Numerical Simulation of Heat and Mass Transfer in Desiccant Coated Rotary Dehumidifiers

Zhang, Huan

A thesis submitted in partial fulfillment of the requirements

for the Degree of Doctor of Philosophy

Department of Building Services Engineering

The Hong Kong Polytechnic University

April 2004

CERTIFICATE OF ORIGINALITY

I hereby declare that this thesis is my own work and that, to the best of my knowledge and belief, it reproduces no material previously published or written nor material which has been accepted for the award of any other degree or diploma, except where due acknowledgement has been made in the text.

_____ (Signed)

Zhang, Huan (Name of student)

Abstract

Abstract of thesis entitled: 'Numerical Simulation of Heat and Mass Transfer in Desiccant Coated Rotary Dehumidifiers'

Submitted by : Zhang, Huan

For the degree of : Doctor of Philosophy

at The Hong Kong Polytechnic University in April, 2004

A numerical model that predicts the heat and moisture transfer during the adsorption and desorption processes in a desiccant-coated, rotary dehumidifier has been developed from fundamental principles. All the assumptions are explained. The model is one-dimensional and transient, and includes all important parameters that affect the performance of desiccant wheels. The influential parameters include energy and mass storage in both the air and the matrix, convection, the axial thermal conduction through both the desiccant and the support material, the axial molecular diffusion within the desiccant coating, and the energy transfer between the air stream and the matrix. No existing models of desiccant coated rotary dehumidifiers include all the above-mentioned important parameters, but literature review indicated a need to accurately model heat and mass transfer in a desiccant-coated, rotary dehumidifier. The model developed in this research can be used in designing or optimizing the desiccant wheels, and in predicting the performance of desiccant enhanced air-conditioning systems.

The model was based on the four governing equations for coupled heat and mass transfer in desiccant wheel. Discretization of the governing equations was performed and all the dependent variables and properties were solved at the nodes. The transient terms were solved using the implicit formulation. The numerical solution scheme was fully implicit, with all dependent variables expressed in their respective current time step values in the algebraic equations. The discretized moisture conservation equations were solved using the Thomas algorithm, also called the Tridiagonal Matrix Algorithm (TDMA), and the discretized energy conservation equations were solved using the Tridiagonal Matrix Algorithm for double variables.

For validation of the numerical model, its predictions were compared with experimental data obtained with a test rig built in accordance with ASHRAE Standard 139 - 1998, Standard Method of Testing for Rating Desiccant Dehumidifiers Utilizing Heat for the Regeneration Process. The accuracy of the simultaneous heat and moisture transfer numerical model of desiccant coated rotary dehumidifier developed in this study has been confirmed by the good agreement with experimental data. The simulated moisture removal capacity agrees with the test data within experimental uncertainty.

The effect of certain parameters on the predicted performance of a desiccant coated rotary dehumidifier was studied. The parameters include regeneration air inlet

temperature and humidity ratio, process air inlet temperature and humidity ratio, and mass flow rate of process airstream. The optimal rotation speed was then found. The variations in parameters of process and regeneration air with angular position and with depth into the tubes are simulated.

The desiccant-coated rotary dehumidifier model developed in this thesis was also applied to predict the performance of desiccant dehumidification and evaporative cooling (DDEC) systems. A two-stage DDEC system using low-temperature heat was proposed, and its performance was predicted. A comparison between a two-stage system and a single-stage system was then made. The required regeneration air inlet temperature of the two-stage DDEC system with intercooling was found to be 35.0°C lower than of the single-stage system. The lowered regeneration temperature will make it possible to utilize low-quality thermal energy such as solar energy and waste heat.

Direct evaporative air coolers are components of DDEC systems. The theoretical and experimental analysis of evaporative coolers filled with corrugated holed aluminum foil fillers (CHAF fillers) is detailed in this thesis. The experimental results show that the direct evaporative cooling effectiveness η_{ec} of the evaporative air cooler using CHAF fillers was about 0.8, and the air flow resistance was less than 200Pa for an air velocity of less than 3m/s. Therefore, CHAF filler is a good pad material.

Acknowledgements

I am deeply indebted to Dr. Jianlei Niu, my chief supervisor, and Professor Chow Wan-ki, my co-supervisor, for their readily available supervision, invaluable suggestions, patient encouragement, and continuous support over the past years.

Table of Contents

List of Figures

List of Tables

Nomenclature

A	adsorption potential energy or the differential molar work of adsorption (kJ/kg_{H_2O})
a	pore radius (m), for regular density (RD) silica gel particles its value can be taken as 11 Å, and for intermediate density (ID) silica gel particles its value can be taken as 68 Å
a_a	thermal diffusivity of air (m^2/s)
A_d	cross-sectional area of desiccant in each tube (m^2)
A_{ec}	contact surface area between air and water in evaporative air cooler (m^2)
A_f	free flow area of each tube (m^2)
A_h	heat transfer surface area per unit length in each tube (m^2/m)
A_m	cross - sectional area of support material in each tube (m^2)
A_s	cross - sectional area of each tube (m^2)
a_v	thermal diffusivity of vapor (m^2/s)
A_w	cross - sectional area of sprinkling water rate in evaporative air cooler (m^2)
a_{wa}	thermal diffusivity of moist air (m^2/s)
C_c	heat capacity rate of the cold fluid flowing through the thermal wheel (kW/K)

c_d specific heat of desiccant, for silica gel its value can be taken as $1.0 kJ/kg_{dry\ \ desiccant} \cdot K$ (Jurinak 1982) or $0.98 kJ/kg_{dry\ \ desiccant} \cdot K$ (Gurgel and Klüppel 1996), and for molecular sieve its value can be taken as $0.615 kJ/kg_{dry\ \ desiccant} \cdot K$ (Simonson and Besant 1997)

C_h heat capacity rate of the hot fluid flowing through the thermal wheel (kW/K)

c_m specific heat of support material, for aluminum its value can be taken as $0.896 kJ/kg \cdot K$ (Kreith and Black 1980)

C_{min} the smaller value between C_h and C_c (kW/K)

COP coefficient of performance of DDEC system (dimensionless)

c_{pa} specific heat of dry air in process channel at constant pressure ($kJ/kg_{dry\ \ air} \cdot K$)

$c_{pa,ev}$ specific heat capacity of air at constant pressure in evaporative air cooler ($kJ/kg \cdot K$)

$c_{pa,heater,in}$ specific heat of regeneration air stream at the inlet of the heater ($kJ/kg_{dry\ \ air} \cdot K$)

$c_{pa,heater,out}$ specific heat of regeneration air stream at the outlet of the heater ($kJ/kg_{dry\ \ air} \cdot K$)

c_{pb} bulk specific heat of desiccant wheel ($kJ/kg \cdot K$)

c_{pc} specific heat of the cold fluid flowing through the thermal wheel $(kJ/kg \cdot K)$

c_{pda} specific heat of dry air in the pore channels of desiccant felt at constant pressure $(kJ/kg_{dry\ \ air} \cdot K)$

c_{ph} specific heat of the hot fluid flowing through the thermal wheel $(kJ/kg \cdot K)$

c_{pva} specific heat of water vapor in process channel at constant pressure $(kJ/kg_{H_2O\ \ vapor} \cdot K)$

c_{pvda} specific heat of water vapor in the pore channels of desiccant felt at constant pressure $(kJ/kg_{H_2O\ \ vapor} \cdot K)$;

c_{pw} specific heat of water liquid at constant pressure, its value can be taken as $4.19 kJ/kg_{H_2O\ \ liquid} \cdot K$

c_{pwa} specific heat of moist air in process channel at constant pressure $(kJ/kg_{dry\ \ air} \cdot K)$

C_s surface concentration $(kg_{H_2O}/m^2_{surface\ \ area})$

D inside diameter of the circular cross-sectional duct of test (m)

$D_{H_2O,air}$ ordinary diffusion coefficient for a water vapor-air mixture through the desiccant felt (m^2/s)

$D_{H_2O,air,c}$ ordinary diffusion coefficient for a water vapor-air mixture in process channel (m^2/s)

$D_{H_2O,air,e}$ effective ordinary diffusion coefficient for a water vapor-air mixture through the desiccant felt (m^2/s)

D_K Knudsen diffusion coefficient (m^2/s)

$D_{K,e}$ effective Knudsen diffusion coefficient (m^2/s)

$D_{o,K}$ combined ordinary and Knudsen diffusion coefficient in water vapor-air mixtures (m^2/s)

$D_{o,K,e}$ effective diffusion coefficient combined ordinary and Knudsen diffusion (m^2/s)

D_s surface diffusion coefficient (m^2/s)

$D_{s,e}$ effective surface diffusion coefficient (m^2/s)

D_w desiccant wheel diameter (m)

E characteristic free energy of adsorption (kJ/kg_{H_2O})

$Ex_{q,s}$ exergy of heat per $kg_{dry\ air}/s$ of the single-stage DDEC system $(kJ/kg_{dry\ air})$

$Ex_{q,t}$ total exergy of heat per $kg_{dry\ air}/s$ of the two-stage DDEC system $(kJ/kg_{dry\ air})$

f_a flux density of dry air at process channel flow area $(kg_{dry\ air}/s \cdot m^2)$

f_v volume fraction of the desiccant in the wheel $(m^3_{desiccant}/m^3_{wheel})$

H_a rate of energy inflow across the x face by convection (kW)

h_a enthalpy of the air stream in process channel ($kJ/kg_{dry\ air}$)

$\bar{h}_{a,p,in}$ average enthalpy over cross-section at the process air inlet of desiccant wheel ($kJ/kg_{dry\ air}$)

$\bar{h}_{a,p,out}$ average enthalpy over cross-section at the process air outlet of desiccant wheel ($kJ/kg_{dry\ air}$)

$\bar{h}_{a,r,in}$ average enthalpy over cross-section at the regeneration air inlet of desiccant wheel ($kJ/kg_{dry\ air}$)

$\bar{h}_{a,r,out}$ average enthalpy over cross-section at the regeneration air outlet of desiccant wheel ($kJ/kg_{dry\ air}$)

$\dot{H}_d$ rate of energy inflow transferred into the desiccant felt across the x face by heat conduction and moisture diffusion

h_d enthalpy of the desiccant solid phase ($kJ/kg_{dry\ desiccant}$)

h_{da} enthalpy of air in the pore channels of desiccant felt or the enthalpy of air in equilibrium with the desiccant solid phase ($kJ/kg_{dry\ air}$)

h_e enthalpy of air stream entering evaporative cooler ($kJ/kg_{dry\ air}$);

h_f enthalpy of the desiccant felt ($kJ/kg_{dry\ desiccant}$)

h_{fg} heat of vaporization of water (kJ/kg_{H_2O})

$h_{fg,0}$ heat of vaporization of water at $0°C$; its value can be taken as $2501.6\,kJ/kg_{H_2O}$

h_i	enthalpy of indoor air ($kJ/kg_{dry\ air}$)
h_l	enthalpy of air stream leaving evaporative cooler ($kJ/kg_{dry\ air}$)
$\dot{H}_m$	rate of energy inflow transferred into the support material across the x face by heat conduction (kW)
h_o	enthalpy of outdoor air ($kJ/kg_{dry\ air}$)
h_s	enthalpy of water molecules in the adsorbed phase (kJ/kg_{H_2O})
h_{va}	enthalpy of water vapor in process channel ($kJ/kg_{H_2O\ vapor}$)
h_{vda}	enthalpy of water vapor in the pore channels of desiccant felt or the enthalpy of water vapor in equilibrium with the desiccant solid phase ($kJ/kg_{H_2O\ vapor}$)
L	filler thickness in evaporative air cooler (m)
l_c	process channel length (m)
Le	Lewis number
l_e	characteristic length of filler in evaporative air cooler (m)
$\dot{M}$	total mass diffusion rate per m^2 of the area normal to the direction of flux ($kg_{H_2O}/m^2 \cdot s$)
$\dot{m}_a$	mass flow rate of dry air in each tube ($kg_{dry\ air}/s$)
$\dot{M}_{a,p}$	total mass flow rate of process air (kg/s)
$\dot{M}_{a,p,in}$	total mass flow rate of process air inlet ($kg_{dry\ air}/s$)
$\dot{M}_{a,p,out}$	total mass flow rate of process air outlet ($kg_{dry\ air}/s$)

$\dot{M}_{a,r}$	total mass flow rate of regeneration air (kg/s)
$\dot{M}_{a,r,in}$	total mass flow rate of regeneration air inlet ($kg_{dry\ air}/s$)
$\dot{M}_{a,r,out}$	total mass flow rate of regeneration air outlet($kg_{dry\ air}/s$)
$\dot{m}_c$	mass flow rate of the cold fluid flowing through the thermal wheel (kg/s)
$\dot{m}_h$	mass flow rate of the hot fluid flowing through the thermal wheel (kg/s)
$\dot{M}_K$	water diffusion rate per m^2 of the area normal to the direction of flux due to Knudsen diffusion ($kg_{H_2O}/s \cdot m^2$)
$\dot{m}_K$	water diffusion rate of one pore due to Knudsen diffusion ($kg_{H_2O}/s \cdot pore$)
$\dot{m}_{K,\tau}$	water diffusion rate of one pore due to Knudsen diffusion accounting for the increase in diffusional length due to tortuous paths of real pores ($kg_{H_2O}/s \cdot pore$)
$\dot{M}_o$	water diffusion rate per m^2 of the area normal to the direction of flux due to ordinary diffusion ($kg_{H_2O}/s \cdot m^2$)
$\dot{m}_o$	water diffusion rate of one pore due to ordinary diffusion ($kg_{H_2O}/s \cdot pore$)

$\dot{M}_{o,K}$ water diffusion rate per m^2 of the area normal to the direction of flux due to combined ordinary and Knudsen diffusion $(kg_{H_2O}/s \cdot m^2)$

$\dot{m}_{o,K}$ combined ordinary and Knudsen diffusion rate of one pore $(kg_{H_2O}/s \cdot pore)$

$\dot{m}_{o,K,\tau}$ combined ordinary and Knudsen diffusion rate of one pore accounting for the increase in diffusional length due to tortuous paths of real pores $(kg_{H_2O}/s \cdot pore)$

$\dot{m}_{o,\tau}$ water diffusion rate of one pore due to ordinary diffusion accounting for the increase in diffusional length due to tortuous paths of real pores $(kg_{H_2O}/s \cdot pore)$

MRC moisture removal capacity (kg_{H_2O}/s)

$\dot{M}_s$ water diffusion rate per m^2 of the area normal to the direction of flux due to surface diffusion $(kg_{H_2O}/s \cdot m^2)$

$\dot{m}_s$ surface diffusion rate of one pore $(kg_{H_2O}/s \cdot pore)$

$\dot{m}_{s,\tau}$ surface diffusion rate of one pore accounting for the increase in diffusional length due to tortuous paths of real pores $(kg_{H_2O}/s \cdot pore)$

M_w total mass of desiccant wheel (kg)

$\dot{m}_w$ water flow rate in evaporative air cooler (kg/s)

M_1	molecular mass of water, its value can be taken as 18 $kg/kmol$
n	number of nodes (dimensionless)
n_{rs}	rotation speed of the rotor $(1/h)$
$n_{rs,op}$	optimal rotation speed of the rotor $(1/h)$
Nu	Nusselt number (dimensionless)
$n_{rs,op}$	optimal rotation speed (1/h)
n_τ	any integer (dimensionless)
Δp	air pressure loss across the evaporative air cooler (pa)
p^*	total pressure of moisture air in the pore channels of desiccant felt (atm)
Pr	Prandtl number of air (dimensionless)
$P_{total,a}$	total pressure of moisture air in process channel (atm)
$P_{total,da}$	total pressure of moisture air in equilibrium with the desiccant solid phase (pa)
$p_{w,da}$	water vapor pressure of moisture air in equilibrium with the desiccant solid phase (pa)
$p_{ws,da}$	water vapor pressure of saturated moisture air in equilibrium with the desiccant solid phase (pa)
q	sprinkling density in evaporative air cooler ($kg/m^2 \cdot s$)
$q_{cool,s}$	cooling capacity per $kg_{dry\ air}/s$ of the single-stage DDEC system ($kJ/kg_{dry\ air}$)

$q_{cool,t}$	total cooling capacity per $kg_{dry\ air}/s$ of the two-stage DDEC system ($kJ/kg_{dry\ air}$)
$q_{cool,tf}$	cooling capacity per $kg_{dry\ air}/s$ of the first thermal wheel ($kJ/kg_{dry\ air}$)
$q_{cool,ts}$	cooling capacity per $kg_{dry\ air}/s$ of the second thermal wheel ($kJ/kg_{dry\ air}$)
$q_{in,s}$	regeneration heat input per $kg_{dry\ air}/s$ of the single-stage DDEC system ($kJ/kg_{dry\ air}$)
$q_{in,t}$	regeneration heat input per $kg_{dry\ air}/s$ of the two-stage DDEC system ($kJ/kg_{dry\ air}$)
q_{st}	heat of adsorption (kJ/kg_{H_2O})
R	gas constant of water vapor ($kJ/kg_{H_2O} \cdot K$), its value can be taken as $0.4516\,kJ/kg_{H_2O} \cdot K$
r	radial coordinate in a particle (m)
r_a	ratio of the free flow area to the face area of a desiccant wheel (dimensionless)
RE	regeneration energy (kW)
Re	Reynolds number (dimensionless)
RH_{da}	relative humidity of the moisture air in equilibrium with the desiccant solid phase (dimensionless)

r_m	ratio of the cross-sectional area of support material to the face area of a desiccant wheel (dimensionless)
RSHI	specific heat input stated in terms of thermal energy input per kilogram of moisture removal (kJ/kg_{H_2O})
r_{sv}	ratio of the desiccant surface area to the wheel volume ($m^2_{desiccant}/m^3_{wheel}$)
S_g	specific surface area of pore ($m^2_{surface\ area}/kg_{dry\ desiccant}$), for RD silica gel its value can be taken as $7.8\times10^5 m^2_{surface\ area}/kg_{dry\ desiccant}$, and for ID silica gel its value can be taken as $3.4\times10^5 m^2_{surface\ area}/kg_{dry\ desiccant}$ (Pesaran and Mills 1987a)specific surface area of pore ($m^2_{surface\ area}/kg_{dry\ desiccant}$)
t_a	temperature of air stream in process channel (°C)
$t_{a,heater,in}$	temperature of the regeneration air stream at the inlet of the heater (°C)
$t_{a,heater,out}$	temperature of the regeneration air stream at the outlet of the heater (°C)
$T_{a,p,in}$	absolute temperature of process air stream inlet condition (K)
$t_{a,p,in}$	temperature of process air stream inlet condition (°C)
$T_{a,r,in}$	absolute temperature of regeneration air stream inlet condition (K)

$t_{a,r,in}$	temperature of regeneration air stream inlet condition (°C)
t_{ce}	air temperature of the cold fluid entering thermal wheel (°C)
T_d	absolute temperature of desiccant or the temperature of the moisture air in equilibrium with the desiccant solid phase (K)
t_d	desiccant temperature or the temperature of the moisture air in equilibrium with the desiccant solid phase (°C), $t_d = T_d - 273.16$
t_e	temperature of air stream entering evaporative cooler (°C)
TET	total energy transfer (kW)
t_{ew}	wet bulb temperature of air stream entering evaporative cooler (°C)
t_{he}	air temperature of the hot fluid entering thermal wheel (°C)
t_{hl}	air temperature of the hot fluid leaving thermal wheel (°C)
t_l	temperature of air stream leaving evaporative cooler (°C)
T_o	absolute temperature of ambient air (K)
V	filler volume in evaporative air cooler (m^3)
v_a	face velocity of air in evaporative air cooler (m/s)
v_c	air velocity at process channel flow area (m/s)
v_f	face air velocity (m/s)
$v_{f,p}$	face velocity of process air (m/s)
$v_{f,r}$	face velocity of regeneration air (m/s)
$\dot{W}_a$	rate of moisture inflow across the x face by convection (kg_{H_2O}/s)
w_a	humidity ratio of air stream in process channel (kg_{H_2O}/kg_{dryair})

$w_{a,p,in}$ humidity ratio of process air stream at inlet of a process channel (kg_{H_2O}/kg_{dryair})

$\bar{w}_{a,p,in}$ average humidity ratio over cross-section at the process air inlet of desiccant wheel ($kg_{H_2O}/kg_{dry\ \ air}$)

$\bar{w}_{a,p,out}$ average humidity ratio over cross-section at the process air outlet of desiccant wheel ($kg_{H_2O}/kg_{dry\ \ air}$)

$w_{a,r,in}$ humidity ratio of regeneration air stream at inlet of a process channel ($kg_{H_2O}/kg_{dry\ \ air}$)

$\bar{w}_{a,r,in}$ average humidity ratio over cross-section at the regeneration air inlet of desiccant wheel ($kg_{H_2O}/kg_{dry\ \ air}$)

$\bar{w}_{a,r,out}$ average humidity ratio over cross-section at the regeneration air outlet of desiccant wheel ($kg_{H_2O}/kg_{dry\ \ air}$)

w_{ce} air humidity ratio of the cold fluid entering thermal wheel ($kg_{H_2O}/kg_{dry\ \ air}$)

w_{cl} air humidity ratio of the cold fluid leaving thermal wheel ($kg_{H_2O}/kg_{dry\ \ air}$)

$\dot{W}_d$ rate of moisture inflow across the x face by diffusion (kg_{H_2O}/s)

w_d water content of desiccant solid phase ($kg_{H_2O}/kg_{dry\ \ desiccant}$)

w_{da} humidity ratio of air in equilibrium with the desiccant solid phase or moisture concentration of air in the pore channels of desiccant felt ($kg_{H_2O}/kg_{dry\ air}$)

$w_{d\max}$ maximum water content of the desiccant solid phase, for silica gel its value can be taken as $0.50kg_{H_2O}/kg_{dry\ desiccant}$ (Jurinak 1982), for molecular sieve its value can be taken as $0.35kg_{H_2O}/kg_{dry\ desiccant}$ (Simonson and Besant 1997), and for the simulations in this thesis its value is taken as $0.35kg_{H_2O}/kg_{dry\ desiccant}$

$w_{d\ total}$ total water content of desiccant felt ($kg_{H_2O}/kg_{dry\ desiccant}$)

Δw_f dehumidifying capacity per $kg_{dry\ air}/s$ of the first desiccant wheel ($kg_{H_2O}/kg_{dry\ air}$)

w_{he} air humidity ratio of the hot fluid entering thermal wheel ($kg_{H_2O}/kg_{dry\ air}$)

w_{hl} air humidity ratio of the hot fluid leaving thermal wheel ($kg_{H_2O}/kg_{dry\ air}$)

w_i humidity ratio of indoor air ($kg_{H_2O}/kg_{dry\ air}$)

w_o humidity ratio of outdoor air ($kg_{H_2O}/kg_{dry\ air}$)

w_s humidity ratio of supply air ($kg_{H_2O}/kg_{dry\ air}$)

Δw_s dehumidifying capacity per $kg_{dry\ air}/s$ of the second desiccant wheel ($kg_{H_2O}/kg_{dry\ air}$)

Δw_t	total dehumidifying capacity per $kg_{dry\ air}/s$ of the DDEC system ($kg_{H_2O}/kg_{dry\ air}$)
x	actual process channel position (m)

Greek Symbols

α	heat transfer coefficient between air and water in evaporative air cooler ($kW/m^2 \cdot K$)
α_h	heat transfer coefficient between air and desiccant in desiccant wheel ($kW/m^2 \cdot K$)
α_m	mass transfer coefficient between air and desiccant in desiccant wheel (m/s)
α_v	average volume heat transfer coefficient between air and water in evaporative air cooler ($kW/m^3 \cdot K$)
β_e	fractional area of regeneration zone, for the desiccant wheel simulated for the sensitivity studies in this chapter is 0.25
ε_p	desiccant felt porosity defined as the volume fraction of dry gel occupied by air (dimensionless)
η_{ec}	saturation effectiveness of evaporative cooler (dimensionless)
η_{hw}	effectiveness of thermal wheel (dimensionless)
λ_a	thermal conductivity of air ($kW/m \cdot K$)

λ_d solid conductivity of the silica gel grain $(kW/m \cdot K)$

λ_m thermal conductivity of support material, for aluminum its value can be taken as $0.236\,kW/m \cdot K$ (Kreith and Black 1980)

μ_f Dynamic viscosity of air at average temperature t_a, $(N \cdot s/m^2)$

μ_w Dynamic viscosity of air at wall temperature t_d, $(N \cdot s/m^2)$

ν_a kinematic viscosity of air (m^2/s)

ρ air density in evaporative air cooler (kg/m^3);

ρ_a density of dry air in process channel $(kg_{dry\ air}/m^3)$

$\rho_{a,o}$ dry air density of outdoor air, its value can be taken as $1.1532\,kg_{dry\ air}/m^3$

ρ_b bulk density of desiccant wheel (kg/m^3_{wheel})

ρ_d density of desiccant felt, for molecular sieve its value can be taken as $350\,kg_{desiccant}/m^3_{desiccant}$ (Simonson and Besant 1997), for RD silica gel its value can be taken as $1129\,kg_{desiccant}/m^3_{desiccant}$, and for ID silica gel its value can be taken as $620\,kg_{desiccant}/m^3_{desiccant}$ (Pesaran and Mills 1987a)

ρ_{da} density of dry air in the pore channels of desiccant felt or density of dry air in equilibrium with the desiccant solid phase $(kg_{dry\ air}/m^3)$

ρ_m density of support material, for aluminum its value can be taken as $2702kg/m^3$ (Kreith and Black 1980)

ρ_{wa} density of moist air in process channel ($kg_{moist\ air}/m^3$)

τ actual time (s)

τ_g tortuosity factor for intraparticle gas diffusion (dimensionless), for regular density (RD) silica gel particles its value can be taken as 2.8, and for intermediate density (ID) silica gel particles its value can be taken as 2.0.

τ_p process air flow period (s)

τ_r regeneration air flow period (s)

τ_s tortuosity factor for intraparticle surface diffusion (dimentionless), for RD silica gel its value can be taken as 2.8, and for ID silica gel its value can be taken as 2.0 (Pesaran and Mills 1987a)

Chapter 1 Introduction and Literature Review

Solid desiccants are generally used in pellet or granular form. However, to minimize pressure drop and thus to increase the energy efficiency of moisture separation, the adsorbents are sometimes formed into adsorbent sheets. A desiccant wheel is a slowly rotating cylindrical wheel with a honeycomb-like internal structure, containing a large number of small parallel channels (also known as tubes). The channels are separated by desiccant coated walls which are substrate sheets (also known as support material) coated with solid desiccant sheets on both sides. The solid desiccants may be silica gels or molecular sieves. The support material could be any rigid nonhygroscopic material, such as ceramic fiber paper or aluminum. A desiccant wheel is often divided into two separately sealed zones: a dehumidifying (adsorption) zone and a regeneration (desorption) zone, through which the regeneration and process air streams flow in opposite directions. In the dehumidifying zone process air stream enters the tubes and transfers moisture to the adsorbents, so that the air stream will leave the wheel at a dried state. In the regeneration zone, the water molecules in the adsorbents are then transferred to the hot regeneration air i.e. desorption occurs. The desorption zone may be occupy up to half of the wheel. Either the dried air or the humid atmospheric air (or a mixture of the two) can be used for regeneration. Figure 1.1 shows a schematic of a desiccant wheel operating in a counterflow arrangement (Figure 1.1(a)), and shows one of the flow tubes in detail (Figure 1.1(b)).

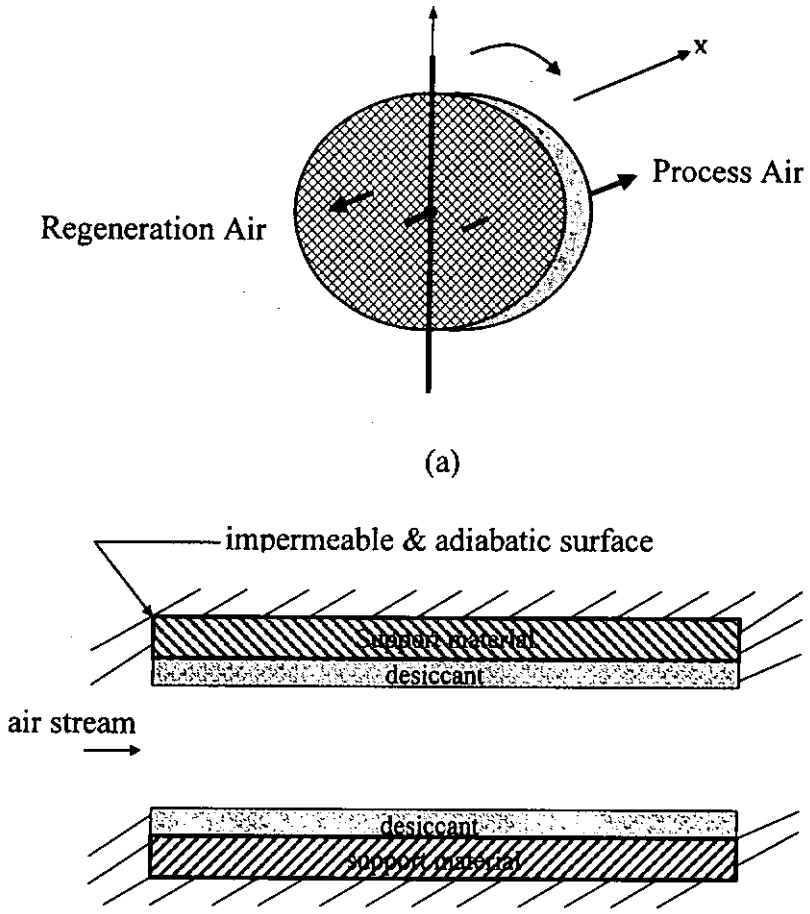

Figure 1.1 Schematic of the desiccant wheel showing
(a) entire wheel
(b) side view of one of the tubes

To remove moisture from the supply air in conventional air-conditioning systems, the required chilled water temperature is typically around 5-7 °C. Alternatively, excessive high humidity may occur. Therefore, a lower evaporating temperature is required and consequently the coefficient of performance, COP, of a

mechanical refrigerating system will be lower. In some cases the supply air is overcooled, reheating used to compensate for this overcooling will waste a lot of energy. When dehumidifying is performed by desiccants, the energy source in desorption can be provided from low-level energy such as waste heat from industries, hot air exhausted from refrigerators , solar collectors and so on. On the other hand, mechanical cooling is required only for sensible heat removal purposes, so a higher evaporating temperature is required and consequently the coefficient of performance, COP, of a mechanical refrigerating system will be higher. Therefore, desiccant wheels are regarded as energy-efficient as air handling equipment.

Solid desiccants have long been used in dehumidification and cooling systems. The application of desiccant dehumidification in a cooling system was first proposed by Pennington (1955). Since that time, much research and many experiments have been conducted on desiccant-based systems. Löf (1955) built and tested an adsorption system that used solar-heated air for the regeneration stream. Dunkle (1965) described an open-cycle desiccant cooling system with an adiabatic rotary dehumidifier. Lunde (1975) showed that the performance of such a system can be improved by introducing interstage cooling. The Institute of Gas Technology developed a desiccant air-conditioning system using a molecular sieve (Staats 1977). The system of AiResearch Manufacturing Co. used 3mm silica gel

particles as the desiccant material packed into a drum (Gunderson 1978). Experimental results showed that the system, operating in a recirculation mode, has a COP of 0.5, which is somewhat lower than the analytical predictions. A cross-cooled, fixed-bed desiccant dehumidifier was built and tested by Mei (1979) and Worek (1980). Workers at Exxon developed a new adiabatic dehumidifier design by incorporating inert material which has been reported to improve the performance of the system (Husky 1982). Investigators at American Solar King used the Exxon dehumidifier design and developed a desiccant cooling system operating in the ventilation mode with a $COP \approx 1.0$ (Venhuizen 1984).

The primary component of a solid-desiccant cooling system is the dehumidifier, which is the most difficult component to simulate, and the simulation of the desiccant wheel is the most time-consuming portion of all solid-desiccant cooling system simulation programs. The subject of heat and mass transfer in rotary desiccant dehumidifiers has been studied extensively over a period of many years.

There is an accepted set of equations that describe the heat and mass transfer in rotary regenerators (e.g., Maclaine – Cross (1972), Kays and Crawford (1980), Jurinak (1982), Van den Bulck (1987), Farooq and Ruthven (1991), Chau and Worek (1995)). The methods that have been used to solve these equations can be classified as direct numerical solution, analogy between heat and mass transfer and heat transfer, and analogy to counter flow exchangers.

Linearized solutions for the adiabatic dehumidifier were given by Banks et al. (1970) using the analogy method. Maclaine-Cross and Banks (1972) predict the exit fluid temperature and humidity of a desiccant dehumidifier wheel using the analogy between the heat and mass transfer processes, and presented a method to solve the coupled heat and mass transfer problem by analogy with heat transfer for any number of components. The method involves transforming the coupled equations into a number of equation sets in which each set describes only one of the characteristic potentials for heat and mass transfer and is of the same form as the equation for heat transfer alone. This allows the solution for sensible rotary heat exchangers to be used to solve each characteristic potential and hence the temperature and moisture content in the air. Banks (1972) and Close and Banks (1972) used the same analogy for heat and mass transfer in fluid flow through a porous medium, assuming thermodynamic equilibrium. They were able to predict the main features of an experiment with a silica gel dryer. However, as pointed out by Banks (1985a), this method contains two significant errors which fortuitously cancel each other out and give acceptable results for a silica gel desiccant. This canceling of errors cannot be guaranteed for other desiccants and operating conditions. Banks (1985b) presented a nonlinear analogy that was deemed to be more accurate for other desiccants than the linear analogy of Maclaine-Cross and Banks (1972), but this nonlinear model reduced only one of the two significant errors and had, in fact, higher errors for a silica gel dehumidifier than the linear

model. The main advantage of using the analogy between heat and mass transfer is that it reduces the computation time necessary to find a solution. With the further development of computers and numerical techniques, this advantage has become less important. As a result, more recent studies have usually solved the coupled heat and mass transfer equations numerically.

Barlow (1982) proposed a pseudo-steady state model and incorporated this model in the DESSIM program, in which a discrete section of dehumidifier was considered as a steady state heat and mass transfer exchanger. The pseudo-steady state model for the heat and mass transfer in the desiccant wheel was modified by Collier et al. (1986) in a later version of the program (i.e., Modified DESSIM). The difference between the approach used by Maclaine-Cross and Banks (1972) and that used by Barlow (1982) and Collier et al. (1986) is that Maclaine-Cross and Banks' method used a heat transfer analogy solution for the entire desiccant wheel and Collier et al. (1986) used a heat and mass exchanger analogy solution to divide the desiccant wheel into discrete elements.

Also, other investigators have performed the heat and mass transfer analysis of a desiccant dehumidifier. Adiabatic dehumidification of moist air was studied, both numerically and experimentally, by Bullock and Threlkeld (1966). Roy and Gidaspow (1972) analyzed a cross-flow regenerator using Green's functions. Mathiprakasam (1979) predicted the performances of a cross-flow, fixed-bed

dehumidifier and an adiabatic dehumidifier using an explicit finite-difference method. Linearized solutions for the adiabatic dehumidifier were given by Mathiprakasam and Lavan (1980) using Laplace transforms. Jurinak (1982) simulated an open-cycle, solid-desiccant cooling system using a finite-difference method for the desiccant wheel. A comparison of several numerical solutions was presented.

Van den Bulck et al. (1985) used a wave theory to model a rotary dehumidifier with infinite transfer coefficients. The result, combined with the solutions of finite transfer coefficients, established the effectiveness correlation of the desiccant wheel. For a given cooling load, Van den Bulck et al. (1986) found an optimum value of regeneration air mass flowrate and wheel rotational speed. The results were presented in a map as a function of several operating conditions. Van den Bulck et al. (1987, 1988) also performed a second-law analysis of a rotary solid-desiccant dehumidifier and simulated compact regenerative dehumidifiers. In 1990, a test procedure for estimating the overall heat and mass transfer coefficient of compact dehumidifier matrices was proposed by Van den Bulck and Klein (1990). The test procedure considers the nonlinear character of the conservation equation. A comparison between several experimental test and theoretical analysis was performed.

Charoensupaya and Worek (1988) also solved the governing equations of an adiabatic dehumidifier using an explicit finite-difference method, which was incorporated in the UIC-Vent1 program, and parametrically studied the performance of open-cycle desiccant cooling systems. In their model, the derivation assumes that there is no axial heat conduction and mass diffusion in the desiccant wall.

In all of the finite-difference methods cited above, explicit finite-difference methods were used. Zheng and Worek (1993) presented an implicit numerical model, which solved heat and mass transfer in adiabatic rotary dehumidifiers. They did extensive work on the numerical model to improve the speed of the simulation. Using the implicit method allowed the numerical scheme to be unconditionally stable and allowed more rapid simulation of desiccant systems. However, the accumulations of energy and moisture in the air stream, and axial heat conduction and mass diffusion in the desiccant wall are negligible in their model. Some results obtained from their numerical model are compared with results from other models but not with experimental measurements. In a subsequent paper, Zheng et al. (1993) used this numerical model to show the effect of wheel speed, type and amount of desiccant and size of the dehumidifier on the performance of adiabatic dehumidifiers. Zheng and Worek (1993) assumed that the energy of phase change is delivered to the matrix, while Collier et al. (1986) assumed that the energy of phase change is delivered to the air. The literature

review did not discuss the effect of the energy of phase change on the performance of a desiccant dehumidifier. Since all models include simplifying assumptions, it is necessary to study the correctness and significance of these assumptions. Furthermore, experimental validation was not completed before a model is used for other applications.

San and Hsiau (1994) established a one-dimensional transient heat and mass transfer model of rotary heat and mass regenerator, in which axial solid heat conduction and mass diffusions are considered but the storage terms $\frac{\partial T}{\partial t_A}$ and $\frac{\partial Y}{\partial t_A}$ are negligible (T is temperature of air, and Y is humidity ratio of air). Their work investigated the effect of the axial heat conduction and mass diffusion on the performance of a solid desiccant wheel. It was found that the axial solid diffusion effect is necessary to consider in the model of solid desiccant wheel.

A computationally simple model was developed by Stiesch et al. (1995) to provide performance estimates for commercially available rotary enthalpy and sensible heat exchangers as a function of matrix design and matrix properties. These properties include the two air inlet states, air flow rates and matrix rotation speed. The model incorporates experimental measurements of the adsorption isotherm of the matrix material together with other relevant properties to enable estimation of the annual (heating and cooling) energy savings which result from the use of rotary enthalpy

and sensible heat exchangers in different climates. The model neglects axial heat conduction through the matrix and the axial molecular diffusion and capillary motion of moisture within the desiccant coating.

Simonson and Besant (1997) developed a numerical model for heat and moisture transfer in rotary energy exchangers, also known as enthalpy wheels or desiccant coated energy wheels. The model includes axial heat conduction through the support material, but neglects axial heat conduction through the desiccant and the axial molecular diffusion and capillary motion of moisture within the desiccant coating. Simonson and Besant (1997) considered the distribution of the heat of sorption between the desiccant and the air. The energy equations for the air and matrix include energy storage, convection, conduction through the support material and energy associated with phase change and are, respectively

$$\rho_g \cdot c_{pg} \cdot A_g \cdot \frac{\partial T_g}{\partial t} + U \cdot \rho_g \cdot c_{pg} \cdot A_g \cdot \frac{\partial T_g}{\partial x} - m' \cdot h_{ad} \cdot \eta + h \cdot p \cdot (T_g - T_m) = 0 \tag{1.1}$$

and

$$\rho_m \cdot c_{pm} \cdot A_m \cdot \frac{\partial T_m}{\partial t} - m \cdot h_{ad} \cdot (1-\eta) - m' \cdot c_{pw} \cdot (T_g - T_m) - h \cdot p \cdot (T_g - T_m)$$

$$= \frac{\partial}{\partial x}(k_{Al} \cdot A_{Al} \frac{\partial T_m}{\partial x}) \tag{1.2}$$

where ρ_g - density of total gas phase (air and water vapor) (kg/m^3);

c_{pg} - specific heat of total gas phase (air and water vapor) ($kJ/kg \cdot K$);

A - cross – sectional area of gas (m^2);

T_g - temperature of gas (K);

t - time (s);

U - mean airflow velocity in tube (m/s);

x - axial coordinate (m);

$\dot{m}'$ - rate of phase change per unit length ($kg/m \cdot s$);

h_{ad} - heat of sorption (adsorption and desorption) (kJ/kg);

η - fraction of the phase change energy that enters the air;

h - convective heat transfer coefficient ($kW/m^2 \cdot K$);

p - perimeter of each tube (m);

T_m - temprature of matrix (including support material, desiccant and moisture) (K);

ρ_m - density of of matrix (including support material, desiccant and moisture) (kg/m^3);

c_{pm} - specific heat of matrix (including support material,desiccant and moisture) ($kJ/kg \cdot K$);

A_m - cross-sectional area of matrix (including support material,desiccant and moisture) (m^2);

c_{pw} - specific heat of liquid water ($kJ/kg \cdot K$);

k_{Al} - thermal conductivity of support material ($kJ/kg \cdot K$);

A_{Al} - cross – sectional area of support material (m^2)

There are two errors in the energy equations for the air and matrix developed by Simonson and Besant (1997)

a. In Equation 1.1 the air gains the energy associated with mass transfer $\dot{m}' \cdot h_{ad} \cdot \eta$, and in Equation 1.2 the matrix gains the energy associated with mass transfer $\dot{m} \cdot h_{ad} \cdot (1-\eta) + \dot{m}' \cdot c_{pw} \cdot (T_g - T_m)$. In fact, it is impossible that both the air and matrix gain energy due to mass transfer. During adsorption the air loses the energy and the matrix gains the energy due to mass transfer. During desorption the result is the opposite.

b. The energy gain of the air associated with mass transfer should be equal to the energy loss of the matrix associated with mass transfer, but in equation (1.1) the energy gain of the air is $\dot{m}' \cdot h_{ad} \cdot \eta$ and in equation (1.2) the energy gain of the matrix is $\dot{m} \cdot h_{ad} \cdot (1-\eta) + \dot{m}' \cdot c_{pw} \cdot (T_g - T_m)$. Therefore, it is an error not only in mathematical signs but also in value.

Simonson and Besant (1997) simulated the effect of the fraction of the energy associated with phase change on predicted performance, but the results can't be used due to the errors in the energy equations.

Although the fundamental physics and surface chemistry of desiccant drying and energy exchange are similar, according to Banks (1985a) the appropriate methods for modeling a regenerative dehumidifier and those for a regenerative energy exchanger may not be the same because the operating conditions are significantly different. As pointed out by Simonson and Besant (1997), desiccant dryers, which use high temperatures to desorb moisture from the wheel, have somewhat different sorption characteristics than energy wheels which operate over a small temperature range. The model developed by Simonson and Besant (1997) was compared with experiments for cold supply air and hot regeneration air inlet conditions of -20°C and 50% rh and 26°C and 40% rh, respectively. The operating condition is significantly different from that of desiccant dehumidifier.

Štěpánek et al. (1998) developed a mathematical model of a desiccant rotor. They assumed thermal equilibrium between the fluid and the solid phase (i.e., the temperature of the gas phase is equal to that of the solid phase), so that they arrived at only three partial differential equations. The correctness and significance of the assumption was not studied in their paper.

In the models developed by Cejudo et al. (2002) and Zhang et al. (2003), the derivation assumes that there is no axial heat conduction and mass diffusion in the desiccant wall.

In the model developed by Niu and Zhang (2002), the axial thermal conduction and water molecular diffusion through desiccant are considered, but the accumulations of energy in the support material and the axial thermal conduction through the support material are negligible.

The studies cited above developed a theory of regenerative dehumidifiers to the point where this theory has been applied to predict the performance of air-conditioning systems. For example, Nimmo et al. (1993) and Rengarajan and Nimmo (1993) used the desiccant wheel numerical model developed by Collier (1988) to show the advantage of using a desiccant wheel together with conventional air conditioning systems. They compared DEAC (Desiccant Enhanced Air Conditioner) to other air conditioning options and found that for a warm humid climate (e.g., Miami) the DEAV had the best performance in energy use, comfort and capital cost. The DEAC system provided the same comfort while using 10% less energy than a current high efficiency air conditioner.

Meckler (1995) introduced a desiccant preconditioning module that can supply dry air to two or more conventional air-conditioning units. Simulation results presented in the paper show that preconditioning ventilation air using desiccant dryers can reduce the required installed air chilling capacity by 30% in the United States. This new system results in improved indoor air quality at a lower cost because temperature and humidity are controlled independently.

The authors (1998, 1999) proposed a two-stage desiccant cooling system with intercooling. They used the analogy method presented by Banks et al. (1970) to show that much lower regeneration temperature will be required as compared with a single-stage desiccant cooling system, which makes low quality thermal energy utilization possible. The energy system analysis using exergy method shows the exergy of a two-stage system is 6 percent less than the exergy of a single-stage system.

A collection of studies by ASHRAE (1992) shows that the inclusion of desiccant dehumidifiers in HAVC systems for large and small office buildings and special applications such as supermarkets, ice rinks, and storage rooms has proven to be effective. The benefits include reduced capital and operating costs together with improved building performance.

The above literature review indicates a need for more research on the desiccant dehumidifiers. The purpose of this thesis is to develop a numerical model for heat and mass transfer in a desiccant coated rotary dehumidifier. This model is intended to be used in designing or optimizing the desiccant wheels and in predicting the performance of desiccant enhanced air-conditioning system, and therefore this model must include all important parameters that affect the performance of desiccant wheels. The model must be complete and accurate, without being overly

complex, in order to facilitate design and optimization. In this thesis, the model includes energy and mass storage in both air and matrix, convection, the axial thermal conduction through both desiccant and the support material, the axial water molecular diffusion within the desiccant coating and the energy transfer between the air stream and the matrix. So far, no reports have been found on the model of a desiccant coated rotary dehumidifier including all important parameters mentioned above. The governing equations and assumptions used to develop the numerical model for desiccant wheel are presented in detail.

The numerical model of a desiccant wheel solves the simultaneous heat and moisture transfer in one tube as it rotates around the axis of the wheel. The analysis is based on the following assumptions.

a. Within each tube shown in Figure 1(b), there are no gradients in radial temperature or moisture content of the air, so the heat and mass transfer process can be modeled using the bulk mean temperatures and moisture concentrations of the air. This assumption simplifies the analysis in the air, because it avoids the problem of determining the radial temperature and moisture concentration distributions in each tube and simplifies the problem to one-dimensional in space for each bulk fluid variable.

b. In each tube shown in Figure 1(b), there are no radial temperature or moisture content gradients within the thickness of the matrix, because the transport of heat and mass from the air stream to the desiccant is controlled by the gas-side film resistance. This assumption is valid if the heat and mass transfer Biot numbers are less than 0.1 (Incropera and Dewitt 1996). Both the heat and mass transfer Biot numbers are less than 0.1 for this problem because the extremely thin-walled tubes that make up the wheel are coated with a thin layer of desiccant. This means that the matrix behaves like a heat-exchanger fin with negligible temperature (and moisture content) differences in the radial direction, but with significant temperature (and moisture content) differences in the axial direction.

c. The axial (x direction) heat conduction and water vapor molecular diffusion in the air are negligible, because the flux, or advection of heat and water vapor in air, is much larger than the axial conduction and molecular diffusion for a wheel under normal operating conditions. The Peclet number for typical operations is in the order of 100, whereas fluid axial heat conduction is generally neglected for Pe>50 and can be neglected for Pe>10 in this specific application (Shah and London 1978).

d. Hysteresis in the sorption isotherm is assumed negligible.

e. The pressure drop across the desiccant wheel does not result in a significant change in the absolute pressure or air density. The pressure drop due to skin friction is negligible compared to atmospheric pressure and thus changes in air pressure within the desiccant wheel will not influence the other properties.

f. The inlet air conditions are uniform radially (r direction), but may vary with time (or rotational angle). Air leakage from the hot side to the cold side, or vice versa, is negligible or zero, but carryover, due to rotation of the air mass within the wheel matrix, is included in the analysis. On the other hand, the tubes that make up the desiccant wheel are identical, i.e. made of the same material and of the same configuration. Therefore, only one of the tubes in the matrix needs to be analyzed.

g. All tubes are assumed to be adiabatic.

The mathematical model of desiccant coated rotary dehumidifier is developed subject to the equilibrium relation of the desiccant material, the heat of adsorption, thermal conduction and moisture diffusion through desiccant material, the heat and mass transfer coefficient, the specific heat capacity, and the other desiccant properties, which are detailed in Chapter 2.

In Chapter 3, the four governing equations for coupled heat and mass transfer in desiccant coated rotary dehumidifier are presented based on above assumptions.

In Chapter 4, the discretization of the governing equations is performed and all the dependent variables and properties are solved at the nodes.

In chapter 5, the test rig built for validation of the numerical model is detailed, and the accuracy of the simultaneous heat and moisture transfer numerical model of desiccant coated rotary dehumidifier, developed in this thesis, is confirmed using experimental data.

In chapter 6, the effect of certain parameters on the predicted performance of a desiccant coated rotary dehumidifier is studied, and a recommendation for the optimal rotation speed is given. The variations in parameters of process and regeneration air with angular position and with depth into the tubes are simulated.

In chapter 7, the numerical model of desiccant-coated, rotary dehumidifier developed in this thesis is applied in prediction of the performance of the desiccant dehumidification and evaporative cooling (DDEC) systems. A two-stage DDEC system using low-temperature heat was proposed, and its performance is predicted. And then a two-stage DDEC system is compared with a single-stage system.

Direct evaporative air coolers are also the components of the DDEC systems. The theoretical and experimental analysis of evaporative coolers filled with corrugated holed aluminum foil fillers is detailed in chapter 7.

Chapter 8 summaries the main achievements of the work reported in this thesis and give some recommendations for future research in the related area.

Chapter 2 Desiccant Properties and Heat and Mass Transfer Coefficients

Desiccant dehumidification is accomplished by adsorption of water molecules present in moist air on the surface and in the pore of the desiccant material. The water molecules do not condense on the surface; rather, they form a solution with the desiccant material. Adsorption is unlike condensation that occurs over a range of temperatures at a fixed pressure.

Water molecules adsorbed in the desiccant material get activated when temperature rises by feeding the heated regeneration air so that the adsorption force gets weakened and water molecules get out from the desiccant material.

There is an equilibrium layer of moist air in contact with desiccant, shown in Figure 2.1. The temperature of the equilibrium layer is equal to the temperature of the desiccant surface. The isotherm determines the relations between the moisture content of desiccant and the relative humidity of moist air in the equilibrium layer at a given temperature.

The heat of adsorption is the amount of heat that is liberated by the phase change of the water from vapor phase to the adsorbed phase. The heat of adsorption can be thought of as two parts: the heat of condensation, and the differential heat of

adsorption (i.e. the adsorption potential energy). The heat of condensation is the energy release associated with the change in phase from vapor to liquid for pure water. The differential heat of adsorption is the energy release associated with the combining of the liquid water and desiccant into a single phase and is usually small compared to the heat of condensation.

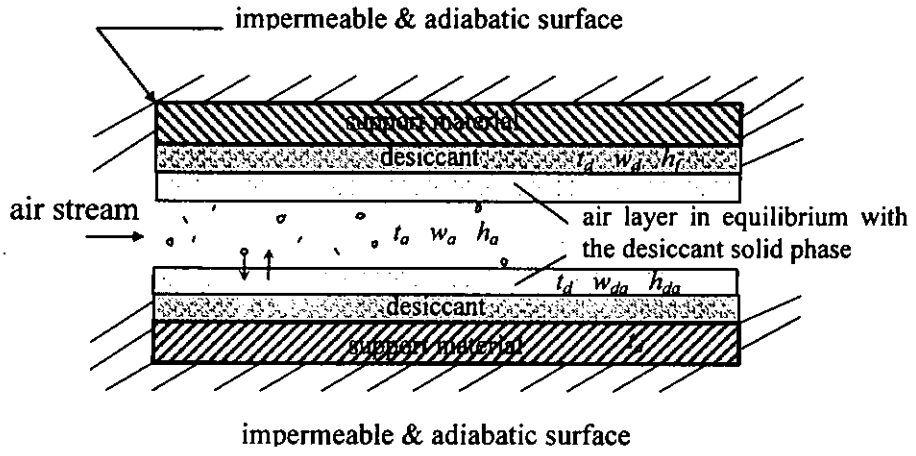

Figure 2.1 Equilibrium layer of moist air in contact with desiccant

Desiccant dehumidifies air and is regenerated through heat and mass transfer processes between the air in the equilibrium layer and air passed through the channel of desiccant wheel. Moist air passes through a desiccant wheel and is dried during the processing period. During adsorption, the dehumidification processes raise the temperature of the process air. The desiccant is heated to a relatively high temperature in order to drive off the water, and this process is referred to as regeneration.

The mathematical model of desiccant wheel is developed subject to the equilibrium relation of the desiccant material, the heat of adsorption, thermal conduction and moisture diffusion through desiccant material, the heat and mass transfer coefficient, the specific heat capacity, and the other desiccant properties.

2.1 Isotherm Shape

A single-sited Dubinin isotherm equation and the adsorption potential theory (Polanyi 1932; Dubinin 1975) are used to describe the isotherm shapes. The adsorption potential theory is valid for microporous adsorbents; that is, adsorbents with pore diameters less than about 20 Å. The single-sited Dubinin isotherm form, which is the most basic form, is used to minimize the number of parameters to consider, and is as follows:

$$w_d = w_{d\max} \cdot \exp\left[-\left(\frac{A}{E}\right)^n\right] \quad (kg_{H_2O}/kg_{dry\ \ desiccant}) \tag{2.1}$$

where w_d - water content of desiccant solid phase ($kg_{H_2O}/kg_{dry\ \ desiccant}$);

$w_{d\max}$ - maximum water content of the desiccant solid phase ($kg_{H_2O}/kg_{dry\ \ desiccant}$);

A - adsorption potential energy or the differential molar work of adsorption (kJ/kg_{H_2O});

E - characteristic free energy of adsorption (kJ/kg_{H_2O})

The temperature of the moisture air in equilibrium with the desiccant material is equal to the desiccant temperature t_d. The adsorption potential energy A is equivalent to the differential Gibb's free energy of adsorption for an ideal gas and is defined as follows:

$$A = -R \cdot T_d \cdot \ln RH_{da} \quad (kJ/kg_{H_2O}) \tag{2.2}$$

where R - gas constant of water vapor, its value can be taken as $0.4516 kJ/kg_{H_2O} \cdot K$;

T_d - absolute temperature of desiccant or the temperature of the moisture air in equilibrium with the desiccant solid (K);

RH_{da} - relative humidity of the moisture air in equilibrium with the desiccant solid phase (dimensionless), defined by

$$RH_{da} = p_{w,da} / p_{ws,da} \tag{2.3}$$

$p_{w,da}$ - water vapor pressure of moisture air in equilibrium with the desiccant solid phase (pa);

$p_{ws,da}$ - water vapor pressure of saturated moisture air in equilibrium with the desiccant solid phase (pa)

The relation between the $p_{w,da}$ and humidity ratio of the moisture air in equilibrium with the desiccant solid phase w_{da} is

$$w_{da} = 0.62198 \cdot \frac{p_{w,da}}{P_{total,da} - p_{w,da}} \quad (kg_{H_2O}/kg_{dry\ air}) \tag{2.4}$$

where $P_{total,da}$ - total pressure of moisture air in equilibrium with the desiccant solid phase, its value can be taken as 101325 (pa)

$p_{ws,da}$ is a function of T_d only.

$$\ln p_{ws,da} = c_8/T_d + c_9 + c_{10} \cdot T_d + c_{11} \cdot T_d^2 + c_{12} \cdot T_d^3 + c_{13} \cdot \ln T_d \qquad (2.5)$$

where c_8 - -5800.2206

c_9 - 1.3914993

c_{10} - -0.048640239

c_{11} - 0.000041764768

c_{12} - -0.000000014452093

c_{13} - 6.5459673

The parameters $w_{d\max}$, E, and n are determined from isotherm data. A maximum moisture content of $0.50 kg_{H_2O}/kg_{dry\ \ desiccant}$ is chosen to represent silica gel (Jurinak 1982), and $0.35 kg_{H_2O}/kg_{dry\ \ desiccant}$ is chosen to represent molecular sieve (Simonson and Besant 1997).

Different isotherm shapes are obtained by varying the characteristic free energy of adsorption E in the Dubinin isotherm equation with a value of n of unity. An n of unity and a high value of E produce the Brunauer type I isotherm shape, and an n of unity and a low value of E produce the Brunauer type III isotherm shape. The

shapes of these curves and the effect of E are shown in Figures 2.2 and 2.3 with desiccant moisture content plotted versus relative humidity and adsorption potential energy respectively. The type I isotherm shape is like that of molecular sieves. The characteristic free energy of adsorption of type I materials, E_I, is $200 kJ/kg_{H_2O}$. The linear isotherm is like that of silica gel, its characteristic free energy, E_{linear}, is $100 kJ/kg_{H_2O}$ and its n is unity. The type III isotherm shape is like that of graphitized carbon. The characteristic free energy of adsorption of type III materials, E_{III}, is $50 kJ/kg_{H_2O}$ (Polanyi 1932; Dubinin 1975).

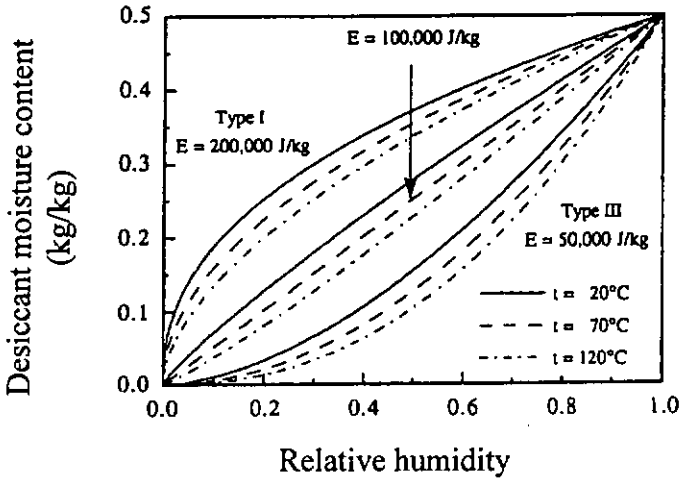

Figure 2.2 Effect of E on the isotherm shapes for a range of temperatures and n=1

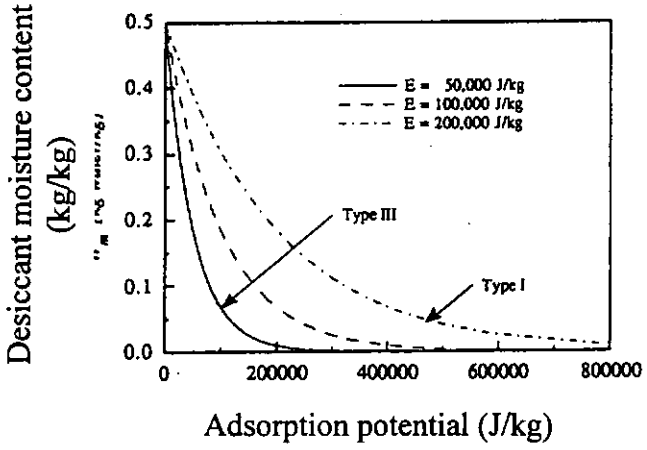

Figure 2.3 Effect of E on the isotherm shapes for *n*=1

From Figure 2.2 or Equations 2.1 and 2.2, it is known that the humidity ratio of air in equilibrium with the desiccant material, w_{da}, increases as (1) the water content of the desiccant material, w_d, increases and (2) the temperature of the desiccant, T_d, increases. Figure 2.3 shows that the temperature variation seen in Figure 2.2 is correlated using the adsorption potential energy.

Equations 2.1 and 2.2 are valid for microporous adsorbents. Substituting Equation 2.2 into 2.1 with a value of n of unity, the water content of desiccant solid phase w_d can be expressed as

$$w_d = w_{d\max} \cdot RH_{da}^{\frac{R \cdot T_d}{E}} \quad (kg_{H_2O}/kg_{dry\ \ desiccant}) \tag{2.6}$$

Equilibrium isotherms also were obtained by fitting fourth – degree polynomials to the manufacturer's data for regular density (RD) and intermediate density (ID) silica gel (Pesaran and Mills 1987a,b):

for RD silica gel

$$RH_{da} = 0.0078 - 0.05759 \cdot w_d + 24.16554 \cdot w_d^{\,2} - 124.478 \cdot w_d^3 + 204.226 \cdot w_d^4 \tag{2.7}$$

for ID silica gel

$$RH_{da} = 1.235 \cdot w_d + 267.99 \cdot w_d^{\,2} - 3170.7 \cdot w_d^{\,3} + 10087.16 \cdot w_d^4$$

$$w_d \le 0.07 \quad (kg_{H_2O}/kg_{dry\ \ desiccant}) \tag{2.8a}$$

$$RH_{da} = 0.3316 + 3.18 \cdot w_d \qquad w_d > 0.07 \quad (kg_{H_2O}/kg_{dry\ \ desiccant}) \tag{2.8b}$$

2.2 Heat of Sorption (Adsorption and Desorption)

The heat of sorption is the heat that is liberated or absorbed during the adsorption/desorption process. The nature of the adsorption process dictates that the heat of sorption is not constant over the entire range of desiccant loadings. The very first molecules that attach themselves to the surface of a desiccant are bonded by the strongest forces. These molecules will, therefore, have the highest adsorption potential energy or the differential molar work of adsorption. As the available sites for bonding fill, i.e., the desiccant loading increases, the less energetic sites become occupied. As the desiccant approaches saturation

conditions, the binding energies approach simple condensation. The heats of sorption will then be the highest at zero water loading and lowest (i.e., heat of condensation for water) at the maximum water loading. The rate at which this energy changes with water loading will vary depending upon the material (Mei et al 1992).

According to the Clausius-Clapeyron equation, the isosteric heat of adsorption, q_{st}, is defined by: (Park 1992)*

$$\left.\frac{\partial \ln p_{w,da}}{\partial T_d}\right|_{w_d} = \frac{q_{st}}{R \cdot T_d^2} \tag{2.9}$$

Therefore, the isosteric heat of adsorption depends on the loading per unit mass of dry desiccant, and temperature and water vapor pressure of moisture air in equilibrium with the desiccant material. From Equation 2.3 the water vapor pressure of moisture air in equilibrium with the desiccant solid phase $p_{w,da}$ can be expressed as:

$$\ln p_{w,da} = \ln RH_{da} + \ln p_{ws,da} \tag{2.10}$$

The water vapor pressure of saturated moisture air in equilibrium with the desiccant material $p_{ws,da}$ is a function of temperature of desiccant T_d only. Substituting Equation 2.2 into 2.10, $\ln p_{w,da}$ can be expressed as a function of adsorption potential energy and temperature as follows:

$$\ln p_{w,da} = -\frac{A}{R \cdot T_d} + \ln p_{ws,da} \tag{2.11}$$

Since $A = A(w_d)$ as shown in Equation 2.1, the lefthand side of Equation 2.9 can be obtained

$$\left.\frac{\partial \ln p_{w,da}}{\partial T_d}\right|_{w_d} = \frac{A}{R \cdot T_d^2} + \left.\frac{\partial \ln p_{ws,da}}{\partial T_d}\right|_{w_d} = \frac{A}{R \cdot T_d^2} + \frac{d \ln p_{ws,da}}{dT_d} \tag{2.12}$$

Substituting Equations 2.12 into Equation 2.9, the isosteric heat of adsorption can be expressed as a function of adsorption potential energy and temperature as follows:

$$q_{st} = A + R \cdot T_d^2 \cdot \frac{d \ln p_{ws,da}}{dT_d} \quad (kJ/kg_{H_2O}) \tag{2.13}$$

According to the Clausius-Clapeyron equation, the heat of vaporization of water at the temperature T_d, h_{fg}, is defined by (Walas 1985):

$$h_{fg} = R \cdot T_d^2 \frac{d \ln p_{ws,da}}{dT_d} \quad (kJ/kg_{H_2O}) \tag{2.14}$$

Therefore, the second term of Equation 2.13 is the heat of vaporization of water, and the isosteric heat of adsorption is the sum of the adsorption potential energy and the condensation heat of water.

$$q_{st} = A + h_{fg} \quad (kJ/kg_{H_2O}) \tag{2.15}$$

Substituting Equation 2.5 into Equation 2.14, the heat of vaporization of water h_{fg} can be obtained

$$h_{fg} = R \cdot (-c_8 + c_{13} \cdot T_d + c_{10} \cdot T_d^2 + 2 \cdot c_{11} \cdot T_d^3 + 3 \cdot c_{12} \cdot T_d^4) \quad (kJ/kg_{H_2O})$$

(2.16)

Substituting Equations 2.2 and 2.16 into Equation 2.15, the isosteric heat of adsorption can be expressed as

$$q_{st} = R \cdot (-T_d \cdot \ln RH_{da} - c_8 + c_{13} \cdot T_d + c_{10} \cdot T_d^2 + 2 \cdot c_{11} \cdot T_d^3 + 3 \cdot c_{12} \cdot T_d^4)$$

(kJ/kg_{H_2O}) (2.17)

Equation 2.17 is valid for microporous adsorbents. For RD silica gel, the heat of adsorption is (Pesaran and Mills 1987)

$$q_{st} = -12400 \cdot w_d + 3500 \quad (kJ/kg_{H_2O}) \qquad w_d \le 0.05 \quad (kg_{H_2O}/kg_{dry\ \ desiccant}) \quad (2.18a)$$

$$q_{st} = -1400 \cdot w_d + 2950 \quad (kJ/kg_{H_2O}) \qquad w_d > 0.05 \quad (kg_{H_2O}/kg_{dry\ \ desiccant}) \quad (2.18b)$$

and for ID silica gel is

$$q_{st} = -300 \cdot w_d + 2095 \quad (kJ/kg_{H_2O}) \qquad w_d \le 0.15 \quad (kg_{H_2O}/kg_{dry\ \ desiccant}) \quad (2.19a)$$

$$q_{st} = 2050 \quad (kJ/kg_{H_2O}) \qquad w_d > 0.15 \quad (kg_{H_2O}/kg_{dry\ \ desiccant}) \quad (2.19b)$$

2.3 Moisture Diffusion (Majumdar 1998, Pesaran 1987)

Water molecules can diffuse through a porous medium by either ordinary diffusion, Knudsen diffusion or surface diffusion or, sometimes, combinations of them, depending on the pore size and pressure. Water molecules move through pores by ordinary diffusion, Knudsen diffusion and surface diffusion, while adsorption takes

place on the pore walls. The adsorption – desorption process is assumed to be rapid with respect to diffusion, and thus the local vapor concentration w_{da} and the local water content of desiccant solid phase w_d are in equilibrium. The temperature of local vapor-air mixture is equal to the desiccant temperature t_d.

2.3.1 Ordinary Diffusion

If the pores are much larger than the mean free path of the vapor, then the molecules collide with each other more frequently than with the pore walls, and ordinary molecular diffusion, as described by Fick's law, is assumed to be the controlling factor. The ordinary diffusion coefficient is calculated based on the kinetic theory of gases and for a water vapor-air mixture the ordinary diffusion coefficient is given by

$$D_{H_2O,air} = 1.735 \times 10^{-9} \cdot \frac{T_d^{1.685}}{p^*} \quad (m^2/s) \tag{2.20}$$

where p^* - total pressure of air in the pore channels of desiccant felt (atm)

Assuming the diffusional path is equivalent to a cylindrical and isothermal tube of radius a, the water diffusion rate of one pore due to ordinary diffusion, $\dot{m}_o$, through the pore in the axial direction x is

$$\dot{m}_o = -\pi \cdot a^2 \cdot D_{H_2O,air} \cdot \frac{\partial(\rho_{da} \cdot w_{da})}{\partial x} \quad (kg_{H_2O}/s \cdot pore) \tag{2.21}$$

where w_{da} - moisture concentration of air in the pore channels of desiccant felt ($kg_{H_2O}/kg_{dry\ air}$);

ρ_{da} - density of dry air in the pore channels of desiccant felt ($kg_{dry\ air}/m^3$);

x - actual process channel position (m);

a - pore radius (m)

Regular density (RD) silica gel has a microporous structure with an average pore radius of 11Å while intermediate density (ID) silica gel is a macroporous material and has an average pore radius of 68Å. (Note that the H – O bond length in a water vapor molecule is 0.958Å with a bond angle of 104.45° and the distance between the two H atoms is 1.515Å.)

Equation 2.21 is, strictly speaking, valid only for long, uniform radius capillaries, and should be modified for application to real porous media. Accounting for the increase in diffusional length due to tortuous paths of real pores, the water diffusion rate of one pore due to ordinary diffusion, $\dot{m}_{o,\tau}$, through the pore in the axial direction x can be expressed as

$$\dot{m}_{o,\tau} = -\pi \cdot a^2 \cdot \frac{D_{H_2O,air}}{\tau_g} \cdot \frac{\partial(\rho_{da} \cdot w_{da})}{\partial x} \quad (kg_{H_2O}/s \cdot pore) \qquad (2.22)$$

where τ_g - tortuosity factor for intraparticle gas diffusion (dimensionless).

For regular density (RD) silica gel particles the value of tortuosity factor τ_g can be taken as 2.8, and for intermediate density (ID) silica gel particles its value can be taken as 2.0.

The water diffusion rate per m^2 of the area normal to the direction of flux due to ordinary diffusion, $\dot{M}_o$, is

$$\dot{M}_o = \frac{\varepsilon_p}{\pi \cdot a^2} \cdot \dot{m}_{o,r} \quad (kg_{H_2O}/s \cdot m^2) \tag{2.23}$$

where ε_p - desiccant felt porosity defined as the volume fraction of dry gel occupied by air (dimensionless)

Substituting Equation 2.22 into Equation 2.23, the water diffusion rate per m^2 of the area normal to the direction of flux due to ordinary diffusion, $\dot{M}_o$, can be expressed as

$$\dot{M}_o = -\frac{\varepsilon_p \cdot D_{H_2O,air}}{\tau_g} \cdot \frac{\partial(\rho_{da} \cdot w_{da})}{\partial x} \quad (kg_{H_2O}/s \cdot m^2) \tag{2.24}$$

where $\varepsilon_p \cdot D_{H_2O,air}/\tau_g$ is defined as the effective ordinary diffusion, $D_{H_2O,air,e}$

$$D_{H_2O,air,e} = \frac{\varepsilon_p}{\tau_g} \cdot D_{H_2O,air} \quad (m^2/s) \tag{2.25}$$

and $\dot{M}_o$, can be expressed as

$$\dot{M}_o = -D_{H_2O,air,e} \cdot \frac{\partial(\rho_{da} \cdot w_{da})}{\partial x} \quad (kg_{H_2O}/s \cdot m^2) \tag{2.26}$$

2.3.2 Knudsen Diffusion

Knudsen diffusion is encountered in the limit of large Knudsen number ($Kn = \lambda/a$, where λ is the mean free path and a is the pore radius), i.e. in smaller pores and low pressure. When water is diffusing through a medium of smaller-size pores, and/or the vapor density is very low, gas molecules collide more frequently with the walls than with each other and the resistance to diffusion along the pore is primarily due to molecular collisions with the walls. Assuming the diffusional path is equivalent to a long circular tube of radius a, and the two ends are maintained at different pressures, a Fick's law type expression can be obtained for this type of flow if a Knudsen diffusion coefficient is defined based on kinetic theory. For water vapor diffusion in straight cylindrical pores of radius a, a dimensional equation for Knudsen diffusion coefficient is

$$D_K = 97 \cdot a \cdot \left(\frac{T_d}{M_1}\right)^{1/2} \quad (m^2/s) \tag{2.27}$$

where M_1 - molecular mass of water, its value can be taken as 18 ($kg/kmol$)

The water diffusion rate of one pore due to Knudsen diffusion, $\dot{m}_K$, through the pore in the axial direction x is

$$\dot{m}_K = -\pi \cdot a^2 \cdot D_K \cdot \frac{\partial(\rho_{da} \cdot w_{da})}{\partial x} \quad (kg_{H_2O}/s \cdot pore) \tag{2.28}$$

Accounting for the increase in diffusional length due to tortuous paths of real pores, the water diffusion rate of one pore due to Knudsen diffusion, $\dot{m}_{K,\tau}$, through the pore in the axial direction x can be obtained by an equation similar to Equation 2.22.

$$\dot{m}_{K,\tau} = -\pi \cdot a^2 \cdot \frac{D_K}{\tau_g} \cdot \frac{\partial(\rho_{da} \cdot w_{da})}{\partial x} \quad (kg_{H_2O}/s \cdot pore) \tag{2.29}$$

The water diffusion rate per m^2 of the area normal to the direction of flux due to Knudsen diffusion, $\dot{M}_K$, through the pore in the axial direction x is

$$\dot{M}_K = \frac{\varepsilon_p}{\pi \cdot a^2} \cdot \dot{m}_{K,\tau} \quad (kg_{H_2O}/s \cdot m^2) \tag{2.30}$$

Substituting Equation 2.29 into Equation 2.30, the water diffusion rate per m^2 of the area normal to the direction of flux due to Knudsen diffusion, $\dot{M}_K$, can be expressed as

$$\dot{M}_K = -\frac{\varepsilon_p \cdot D_K}{\tau_g} \cdot \frac{\partial(\rho_{da} \cdot w_{da})}{\partial x} \quad (kg_{H_2O}/s \cdot m^2) \tag{2.31}$$

where $\varepsilon_p \cdot D_K/\tau_g$ is defined as the effective Knudsen diffusion, $D_{K,e}$

$$D_{K,e} = \frac{\varepsilon_p}{\tau_g} \cdot D_K \quad (m^2/s) \tag{2.32}$$

and $\dot{M}_K$, can be expressed as

$$\dot{M}_K = -D_{K,e} \cdot \frac{\partial(\rho_{da} \cdot w_{da})}{\partial x} \quad (kg_{H_2O}/s \cdot m^2) \tag{2.33}$$

2.3.3 Combined Ordinary Diffusion and Knudsen Diffusion

Table 2.1 Comparison of Knudsen and ordinary diffusion coefficients in water vapor-air mixtures for various values of pore radius (T^*=313.15K, p^*=1atm)

a(Å)	D_{K,H_2O} (m^2/s)	$D_{H_2O,air}$ (m^2/s)	$\frac{D_{K,H_2O}}{D_{H_2O,air}}$
11	4.45×10^{-7}	2.79×10^{-5}	0.0159
68	2.75×10^{-6}	2.79×10^{-5}	0.099
100	4.04×10^{-6}	2.79×10^{-5}	0.145
200	8.08×10^{-6}	2.79×10^{-5}	0.290
1000	4.04×10^{-5}	2.79×10^{-5}	1.450

Table 2.1 compares Knudsen and ordinary diffusion coefficient in water vapor-air mixtures for various values of pore radius. Note that combined ordinary diffusion and Knudsen diffusion may be approximately represented by assuming additive parallel resistance, that is

$$D_{o,K} = \left(\frac{1}{D_{H_2O,air}} + \frac{1}{D_K} \right)^{-1} \quad (m^2/s) \tag{2.34}$$

The combined ordinary and Knudsen diffusion rate of one pore, $\dot{m}_{o,K}$, through the pore in the axial direction x is

$$\dot{m}_{o,K} = -\pi \cdot a^2 \cdot D_{o,K} \cdot \frac{\partial(\rho_{da} \cdot w_{da})}{\partial x} \quad (kg_{H_2O}/s \cdot pore) \tag{2.35}$$

Accounting for the increase in diffusional length due to tortuous paths of real pores, the combined ordinary and Knudsen diffusion rate of one pore, $\dot{m}_{o,K,\tau}$, through the pore in the axial direction x can be expressed as

$$\dot{m}_{o,K,\tau} = -\pi \cdot a^2 \cdot \frac{D_{o,K}}{\tau_g} \cdot \frac{\partial(\rho_{da} \cdot w_{da})}{\partial x} \quad (kg_{H_2O}/s \cdot pore) \tag{2.36}$$

The water diffusion rate per m^2 of the area normal to the direction of flux due to combined ordinary and Knudsen diffusion, $\dot{M}_{o,K}$, through the pore in the axial direction x is

$$\dot{M}_{o,K} = \frac{\varepsilon_p}{\pi \cdot a^2} \cdot \dot{m}_{o,K,\tau} \quad (kg_{H_2O}/s \cdot m^2) \tag{2.37}$$

Substituting Equation 2.36 into Equation 2.37, the water diffusion rate per m^2 of the area normal to the direction of flux due to combined ordinary and Knudsen diffusion, $\dot{M}_{o,K}$, can be expressed as

$$\dot{M}_{o,K} = -\frac{\varepsilon_p \cdot D_{o,K}}{\tau_g} \cdot \frac{\partial(\rho_{da} \cdot w_{da})}{\partial x} \quad (kg_{H_2O}/s \cdot m^2) \tag{2.38}$$

where $\varepsilon_p \cdot D_{o,K}/\tau_g$ is defined as the effective diffusion coefficient combined ordinary and Knudsen diffusion, $D_{o,K,e}$

$$D_{o,K,e} = \frac{\varepsilon_p}{\tau_g} \cdot D_{o,K} \quad (m^2/s) \tag{2.39}$$

and $\dot{M}_{o,K}$, can be expressed as

$$\dot{M}_{o,K} = -D_{o,K,e} \cdot \frac{\partial(\rho_{da} \cdot w_{da})}{\partial x} \quad (kg_{H_2O}/s \cdot m^2) \tag{2.40}$$

In Table 1 Knudsen diffusion is dominant for pore sizes smaller than about 200 Å, because the resistance to Knudsen diffusion, $\frac{1}{D_K}$, is much higher than the resistance to ordinary diffusion, $\frac{1}{D_{H_2O,air}}$, for pore sizes smaller than about 200 Å. Since most of the pores of silica gel are less than 100 Å, it is clear that ordinary diffusion can be ignored in usual silica gel applications, but in the model developed in this thesis combined ordinary diffusion and Knudsen diffusion coefficient, $D_{o,K} = \left(\frac{1}{D_{H_2O,air}} + \frac{1}{D_K} \right)^{-1} \quad (m^2/s)$, is used to accurately represent any desiccant material. The model developed in this thesis can be applied to simulate any desiccant coated rotary dehumidifiers besides silica gel coated rotary dehumidifiers, if other desiccant properties are used in the model.

2.3.4 Surface Diffusion

Surface diffusion is the transport of adsorbed molecules on the pore surface. A number of models representing the possible mechanisms for movement of adsorbed molecules on surfaces are available. These are the hydrodynamic model, the mechanistic hopping model and Fick's law model. In the Fick's law model, the surface diffusion rate of one pore is assumed to be proportional to the surface concentration gradient and expressed as

$$\dot{m}_s = -2 \cdot \pi \cdot a \cdot D_s \cdot \frac{\partial C_s}{\partial x} \quad (kg_{H_2O}/s \cdot pore) \tag{2.41}$$

where D_s - surface diffusion coefficient (m^2/s)

C_s – surface concentration ($kg_{H_2O}/m^2_{surface\ \ area}$), defined by

$$C_s = \frac{w_d}{S_g} \tag{2.42}$$

S_g – specific surface area of pore, for RD silica gel its value can be taken as $7.8\times10^5 m^2_{surface\ \ area}/kg_{dry\ \ desiccant}$, and for ID silica gel its value can be taken as $3.4\times10^5 m^2_{surface\ \ area}/kg_{dry\ \ desiccant}$ (Pesaran and Mills 1987a)

Substituting Equation 2.42 into Equation 2.41, the surface diffusion rate of one pore can be expressed as

$$\dot{m}_s = -2 \cdot \pi \cdot a \cdot \frac{D_s}{S_g} \cdot \frac{\partial w_d}{\partial x} \quad (kg_{H_2O}/s \cdot pore) \tag{2.43}$$

The surface diffusion coefficient D_s was estimated experimentally by various investigators (Gilliland et al., 1974; Sladek et al., 1974; Kruckles, 1973; Pesaran et al. 1987, Lu et al., 1991). Kruckles (1973) studied the surface diffusion of water through isothermal (RD) silica gel particles. He considered the submonolayer concentration range (concentrations up to about half of the saturation loading of silica gel particles), and proposed that the mechanism of surface diffusion was that of the activated hopping of molecules in a random walk process. He proposed a formula with several parameters based on a combined mathematical model and experimental data. Since the theoretical estimation of these parameters was difficult, they were calculated by a nonlinear least squares fit between the mathematical model and experimental data at 40°C. The resulting formula for the surface diffusion coefficient can be extrapolated to other temperatures using the assumption of Arrhenius type behavior:

$$D_s = 1.287\times10^{-8}\cdot\exp\left(-811.30\cdot\frac{w_d}{T_d}\right)\cdot\left[1+3112\cdot w_d\cdot\frac{\tanh\left(0.265\times10^{-2}\cdot\frac{\partial w_d}{\partial r}\right)}{\frac{\partial w_d}{\partial r}}\right]\quad\left(m^2/s\right)\qquad(2.44)$$

where r – radial coordinate in a particle (m)

This formula shows a decrease of D_s with increasing w_d. However, it requires considerable computational effort and is only valid for RD gels at low concentrations.

Lu et al. (1991) obtained apparent solid-side diffusivity by matching the analytical solution to the experimental data and showed the dependence of surface diffusivity on the particle size and moisture content.

A simpler formula which can be used for both RD and ID silica gel at both high and low concentrations was therefore sought. Sladek et al. (1974) proposed a simpler correlation for silica gel, which is valid for both low and high surface coverages. They assumed a mechanistic hopping model with the assumption that the jumping frequency is a function of surface concentration (through the heat of adsorption) and obtained the following expression for the surface diffusion coefficient

$$D_s = D_o \cdot \exp\left(-\frac{a_0 \cdot q_{st}}{R \cdot T_d}\right) \quad (m^2/s) \tag{2.45}$$

They later correlated some available data on surface diffusion of various adsorbates into different adsorbents (not H_2O – silica gel system) with this equation and found that D_o should be set at $1.6\times10^{-6}\ m^2/s$ and $a_0=0.45/b$ where b is obtained from the type of adsorption bond. For silica gel, b is unity so the surface diffusivity becomes

$$D_s = D_o \cdot \exp\left(-0.974\times10^{-3} \cdot \frac{q_{st}}{T_d}\right) \quad (m^2/s) \tag{2.46}$$

where an approximation to D_o is

$$D_0 = 1.6\times10^{-6} \quad (m^2/s) \tag{2.47}$$

However, D_o can be obtained by matching the experimental and theoretical results of the transient response of packed bed of silica gel (Pesaran and Mills 1987 b).

A comparison of Knudsen and surface diffusion rates in pores shows that surface diffusion dominates in a pore with RD gel characteristics, whereas both are important for a pore with ID gel characteristics (Pesaran and Mills 1987 a).

Equation 2.43 given above is valid for smooth surfaces, and should be modified to account for the rough walls of the porous media. Accounting for the increase in diffusional length due to tortuous paths of real pores, the surface diffusion rate of one pore can be expressed as

$$\dot{m}_{s,r} = -\frac{2 \cdot \pi \cdot a}{S_g} \cdot \frac{D_s}{\tau_s} \cdot \frac{\partial w_d}{\partial x} \quad (kg_{H_2O}/s \cdot pore) \tag{2.48}$$

where τ_s - tortuosity factor for intraparticle surface diffusion (dimentionless), for RD silica gel its value can be taken as 2.8, and for ID silica gel its value can be taken as 2.0 (Pesaran and Mills 1987a)

and D_s/τ_g is defined as the effective surface diffusion coefficient, $D_{s,e}$

$$D_{s,e} = \frac{D_s}{\tau_s} \tag{2.49}$$

thus $\dot{m}_{s,r}$, can be expressed as

$$\dot{m}_{s,\tau} = -\frac{2 \cdot \pi \cdot a}{S_g} \cdot D_{s,e} \cdot \frac{\partial w_d}{\partial x} \quad (kg_{H_2O}/s \cdot pore) \tag{2.50}$$

The water diffusion rate per m^2 of the area normal to the direction of flux due to surface diffusion, $\dot{M}_s$, through the pore in the axial direction x is

$$\dot{M}_s = \frac{\varepsilon_p}{\pi \cdot a^2} \cdot \dot{m}_{s,\tau} \quad (kg_{H_2O}/s \cdot m^2) \tag{2.51}$$

Substituting Equation 2.50 into Equation 2.51, the water diffusion rate per m^2 of the area normal to the direction of flux due to surface diffusion, $\dot{M}_s$, can be expressed as

$$\dot{M}_s = -\frac{2 \cdot \varepsilon_p}{a \cdot S_g} \cdot D_{s,e} \cdot \frac{\partial w_d}{\partial x} \quad (kg_{H_2O}/s \cdot m^2) \tag{2.52}$$

where $\frac{2 \cdot \varepsilon_p}{a \cdot S_g}$ is the density of desiccant felt ρ_d, for molecular sieve its value can be taken as $350\, kg_{desiccant}/m^3_{desiccant}$ (Simonson and Besant 1997), for RD silica gel its value can be taken as $1129\, kg_{desiccant}/m^3_{desiccant}$, and for ID silica gel its value can be taken as $620\, kg_{desiccant}/m^3_{desiccant}$ (Pesaran and Mills 1987a).

Substituting $\rho_d = \frac{2 \cdot \varepsilon_p}{a \cdot S_g}$ into Equation 2.52, $\dot{M}_s$ can be expressed as

$$\dot{M}_s = -\rho_d \cdot D_{s,e} \cdot \frac{\partial w_d}{\partial x} \quad (kg_{H_2O}/s \cdot m^2) \tag{2.53}$$

2.3.5 Total Moisture Diffusion Rate

If surface diffusion of the adsorbed layer is important, along with molecular and Knudsen diffusion, while adsorption takes place on the pore walls. Since ordinary, Knudsen and surface diffusion are parallel processes, they are additive if the interactions between them are ignored. Adding the contributions to the mass diffusion, then the total mass diffusion rate per m^2 of the area normal to the direction of flux can be obtained

$$\dot{M} = \dot{M}_{o,K} + \dot{M}_s \quad (kg_{H_2O}/s \cdot m^2) \tag{2.54}$$

Substituting Equations 2.40 and 2.53 into Equation 2.54, the total mass diffusion rate per m^2 of the area normal to the direction of flux can be expressed

$$\dot{M} = -D_{o,K,e} \cdot \frac{\partial(\rho_{da} \cdot w_{da})}{\partial x} - \rho_d \cdot D_{s,e} \cdot \frac{\partial w_d}{\partial x} \quad (kg_{H_2O}/m^2 \cdot s) \tag{2.55}$$

Equation 2.55 can be applied to any combination of ordinary, Knudsen and surface diffusion. Since ordinary diffusion can be ignored in usual silica gel applications, the mass diffusion rate per m^2 of the area normal to the direction of flux can be expressed as

$$\dot{M} = -D_{K,e} \cdot \frac{\partial(\rho_{da} \cdot w_{da})}{\partial x} - \rho_d \cdot D_{s,e} \cdot \frac{\partial w_d}{\partial x} \quad (kg_{H_2O}/m^2 \cdot s) \tag{2.56}$$

As surface diffusion dominates in a pore with RD silica gel characteristics, the mass diffusion rate per m^2 of the area normal to the direction of flux can be expressed as

$$\dot{M} = -\rho_d \cdot D_{s,e} \cdot \frac{\partial w_d}{\partial x} \quad (kg_{H_2O}/m^2 \cdot s) \tag{2.57}$$

2.4 Thermal Conductivity (Gurgel and Klüppel 1996)

The thermal conductivity of silica gel was investigated by Gurgel and Klüppel (1996) and found to vary linearly with the water content of the silica gel. The thermal conductivity of silica gel was measured by steady - state procedures, using silica gel with different loads, w_d, in the range $0.0-0.3 kg_{H_2O}/kg_{dry\ \ desiccant}$, under water vapor in chemical equilibrium with the sorbent, and under humid air at 100 kPa total pressure.

The total water content of desiccant felt is given by

$$w_{d,total} = w_d + \varepsilon_p \cdot \frac{\rho_{da}}{\rho_d} \cdot w_{da} \quad (kg_{H_2O}/kg_{dry\ \ desiccant}) \tag{2.58}$$

The solid conductivity of the silica gel grain λ_d is a function of the water concentration in the silica gel w_d.

$$\lambda_d = (0.966 \cdot w_d + 0.683) \times 10^{-3} \quad (kW/m \cdot K) \tag{2.59}$$

2.5 Enthalpy of Desiccant

The enthalpy of air in process channel is

$$h_a = c_{pa} \cdot t_a + w_a \cdot h_{va} \quad (kJ/kg_{dry\ air}) \tag{2.60}$$

where c_{pa} - specific heat of dry air in process channel at constant pressure $(kJ/kg_{dry\ air} \cdot K)$;

t_a - temperature of air stream in process channel (°C);

w_a - humidity ratio of air stream in process channel (kg_{H_2O}/kg_{dryair});

h_{va} - enthalpy of water vapor in process channel $(kJ/kg_{H_2O\ vapor})$

$$h_{va} = h_{fg,0} + c_{pva} \cdot t_a \quad (kJ/kg_{H_2O\ vapor}) \tag{2.61}$$

$h_{fg,0}$ - heat of vaporization of water at $0°C$; its value can be taken as $2501.6 kJ/kg_{H_2O}$;

c_{pva} - specific heat of water vapor in process channel at constant pressure $(kJ/kg_{H_2O\ vapor} \cdot K)$

The enthalpy of air in the pore channels of desiccant felt is

$$h_{da} = c_{pda} \cdot t_d + w_{da} \cdot h_{vda} \quad (kJ/kg_{dry\ air}) \tag{2.62}$$

where c_{pda} - specific heat of dry air in the pore channels of desiccant felt at constant pressure $(kJ/kg_{dry\ air} \cdot K)$;

h_{vda} - enthalpy of water vapor in the pore channels of desiccant felt ($kJ/kg_{H_2O\ vapor}$)

$$h_{vda} = h_{fg,0} + c_{pvda} \cdot t_d \quad (kJ/kg_{H_2O\ vapor}) \tag{2.63a}$$

or $$h_{vda} = h_{fg} + c_{pw} \cdot t_d \quad (kJ/kg_{H_2O\ vapor}) \tag{2.63b}$$

c_{pvda} - specific heat of water vapor in the pore channels of desiccant felt at constant pressure ($kJ/kg_{H_2O\ vapor} \cdot K$);

h_{fg} - heat of vaporization of water (kJ/kg_{H_2O});

c_{pw} - specific heat of water liquid in the pore channels of desiccant felt at constant pressure, its value can be taken as $4.19 kJ/kg_{H_2O\ liquid} \cdot K$

Substituting Equation 2.61 into Equation 2.60, the enthalpy of air in process channel can be expressed as

$$h_a = c_{pa} \cdot t_a + w_a \cdot (h_{fg,0} + c_{pva} \cdot t_a) \quad (kJ/kg_{dry\ air}) \tag{2.64}$$

Substituting Equation 2.63a into Equation 2.62, the enthalpy of air in the pore channels of desiccant felt can be expressed as

$$h_{da} = c_{pa} \cdot t_d + w_{da} \cdot (h_{fg,0} + c_{pvda} \cdot t_d) \quad (kJ/kg_{dry\ air}) \tag{2.65}$$

The enthalpy of the desiccant solid phase h_d is a function of desiccant temperature t_d and moisture content of the desiccant solid w_d

$$h_d = c_d \cdot t_d + w_d \cdot t_d \quad (kJ/kg_{dry\ desiccant}) \tag{2.66}$$

where c_d - specific heat of desiccant, for silica gel its value can be taken as $1.0\,kJ/kg_{dry\ \ desiccant}\cdot K$ (Jurinak 1982) or $0.98\,kJ/kg_{dry\ \ desiccant}\cdot K$ (Gurgel and Klüppel 1996), and for molecular sieve its value can be taken as $0.615\,kJ/kg_{dry\ \ desiccant}\cdot K$ (Simonson and Besant 1997)

h_s - enthalpy of water molecules in the adsorbed phase (kJ/kg_{H_2O})

The enthalpy of water molecules in the adsorbed phase h_s equals the enthalpy of water molecules in vapor phase minus the heat of adsorption.

$$h_s = h_{vda} - q_{st} \quad (kJ/kg_{H_2O}) \tag{2.67}$$

Equation 2.67 can be applied to any adsorbent. Substituting Equation 2.63a into Equation 2.67, the enthalpy of water molecules in adsorbed phase h_s for any adsorbent can be expressed as

$$h_s = h_{fg,0} + c_{pvda}\cdot t_d - q_{st} \quad (kJ/kg_{H_2O}) \tag{2.68a}$$

For microporous adsorbents, substituting Equations 2.15 and 2.63b into Equation 2.67 the enthalpy of water molecules in the adsorbed phase h_s can be expressed

$$h_s = c_{pw}\cdot t_d - A \quad (kJ/kg_{H_2O}) \tag{2.68b}$$

Substituting Equations 2.68a and 2.68b into Equation 2.66 respectively, the enthalpy of the desiccant solid phase h_d can be expressed as

$$h_d = c_d\cdot t_d + w_d\cdot(h_{fg,0} + c_{pvda}\cdot t_d - q_{st}) \quad (kJ/kg_{dry\ \ desiccant}) \tag{2.69a}$$

for any adsorbent

and $h_d = c_d \cdot t_d + w_d \cdot (c_{pw} \cdot t_d - A) \quad (kJ/kg_{dry\ \ desiccant})$ (2.69b)

for microporous adsorbents.

The enthalpy of the desiccant felt h_f is

$$h_f = \varepsilon_p \cdot \frac{\rho_{da}}{\rho_d} \cdot h_{da} + h_d \quad (kJ/kg_{dry\ \ desiccant}) \tag{2.70}$$

Substituting Equations 2.65 and 2.69a into Equation 2.70, the enthalpy of the desiccant felt h_f can be expressed as

$$h_f = \varepsilon_p \cdot \frac{\rho_{da}}{\rho_d} \cdot \left[c_{pda} \cdot t_d + w_{da} \cdot (h_{fg,0} + c_{pvda} \cdot t_d)\right]$$

$$+c_d \cdot t_d + w_d \cdot (h_{fg,0} + c_{pvda} \cdot t_d - q_{st}) \quad (kJ/kg_{dry\ \ desiccant}) \tag{2.71}$$

Substituting $\rho_d = \frac{2 \cdot \varepsilon_p}{a \cdot S_g}$ into Equation 2.71, the enthalpy of the desiccant felt h_f can be expressed as

$$h_f = \frac{a \cdot s_g \cdot \rho_{da}}{2} \cdot \left[c_{pda} \cdot t_d + w_{da} \cdot (h_{fg,0} + c_{pvda} \cdot t_d)\right]$$

$$+c_d \cdot t_d + w_d \cdot (h_{fg,0} + c_{pvda} \cdot t_d - q_{st}) \quad (kJ/kg_{dry\ \ desiccant}) \tag{2.72}$$

2.6 Heat and Mass Transfer Coefficient

Modeling the heat and moisture transfer coefficient is one of the most important parts of the model.

The following relation holds for $\mathrm{Re} \leq 50$ (Incropera and Dewitt 1996)*:

$$Nu = 0.13 \cdot (\mathrm{Re} \cdot \mathrm{Pr} \cdot \frac{d_e}{l_c})^{\frac{1}{3}} \cdot (\frac{\mu_f}{\mu_w})^{0.14} \tag{2.73}$$

where Nu - Nusselt number, $Nu = \frac{\alpha_h \cdot d_e}{\lambda_a}$;

α_h - heat transfer coefficient ($kW/m^2 \cdot K$);

λ_a - thermal conductivity of air ($kW/m \cdot K$);

Re - Reynolds number, $\mathrm{Re} = \frac{v_c \cdot d_e}{\nu_a}$;

v_c - air velocity at process channel flow area (m/s)

ν_a - kinematic viscosity of air (m^2/s);

Pr - Prandtl number, $\mathrm{Pr} = \frac{\nu_a}{a_a}$;

a_a - thermal diffusivity of air (m^2/s);

μ_f - Dynamic viscosity of air at average temperature t_a ($N \cdot s/m^2$);

μ_w - Dynamic viscosity of air at wall temperature t_d ($N \cdot s/m^2$)

l_c - process channel length (m)

d_e - equivalent diameter (m)

When the cross-sectional area of a channel is not circular, the appropriate dimension to use in place of the channel diameter is the hydraulic diameter defined by the relation

$$d_e = 4(\frac{cross-sectional\ \ area}{wetted\ \ perimeter}) = \frac{4 \cdot r_a}{r_{sv}} \quad (m) \tag{2.74}$$

The mass transfer coefficient α_m can be obtained from the relation (Zhang, 1993)

$$\alpha_m = \frac{\alpha_h}{c_{pwa} \cdot \rho_{wa}} \cdot Le^{-\frac{2}{3}} \quad (m/s) \tag{2.75}$$

where c_{pwa} - specific heat of moist air in process channel at constant pressure $(kJ/kg_{dry\ \ air} \cdot K)$

$$c_{pwa} = c_{pa} + w_a \cdot c_{pva} \tag{2.76}$$

ρ_{wa} - density of moist air in process channel $(kg_{moist\ \ air}/m^3)$

$$\rho_{wa} = \rho_a \cdot (1 + w_a) \tag{2.77}$$

Le - Lewis number

$$Le = \frac{a_{wa}}{D_{H_2O,air,c}} \tag{2.78}$$

a_{wa} - thermal diffusivity of moist air (m^2/s)

$$a_{wa} = a_a + w_a \cdot a_v \tag{2.79}$$

a_v - thermal diffusivity of vapor (m^2/s)

$D_{H_2O,air,c}$ - ordinary diffusion coefficient for a water vapor-air mixture in process channel (m^2/s)

$$D_{H_2O,air,c} = 1.735 \times 10^{-9} \cdot \frac{T_a^{1.685}}{P_{total,a}} \quad (m^2/s) \tag{2.80}$$

$P_{total,a}$ - total pressure of moisture air in process channel (atm)

Chapter 3 Governing Equations for Modeling Desiccant Wheel

Based on the assumptions in Chapter 1, a one-dimensional transient heat and mass transfer model of desiccant coated rotary dehumidifier, including energy and mass storage in both air and matrix, convection, the axial thermal conduction through both desiccant and the support material, the axial molecular diffusion within the desiccant coating and the energy transfer between the air stream and the matrix, is developed. The governing equations for coupled heat and moisture transfer in desiccant wheel are now presented for one tube.

3.1 Conservation of Moisture

3.1.1 Control Volume

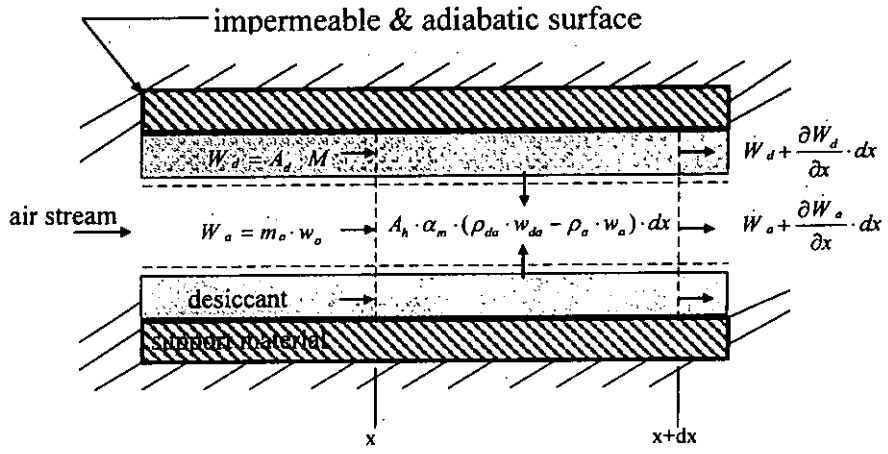

Figure 3.1 Schematic showing a moisture balance on an elemental volume dx long

Consider a differential element dx fixed in one of the tubes of which the desiccant wheel consists, as shown in Figure 3.1. Two control volumes $A_f \cdot dx$ (m^3) and $A_d \cdot dx$ (m^3) are used for the moisture conservation equations. A_f (m^2) is the free flow area of each tube, and A_d (m^2) is the cross-sectional area of desiccant in each tube.

3.1.2 Conservation of Moisture on Air Stream

Moisture Storage

The rate at which moisture is stored in the control volume $A_f \cdot dx$ (m^3) is

$$A_f \cdot \frac{\partial(\rho_a \cdot w_a)}{\partial \tau} \cdot dx \quad (kg_{H_2O}/s) \tag{3.1}$$

where τ - actual time (s);

x - actual process channel position (m)

Moisture Inflow

Moisture can cross the control volume boundaries by the axial convection. The rate of moisture inflow across the x face by convection is

$$\dot{W}_a = \dot{m}_a \cdot w_a \quad (kg_{H_2O}/s) \tag{3.2}$$

where $\dot{m}_a$ - mass flow rate of dry air in each tube ($kg_{dry\ air}/s$)

$$\dot{m}_a = A_f \cdot f_a \quad (kg_{dry\ air}/s) \tag{3.3}$$

f_a - flux density of dry air at process channel flow area ($kg_{dry\ air}/s \cdot m^2$)

Substituting Equation 3.3 into 3.2 the rate of moisture inflow across the x face by convection can be expressed as

$$\dot{W}_a = A_f \cdot f_a \cdot w_a \quad (kg_{H_2O}/s) \tag{3.4}$$

The rate of moisture outflow across the $x+dx$ face by convection is

$$\dot{W}_a + \frac{\partial \dot{W}_a}{\partial x} \cdot dx \quad (kg_{H_2O}/s) \tag{3.5}$$

The net rate of inflow is found by subtracting the outflow from the inflow

$$-\frac{\partial \dot{W}_a}{\partial x} \cdot dx \quad (kg_{H_2O}/s) \tag{3.6}$$

Substituting Equation 3.4 into Equation 3.6 the net rate of inflow can be obtained as

$$-A_f \cdot f_a \cdot \frac{\partial w_a}{\partial x} \cdot dx \quad (kg_{H_2O}/s) \tag{3.7}$$

Moisture Transfer

The rate of moisture transfer between the air stream and the desiccant is

$$A_h \cdot \alpha_m \cdot (\rho_{da} \cdot w_{da} - \rho_a \cdot w_a) \cdot dx \quad (kg_{H_2O}/s) \tag{3.8}$$

where A_h - heat transfer surface area per unit length in each tube (m^2/m);

Moisture Conservation Equation

The rate at which moisture is stored in the control volume $A_f \cdot dx$ (m^3) equals the net rate of inflow of moisture across the control volume boundary by the axial convection, plus the rate of moisture transfer between the air stream and the desiccant. Substituting all the preceding terms in the statement of conservation of moisture and dividing by the *dx* gives the equation of moisture conservation on air stream,

$$A_f \cdot \frac{\partial(\rho_a \cdot w_a)}{\partial \tau} = -A_f \cdot f_a \cdot \frac{\partial w_a}{\partial x} + A_h \cdot \alpha_m \cdot (\rho_{da} \cdot w_{da} - \rho_a \cdot w_a) \qquad (3.9)$$

Divide throughout by the cross-sectional area of each tube A_s (m^2),

$$\frac{A_f}{A_s} \cdot \frac{\partial(\rho_a \cdot w_a)}{\partial \tau} = -\frac{A_f}{A_s} \cdot f_a \cdot \frac{\partial w_a}{\partial x} + \frac{A_h}{A_s} \cdot \alpha_m \cdot (\rho_{da} \cdot w_{da} - \rho_a \cdot w_a) \qquad (3.10)$$

where A_f/A_s which is the ratio of the free flow area to the face area of a desiccant wheel, can be expressed as r_a (m^2/m^2); and $(A_h \cdot l_c)/(A_s \cdot l_c)$ which is the ratio of the heat transfer surface area to the wheel volume, can be expressed as r_{sv} ($m^2_{desiccant}/m^3_{wheel}$); thus,

$$r_a \cdot \frac{\partial(\rho_a \cdot w_a)}{\partial \tau} = -r_a \cdot f_a \cdot \frac{\partial w_a}{\partial x} + r_{sv} \cdot \alpha_m \cdot (\rho_{da} \cdot w_{da} - \rho_a \cdot w_a) \qquad (3.11)$$

3.1.3 Conservation of Moisture on Desiccant

Moisture Storage

The moisture stored in the control volume $A_d \cdot dx$ (m^3) includes the moisture stored on the surface and in the pore of the desiccant felt material. The rate at which moisture is stored is:

$$A_d \cdot \varepsilon_p \cdot \frac{\partial(\rho_{da} \cdot w_{da})}{\partial \tau} \cdot dx + A_d \cdot \rho_d \cdot \frac{\partial w_d}{\partial \tau} \cdot dx \quad (kg_{H_2O}/s) \tag{3.12}$$

Moisture Inflow

Moisture can be transferred into the control volume by diffusion. The rate of moisture inflow across the x face by diffusion is

$$\dot{W}_d = A_d \cdot \dot{M} \quad (kg_{H_2O}/s) \tag{3.13}$$

Substituting Equation 2.55 into Equation 3.13, the rate of moisture inflow across the x face by diffusion can be expressed as

$$\dot{W}_d = -A_d \cdot D_{o,K,e} \cdot \frac{\partial(\rho_{da} \cdot w_{da})}{\partial x} - A_d \cdot \rho_d \cdot D_{s,e} \cdot \frac{\partial w_d}{\partial x} \quad (kg_{H_2O}/s) \tag{3.14}$$

and the rate of outflow across the $x+dx$ face is

$$\dot{W}_d + \frac{\partial \dot{W}_d}{\partial x} \cdot dx \quad (kg_{H_2O}/s) \tag{3.15}$$

The net rate of inflow for the two faces is

$$-\frac{\partial \dot{W}_d}{\partial x}\cdot dx \quad (kg_{H_2O}/s) \tag{3.16}$$

Substituting Equation 3.14 into Equation 3.16 the net rate of inflow for the two faces can be obtained as

$$A_d\cdot\frac{\partial\left[D_{o,K,e}\cdot\dfrac{\partial(\rho_{da}\cdot w_{da})}{\partial x}\right]}{\partial x}\cdot dx + A_d\cdot\rho_d\cdot\frac{\partial(D_{s,e}\cdot\dfrac{\partial w_d}{\partial x})}{\partial x}\cdot dx \quad (kg_{H_2O}/s) \tag{3.17}$$

Moisture Conservation Equation

The rate at which moisture is stored in the control volume $A_d\cdot dx$ (m^3) equals the net rate of inflow for the two faces by diffusion, minus the rate of moisture transfer between the air stream and the desiccant. Substituting all the preceding terms in the statement of conservation of moisture and dividing by the dx gives the equation of moisture conservation on desiccant,

$$\begin{aligned} &A_d\cdot\varepsilon_p\cdot\frac{\partial(\rho_{da}\cdot w_{da})}{\partial\tau}+A_d\cdot\rho_d\cdot\frac{\partial w_d}{\partial\tau}\\ &=A_d\cdot\frac{\partial\left[D_{o,K,e}\cdot\dfrac{\partial(\rho_{da}\cdot w_{da})}{\partial x}\right]}{\partial x}+A_d\cdot\rho_d\cdot\frac{\partial(D_{s,e}\cdot\dfrac{\partial w_d}{\partial x})}{\partial x}\\ &-A_h\cdot\alpha_m\cdot(\rho_{da}\cdot w_{da}-\rho_a\cdot w_a) \end{aligned} \tag{3.18}$$

Divide throughout by the cross-sectional area of each tube A_s (m^2)

$$\frac{A_d}{A_s}\cdot\varepsilon_p\cdot\frac{\partial(\rho_{da}\cdot w_{da})}{\partial\tau}+\frac{A_d}{A_s}\cdot\rho_d\cdot\frac{\partial w_d}{\partial\tau}$$

$$=\frac{A_d}{A_s}\cdot\frac{\partial\left[D_{o,K,e}\cdot\dfrac{\partial(\rho_{da}\cdot w_{da})}{\partial x}\right]}{\partial x}+\frac{A_d}{A_s}\cdot\rho_d\cdot\frac{\partial(D_{s,e}\cdot\dfrac{\partial w_d}{\partial x})}{\partial x}$$

$$-\frac{A_h}{A_s}\cdot\alpha_m\cdot(\rho_{da}\cdot w_{da}-\rho_a\cdot w_a) \tag{3.19}$$

where $(A_d\cdot l_c)/(A_s\cdot l_c)$ which is the fraction of the desiccant in the wheel, can be expressed as f_v $(m^3_{desiccant}/m^3_{wheel})$; thus,

$$f_v\cdot\varepsilon_p\cdot\frac{\partial(\rho_{da}\cdot w_{da})}{\partial\tau}+f_v\cdot\rho_d\cdot\frac{\partial w_d}{\partial\tau}$$

$$=f_v\cdot\frac{\partial\left[D_{o,K,e}\cdot\dfrac{\partial(\rho_{da}\cdot w_{da})}{\partial x}\right]}{\partial x}+f_v\cdot\rho_d\cdot\frac{\partial(D_{s,e}\cdot\dfrac{\partial w_d}{\partial x})}{\partial x}$$

$$-r_{sv}\cdot\alpha_m\cdot(\rho_{da}\cdot w_{da}-\rho_a\cdot w_a) \tag{3.20}$$

3.2 Conservation of Energy

3.2.1 Control Volume

Two control volumes $A_f\cdot dx$ (m^3) and $(A_d+A_m)\cdot dx$ (m^3) are used for the energy conservation equations, as shown in Figure 3.2. A_m (m^2) is the cross-sectional area of support material in each tube.

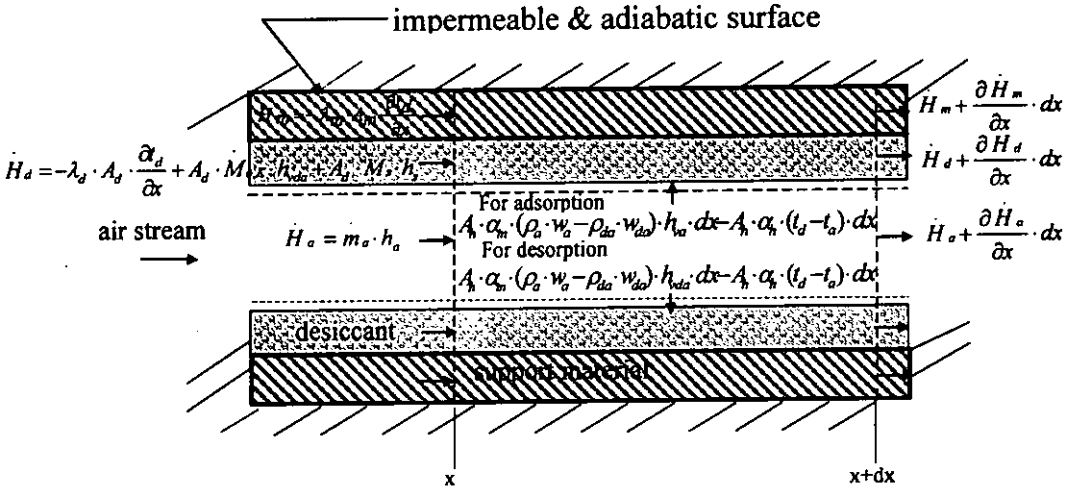

Figure 3.2 Schematic showing an energy balance on an elemental volume dx long

3.2.2 Conservation of Energy on Air Stream

Energy Storage

The rate at which energy is stored in the control volume $A_f \cdot dx$ (m^3) is

$$A_f \cdot \frac{\partial(\rho_a \cdot h_a)}{\partial \tau} \cdot dx \quad (kW) \tag{3.21}$$

Energy Inflow

Energy can flow into the control volume by convection. The convection across the x face per unit time is

$$\dot{H}_a = \dot{m}_a \cdot h_a \quad (kW) \tag{3.22}$$

Substituting Equation 3.3 into 3.22, the rate of energy inflow across the x face by convection per unit time can be expressed as

$$\dot{H}_a = A_f \cdot f_a \cdot h_a \quad (kW) \tag{3.23}$$

and the convection out across the $x+dx$ face is

$$\dot{H}_a + \frac{\partial \dot{H}_a}{\partial x} \cdot dx \quad (kW) \tag{3.24}$$

The net rate of inflow for the two faces is

$$-\frac{\partial \dot{H}_a}{\partial x} \cdot dx \quad (kW) \tag{3.25}$$

Substituting Equation 3.23 into 3.25 the net rate of inflow for the two faces can be expressed as

$$-A_f \cdot f_a \cdot \frac{\partial h_a}{\partial x} \cdot dx \quad (kW) \tag{3.26}$$

Energy Transfer

Zheng and Worek (1993) assumed that the heat of sorption is delivered to the matrix, while Collier et al. (1986) assumed that the heat of sorption is delivered to the air. Simonson and Besant (1997) considered the distribution of the heat of sorption between the desiccant and the air. The correctness and significance of these assumptions needs to be investigated.

In fact, during adsorption the water vapor in process channel enters the air layer in equilibrium with the desiccant solid phase and the process air loses the enthalpy of water vapor h_{va}. For the process air, the rate of energy transfer due to heat and moisture transfer between the matrix and the air stream is described by

$$A_h \cdot \alpha_m \cdot (\rho_a \cdot w_a - \rho_{da} \cdot w_{da}) \cdot h_{va} \cdot dx - A_h \cdot \alpha_h \cdot (t_d - t_a) \cdot dx \quad (kW) \quad (3.27a)$$

During desorption the water vapor leaves the air layer in equilibrium with the desiccant solid phase and the regeneration air gains the enthalpy of water vapor h_{vda}. For the regeneration air, the rate of energy transfer due to heat and moisture transfer between the matrix and the air stream is described by

$$A_h \cdot \alpha_m \cdot (\rho_a \cdot w_a - \rho_{da} \cdot w_{da}) \cdot h_{vda} \cdot dx - A_h \cdot \alpha_h \cdot (t_d - t_a) \cdot dx \quad (kW) \quad (3.27b)$$

Energy Conservation Equation

The rate at which energy is stored in the control volume $A_f \cdot dx$ (m^3) equals the net rate of inflow of energy across the control volume boundary by the axial convection, minus the rate of energy transfer between the air stream and the desiccant. Substituting all the preceding terms in the statement of conservation of energy and dividing by the dx gives the equation of energy conservation on air stream, the energy conservation equations are:

$$A_f \cdot \frac{\partial(\rho_a \cdot h_a)}{\partial \tau} = -A_f \cdot f_a \cdot \frac{\partial h_a}{\partial x} - A_h \cdot \alpha_m \cdot (\rho_a \cdot w_a - \rho_{da} \cdot w_{da}) \cdot h_{va}$$

$$+ A_h \cdot \alpha_h \cdot (t_d - t_a) \qquad (3.28a)$$

and

$$A_f \cdot \frac{\partial(\rho_a \cdot h_a)}{\partial \tau} = -A_f \cdot f_a \cdot \frac{\partial h_a}{\partial x} - A_h \cdot \alpha_m \cdot (\rho_a \cdot w_a - \rho_{da} \cdot w_{da}) \cdot h_{vda}$$

$$+ A_h \cdot \alpha_h \cdot (t_d - t_a) \qquad (3.28b)$$

for adsorption and desorption respectively.

Divide throughout by the cross-sectional area of each tube A_s (m^2).

$$r_a \cdot \frac{\partial(\rho_a \cdot h_a)}{\partial \tau} = -r_a \cdot f_a \cdot \frac{\partial h_a}{\partial x} - r_{sv} \cdot \alpha_m \cdot (\rho_a \cdot w_a - \rho_{da} \cdot w_{da}) \cdot h_{va}$$

$$+ r_{sv} \cdot \alpha_h \cdot (t_d - t_a) \qquad (3.29a)$$

$$r_a \cdot \frac{\partial(\rho_a \cdot h_a)}{\partial \tau} = -r_a \cdot f_a \cdot \frac{\partial h_a}{\partial x} - r_{sv} \cdot \alpha_m \cdot (\rho_a \cdot w_a - \rho_{da} \cdot w_{da}) \cdot h_{vda}$$

$$+ r_{sv} \cdot \alpha_h \cdot (t_d - t_a) \qquad (3.29b)$$

3.2.3 Conservation of Energy on Matrix

Energy Storage

The rate at which energy is stored in the desiccant volume $A_d \cdot dx$ (m^3) is

$$A_d \cdot \rho_d \cdot \frac{\partial h_f}{\partial \tau} \cdot dx \quad (kW) \qquad (3.30)$$

The rate at which energy is stored in the support material volume $A_m \cdot dx$ (m^3) is

$$A_m \cdot \rho_m \cdot c_m \cdot \frac{\partial t_d}{\partial \tau} \cdot dx \quad (kW) \tag{3.31}$$

where ρ_m - density of support material, for aluminum its value can be taken as $2702 kg/m^3$ (Kreith and Black 1980);

c_m - specific heat of support material, for aluminum its value can be taken as $0.896 kJ/kg \cdot K$ (Kreith and Black 1980);

When a desiccant wheel is made of ceramic fiber paper as a substratum, the low density (normally 190kg/m^3) and low specific heat (normally $0.8 kJ/kg \cdot K$) of ceramic fiber paper give low heat storage.

The rate of the whole energy storage in the control volume $(A_d + A_m) \cdot dx$ per unit time thus

$$A_d \cdot \rho_d \cdot \frac{\partial h_f}{\partial \tau} \cdot dx + A_m \cdot \rho_m \cdot c_m \cdot \frac{\partial t_d}{\partial \tau} \cdot dx \quad (kW) \tag{3.32}$$

Energy Inflow

Energy can be transferred into the desiccant volume $A_d \cdot dx$ by heat conduction and moisture diffusion. The rate of energy inflow across the x face by heat conduction and moisture diffusion is

$$\dot{H}_d = -\lambda_d \cdot A_d \cdot \frac{\partial t_d}{\partial x} + A_d \cdot \dot{M}_{o,K} \cdot h_{vda} + A_d \cdot \dot{M}_s \cdot h_s \quad (kW) \tag{3.33}$$

Substituting Equations 2.40 and 2.53 into Equation 3.33 the rate of energy inflow across the x face by heat conduction and moisture diffusion can be expressed as

$$\dot{H}_d = -\lambda_d \cdot A_d \cdot \frac{\partial t_d}{\partial x} - A_d \cdot h_{vda} \cdot D_{o,K,e} \cdot \frac{\partial(\rho_{da} \cdot w_{da})}{\partial x}$$

$$- A_d \cdot \rho_d \cdot h_s \cdot D_{s,e} \frac{\partial w_d}{\partial x} \quad (kW) \tag{3.34}$$

The rate of outflow across the $x+dx$ face is

$$\dot{H}_d + \frac{\partial \dot{H}_d}{\partial x} \cdot dx \quad (kW) \tag{3.35}$$

The net rate of inflow for the two faces is

$$-\frac{\partial \dot{H}_d}{\partial x} \cdot dx \quad (kW) \tag{3.36}$$

Substituting Equation 3.34 into Equation 3.36 the net rate of inflow for the two faces can be expressed as

$$A_d \cdot \frac{\partial(\lambda_d \cdot \frac{\partial t_d}{\partial x})}{\partial x} \cdot dx + A_d \cdot \frac{\partial\left[D_{o,K,e} \cdot h_{vda} \cdot \frac{\partial(\rho_{da} \cdot w_{da})}{\partial x} \right]}{\partial x} \cdot dx$$

$$+ A_d \cdot \rho_d \cdot \frac{\partial(D_{s,e} \cdot h_s \cdot \frac{\partial w_d}{\partial x})}{\partial x} \cdot dx \quad (kW) \tag{3.37}$$

Energy can be transferred into the support material volume $A_m \cdot dx$ by heat conduction. The temperature of support material is equal to the desiccant temperature t_d. The rate of energy inflow across the x face by heat conduction is

$$\dot{H}_m = -\lambda_m \cdot A_m \cdot \frac{\partial t_d}{\partial x} \quad (kW) \tag{3.38}$$

where λ_m - thermal conductivity of support material, for aluminum and ceramic fiber paper their values can be taken as $0.236 kW/m \cdot K$ (Kreith and Black 1980) and $0.015 \times 10^{-3} kW/m \cdot K$

The rate of outflow across the $x+dx$ face is

$$\dot{H}_m + \frac{\partial \dot{H}_m}{\partial x} \cdot dx \quad (kW) \tag{3.39}$$

The net rate of inflow for the two faces is

$$-\frac{\partial \dot{H}_m}{\partial x} \cdot dx \quad (kW) \tag{3.40}$$

Substituting Equation 3.38 into Equation 3.40 the net rate of inflow for the two faces can be expressed as

$$\lambda_m \cdot A_m \cdot \frac{\partial^2 t_d}{\partial x^2} \cdot dx \quad (kW) \tag{3.41}$$

The sum for desiccant and support material can be written

$$\lambda_m \cdot A_m \frac{\partial^2 t_d}{\partial x^2} \cdot dx + A_d \cdot \frac{\partial(\lambda_d \cdot \frac{\partial t_d}{\partial x})}{\partial x} \cdot dx$$

$$+ A_d \cdot \frac{\partial\left[D_{o,K,e} \cdot h_{vda} \cdot \frac{\partial(\rho_{da} \cdot w_{da})}{\partial x}\right]}{\partial x} \cdot dx + A_d \cdot \rho_d \cdot \frac{\partial(D_{s,e} \cdot h_s \cdot \frac{\partial w_d}{\partial x})}{\partial x^2} \cdot dx \quad (kW)$$

(3.42)

Energy Conservation Equation

The rate at which energy is stored in the control volume $(A_d + A_m) \cdot dx$ (m^3) equals the net rate of inflow of energy across the control volume boundary by the axial heat conduction and moisture diffusion, plus the rate of energy transfer between the air stream and the matrix. Substituting all the preceding terms in the statement of conservation of energy and dividing by the dx gives the equation of energy conservation on matrix, the energy conservation equations are

$$A_d \cdot \rho_d \cdot \frac{\partial h_f}{\partial \tau} + A_m \cdot \rho_m \cdot c_m \cdot \frac{\partial t_d}{\partial \tau}$$

$$= A_m \cdot \lambda_m \cdot \frac{\partial^2 t_d}{\partial x^2} + A_d \cdot \frac{\partial(\lambda_d \cdot \frac{\partial t_d}{\partial x})}{\partial x} + A_d \cdot \frac{\partial\left[D_{o,K,e} \cdot h_{vda} \cdot \frac{\partial(\rho_{da} \cdot w_{da})}{\partial x}\right]}{\partial x}$$

$$+ A_d \cdot \rho_d \cdot \frac{\partial(D_{s,e} \cdot h_s \cdot \frac{\partial w_d}{\partial x})}{\partial x} + A_h \cdot \alpha_m \cdot (\rho_a \cdot w_a - \rho_{da} \cdot w_{da}) \cdot h_{va}$$

$$- A_h \cdot \alpha_h \cdot (t_d - t_a) \qquad (3.43a)$$

and

$$A_d \cdot \rho_d \cdot \frac{\partial h_f}{\partial \tau} + A_m \cdot \rho_m \cdot c_m \cdot \frac{\partial t_d}{\partial \tau}$$

$$= A_m \cdot \lambda_m \cdot \frac{\partial^2 t_d}{\partial x^2} + A_d \cdot \frac{\partial(\lambda_d \cdot \frac{\partial t_d}{\partial x})}{\partial x} + A_d \cdot \frac{\partial\left[D_{o,K,e} \cdot h_{vda} \cdot \frac{\partial(\rho_{da} \cdot w_{da})}{\partial x} \right]}{\partial x}$$

$$+ A_d \cdot \rho_d \cdot \frac{\partial(D_{s,e} \cdot h_s \cdot \frac{\partial w_d}{\partial x})}{\partial x} + A_h \cdot \alpha_m \cdot (\rho_a \cdot w_a - \rho_{da} \cdot w_{da}) \cdot h_{vda} \cdot dx$$

$$- A_h \cdot \alpha_h \cdot (t_d - t_a) \cdot dx \qquad (3.43b)$$

for adsorption and desorption respectively.

Divide throughout by the cross-sectional area of each tube A_s (m^2). A_m / A_s is the ratio of the cross-sectional area of support material to the face area of a desiccant wheel, can be expressed as r_m (m^2/m^2) $(r_a + f_v + r_m = 1)$.

$$f_v \cdot \rho_d \cdot \frac{\partial h_f}{\partial \tau} + r_m \cdot \rho_m \cdot c_m \cdot \frac{\partial t_d}{\partial \tau}$$

$$= r_m \cdot \lambda_m \cdot \frac{\partial^2 t_d}{\partial x^2} + f_v \cdot \frac{\partial(\lambda_d \cdot \frac{\partial t_d}{\partial x})}{\partial x} + f_v \cdot \frac{\partial\left[D_{o,K,e} \cdot h_{vda} \cdot \frac{\partial(\rho_{da} \cdot w_{da})}{\partial x} \right]}{\partial x}$$

$$+ f_v \cdot \rho_d \cdot \frac{\partial(D_{s,e} \cdot h_s \cdot \frac{\partial w_d}{\partial x})}{\partial x} + r_{sv} \cdot \alpha_m \cdot (\rho_a \cdot w_a - \rho_{da} \cdot w_{da}) \cdot h_{va}$$

$$- r_{sv} \cdot \alpha_h \cdot (t_d - t_a) \qquad (3.44a)$$

$$f_v \cdot \rho_d \cdot \frac{\partial h_f}{\partial \tau} + r_m \cdot \rho_m \cdot c_m \cdot \frac{\partial t_d}{\partial \tau}$$

$$= r_m \cdot \lambda_m \cdot \frac{\partial^2 t_d}{\partial x^2} + f_v \cdot \frac{\partial(\lambda_d \cdot \frac{\partial t_d}{\partial x})}{\partial x} + f_v \cdot \frac{\partial\left[D_{o,K,e} \cdot h_{vda} \cdot \frac{\partial(\rho_{da} \cdot w_{da})}{\partial x} \right]}{\partial x}$$

$$+ f_v \cdot \rho_d \cdot \frac{\partial(D_{s,e} \cdot h_s \cdot \frac{\partial w_d}{\partial x})}{\partial x} + r_{sv} \cdot \alpha_m \cdot (\rho_a \cdot w_a - \rho_{da} \cdot w_{da}) \cdot h_{vda}$$

$$- r_{sv} \cdot \alpha_h \cdot (t_d - t_a) \qquad (3.44b)$$

3.3 Summary of the Governing Equations

The governing equations will now be summarized. Conservation of moisture on air stream:

$$r_a \cdot \frac{\partial(\rho_a \cdot w_a)}{\partial \tau} = -r_a \cdot f_a \cdot \frac{\partial w_a}{\partial x} + r_{sv} \cdot \alpha_m \cdot (\rho_{da} \cdot w_{da} - \rho_a \cdot w_a) \qquad (3.11)$$

Conservation of moisture on matrix:

$$f_v \cdot \varepsilon_p \cdot \frac{\partial(\rho_{da} \cdot w_{da})}{\partial \tau} + f_v \cdot \rho_d \cdot \frac{\partial w_d}{\partial \tau}$$

$$= f_v \cdot \frac{\partial\left[D_{o,K,e} \cdot \frac{\partial(\rho_{da} \cdot w_{da})}{\partial x} \right]}{\partial x} + f_v \cdot \rho_d \cdot \frac{\partial(D_{s,e} \cdot \frac{\partial w_d}{\partial x})}{\partial x})$$

$$- r_{sv} \cdot \alpha_m \cdot (\rho_{da} \cdot w_{da} - \rho_a \cdot w_a) \qquad (3.20)$$

Conservation of energy on air stream:

$$r_a \cdot \frac{\partial(\rho_a \cdot h_a)}{\partial \tau} = -r_a \cdot f_a \cdot \frac{\partial h_a}{\partial x} - r_{sv} \cdot \alpha_m \cdot (\rho_a \cdot w_a - \rho_{da} \cdot w_{da}) \cdot h_{va}$$

$$+ r_{sv} \cdot \alpha_h \cdot (t_d - t_a) \qquad (3.29a)$$

for adsorption and

$$r_a \cdot \frac{\partial(\rho_a \cdot h_a)}{\partial \tau} = -r_a \cdot f_a \cdot \frac{\partial h_a}{\partial x} - r_{sv} \cdot \alpha_m \cdot (\rho_a \cdot w_a - \rho_{da} \cdot w_{da}) \cdot h_{vda}$$

$$+ r_{sv} \cdot \alpha_h \cdot (t_d - t_a) \qquad (3.29b)$$

for desorption.

Conservation of energy on matrix

$$f_v \cdot \rho_d \cdot \frac{\partial h_f}{\partial \tau} + r_m \cdot \rho_m \cdot c_m \cdot \frac{\partial t_d}{\partial \tau}$$

$$= r_m \cdot \lambda_m \cdot \frac{\partial^2 t_d}{\partial x^2} + f_v \cdot \frac{\partial(\lambda_d \cdot \frac{\partial t_d}{\partial x})}{\partial x} + f_v \cdot \frac{\partial\left[D_{o,K,e} \cdot h_{vda} \cdot \frac{\partial(\rho_{da} \cdot w_{da})}{\partial x} \right]}{\partial x}$$

$$+ f_v \cdot \rho_d \cdot \frac{\partial(D_{s,e} \cdot h_s \cdot \frac{\partial w_d}{\partial x})}{\partial x} + r_{sv} \cdot \alpha_m \cdot (\rho_a \cdot w_a - \rho_{da} \cdot w_{da}) \cdot h_{va}$$

$$- r_{sv} \cdot \alpha_h \cdot (t_d - t_a) \qquad (3.44a)$$

for adsorption and

$$f_v \cdot \rho_d \cdot \frac{\partial h_f}{\partial \tau} + r_m \cdot \rho_m \cdot c_m \cdot \frac{\partial t_d}{\partial \tau}$$

$$= r_m \cdot \lambda_m \cdot \frac{\partial^2 t_d}{\partial x^2} + f_v \cdot \frac{\partial(\lambda_d \cdot \frac{\partial t_d}{\partial x})}{\partial x} + f_v \cdot \frac{\partial\left[D_{o,K,e} \cdot h_{vda} \cdot \frac{\partial(\rho_{da} \cdot w_{da})}{\partial x} \right]}{\partial x}$$

$$+ f_v \cdot \rho_d \cdot \frac{\partial(D_{s,e} \cdot h_s \cdot \frac{\partial w_d}{\partial x})}{\partial x} + r_{sv} \cdot \alpha_m \cdot (\rho_a \cdot w_a - \rho_{da} \cdot w_{da}) \cdot h_{vda}$$

$$- r_{sv} \cdot \alpha_h \cdot (t_d - t_a) \qquad (3.44b)$$

for desorption.

3.4 Boundary and Initial Conditions

The above governing equations are subject to the following boundary and initial conditions.

The required boundary conditions for the problem are the process and regeneration air stream inlet conditions. These conditions can generally vary with time on both the process and regeneration sides of the desiccant wheel for any integer (n_τ):

Regeneration air side $[n_\tau \cdot (\tau_r + \tau_p) \le \tau \le n_\tau \cdot (\tau_r + \tau_p) + \tau_h)]$:

$$w_a(\tau,0) = w_{a,r,in}(\tau) \qquad (3.45)$$

$$t_a(\tau,0) = t_{a,r,in}(\tau) \qquad (3.46)$$

where τ_r - regeneration air flow period (s);

τ_p - process air flow period (s);

$w_{a,r,in}$ - humidity ratio of regeneration air stream inlet condition ($kg_{H_2O}/kg_{dry\ air}$);

$t_{a,r,in}$ - temperature of regeneration air stream inlet condition (°C)

Process air side $[n_\tau \cdot (\tau_r + \tau_p) + \tau_r \le \overset{\bullet}{\tau} \le (\tau_\tau + 1)(\tau_r + \tau_p)]$:

$$w_a(\tau, l_c) = w_{a,p,in}(\tau) \tag{3.47}$$

$$t_a(\tau, l_c) = t_{a,p,in}(\tau) \tag{3.48}$$

where $w_{a,p,in}$ - humidity ratio of process air stream inlet condition ($kg_{H_2O}/kg_{dry\ air}$);

$t_{a,p,in}$ - temperature of process air stream inlet condition (°C)

Because time is a continuous variable from $\tau = 0$ to $\tau = (\tau_r + \tau_p)$ to $\tau = n(\tau_r + \tau_p)$, the periodic boundary conditions are inherently included in the formulation.

The end surfaces of the matrix at the air flow entrance and exit from the wheel make up less than 0.1% of the total heat and mass transfer area of the matrix. The heat transfer through the ends will therefore be negligible compared to the heat transfer within the tube. Hence, the boundary conditions for the matrix are chosen to be moisture-tight and adiabatic. Mathematically this is,

$$\left.\frac{\partial w_d}{\partial x}\right|_{x=0} = 0 \tag{3.49}$$

$$\left.\frac{\partial w_d}{\partial x}\right|_{x=l_c} = 0 \tag{3.50}$$

$$\left.\frac{\partial h_f}{\partial x}\right|_{x=0} = 0 \tag{3.51}$$

and $$\left.\frac{\partial h_f}{\partial x}\right|_{x=l_c} = 0 \tag{3.52}$$

It should be noted that the initial conditions for the problem are not critical because the desired solution is the quasi-steady-state solution for a desiccant wheel rotating at constant speed with constant inlet condition for both the hot and cold air flows.

Chapter 4 Numerical Scheme

The discretization of the governing equations is performed based on the control volume shown in Figure 4.1. All the dependent variables and properties are solved at the nodes. The transient terms are solved using the implicit formulation. The numerical solution scheme is fully implicit for all of the dependent variables in that the most updated value is used in each algebraic equation. The discretized equations of moisture conservation are solved using the Thomas algorithm, also called the Tridiagonal Matrix Algorithm (TDMA), and the discretized equations of energy conservation are solved using the Tridiagonal Matrix Algorithm for double variables.

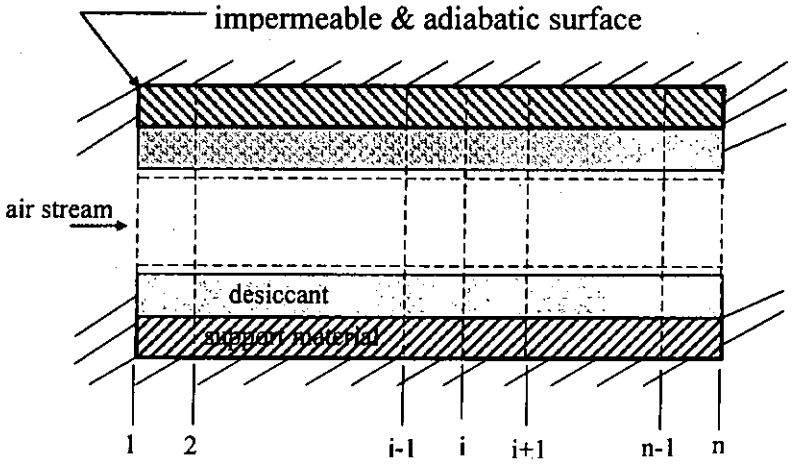

Figure 4.1 Discretization of energy and moisture conservation equations

The governing equations were discretized using a central – difference formula, for the derivatives $\frac{\partial w_a}{\partial x}$ in Equation 3.11, $\frac{\partial h_a}{\partial x}$ in Equation 3.29, $\frac{\partial\left[D_{o,K,e}\cdot\frac{\partial(\rho_{da}\cdot w_{da})}{\partial x}\right]}{\partial x}$ and $\frac{\partial(D_{s,e}\cdot\frac{\partial w_d}{\partial x})}{\partial x}$ in Equation 3.20, and $\frac{\partial^2 t_d}{\partial x^2}$, $\frac{\partial(\lambda_d\cdot\frac{\partial t_d}{\partial x})}{\partial x}$, $\frac{\partial\left[D_{o,K,e}\cdot h_{vda}\cdot\frac{\partial(\rho_{da}\cdot w_{da})}{\partial x}\right]}{\partial x}$, and $\frac{\partial(D_{s,e}\cdot h_s\cdot\frac{\partial w_d}{\partial x})}{\partial x}$ in Equation 3.44 at the point (k, i), where k is the time step index and i is the position step index.

$$\frac{\partial w_a}{\partial x}=\frac{w_{a\ i+1}^{k}-w_{a\ i-1}^{k}}{2\cdot\Delta x} \tag{4.1}$$

$$\frac{\partial h_a}{\partial x}=\frac{h_{a\ i+1}^{k}-h_{a\ i-1}^{k}}{2\cdot\Delta x} \tag{4.2}$$

$$\frac{\partial\left[D_{o,K,e}\cdot\frac{\partial(\rho_{da}\cdot w_{da})}{\partial x}\right]}{\partial x}$$

$$=D_{o,K,e\ i}^{k}\cdot\frac{\rho_{da\ i+1}^{k}\cdot w_{da\ i+1}^{k}-2\cdot\rho_{da\ i}^{k}\cdot w_{da\ i}^{k}+\rho_{da\ i-1}^{k}\cdot w_{da\ i-1}^{k}}{\Delta x^2} \tag{4.3}$$

$$\frac{\partial\left[D_{o,K,e}\cdot h_{vda}\cdot\frac{\partial(\rho_{da}\cdot w_{da})}{\partial x}\right]}{\partial x}$$

$$=D_{o,K,e\ i}^{k}\cdot h_{vda\ i}^{k}\frac{\rho_{da\ i+1}^{k}\cdot w_{da\ i+1}^{k}-2\cdot\rho_{da\ i}^{k}\cdot w_{da\ i}^{k}+\rho_{da\ i-1}^{k}\cdot w_{da\ i-1}^{k}}{\Delta x^2} \tag{4.4}$$

$$\frac{\partial(D_{s,e}\cdot\frac{\partial w_d}{\partial x})}{\partial x}=D_{se\ i}^{k}\cdot\frac{w_{d\ i+1}^{k}-2\cdot w_{d\ i}^{k}+w_{d\ i-1}^{k}}{\Delta x^2} \tag{4.5}$$

$$\frac{\partial(D_{s,e}\cdot h_s\cdot\frac{\partial w_d}{\partial x})}{\partial x}=D^k_{se\ i}\cdot h^k_{s\ i}\cdot\frac{w^k_{d\ i+1}-2\cdot w^k_{d\ i}+w^k_{d\ i-1}}{\Delta x^2} \tag{4.6}$$

$$\frac{\partial^2 t_d}{\partial x^2}=\frac{t^k_{d\ i+1}-2\cdot t^k_{d\ i}+t^k_{d\ i-1}}{\Delta x^2} \tag{4.7}$$

$$\frac{\partial(\lambda_d\cdot\frac{\partial t_d}{\partial x})}{\partial x}=\lambda^k_{d\ i}\frac{t^k_{d\ i+1}-2\cdot t^k_{d\ i}+t^k_{d\ i-1}}{\Delta x^2} \tag{4.8}$$

The governing equations were discretized using a downwind – difference scheme, for the derivatives $\frac{\partial(\rho_a\cdot w_a)}{\partial\tau}$ in Equation 3.11, $\frac{\partial(\rho_a\cdot h_a)}{\partial\tau}$ in Equation 3.29, $\frac{\partial(\rho_{da}\cdot w_{da})}{\partial\tau}$ and $\frac{\partial w_d}{\partial\tau}$ in Equation 3.20, and $\frac{\partial h_f}{\partial\tau}$ and $\frac{\partial t_d}{\partial\tau}$ in Equation 3.44 at the point (k, i).

$$\frac{\partial(\rho_a\cdot w_a)}{\partial\tau}=\frac{\rho^k_{a\ i}\cdot w^k_{a\ i}-\rho^{k-1}_{a\ i}\cdot w^{k-1}_{a\ i}}{\Delta\tau} \tag{4.9}$$

$$\frac{\partial(\rho_a\cdot h_a)}{\partial\tau}=\frac{\rho^k_{a\ i}\cdot h^k_{a\ i}-\rho^{k-1}_{a\ i}\cdot h^{k-1}_{a\ i}}{\Delta\tau} \tag{4.10}$$

$$\frac{\partial(\rho_{da}\cdot w_{da})}{\partial\tau}=\frac{\rho^k_{da\ i}\cdot w^k_{da\ i}-\rho^{k-1}_{da\ i}\cdot w^{k-1}_{da\ i}}{\Delta\tau} \tag{4.11}$$

$$\frac{\partial w_d}{\partial\tau}=\frac{w^k_{d\ i}-w^{k-1}_{d\ i}}{\Delta\tau} \tag{4.12}$$

$$\frac{\partial h_f}{\partial\tau}=\frac{h^k_{f\ i}-h^{k-1}_{f\ i}}{\Delta\tau} \tag{4.13}$$

$$\frac{\partial t_d}{\partial\tau}=\frac{t^k_{d\ i}-t^{k-1}_{d\ i}}{\Delta\tau} \tag{4.14}$$

4.1 Solution of Moisture Conservation Equation on Air Stream

The discretized moisture conservation equation for air (Equation 3.11) can be approximated in finite-difference form as

$$r_a \cdot \frac{\rho_{a\ i}^{k} \cdot w_{a\ i}^{k} - \rho_{a\ i}^{k-1} \cdot w_{a\ i}^{k-1}}{\Delta\tau}$$

$$= -r_a \cdot f_a \cdot \frac{w_{a\ i+1}^{k} - w_{a\ i-1}^{k}}{2 \cdot \Delta x} + r_{sv} \cdot \alpha_{m\ i}^{k} \cdot (\rho_{da\ i}^{k} \cdot w_{da\ i}^{k} - \rho_{a\ i}^{k} \cdot w_{a\ i}^{k}) \qquad (i = 2,\ 3,\ \cdots,\ n-1) \quad (4.15)$$

and

$$r_a \cdot \frac{\rho_{a\ n}^{k} \cdot w_{a\ n}^{k} - \rho_{a\ n}^{k-1} \cdot w_{a\ n}^{k-1}}{\Delta\tau}$$

$$= -r_a \cdot f_a \cdot \frac{w_{a\ n}^{k} - w_{a\ n-1}^{k}}{\Delta x} + r_{sv} \cdot \alpha_{m\ n}^{k} \cdot (\rho_{da\ n}^{k} \cdot w_{da\ n}^{k} - \rho_{a\ n}^{k} \cdot w_{a\ n}^{k}) \qquad (4.16)$$

where n is the number of nodes.

The boundary condition equations 3.45 and 3.47 at point (k, 1) can be written as

$$w_{a\ 1}^{k} = w_{a,p,in}^{k} \quad \text{(adsorption)} \quad \text{and} \quad w_{a\ 1}^{k} = w_{a,r,in}^{k} \quad \text{(desorption)} \quad (4.17)$$

The coefficient matrix of the discretized equations A is tridiagonal, because its only nonzero elements are on the main diagonal or immediately above or below that diagonal. That is, the elements a_{ij} of the matrix satisfy

$$a_{ij} = 0 \qquad \text{whenever } |i-j| > 1 \tag{4.18}$$

It is convenient to use the notation b_i for the elements of the diagonal, c_i for the superdiagonal, and a_i for the subdiagonal. In detail set

$$a_i = a_{i,i-1} \qquad b_i = a_{ii} \qquad c_i = a_{i,i+1} \tag{4.19}$$

With the notation just introduced, such a system of discretized equations will be of the form

$$\begin{aligned}
b_1 \cdot w_{a\ 1}^k + c_1 \cdot w_{a\ 2}^k &= d_1 \\
a_2 \cdot w_{a\ 1}^k + b_2 \cdot w_{a\ 2}^k + c_2 \cdot w_{a\ 3}^k &= d_2 \\
a_3 \cdot w_{a\ 2}^k + b_3 \cdot w_{a\ 3}^k + c_3 \cdot w_{a\ 4}^k &= d_3 \\
&\cdots\cdots \\
a_i \cdot w_{a\ i-1}^k + b_i \cdot w_{a\ i}^k + c_i \cdot w_{a\ i+1}^k &= d_i \qquad (4.20) \\
&\cdots\cdots \\
a_{n-1} \cdot w_{a\ n-2}^k + b_{n-1} \cdot w_{a\ n-1}^k + c_{n-1} \cdot w_{a\ n}^k &= d_{n-1} \\
a_n \cdot w_{a\ n-1}^k + b_n \cdot w_{a\ n}^k &= d_n
\end{aligned}$$

where $a_1 = 0$ (4.21)

$b_1 = 1$ (4.22)

$$c_1 = 0 \tag{4.23}$$

$$d_1 = w^k_{a,p,in} \quad \text{(adsorption)} \qquad d_1 = w^k_{a,r,in} \quad \text{(desorption)} \tag{4.24}$$

$$a_i = -\frac{r_a \cdot f_a}{2 \cdot \Delta x} \qquad (i = 2,\ 3,\ \cdots,\ n-1) \tag{4.25}$$

$$b_i = \frac{r_a \cdot \rho^k_{a\ i}}{\Delta \tau} + r_{sv} \cdot \alpha^k_{m\ i} \cdot \rho^k_{a\ i} \qquad (i = 2,\ 3,\ \cdots,\ n-1) \tag{4.26}$$

$$c_i = \frac{r_a \cdot f_a}{2 \cdot \Delta x} \qquad (i = 2,\ 3,\ \cdots,\ n-1) \tag{4.27}$$

$$d_i = \frac{r_a \cdot \rho^{k-1}_{a\ i} \cdot w^{k-1}_{a\ i}}{\Delta \tau} + r_{sv} \cdot \alpha^k_{m\ i} \cdot \rho^k_{da\ i} \cdot w^k_{da\ i} \qquad (i = 2,\ 3,\ \cdots,\ n-1) \tag{4.28}$$

$$a_n = -\frac{r_a \cdot f_a}{\Delta x} \tag{4.29}$$

$$b_n = \frac{r_a \cdot \rho^k_{a\ n}}{\Delta \tau} + \cdot\frac{r_a \cdot f_a}{\Delta x} + r_{sv} \cdot \alpha^k_{m\ n} \cdot \rho^k_{a\ n} \tag{4.30}$$

$$c_n = 0 \tag{4.31}$$

$$d_n = \frac{r_a \cdot \rho^{k-1}_{a\ n} \cdot w^{k-1}_{a\ n}}{\Delta \tau} + r_{sv} \cdot \alpha^k_{m\ n} \cdot \rho^k_{da\ n} \cdot w^k_{da\ n} \tag{4.32}$$

Applying Equation 4.20 for $i = 2$ (the first interior point) yields

$$\cdot w^k_{a\ 2} = -\frac{a_2}{b_2} \cdot w^k_{a\ 1} - \frac{c_2}{b_2} \cdot w^k_{a\ 3} + \frac{d_2}{b_2} \tag{4.33}$$

Since $w^k_{a\ 1}$ is known, Equation 4.33 is effectively a relation between $w^k_{a\ 2}$ and $w^k_{a\ 3}$. Next, applying Equation 4.20 for $i = 3$ yields a relation between $w^k_{a\ 2}$, $w^k_{a\ 3}$, and $w^k_{a\ 4}$. However, utilizing Equation 4.33 to eliminate $w^k_{a\ 2}$, this relation

becomes effectively one between $w_{a\ 3}^{k}$ and $w_{a\ 4}^{k}$. This process continues all the way until $n-1$. Applying Equation 4.20 for $i=n-1$ yields

$$w_{a\ n-1}^{k}=-\frac{a_{n-1}}{b_{n-1}}\cdot w_{a\ n-2}^{k}-\frac{c_{n-1}}{b_{n-1}}\cdot w_{a\ n}^{k}+\frac{d_{n-1}}{b_{n-1}} \tag{4.34}$$

Since a relation between $w_{a\ n-1}^{k}$ and $w_{a\ n-2}^{k}$ exists from the earlier application of Equation 4.20 for $i=n-2$, Equation 4.34 is, effectively, a relation between $w_{a\ n-1}^{k}$ and $w_{a\ n}^{k}$. Further, since information on $w_{a\ n}^{k}$ is provided by Equation 4.15, Equation 4.34 can be solved for the value of $w_{a\ n-1}^{k}$ and $w_{a\ n}^{k}$. With $w_{a\ n-1}^{k}$ known, a process of back substitution can be initiated to obtain $w_{a\ n-2}^{k}$ from $w_{a\ n-1}^{k}$, $w_{a\ n-3}^{k}$ from $w_{a\ n-2}^{k}\ldots w_{a\ 3}^{k}$ from $w_{a\ 4}^{k}$ and $w_{a\ 2}^{k}$ from $w_{a\ 3}^{k}$.

The discussion above describes the basic principles of the Thomas algorithm. In term of programming, at each point a relation of the type

$$w_{a\ i}^{k}=P_i\cdot w_{a\ i+1}^{k}+Q_i \tag{4.35}$$

needs to be constructed during the forward marching process from ($i=2$) to ($i=n-1$). Equation 4.35 connects the humidity ratio of air stream w_a of two sequential grid points. Written for point $i-1$, Equation 4.35 reads

$$w_{a\ i-1}^{k}=P_{i-1}\cdot w_{a\ i}^{k}+Q_{i-1} \tag{4.36}$$

Combining Equations 4.36 and 4.20 to eliminate $w_{a\ i-1}^{k}$ yields, after some rearranging,

$$w_{a\ i}^{k} = -\frac{c_i}{a_i \cdot P_{i-1} + b_i} \cdot w_{a\ i+1}^{k} + \frac{d_i - a_i \cdot Q_{i-1}}{a_i \cdot P_{i-1} + b_i} \qquad (i = 2,\ 3,\ \cdots,\ n-1) \quad (4.37)$$

Note that Equation 4.37 is identical to Equation 4.35 with

$$P_i = -\frac{c_i}{a_i \cdot P_{i-1} + b_i} \quad (4.38)$$

$$Q_i = \frac{d_i - a_i \cdot Q_{i-1}}{a_i \cdot P_{i-1} + b_i} \quad (4.39)$$

To start the calculation process, applying Equations 4.38 and 4.39 for $i = 1$ yields

$$P_1 = -\frac{c_1}{b_1} \quad (4.40)$$

$$Q_1 = \frac{d_1}{b_1} \quad (4.41)$$

Next, Equations 4.38 and 4.39 should be used to obtain P_i and Q_i for *i = 2, 3, ···, n.* Since $c_n = 0$, applying Equation 4.38 yields $P_n = 0$, and then applying Equation 4.35 yields $w_{a\ n}^{k} = Q_n$. Finally, Equation 4.35 needs to be employed for *i=n-1, n-2, ···, 3, 2,* to yield the humidity ratio of air stream w_a at all interior points.

4.2 Solution of Moisture Conservation Equation on Desiccant

The discretized moisture conservation equation for desiccant (Equation 3.20) can be approximated in finite-difference form as

$$f_v \cdot \varepsilon_p \cdot \frac{\rho^k_{da\ i} \cdot w^k_{da\ i} - \rho^{k-1}_{da\ i} \cdot w^{k-1}_{da\ i}}{\Delta\tau} + f_v \cdot \rho_d \cdot \frac{w^k_{d\ i} - w^{k-1}_{d\ i}}{\Delta\tau}$$

$$= f_v \cdot D^k_{o,K,e\ i} \cdot \frac{\rho^k_{da\ i+1} \cdot w^k_{da\ i+1} - 2 \cdot \rho^k_{da\ i} \cdot w^k_{da\ i} + \rho^k_{da\ i-1} w^k_{da\ i-1}}{\Delta x^2}$$

$$+ f_v \cdot \rho_d \cdot D^k_{se\ i} \cdot \frac{w^k_{d\ i+1} - 2 \cdot w^k_{d\ i} + w^k_{d\ i-1}}{\Delta x^2}$$

$$- r_{sv} \cdot \alpha^k_{m\ i} \cdot (\rho^k_{da\ i} \cdot w^k_{da\ i} - \rho^k_{a\ i} \cdot w^k_{a\ i}) \qquad (i = 2,\ 3,\ \cdots,\ n-1) \quad (4.42)$$

Utilizing the boundary conditions $\left.\frac{\partial w_d}{\partial x}\right|_{x=0} = 0$ (3.49) and $\left.\frac{\partial w_d}{\partial x}\right|_{x=l_c} = 0$ (3.50), the discretized boundary condition equations of moisture conservation on desiccant can be expressed as

$$f_v \cdot \varepsilon_p \cdot \frac{\rho^k_{da\ 1} \cdot w^k_{da\ 1} - \rho^{k-1}_{da\ 1} \cdot w^{k-1}_{da\ 1}}{2 \cdot \Delta\tau} + f_v \cdot \rho_d \cdot \frac{w^k_{d\ 1} - w^{k-1}_{d\ 1}}{2 \cdot \Delta\tau}$$

$$= f_v \cdot D^k_{o,K,e\ 1} \cdot \frac{\rho^k_{da\ 2} \cdot w^k_{da\ 2} - \rho^k_{da\ 1} \cdot w^k_{da\ 1}}{\Delta x^2}$$

$$+ f_v \cdot \rho_d \cdot D^k_{se\ 1} \cdot \frac{w^k_{d\ 2} - w^k_{d\ 1}}{\Delta x^2} - \frac{r_{sv} \cdot \alpha^k_{m\ 1} \cdot (\rho^k_{da\ 1} \cdot w^k_{da\ 1} - \rho^k_{a\ 1} \cdot w^k_{a\ 1})}{2} \quad (4.43)$$

and $$f_v \cdot \varepsilon_p \cdot \frac{\rho^k_{da\ n} \cdot w^k_{da\ n} - \rho^{k-1}_{da\ n} \cdot w^{k-1}_{da\ n}}{2 \cdot \Delta\tau} + f_v \cdot \rho_d \cdot \frac{w^k_{d\ n} - w^{k-1}_{d\ n}}{2 \cdot \Delta\tau}$$

$$= -f_v \cdot D^k_{o,K,e\ n} \cdot \frac{\rho^k_{da\ n} \cdot w^k_{da\ n} - \rho^k_{da\ n-1} \cdot w^k_{da\ n-1}}{\Delta x^2}$$

$$- f_v \cdot \rho_d \cdot D^k_{se\ n} \cdot \frac{w^k_{d\ n} - w^k_{d\ n-1}}{\Delta x^2} + \frac{r_{sv} \cdot \alpha^k_{m\ n} \cdot (\rho^k_{a\ n} \cdot w^k_{a\ n} - \rho^k_{da\ n} \cdot w^k_{da\ n})}{2}$$

(4.44)

The Equations 4.42, 4.43 and 4.44 can be written in the following form:

$$a_i \cdot w_{d\ i-1}^k + b_i \cdot w_{d\ i}^k + c_i \cdot w_{d\ i+1}^k = d_i \tag{4.45}$$

where the coefficients are all known and are defined as

$$a_1 = 0 \tag{4.46}$$

$$b_1 = \frac{f_v \cdot \rho_d}{2 \cdot \Delta\tau} + \frac{f_v \cdot \rho_d \cdot D_{se\ 1}^k}{\Delta x^2} \tag{4.47}$$

$$c_1 = -\frac{f_v \cdot \rho_d \cdot D_{se\ 1}^k}{\Delta x^2} \tag{4.48}$$

$$\begin{aligned} d_1 = & -f_v \cdot \varepsilon_p \cdot \frac{\rho_{da\ 1}^k \cdot w_{da\ 1}^k - \rho_{da\ 1}^{k-1} \cdot w_{da\ 1}^{k-1}}{2 \cdot \Delta\tau} + \frac{f_v \cdot \rho_d \cdot w_{d\ 1}^{k-1}}{2 \cdot \Delta\tau} \\ & + f_v \cdot D_{o,K,e\ 1}^k \cdot \frac{\rho_{da\ 2}^k \cdot w_{da\ 2}^k - \rho_{da\ 1}^k \cdot w_{da\ 1}^k}{\Delta x^2} \\ & - \frac{r_{sv} \cdot \alpha_{m\ 1}^k \cdot (\rho_{da\ 1}^k \cdot w_{da\ 1}^k - \rho_{a\ 1}^k \cdot w_{a\ 1}^k)}{2} \end{aligned} \tag{4.49}$$

$$a_i = -\frac{f_v \cdot \rho_d \cdot D_{se\ i}^k}{\Delta x^2} \qquad (i = 2,\ 3,\ \cdots,\ n-1) \tag{4.50}$$

$$b_i = \frac{f_v \cdot \rho_d}{\Delta\tau} + \frac{2 \cdot f_v \cdot \rho_d \cdot D_{se\ i}^k}{\Delta x^2} \qquad (i = 2,\ 3,\ \cdots,\ n-1) \tag{4.51}$$

$$c_i = -\frac{f_v \cdot \rho_d \cdot D_{se\ i}^k}{\Delta x^2} \qquad (i = 2,\ 3,\ \cdots,\ n-1) \tag{4.52}$$

$$d_i = -f_v \cdot \varepsilon_p \cdot \frac{\rho^k_{da\ i} \cdot w^k_{da\ i} - \rho^{k-1}_{da\ i} w^{k-1}_{da\ i}}{\Delta\tau} + \frac{f_v \cdot \rho_d \cdot w^{k-1}_{d\ i}}{\Delta\tau}$$

$$+ f_v \cdot D^k_{o,K,e\ i} \cdot \frac{\rho^k_{da\ i+1} \cdot w^k_{da\ i+1} - 2 \cdot \rho^k_{da\ i} \cdot w^k_{da\ i} + \rho^k_{da\ i-1} \cdot w^k_{da\ i-1}}{\Delta x^2}$$

$$- r_{sv} \cdot \alpha^k_{m\ i} \cdot (\rho^k_{da\ i} \cdot w^k_{da\ i} - \rho^k_{a\ i} \cdot w^k_{a\ i}) \quad (i = 2,\ 3,\ \cdots,\ n-1) \tag{4.53}$$

$$a_n = -\frac{f_v \cdot \rho_d \cdot D^k_{se\ n}}{\Delta x^2} \tag{4.54}$$

$$b_n = \frac{f_v \cdot \rho_d}{2 \cdot \Delta\tau} + \frac{f_v \cdot \rho_d \cdot D^k_{se\ n}}{\Delta x^2} \tag{4.55}$$

$$c_n = 0 \tag{4.56}$$

$$d_n = -f_v \cdot \varepsilon_p \cdot \frac{\rho^k_{da\ n} \cdot w^k_{da\ n} - \rho^{k-1}_{da\ n} \cdot w^{k-1}_{da\ n}}{2 \cdot \Delta\tau} + \frac{f_v \cdot \rho_d \cdot w^{k-1}_{d\ n}}{2 \cdot \Delta\tau}$$

$$- f_v \cdot D^k_{o,K,e\ n} \cdot \frac{\rho^k_{da\ n} \cdot w^k_{da\ n} - \rho^k_{da\ n-1} w^k_{da\ n-1}}{\Delta x^2}$$

$$+ \frac{r_{sv} \cdot \alpha^k_{m\ n} \cdot (\rho^k_{a\ n} \cdot w^k_{a\ n} - \rho^k_{da\ n} \cdot w^k_{da\ n})}{2} \tag{4.57}$$

At each point a relation of the type

$$w^k_{d\ i} = P_i \cdot w^k_{d\ i+1} + Q_i \tag{4.58}$$

needs to be constructed according to the eariler discussion on the solusion of w_a, finally to yield the water content of desiccant solid phase w_d at all points.

4.3 Discretization of Energy Conservation Equations on Air Stream

The discretized energy conservation equations on air stream (Equations 3.29) can be approximated in finite-difference form as

$$r_a \cdot \frac{\rho_{a\ i}^k \cdot h_{a\ i}^k - \rho_{a\ i}^{k-1} \cdot h_{a\ i}^{k-1}}{\Delta\tau}$$

$$= -r_a \cdot f_a \cdot \frac{h_{a\ i+1}^k - h_{a\ i-1}^k}{2 \cdot \Delta x} - r_{sv} \cdot \alpha_{m\ i}^k \cdot (\rho_{a\ i}^k \cdot w_{a\ i}^k - \rho_{da\ i}^k \cdot w_{da\ i}^k) \cdot h_{va\ i}^k$$

$$+ r_{sv} \cdot \alpha_{h\ i}^k \cdot (t_{d\ i}^k - t_{a\ i}^k) \qquad (i = 2,\ 3,\ \cdots,\ n-1) \quad (4.59a)$$

for adsorption,

$$r_a \cdot \frac{\rho_{a\ i}^k \cdot h_{a\ i}^k - \rho_{a\ i}^{k-1} \cdot h_{a\ i}^{k-1}}{\Delta\tau}$$

$$= -r_a \cdot f_a \cdot \frac{h_{a\ i+1}^k - h_{a\ i-1}^k}{2 \cdot \Delta x} - r_{sv} \cdot \alpha_{m\ i}^k \cdot (\rho_{a\ i}^k \cdot w_{a\ i}^k - \rho_{da\ i}^k \cdot w_{da\ i}^k) \cdot h_{vda\ i}^k$$

$$+ r_{sv} \cdot \alpha_{h\ i}^k \cdot (t_{d\ i}^k - t_{a\ i}^k) \qquad (i = 2,\ 3,\ \cdots,\ n-1) \quad (4.59b)$$

for desorption,

$$r_a \cdot \frac{\rho_{a\ n}^k \cdot h_{a\ n}^k - \rho_{a\ n}^{k-1} \cdot h_{a\ n}^{k-1}}{\Delta\tau}$$

$$= -r_a \cdot f_a \cdot \frac{h_{a\ n}^k - h_{a\ n-1}^k}{\Delta x} - r_{sv} \cdot \alpha_{m\ n}^k \cdot (\rho_{a\ n}^k \cdot w_{a\ n}^k - \rho_{da\ n}^k \cdot w_{da\ n}^k) \cdot h_{va\ n}^k$$

$$+ r_{sv} \cdot \alpha_{h\ n}^k \cdot (t_{d\ n}^k - t_{a\ n}^k) \qquad (4.60a)$$

for adsorption, and

$$r_a \cdot \frac{\rho_{a\ n}^{k} \cdot h_{a\ n}^{k} - \rho_{a\ n}^{k-1} \cdot h_{a\ n}^{k-1}}{\Delta\tau}$$

$$= -r_a \cdot f_a \cdot \frac{h_{a\ n}^{k} - h_{a\ n-1}^{k}}{\Delta x} - r_{sv} \cdot \alpha_{m\ n}^{k} \cdot (\rho_{a\ n}^{k} \cdot w_{a\ n}^{k} - \rho_{da\ n}^{k} \cdot w_{da\ n}^{k}) \cdot h_{vda\ n}^{k}$$

$$+ r_{sv} \cdot \alpha_{h\ n}^{k} \cdot (t_{d\ n}^{k} - t_{a\ n}^{k}) \qquad (4.60b)$$

for desorption.

Substituting Equations 2.60, 2.61 and 2.63a into Equations 4.59 and 4.60, the discretized energy conservation equations on air stream can be expressed as

$$r_a \cdot \rho_{a\ i}^{k} \cdot \frac{c_{pa\ i}^{k} \cdot t_{a\ i}^{k} + w_{a\ i}^{k} \cdot (h_{fg,0} + c_{pva\ i}^{k} \cdot t_{a\ i}^{k})}{\Delta\tau} - \frac{r_a \cdot \rho_{a\ i}^{k-1} \cdot h_{a\ i}^{k-1}}{\Delta\tau}$$

$$= -r_a \cdot f_a \cdot \frac{c_{pa\ i+1}^{k} \cdot t_{a\ i+1}^{k} + w_{a\ i+1}^{k} \cdot (h_{fg,0} + c_{pva\ i+1}^{k} \cdot t_{a\ i+1}^{k})}{2 \cdot \Delta x}$$

$$+ r_a \cdot f_a \cdot \frac{c_{pa\ i-1}^{k} \cdot t_{a\ i-1}^{k} + w_{a\ i-1}^{k} \cdot (h_{fg,0} + c_{pva\ i-1}^{k} \cdot t_{a\ i-1}^{k})}{2 \cdot \Delta x}$$

$$- r_{sv} \cdot \alpha_{m\ i}^{k} \cdot (\rho_{a\ i}^{k} \cdot w_{a\ i}^{k} - \rho_{da\ i}^{k} \cdot w_{da\ i}^{k}) \cdot (h_{fg,0} + c_{pva\ i}^{k} \cdot t_{a\ i}^{k})$$

$$+ r_{sv} \cdot \alpha_{h\ i}^{k} \cdot (t_{d\ i}^{k} - t_{a\ i}^{k}) \qquad (i = 2,\ 3,\ \cdots,\ n-1) \quad (4.61a)$$

for adsorption,

$$r_a \cdot \rho_{a\ i}^{k} \cdot \frac{c_{pa\ i}^{k} \cdot t_{a\ i}^{k} + w_{a\ i}^{k} \cdot (h_{fg,0} + c_{pva\ i}^{k} \cdot t_{a\ i}^{k})}{\Delta\tau} - \frac{r_a \cdot \rho_{a\ i}^{k-1} \cdot h_{a\ i}^{k-1}}{\Delta\tau}$$

$$= -r_a \cdot f_a \cdot \frac{c_{pa\ i+1}^{k} \cdot t_{a\ i+1}^{k} + w_{a\ i+1}^{k} \cdot (h_{fg,0} + c_{pva\ i+1}^{k} \cdot t_{a\ i+1}^{k})}{2 \cdot \Delta x}$$

$$+ r_a \cdot f_a \cdot \frac{c_{pa\ i-1}^{k} \cdot t_{a\ i-1}^{k} + w_{a\ i-1}^{k} \cdot (h_{fg,0} + c_{pva\ i-1}^{k} \cdot t_{a\ i-1}^{k})}{2 \cdot \Delta x}$$

$$- r_{sv} \cdot \alpha_{m\ i}^{k} \cdot (\rho_{a\ i}^{k} \cdot w_{a\ i}^{k} - \rho_{da\ i}^{k} \cdot w_{da\ i}^{k}) \cdot (h_{fg,0} + c_{pvda\ i}^{k} \cdot t_{d\ i}^{k})$$

$$+ r_{sv} \cdot \alpha_{h\ i}^{k} \cdot (t_{d\ i}^{k} - t_{a\ i}^{k}) \qquad (i = 2,\ 3,\ \cdots,\ n-1) \quad (4.61b)$$

for desorption,

$$r_a \cdot \rho_{a\ n}^{k} \cdot \frac{c_{pa\ n}^{k} \cdot t_{a\ n}^{k} + w_{a\ n}^{k} \cdot (h_{fg,0} + c_{pva\ n}^{k} \cdot t_{a\ n}^{k})}{\Delta\tau} - \frac{r_a \cdot \rho_{a\ n}^{k-1} \cdot h_{a\ n}^{k-1}}{\Delta\tau}$$

$$= -r_a \cdot f_a \cdot \frac{c_{pa\ n}^{k} \cdot t_{a\ n}^{k} + w_{a\ n}^{k} \cdot (h_{fg,0} + c_{pva\ n}^{k} \cdot t_{a\ n}^{k})}{\Delta x}$$

$$+ r_a \cdot f_a \cdot \frac{c_{pa\ n-1}^{k} \cdot t_{a\ n-1}^{k} + w_{a\ n-1}^{k} \cdot (h_{fg,0} + c_{pva\ n-1}^{k} \cdot t_{a\ n-1}^{k})}{\Delta x}$$

$$- r_{sv} \cdot \alpha_{m\ n}^{k} \cdot (\rho_{a\ n}^{k} \cdot w_{a\ n}^{k} - \rho_{da\ n}^{k} \cdot w_{da\ n}^{k}) \cdot (h_{fg,0} + c_{pva\ n}^{k} \cdot t_{a\ n}^{k})$$

$$+ r_{sv} \cdot \alpha_{h\ n}^{k} \cdot (t_{d\ n}^{k} - t_{a\ n}^{k}) \qquad (4.62a)$$

for adsorption, and

$$r_a \cdot \rho_{a\ n}^{k} \cdot \frac{c_{pa\ n}^{k} \cdot t_{a\ n}^{k} + w_{a\ n}^{k} \cdot (h_{fg,0} + c_{pva\ n}^{k} \cdot t_{a\ n}^{k})}{\Delta\tau} - \frac{r_a \cdot \rho_{a\ n}^{k-1} \cdot h_{a\ n}^{k-1}}{\Delta\tau}$$

$$= -r_a \cdot f_a \cdot \frac{c_{pa\ n}^{k} \cdot t_{a\ n}^{k} + w_{a\ n}^{k} \cdot (h_{fg,0} + c_{pva\ n}^{k} \cdot t_{a\ n}^{k})}{\Delta x}$$

$$+ r_a \cdot f_a \cdot \frac{c_{pa\ n-1}^{k} \cdot t_{a\ n-1}^{k} + w_{a\ n-1}^{k} \cdot (h_{fg,0} + c_{pva\ n-1}^{k} \cdot t_{a\ n-1}^{k})}{\Delta x}$$

$$- r_{sv} \cdot \alpha_{m\ n}^{k} \cdot (\rho_{a\ n}^{k} \cdot w_{a\ n}^{k} - \rho_{da\ n}^{k} \cdot w_{da\ n}^{k}) \cdot (h_{fg,0} + c_{pvda\ n}^{k} \cdot t_{d\ n}^{k})$$

$$+ r_{sv} \cdot \alpha_{h\ n}^{k} \cdot (t_{d\ n}^{k} - t_{a\ n}^{k}) \qquad (4.62b)$$

for desorption.

The boundary condition equations 3.46 and 3.48 at point (k, 1) can be written as

$$t_{a\ 1}^{k} = t_{a,p,in}^{k} \qquad (4.63)$$

and $$t_{a\ 1}^{k} = t_{a,r,in}^{k} \qquad (4.64)$$

4.4 Discretization of Energy Conservation Equations on Matrix

The discretized energy conservation equation on matrix (Equations 3.44) can be approximated in finite-difference form as

$$f_v \cdot \rho_d \cdot \frac{h_{f\ i}^k - h_{f\ i}^{k-1}}{\Delta\tau} + r_m \cdot \rho_m \cdot c_m \cdot \frac{t_{d\ i}^k - t_{d\ i}^{k-1}}{\Delta\tau}$$

$$= (\lambda_{d\ i}^k \cdot f_v + \lambda_m \cdot r_m) \cdot \frac{t_{d\ i+1}^k - 2 \cdot t_{d\ i}^k + t_{d\ i-1}^k}{\Delta x^2}$$

$$+ f_v \cdot D_{o,K,e\ i}^k \cdot h_{vda\ i}^k \cdot \frac{\rho_{da\ i+1}^k \cdot w_{da\ i+1}^k - 2 \cdot \rho_{da\ i}^k \cdot w_{da\ i}^k + \rho_{da\ i-1}^k w_{da\ i-1}^k}{\Delta x^2}$$

$$+ f_v \cdot \rho_d \cdot D_{s,e\ i}^k \cdot h_{s\ i}^k \cdot \frac{w_{d\ i+1}^k - 2 \cdot w_{d\ i}^k + w_{d\ i-1}^k}{\Delta x^2}$$

$$+ r_{sv} \cdot \alpha_{m\ i}^k \cdot (\rho_{a\ i}^k \cdot w_{a\ i}^k - \rho_{da\ i}^k \cdot w_{da\ i}^k) \cdot h_{va\ i}^k - r_{sv} \cdot \alpha_{h\ i}^k \cdot (t_{d\ i}^k - t_{a\ i}^k)$$

$(i = 2,\ 3,\ \cdots,\ n-1)$ (4.65a)

for adsorption, and

$$f_v \cdot \rho_d \cdot \frac{h_{f\ i}^k - h_{f\ i}^{k-1}}{\Delta\tau} + r_m \cdot \rho_m \cdot c_m \cdot \frac{t_{d\ i}^k - t_{d\ i}^{k-1}}{\Delta\tau}$$

$$= (\lambda_{d\ i}^k \cdot f_v + \lambda_m \cdot r_m) \cdot \frac{t_{d\ i+1}^k - 2 \cdot t_{d\ i}^k + t_{d\ i-1}^k}{\Delta x^2}$$

$$+ f_v \cdot D_{o,K,e\ i}^k \cdot h_{vda\ i}^k \cdot \frac{\rho_{da\ i+1}^k \cdot w_{da\ i+1}^k - 2 \cdot \rho_{da\ i}^k \cdot w_{da\ i}^k + \rho_{da\ i-1}^k w_{da\ i-1}^k}{\Delta x^2}$$

$$+ f_v \cdot \rho_d \cdot D_{s,e\ i}^k \cdot h_{s\ i}^k \cdot \frac{w_{d\ i+1}^k - 2 \cdot w_{d\ i}^k + w_{d\ i-1}^k}{\Delta x^2}$$

$$+ r_{sv} \cdot \alpha_{m\ i}^k \cdot (\rho_{a\ i}^k \cdot w_{a\ i}^k - \rho_{da\ i}^k \cdot w_{da\ i}^k) \cdot h_{vda\ i}^k - r_{sv} \cdot \alpha_{h\ i}^k \cdot (t_{d\ i}^k - t_{a\ i}^k)$$

$(i = 2,\ 3,\ \cdots,\ n-1)$ (4.65b)

for desorption.

Utilizing the boundary conditions $\left.\frac{\partial h_f}{\partial x}\right|_{x=0} = 0$ (3.51) and $\left.\frac{\partial h_f}{\partial x}\right|_{x=l_c} = 0$ (3.52), the discretized boundary condition equations of energy conservation on matrixcan be expressed as

$$f_v \cdot \rho_d \cdot \frac{h_{f\ 1}^{k} - h_{f\ 1}^{k-1}}{2 \cdot \Delta\tau} + r_m \cdot \rho_m \cdot c_m \cdot \frac{t_{d\ 1}^{k} - t_{d\ 1}^{k-1}}{2 \cdot \Delta\tau}$$

$$= (\lambda_{d\ 1}^{k} \cdot f_v + \lambda_m \cdot r_m) \cdot \frac{t_{d\ 2}^{k} - t_{d\ 1}^{k}}{\Delta x^2}$$

$$+ f_v \cdot D_{o,K,e\ 1}^{k} \cdot h_{vda\ 1}^{k} \cdot \frac{\rho_{da\ 2}^{k} \cdot w_{da\ 2}^{k} - \rho_{da\ 1}^{k} \cdot w_{da\ 1}^{k}}{\Delta x^2}$$

$$+ f_v \cdot \rho_d \cdot D_{s,e\ 1}^{k} \cdot h_{s\ 1}^{k} \cdot \frac{w_{d\ 2}^{k} - w_{d\ 1}^{k}}{\Delta x^2}$$

$$+ \frac{r_{sv} \cdot \alpha_{m\ 1}^{k} \cdot (\rho_{a\ 1}^{k} \cdot w_{a\ 1}^{k} - \rho_{da\ 1}^{k} \cdot w_{da\ 1}^{k}) \cdot h_{va\ 1}^{k}}{2} - \frac{r_{sv} \cdot \alpha_{h\ 1}^{k} \cdot (t_{d\ 1}^{k} - t_{a\ 1}^{k})}{2}$$

(4.66a)

for adsorption,

$$f_v \cdot \rho_d \cdot \frac{h_{f\ 1}^{k} - h_{f\ 1}^{k-1}}{2 \cdot \Delta\tau} + r_m \cdot \rho_m \cdot c_m \cdot \frac{t_{d\ 1}^{k} - t_{d\ 1}^{k-1}}{2 \cdot \Delta\tau}$$

$$= (\lambda_{d\ 1}^{k} \cdot f_v + \lambda_m \cdot r_m) \cdot \frac{t_{d\ 2}^{k} - t_{d\ 1}^{k}}{\Delta x^2}$$

$$+ f_v \cdot D_{o,K,e\ 1}^{k} \cdot h_{vda\ 1}^{k} \cdot \frac{\rho_{da\ 2}^{k} \cdot w_{da\ 2}^{k} - \rho_{da\ 1}^{k} \cdot w_{da\ 1}^{k}}{\Delta x^2}$$

$$+ f_v \cdot \rho_d \cdot D_{s,e\ 1}^{k} \cdot h_{s\ 1}^{k} \cdot \frac{w_{d\ 2}^{k} - w_{d\ 1}^{k}}{\Delta x^2}$$

$$+ \frac{r_{sv} \cdot \alpha_{m\ 1}^{k} \cdot (\rho_{a\ 1}^{k} \cdot w_{a\ 1}^{k} - \rho_{da\ 1}^{k} \cdot w_{da\ 1}^{k}) \cdot h_{vda\ 1}^{k}}{2} - \frac{r_{sv} \cdot \alpha_{h\ 1}^{k} \cdot (t_{d\ 1}^{k} - t_{a\ 1}^{k})}{2}$$

(4.66b)

for desorption,

$$f_v \cdot \rho_d \cdot \frac{h_{f\ n}^{k} - h_{f\ n}^{k-1}}{2 \cdot \Delta\tau} + r_m \cdot \rho_m \cdot c_m \cdot \frac{t_{d\ n}^{k} - t_{d\ n}^{k-1}}{2 \cdot \Delta\tau}$$

$$= -(\lambda_{d\ n}^{k} \cdot f_v + \lambda_m \cdot r_m) \cdot \frac{t_{d\ n}^{k} - t_{d\ n-1}^{k}}{\Delta x^2}$$

$$- f_v \cdot D_{o,K,e\ n}^{k} \cdot h_{vda\ n}^{k} \cdot \frac{\rho_{da\ n}^{k} \cdot w_{da\ n}^{k} - \rho_{da\ n-1}^{k} \cdot w_{da\ n-1}^{k}}{\Delta x^2}$$

$$- f_v \cdot \rho_d \cdot D_{s,e\ n}^{k} \cdot h_{s\ n}^{k} \cdot \frac{w_{d\ n}^{k} - w_{d\ n-1}^{k}}{\Delta x^2}$$

$$+ \frac{r_{sv} \cdot \alpha_{m\ n}^{k} \cdot (\rho_{a\ n}^{k} \cdot w_{a\ n}^{k} - \rho_{da\ n}^{k} \cdot w_{da\ n}^{k}) \cdot h_{va\ n}^{k}}{2} - \frac{r_{sv} \cdot \alpha_{h\ n}^{k} \cdot (t_{d\ n}^{k} - t_{a\ n}^{k})}{2}$$

(4.67a)

for adsorption and

$$f_v \cdot \rho_d \cdot \frac{h_{f\ n}^{k} - h_{f\ n}^{k-1}}{2 \cdot \Delta\tau} + r_m \cdot \rho_m \cdot c_m \cdot \frac{t_{d\ n}^{k} - t_{d\ n}^{k-1}}{2 \cdot \Delta\tau}$$

$$= -(\lambda_{d\ n}^{k} \cdot f_v + \lambda_m \cdot r_m) \cdot \frac{t_{d\ n}^{k} - t_{d\ n-1}^{k}}{\Delta x^2}$$

$$- f_v \cdot D_{o,K,e\ n}^{k} \cdot h_{vda\ n}^{k} \cdot \frac{\rho_{da\ n}^{k} \cdot w_{da\ n}^{k} - \rho_{da\ n-1}^{k} \cdot w_{da\ n-1}^{k}}{\Delta x^2}$$

$$- f_v \cdot \rho_d \cdot D_{s,e\ n}^{k} \cdot h_{s\ n}^{k} \cdot \frac{w_{d\ n}^{k} - w_{d\ n-1}^{k}}{\Delta x^2}$$

$$+ \frac{r_{sv} \cdot \alpha_{m\ n}^{k} \cdot (\rho_{a\ n}^{k} \cdot w_{a\ n}^{k} - \rho_{da\ n}^{k} \cdot w_{da\ n}^{k}) \cdot h_{vda\ n}^{k}}{2} - \frac{r_{sv} \cdot \alpha_{h\ n}^{k} \cdot (t_{d\ n}^{k} - t_{a\ n}^{k})}{2}$$

(4.67b)

for desorption.

Substituting Equations 2.61, 2.63a, 2.68a and 2.71 into Equations 4.65, 4.66 and 4.67 the discretized energy conservation equations on matrixcan be expressed as

$$f_v \cdot \varepsilon_p \cdot \rho_{da\ i}^k \cdot \frac{c_{pda\ i}^k \cdot t_{d\ i}^k + w_{da\ i}^k \cdot (h_{fg,0} + c_{pvda\ i}^k \cdot t_{d\ i}^k)}{\Delta\tau}$$

$$+ f_v \cdot \rho_d \cdot \frac{c_d \cdot t_{d\ i}^k + w_{d\ i}^k \cdot (h_{fg,0} + c_{pvda\ i}^k \cdot t_{d\ i}^k - q_{st\ i}^k)}{\Delta\tau}$$

$$- \frac{f_v \cdot \rho_d \cdot h_{f\ i}^{k-1}}{\Delta\tau} + r_m \cdot \rho_m \cdot c_m \cdot \frac{t_{d\ i}^k - t_{d\ i}^{k-1}}{\Delta\tau}$$

$$= (\lambda_{d\ i}^k \cdot f_v + \lambda_m \cdot r_m) \cdot \frac{t_{d\ i+1}^k - 2 \cdot t_{d\ i}^k + t_{d\ i-1}^k}{\Delta x^2}$$

$$+ f_v \cdot D_{o,K,e\ i}^k \cdot (h_{fg,0} + c_{pvda\ i}^k \cdot t_{d\ i}^k) \cdot \frac{\rho_{da\ i+1}^k \cdot w_{da\ i+1}^k - 2 \cdot \rho_{da\ i}^k \cdot w_{da\ i}^k + \rho_{da\ i-1}^k \cdot w_{da\ i-1}^k}{\Delta x^2}$$

$$+ f_v \cdot \rho_d \cdot D_{s,e\ i}^k \cdot (h_{fg,0} + c_{pvda\ i}^k \cdot t_{d\ i}^k - q_{st\ i}^k) \cdot \frac{w_{d\ i+1}^k - 2 \cdot w_{d\ i}^k + w_{d\ i-1}^k}{\Delta x^2}$$

$$+ r_{sv} \cdot \alpha_{m\ i}^k \cdot (\rho_{a\ i}^k \cdot w_{a\ i}^k - \rho_{da\ i}^k \cdot w_{da\ i}^k) \cdot (h_{fg,0} + c_{pva\ i}^k \cdot t_{a\ i}^k)$$

$$- r_{sv} \cdot \alpha_{h\ i}^k \cdot (t_{d\ i}^k - t_{a\ i}^k) \qquad (i = 2,\ 3,\ \cdots,\ n-1) \quad (4.68a)$$

for adsorption,

$$f_v \cdot \varepsilon_p \cdot \rho_{da\ i}^k \cdot \frac{c_{pda\ i}^k \cdot t_{d\ i}^k + w_{da\ i}^k \cdot (h_{fg,0} + c_{pvda\ i}^k \cdot t_{d\ i}^k)}{\Delta\tau}$$

$$+ f_v \cdot \rho_d \cdot \frac{c_d \cdot t_{d\ i}^k + w_{d\ i}^k \cdot (h_{fg,0} + c_{pvda\ i}^k \cdot t_{d\ i}^k - q_{st\ i}^k)}{\Delta\tau}$$

$$- \frac{f_v \cdot \rho_d \cdot h_{f\ i}^{k-1}}{\Delta\tau} + r_m \cdot \rho_m \cdot c_m \cdot \frac{t_{d\ i}^k - t_{d\ i}^{k-1}}{\Delta\tau}$$

$$= (\lambda_{d\ i}^k \cdot f_v + \lambda_m \cdot r_m) \cdot \frac{t_{d\ i+1}^k - 2 \cdot t_{d\ i}^k + t_{d\ i-1}^k}{\Delta x^2}$$

$$+ f_v \cdot D_{o,K,e\ i}^k \cdot (h_{fg,0} + c_{pvda\ i}^k \cdot t_{d\ i}^k)$$

$$\cdot \frac{\rho_{da\ i+1}^k \cdot w_{da\ i+1}^k - 2 \cdot \rho_{da\ i}^k \cdot w_{da\ i}^k + \rho_{da\ i-1}^k \cdot w_{da\ i-1}^k}{\Delta x^2}$$

$$+ f_v \cdot \rho_d \cdot D_{s,e\ i}^k \cdot (h_{fg,0} + c_{pvda\ i}^k \cdot t_{d\ i}^k - q_{st\ i}^k) \cdot \frac{w_{d\ i+1}^k - 2 \cdot w_{d\ i}^k + w_{d\ i-1}^k}{\Delta x^2}$$

$$+ r_{sv} \cdot \alpha_{m\ i}^k \cdot (\rho_{a\ i}^k \cdot w_{a\ i}^k - \rho_{da\ i}^k \cdot w_{da\ i}^k) \cdot (h_{fg,0} + c_{pvda\ i}^k \cdot t_{d\ i}^k)$$

$$- r_{sv} \cdot \alpha_{h\ i}^k \cdot (t_{d\ i}^k - t_{a\ i}^k) \qquad (i = 2,\ 3,\ \cdots,\ n-1) \quad (4.68b)$$

for desorption,

$$f_v \cdot \varepsilon_p \cdot \rho^k_{da\ 1} \cdot \frac{c^k_{pda\ 1} \cdot t^k_{d\ 1} + w^k_{da\ 1} \cdot (h_{fg,0} + c^k_{pvda\ 1} \cdot t^k_{d\ 1})}{2 \cdot \Delta\tau}$$

$$+ f_v \cdot \rho_d \cdot \frac{c_d \cdot t^k_{d\ 1} + w^k_{d\ 1} \cdot (h_{fg,0} + c^k_{pvda\ 1} \cdot t^k_{d\ 1} - q^k_{st\ 1})}{2 \cdot \Delta\tau}$$

$$- \frac{f_v \cdot \rho_d \cdot h^{k-1}_{f\ 1}}{2 \cdot \Delta\tau} + r_m \cdot \rho_m \cdot c_m \cdot \frac{t^k_{d\ 1} - t^{k-1}_{d\ 1}}{2 \cdot \Delta\tau}$$

$$= (\lambda^k_{d\ 1} \cdot f_v + \lambda_m \cdot r_m) \cdot \frac{t^k_{d\ 2} - t^k_{d\ 1}}{\Delta x^2}$$

$$+ f_v \cdot D^k_{o,K,e\ 1} \cdot (h_{fg,0} + c^k_{pvda\ 1} \cdot t^k_{d\ 1}) \cdot \frac{\rho^k_{da\ 2} \cdot w^k_{da\ 2} - \rho^k_{da\ 1} \cdot w^k_{da\ 1}}{\Delta x^2}$$

$$+ f_v \cdot \rho_d \cdot D^k_{s,e\ 1} \cdot (h_{fg,0} + c^k_{pvda\ 1} \cdot t^k_{d\ 1} - q^k_{st\ 1}) \cdot \frac{w^k_{d\ 2} - w^k_{d\ 1}}{\Delta x^2}$$

$$+ \frac{r_{sv} \cdot \alpha^k_{m\ 1} \cdot (\rho^k_{a\ 1} \cdot w^k_{a\ 1} - \rho^k_{da\ 1} \cdot w^k_{da\ 1}) \cdot (h_{fg,0} + c^k_{pva\ 1} \cdot t^k_{a\ 1})}{2}$$

$$- \frac{r_{sv} \cdot \alpha^k_{h\ 1} \cdot (t^k_{d\ 1} - t^k_{a\ 1})}{2} \qquad (4.69a)$$

for adsorption,

$$f_v \cdot \varepsilon_p \cdot \rho_{da\ 1}^k \cdot \frac{c_{pda\ 1}^k \cdot t_{d\ 1}^k + w_{da\ 1}^k \cdot (h_{fg,0} + c_{pvda\ 1}^k \cdot t_{d\ 1}^k)}{2 \cdot \Delta\tau}$$

$$+ f_v \cdot \rho_d \cdot \frac{c_d \cdot t_{d\ 1}^k + w_{d\ 1}^k \cdot (h_{fg,0} + c_{pvda\ 1}^k \cdot t_{d\ 1}^k - q_{st\ 1}^k)}{2 \cdot \Delta\tau}$$

$$- \frac{f_v \cdot \rho_d \cdot h_{f\ 1}^{k-1}}{2 \cdot \Delta\tau} + r_m \cdot \rho_m \cdot c_m \cdot \frac{t_{d\ 1}^k - t_{d\ 1}^{k-1}}{2 \cdot \Delta\tau}$$

$$= (\lambda_{d\ 1}^k \cdot f_v + \lambda_m \cdot r_m) \cdot \frac{t_{d\ 2}^k - t_{d\ 1}^k}{\Delta x^2}$$

$$+ f_v \cdot D_{o,K,e\ 1}^k \cdot (h_{fg,0} + c_{pvda\ 1}^k \cdot t_{d\ 1}^k) \cdot \frac{\rho_{da\ 2}^k \cdot w_{da\ 2}^k - \rho_{da\ 1}^k \cdot w_{da\ 1}^k}{\Delta x^2}$$

$$+ f_v \cdot \rho_d \cdot D_{s,e\ 1}^k \cdot (h_{fg,0} + c_{pvda\ 1}^k \cdot t_{d\ 1}^k - q_{st\ 1}^k) \cdot \frac{w_{d\ 2}^k - w_{d\ 1}^k}{\Delta x^2}$$

$$+ \frac{r_{sv} \cdot \alpha_{m\ 1}^k \cdot (\rho_{a\ 1}^k \cdot w_{a\ 1}^k - \rho_{da\ 1}^k \cdot w_{da\ 1}^k) \cdot (h_{fg,0} + c_{pvda\ 1}^k \cdot t_{d\ 1}^k)}{2}$$

$$- \frac{r_{sv} \cdot \alpha_{h\ 1}^k \cdot (t_{d\ 1}^k - t_{a\ 1}^k)}{2} \qquad (4.69b)$$

for desorption,

$$f_v \cdot \varepsilon_p \cdot \rho^k_{da\ n} \cdot \frac{c^k_{pda\ n} \cdot t^k_{d\ n} + w^k_{da\ n} \cdot (h_{fg,0} + c^k_{pvda\ n} \cdot t^k_{d\ n})}{2 \cdot \Delta\tau}$$

$$+ f_v \cdot \rho_d \cdot \frac{c_d \cdot t^k_{d\ n} + w^k_{d\ n} \cdot (h_{fg,0} + c^k_{pvda\ n} \cdot t^k_{d\ n} - q^k_{si\ n})}{2 \cdot \Delta\tau}$$

$$- \frac{f_v \cdot \rho_d \cdot h^{k-1}_{f\ n}}{2 \cdot \Delta\tau} + r_m \cdot \rho_m \cdot c_m \cdot \frac{t^k_{d\ n} - t^{k-1}_{d\ n}}{2 \cdot \Delta\tau}$$

$$= -(\lambda^k_{d\ n} \cdot f_v + \lambda_m \cdot r_m) \cdot \frac{t^k_{d\ n} - t^k_{d\ n-1}}{\Delta x^2}$$

$$- f_v \cdot D^k_{o,K,e\ n} \cdot (h_{fg,0} + c^k_{pvda\ n} \cdot t^k_{d\ n}) \cdot \frac{\rho^k_{da\ n} \cdot w^k_{da\ n} - \rho^k_{da\ n-1} \cdot w^k_{da\ n-1}}{\Delta x^2}$$

$$- f_v \cdot \rho_d \cdot D^k_{s,e\ n} \cdot (h_{fg,0} + c^k_{pvda\ n} \cdot t^k_{d\ n} - q^k_{si\ n}) \cdot \frac{w^k_{d\ n} - w^k_{d\ n-1}}{\Delta x^2}$$

$$+ \frac{r_{sv} \cdot \alpha^k_{m\ n} \cdot (\rho^k_{a\ n} \cdot w^k_{a\ n} - \rho^k_{da\ n} \cdot w^k_{da\ n}) \cdot (h_{fg,0} + c^k_{pva\ n} \cdot t^k_{a\ n})}{2}$$

$$- \frac{r_{sv} \cdot \alpha^k_{h\ n} \cdot (t^k_{d\ n} - t^k_{a\ n})}{2} \qquad (4.70a)$$

for adsorption, and

$$f_v \cdot \varepsilon_p \cdot \rho^k_{da\ n} \cdot \frac{c^k_{pda\ n} \cdot t^k_{d\ n} + w^k_{da\ n} \cdot (h_{fg,0} + c^k_{pvda\ n} \cdot t^k_{d\ n})}{2 \cdot \Delta\tau}$$

$$+ f_v \cdot \rho_d \cdot \frac{c_d \cdot t^k_{d\ n} + w^k_{d\ n} \cdot (h_{fg,0} + c^k_{pvda\ n} \cdot t^k_{d\ n} - q^k_{st\ n})}{2 \cdot \Delta\tau}$$

$$- \frac{f_v \cdot \rho_d \cdot h^{k-1}_{f\ n}}{2 \cdot \Delta\tau} + r_m \cdot \rho_m \cdot c_m \cdot \frac{t^k_{d\ n} - t^{k-1}_{d\ n}}{2 \cdot \Delta\tau}$$

$$= -(\lambda^k_{d\ n} \cdot f_v + \lambda_m \cdot r_m) \cdot \frac{t^k_{d\ n} - t^k_{d\ n-1}}{\Delta x^2}$$

$$- f_v \cdot D^k_{o,K,e\ n} \cdot (h_{fg,0} + c^k_{pvda\ n} \cdot t^k_{d\ n}) \cdot \frac{\rho^k_{da\ n} \cdot w^k_{da\ n} - \rho^k_{da\ n-1} \cdot w^k_{da\ n-1}}{\Delta x^2}$$

$$- f_v \cdot \rho_d \cdot D^k_{s,e\ n} \cdot (h_{fg,0} + c^k_{pvda\ n} \cdot t^k_{d\ n} - q^k_{st\ n}) \cdot \frac{w^k_{d\ n} - w^k_{d\ n-1}}{\Delta x^2}$$

$$+ \frac{r_{sv} \cdot \alpha^k_{m\ n} \cdot (\rho^k_{a\ n} \cdot w^k_{a\ n} - \rho^k_{da\ n} \cdot w^k_{da\ n}) \cdot (h_{fg,0} + c^k_{pdva\ n} \cdot t^k_{d\ n})}{2}$$

$$- \frac{r_{sv} \cdot \alpha^k_{h\ n} \cdot (t^k_{d\ n} - t^k_{a\ n})}{2} \qquad (4.70b)$$

for desorption.

4.5 Solution of Energy Conservation Equations

The discretized equations of energy conservation were solved using the Tridiagonal Matrix Algorithm for double variables. The Equations 4.61 to 4.64, and 4.68 to 4.70 can be written in the following form:

$$a_i \cdot t^k_{a\ i} = b_i \cdot t^k_{a\ i+1} + c_i \cdot t^k_{a\ i-1} + d_i + e_i \cdot t^k_{d\ i} \qquad (4.71)$$

for energy conservation equations on air stream, and

$$A_i \cdot t_{d\ i}^{k} = B_i \cdot t_{d\ i+1}^{k} + C_i \cdot t_{d\ i-1}^{k} + D_i + E_i \cdot t_{a\ i}^{k} \tag{4.72}$$

for energy conservation equations on matrix

where the coefficients are all known and are defined as

$$a_1 = 1 \tag{4.73}$$

$$b_1 = 0 \tag{4.74}$$

$$c_1 = 0 \tag{4.75}$$

$$d_1 = t_{a,p,in}^{k} \quad \text{(adsorption)} \qquad d_1 = t_{a,r,in}^{k} \quad \text{(desorption)} \tag{4.76}$$

$$e_1 = 0 \tag{4.77}$$

$$a_i = \frac{r_a \cdot \rho_{a\ i}^{k} \cdot c_{pa\ i}^{k}}{\Delta\tau} + \frac{r_a \cdot \rho_{a\ i}^{k} \cdot w_{a\ i}^{k} \cdot c_{pva\ i}^{k}}{\Delta\tau}$$

$$+ r_{sv} \cdot \alpha_{m\ i}^{k} \cdot (\rho_{a\ i}^{k} \cdot w_{a\ i}^{k} - \rho_{da\ i}^{k} \cdot w_{da\ i}^{k}) \cdot c_{pva\ i}^{k} + r_{sv} \cdot \alpha_{h\ i}^{k}$$

(adsorption) (4.78a)

$$a_i = \frac{r_a \cdot \rho_{a\ i}^{k} \cdot c_{pa\ i}^{k}}{\Delta\tau} + \frac{r_a \cdot \rho_{a\ i}^{k} \cdot w_{a\ i}^{k} \cdot c_{pva\ i}^{k}}{\Delta\tau} + r_{sv} \cdot \alpha_{h\ i}^{k}$$

(desorption) (4.78b)

$$b_i = -\frac{r_a \cdot f_a \cdot c_{pa\ i+1}^{k}}{2 \cdot \Delta x} - \frac{r_a \cdot f_a \cdot w_{a\ i+1}^{k} \cdot c_{pva\ i+1}^{k}}{2 \cdot \Delta x} \tag{4.79}$$

$$c_i = \frac{r_a \cdot f_a \cdot c_{pa\ i-1}^{k}}{2 \cdot \Delta x} + \frac{r_a \cdot f_a \cdot w_{a\ i-1}^{k} \cdot c_{pva\ i-1}^{k}}{2 \cdot \Delta x} \tag{4.80}$$

$$d_i = -\frac{r_a \cdot \rho_{a\ i}^k \cdot w_{a\ i}^k \cdot h_{fg,0}}{\Delta\tau} + \frac{r_a \cdot \rho_{a\ i}^{k-1} \cdot h_{a\ i}^{k-1}}{\Delta\tau} - \frac{r_a \cdot f_a \cdot w_{a\ i+1}^k \cdot h_{fg,0}}{2 \cdot \Delta x}$$

$$+ \frac{r_a \cdot f_a \cdot w_{a\ i-1}^k \cdot h_{fg,0}}{2 \cdot \Delta x} - r_{sv} \cdot \alpha_{m\ i}^k \cdot (\rho_{a\ i}^k \cdot w_{a\ i}^k - \rho_{da\ i}^k \cdot w_{da\ i}^k) \cdot h_{fg,0}$$

(4.81)

$$e_i = r_{sv} \cdot \alpha_{h\ i}^k \qquad \text{(adsorption)} \quad (4.82a)$$

$$e_i = -r_{sv} \cdot \alpha_{m\ i}^k \cdot (\rho_{a\ i}^k \cdot w_{a\ i}^k - \rho_{da\ i}^k \cdot w_{da\ i}^k) \cdot c_{pvda\ i}^k + r_{sv} \cdot \alpha_{h\ i}^k$$

(desorption) (4.82b)

$$a_n = \frac{r_a \cdot \rho_{a\ n}^k \cdot c_{pa\ n}^k}{\Delta\tau} + \frac{r_a \cdot \rho_{a\ n}^k \cdot w_{a\ n}^k \cdot c_{pva\ n}^k}{\Delta\tau} + \frac{r_a \cdot f_a \cdot c_{pa\ n}^k}{\Delta x}$$

$$+ \frac{r_a \cdot f_a \cdot w_{a\ n}^k \cdot c_{pva\ n}^k}{\Delta x} + r_{sv} \cdot \alpha_{m\ n}^k \cdot (\rho_{a\ n}^k \cdot w_{a\ n}^k - \rho_{da\ n}^k \cdot w_{da\ n}^k) \cdot c_{pva\ n}^k$$

$$+ r_{sv} \cdot \alpha_{h\ n}^k \qquad \text{(adsorption)} \quad (4.83a)$$

$$a_n = \frac{r_a \cdot \rho_{a\ n}^k \cdot c_{pa\ n}^k}{\Delta\tau} + \frac{r_a \cdot \rho_{a\ n}^k \cdot w_{a\ n}^k \cdot c_{pva\ n}^k}{\Delta\tau} + \frac{r_a \cdot f_a \cdot c_{pa\ n}^k}{\Delta x}$$

$$+ \frac{r_a \cdot f_a \cdot w_{a\ n}^k \cdot c_{pva\ n}^k}{\Delta x} + r_{sv} \cdot \alpha_{h\ n}^k \qquad \text{(desorption)} \quad (4.83b)$$

$$b_n = 0 \qquad (4.84)$$

$$c_n = \frac{r_a \cdot f_a \cdot c_{pa\ n-1}^k}{\Delta x} + \frac{r_a \cdot f_a \cdot w_{a\ n-1}^k \cdot c_{pva\ n-1}^k}{\Delta x} \qquad (4.85)$$

$$d_n = -\frac{r_a \cdot \rho_{a\ n}^{k} \cdot w_{a\ n}^{k} \cdot h_{fg,0}}{\Delta\tau} + \frac{r_a \cdot \rho_{a\ n}^{k-1} \cdot h_{a\ n}^{k-1}}{\Delta\tau} - \frac{r_a \cdot f_a \cdot w_{a\ n}^{k} \cdot h_{fg,0}}{\Delta x}$$

$$+ \frac{r_a \cdot f_a \cdot w_{a\ n-1}^{k} \cdot h_{fg,0}}{\Delta x} - r_{sv} \cdot \alpha_{m\ n}^{k} \cdot (\rho_{a\ n}^{k} \cdot w_{a\ n}^{k} - \rho_{da\ n}^{k} \cdot w_{da\ n}^{k}) \cdot h_{fg,0}$$

(4.86)

$$e_n = r_{sv} \cdot \alpha_{h\ n}^{k} \qquad \text{(adsorption)} \quad (4.87a)$$

$$e_n = -r_{sv} \cdot \alpha_{m\ n}^{k} \cdot (\rho_{a\ n}^{k} \cdot w_{a\ n}^{k} - \rho_{da\ n}^{k} \cdot w_{da\ n}^{k}) \cdot c_{pvda\ n}^{k} + r_{sv} \cdot \alpha_{h\ n}^{k}$$

(desorption) (4.87b)

$$A_1 = \frac{f_v \cdot \varepsilon_p \cdot \rho_{da\ 1}^{k} \cdot c_{pda\ 1}^{k}}{2 \cdot \Delta\tau} + \frac{f_v \cdot \varepsilon_p \cdot \rho_{da\ 1}^{k} \cdot w_{da\ 1}^{k} \cdot c_{pvda\ 1}^{k}}{2 \cdot \Delta\tau} + \frac{f_v \cdot \rho_d \cdot c_d}{2 \cdot \Delta\tau}$$

$$+ \frac{f_v \cdot \rho_d \cdot w_{d\ 1}^{k} c_{pvda\ 1}^{k}}{2 \cdot \Delta\tau} + \frac{r_m \cdot \rho_m \cdot c_m}{2 \cdot \Delta\tau} + \frac{(\lambda_{d\ 1}^{k} \cdot f_v + \lambda_m \cdot r_m)}{\Delta x^2}$$

$$- f_v \cdot \rho_{da\ 1}^{k} \cdot D_{o,K,e\ 1}^{k} \cdot c_{pvda\ 1}^{k} \cdot \frac{w_{da\ 2}^{k} - w_{da\ 1}^{k}}{\Delta x^2}$$

$$- f_v \cdot \rho_d \cdot D_{s,e\ 1}^{k} \cdot c_{pvda\ 1}^{k} \cdot \frac{w_{d\ 2}^{k} - w_{d\ 1}^{k}}{\Delta x^2} + \frac{r_{sv} \cdot \alpha_{h\ 1}^{k}}{2}$$

(adsorption) (4.88a)

$$A_1 = \frac{f_v \cdot \varepsilon_p \cdot \rho^k_{da\ 1} \cdot c^k_{pda\ 1}}{2 \cdot \Delta\tau} + \frac{f_v \cdot \varepsilon_p \cdot \rho^k_{da\ 1} \cdot w^k_{da\ 1} \cdot c^k_{pvda\ 1}}{2 \cdot \Delta\tau} + \frac{f_v \cdot \rho_d \cdot c_d}{2 \cdot \Delta\tau}$$

$$+ \frac{f_v \cdot \rho_d \cdot w^k_{d\ 1} c^k_{pvda\ 1}}{2 \cdot \Delta\tau} + \frac{r_m \cdot \rho_m \cdot c_m}{2 \cdot \Delta\tau} + \frac{(\lambda^k_{d\ 1} \cdot f_v + \lambda_m \cdot r_m)}{\Delta x^2}$$

$$- f_v \cdot \rho^k_{da\ 1} \cdot D^k_{o,K,e\ 1} \cdot c^k_{pvda\ 1} \cdot \frac{w^k_{da\ 2} - w^k_{da\ 1}}{\Delta x^2}$$

$$- f_v \cdot \rho_d \cdot D^k_{s,e\ 1} \cdot c^k_{pvda\ 1} \cdot \frac{w^k_{d\ 2} - w^k_{d\ 1}}{\Delta x^2} + \frac{r_{sv} \cdot \alpha^k_{h\ 1}}{2}$$

$$- \frac{r_{sv} \cdot \alpha^k_{m\ 1} \cdot (\rho^k_{a\ 1} \cdot w^k_{a\ 1} - \rho^k_{da\ 1} \cdot w^k_{da\ 1}) \cdot c^k_{pvda\ 1}}{2} \quad \text{(desorption)} \qquad (4.88b)$$

$$B_1 = \frac{(\lambda^k_{d\ 1} \cdot f_v + \lambda_m \cdot r_m)}{\Delta x^2} \qquad (4.89)$$

$$C_1 = 0 \qquad (4.90)$$

$$D_1 = -\frac{f_v \cdot \varepsilon_p \cdot \rho^k_{da\ 1} \cdot w^k_{da\ 1} \cdot h_{fg,0}}{2 \cdot \Delta\tau} - f_v \cdot \rho_d \cdot \frac{w^k_{d\ 1} \cdot (h_{fg,0} - q^k_{st\ 1})}{2 \cdot \Delta\tau}$$

$$+ f_v \cdot \rho_d \cdot \frac{h^{k-1}_{f\ 1}}{2 \cdot \Delta\tau} + \frac{r_m \cdot \rho_m \cdot c_m \cdot t^{k-1}_{d\ 1}}{2 \cdot \Delta\tau}$$

$$+ f_v \cdot D^k_{o,K,e\ 1} \cdot h_{fg,0} \cdot \frac{\rho^k_{da\ 2} \cdot w^k_{da\ 2} - \rho^k_{da\ 1} \cdot w^k_{da\ 1}}{\Delta x^2}$$

$$+ f_v \cdot \rho_d \cdot D^k_{s,e\ 1} \cdot (h_{fg,0} - q^k_{st\ 1}) \cdot \frac{w^k_{d\ 2} - w^k_{d\ 1}}{\Delta x^2}$$

$$+ \frac{r_{sv} \cdot \alpha^k_{m\ 1} \cdot (\rho^k_{a\ 1} \cdot w^k_{a\ 1} - \rho^k_{da\ 1} \cdot w^k_{da\ 1}) \cdot h_{fg,0}}{2} \qquad (4.91)$$

$$E_1 = \frac{r_{sv} \cdot \alpha_{m\ 1}^{k} \cdot (\rho_{a\ 1}^{k} \cdot w_{a\ 1}^{k} - \rho_{da\ 1}^{k} \cdot w_{da\ 1}^{k}) \cdot c_{pva\ 1}^{k}}{2} + \frac{r_{sv} \cdot \alpha_{h\ 1}^{k}}{2}$$

(adsorption) (4.92a)

$$E_1 = \frac{r_{sv} \cdot \alpha_{h\ 1}^{k}}{2}$$ (adsorption) (4.92b)

$$A_i = \frac{f_v \cdot \varepsilon_p \cdot \rho_{da\ i}^{k} \cdot c_{pda\ i}^{k}}{\Delta\tau} + \frac{f_v \cdot \varepsilon_p \cdot \rho_{da\ i}^{k} \cdot w_{da\ i}^{k} \cdot c_{pvda\ i}^{k}}{\Delta\tau} + \frac{f_v \cdot \rho_d \cdot c_d}{\Delta\tau}$$

$$+ \frac{f_v \cdot \rho_d \cdot w_{d\ i}^{k} \cdot c_{pvda\ i}^{k}}{\Delta\tau} + \frac{r_m \cdot \rho_m \cdot c_m}{\Delta\tau} + \frac{2 \cdot (\lambda_{d\ i}^{k} \cdot f_v + \lambda_m \cdot r_m)}{\Delta x^2}$$

$$- f_v \cdot D_{o,K,e\ i}^{k} \cdot c_{pvda\ i}^{k} \cdot \frac{\rho_{da\ i+1}^{k} \cdot w_{da\ i+1}^{k} - 2 \cdot \rho_{da\ i}^{k} \cdot w_{da\ i}^{k} + \rho_{da\ i-1}^{k} \cdot w_{da\ i-1}^{k}}{\Delta x^2}$$

$$- f_v \cdot \rho_d \cdot D_{s,e\ i}^{k} \cdot c_{pvda\ i}^{k} \cdot \frac{w_{d\ i+1}^{k} - 2 \cdot w_{d\ i}^{k} + w_{d\ i-1}^{k}}{\Delta x^2} + r_{sv} \cdot \alpha_{h\ i}^{k}$$

(adsorption) (4.93a)

$$A_i = \frac{f_v \cdot \varepsilon_p \cdot \rho_{da\ i}^{k} \cdot c_{pda\ i}^{k}}{\Delta\tau} + \frac{f_v \cdot \varepsilon_p \cdot \rho_{da\ i}^{k} \cdot w_{da\ i}^{k} \cdot c_{pvda\ i}^{k}}{\Delta\tau} + \frac{f_v \cdot \rho_d \cdot c_d}{\Delta\tau}$$

$$+ \frac{f_v \cdot \rho_d \cdot w_{d\ i}^{k} \cdot c_{pvda\ i}^{k}}{\Delta\tau} + \frac{r_m \cdot \rho_m \cdot c_m}{\Delta\tau} + \frac{2 \cdot (\lambda_{d\ i}^{k} \cdot f_v + \lambda_m \cdot r_m)}{\Delta x^2}$$

$$- f_v \cdot D_{o,K,e\ i}^{k} \cdot c_{pvda\ i}^{k} \cdot \frac{\rho_{da\ i+1}^{k} \cdot w_{da\ i+1}^{k} - 2 \cdot \rho_{da\ i}^{k} \cdot w_{da\ i}^{k} + \rho_{da\ i-1}^{k} \cdot w_{da\ i-1}^{k}}{\Delta x^2}$$

$$- f_v \cdot \rho_d \cdot D_{s,e\ i}^{k} \cdot c_{pvda\ i}^{k} \cdot \frac{w_{d\ i+1}^{k} - 2 \cdot w_{d\ i}^{k} + w_{d\ i-1}^{k}}{\Delta x^2} + r_{sv} \cdot \alpha_{h\ i}^{k}$$

$$- r_{sv} \cdot \alpha_{m\ i}^{k} \cdot (\rho_{a\ i}^{k} \cdot w_{a\ i}^{k} - \rho_{da\ i}^{k} \cdot w_{da\ i}^{k}) \cdot c_{pvda\ i}^{k}$$ (desorption) (4.93b)

$$B_i = \frac{(\lambda_{d\ i}^{k} \cdot f_v + \lambda_m \cdot r_m)}{\Delta x^2}$$ (4.94)

$$C_i = \frac{(\lambda_{d\ i}^{k} \cdot f_v + \lambda_m \cdot r_m)}{\Delta x^2} \tag{4.95}$$

$$D_i = -\frac{f_v \cdot \varepsilon_p \cdot \rho_{da\ i}^{k} \cdot w_{da\ i}^{k} \cdot h_{fg,0}}{\Delta \tau} - f_v \cdot \rho_d \cdot \frac{w_{d\ i}^{k} \cdot (h_{fg,0} - q_{st\ i}^{k})}{\Delta \tau} + \frac{f_v \cdot \rho_d \cdot h_{f\ i}^{k-1}}{\Delta \tau}$$

$$+ \frac{r_m \cdot \rho_m \cdot c_m \cdot t_{d\ i}^{k-1}}{\Delta \tau}$$

$$+ f_v \cdot \rho_{da\ i}^{k} \cdot D_{o,K,e\ i}^{k} \cdot h_{fg,0} \cdot \frac{\rho_{da\ i+1}^{k} \cdot w_{da\ i+1}^{k} - 2 \cdot \rho_{da\ i}^{k} \cdot w_{da\ i}^{k} + \rho_{da\ i-1}^{k} \cdot w_{da\ i-1}^{k}}{\Delta x^2}$$

$$+ f_v \cdot \rho_d \cdot D_{s,e\ i}^{k} \cdot (h_{fg,0} - q_{st\ i}^{k}) \cdot \frac{w_{d\ i+1}^{k} - 2 \cdot w_{d\ i}^{k} + w_{d\ i-1}^{k}}{\Delta x^2}$$

$$+ r_{sv} \cdot \alpha_{m\ i}^{k} \cdot (\rho_{a\ i}^{k} \cdot w_{a\ i}^{k} - \rho_{da\ i}^{k} \cdot w_{da\ i}^{k}) \cdot h_{fg,0} \tag{4.96}$$

$$E_i = r_{sv} \cdot \alpha_{m\ i}^{k} \cdot (\rho_{a\ i}^{k} \cdot w_{a\ i}^{k} - \rho_{da\ i}^{k} \cdot w_{da\ i}^{k}) \cdot c_{pva\ i}^{k} + r_{sv} \cdot \alpha_{h\ i}^{k}$$

(adsorption) (4.97a)

$$E_i = r_{sv} \cdot \alpha_{h\ i}^{k} \qquad \text{(desorption)} \quad (4.97b)$$

$$A_n = \frac{f_v \cdot \varepsilon_p \cdot \rho_{da\ n}^{k} \cdot c_{pda\ n}^{k}}{2 \cdot \Delta \tau} + \frac{f_v \cdot \varepsilon_p \cdot \rho_{da\ n}^{k} \cdot w_{da\ n}^{k} \cdot c_{pvda\ n}^{k}}{2 \cdot \Delta \tau} + \frac{f_v \cdot \rho_d \cdot c_d}{2 \cdot \Delta \tau}$$

$$+ \frac{f_v \cdot \rho_d \cdot w_{d\ n}^{k} \cdot c_{pvda\ n}^{k}}{2 \cdot \Delta \tau} + \cdot \frac{r_m \cdot \rho_m \cdot c_m}{2 \cdot \Delta \tau} + \frac{(\lambda_{d\ n}^{k} \cdot f_v + \lambda_m \cdot r_m)}{\Delta x^2}$$

$$+ f_v \cdot D_{o,K,e\ n}^{k} \cdot c_{pvda\ n}^{k} \cdot \frac{\rho_{da\ n}^{k} \cdot w_{da\ n}^{k} - \rho_{da\ n-1}^{k} \cdot w_{da\ n-1}^{k}}{\Delta x^2}$$

$$+ f_v \cdot \rho_d \cdot D_{s,e\ n}^{k} \cdot c_{pvda\ n}^{k} \cdot \frac{w_{d\ n}^{k} - w_{d\ n-1}^{k}}{\Delta x^2} + \frac{r_{sv} \cdot \alpha_{h\ n}^{k}}{2}$$

(adsorption) (4.98a)

$$A_n = \frac{f_v \cdot \varepsilon_p \cdot \rho^k_{da\ n} \cdot c^k_{pda\ n}}{2 \cdot \Delta\tau} + \frac{f_v \cdot \varepsilon_p \cdot \rho^k_{da\ n} \cdot w^k_{da\ n} \cdot c^k_{pvda\ n}}{2 \cdot \Delta\tau} + \frac{f_v \cdot \rho_d \cdot c_d}{2 \cdot \Delta\tau}$$

$$+ \frac{f_v \cdot \rho_d \cdot w^k_{d\ n} \cdot c^k_{pvda\ n}}{2 \cdot \Delta\tau} + \cdot \frac{r_m \cdot \rho_m \cdot c_m}{2 \cdot \Delta\tau} + \frac{(\lambda^k_{d\ n} \cdot f_v + \lambda_m \cdot r_m)}{\Delta x^2}$$

$$+ f_v \cdot D^k_{o,K,e\ n} \cdot c^k_{pvda\ n} \cdot \frac{\rho^k_{da\ n} \cdot w^k_{da\ n} - \rho^k_{da\ n-1} \cdot w^k_{da\ n-1}}{\Delta x^2}$$

$$+ f_v \cdot \rho_d \cdot D^k_{s,e\ n} \cdot c^k_{pvda\ n} \cdot \frac{w^k_{d\ n} - w^k_{d\ n-1}}{\Delta x^2} + \frac{r_{sv} \cdot \alpha^k_{h\ n}}{2}$$

$$- \frac{r_{sv} \cdot \alpha^k_{m\ n} \cdot (\rho^k_{a\ n} \cdot w^k_{a\ n} - \rho^k_{da\ n} \cdot w^k_{da\ n}) \cdot c^k_{pvda\ n}}{2}$$

(desorption) (4.98b)

$$B_n = 0 \tag{4.99}$$

$$C_n = \frac{(\lambda^k_{d\ n} \cdot f_v + \lambda_m \cdot r_m)}{\Delta x^2} \tag{4.100}$$

$$D_n = -\frac{f_v \cdot \varepsilon_p \cdot \rho^k_{da\ n} \cdot w^k_{da\ n} \cdot h_{fg,0}}{2 \cdot \Delta\tau} - \frac{f_v \cdot \rho_d \cdot w^k_{d\ n} \cdot (h_{fg,0} - q^k_{st\ n})}{2 \cdot \Delta\tau} + \frac{f_v \cdot \rho_d \cdot h^{k-1}_{f\ n}}{2 \cdot \Delta\tau}$$

$$+ \frac{r_m \cdot \rho_m \cdot c_m \cdot t^{k-1}_{d\ n}}{2 \cdot \Delta\tau} - f_v \cdot D^k_{o,K,e\ n} \cdot h_{fg,0} \cdot \frac{\rho^k_{da\ n} \cdot w^k_{da\ n} - \rho^k_{da\ n-1} \cdot w^k_{da\ n-1}}{\Delta x^2}$$

$$- f_v \cdot \rho_d \cdot D^k_{s,e\ n} \cdot (h_{fg,0} - q^k_{st\ n}) \cdot \frac{w^k_{d\ n} - w^k_{d\ n-1}}{\Delta x^2}$$

$$+ \frac{r_{sv} \cdot \alpha^k_{m\ n} \cdot (\rho^k_{a\ n} \cdot w^k_{a\ n} - \rho^k_{da\ n} \cdot w^k_{da\ n}) \cdot h_{fg,0}}{2} \tag{4.101}$$

$$E_n = \frac{r_{sv} \cdot \alpha^k_{m\ n} \cdot (\rho^k_{a\ n} \cdot w^k_{a\ n} - \rho^k_{da\ n} \cdot w^k_{da\ n}) \cdot c^k_{pva\ n}}{2} + \frac{r_{sv} \cdot \alpha^k_{h\ n}}{2}$$

(adsorption) (4.102a)

$$E_n = \frac{r_{sv} \cdot \alpha_{h\ n}^{k}}{2} \qquad \text{(desorption)} \quad (4.102b)$$

At each point the relations of the type

$$t_{a\ i}^{k} = p_i \cdot t_{a\ i+1}^{k} + q_i + r_i \cdot t_{d\ i}^{k} \qquad (4.103)$$

and $$t_{d\ i}^{k} = PP_i \cdot t_{d\ i+1}^{k} + Q_i + R_i \cdot t_{a\ i}^{k} \qquad (4.104)$$

need to be constructed during the forward marching process from ($i = 2$) to ($i = n-1$). Written for point $i-1$, equations 4.103 and 4.104 read

$$t_{a\ i-1}^{k} = p_{i-1} \cdot t_{a\ i}^{k} + q_{i-1} + r_{i-1} \cdot t_{d\ i-1}^{k} \qquad (4.105)$$

and $$t_{d\ i-1}^{k} = PP_{i-1} \cdot t_{d\ i}^{k} + Q_{i-1} + R_{i-1} \cdot t_{a\ i-1}^{k} \qquad (4.106)$$

Combining Equations 4.105 and 4.106 to eliminate $t_{d\ i-1}^{k}$ yields, after some rearranging,

$$t_{a\ i-1}^{k} = \frac{1}{1 - r_{i-1} \cdot R_{i-1}} \cdot (p_{i-1} \cdot t_{a\ i}^{k} + r_{i-1} \cdot PP_{i-1} \cdot t_{d\ i}^{k} + q_{i-1} + r_{i-1} \cdot Q_{i-1}) \qquad (4.107)$$

Substituting Equation 4.107 into Equation 4.71 yields, after some rearranging,

$$t_{a\ i}^{k} = \frac{b_i \cdot (1 - r_{i-1} \cdot R_{i-1})}{a_i \cdot (1 - r_{i-1} \cdot R_{i-1}) - c_i \cdot p_{i-1}} \cdot t_{a\ i+1}^{k} + \frac{c_i \cdot (q_{i-1} + r_{i-1} \cdot Q_{i-1}) + d_i \cdot (1 - r_{i-1} \cdot R_{i-1})}{a_i \cdot (1 - r_{i-1} \cdot R_{i-1}) - c_i \cdot p_{i-1}}$$

$$+ \frac{e_i \cdot (1 - r_{i-1} \cdot R_{i-1}) + c_i \cdot r_{i-1} \cdot PP_{i-1}}{a_i \cdot (1 - r_{i-1} \cdot R_{i-1}) - c_i \cdot p_{i-1}} \cdot t_{d\ i}^{k} \qquad (4.108)$$

Note that Equation 4.108 is identical to Equation 4.103 with

$$p_i = \frac{b_i \cdot (1 - r_{i-1} \cdot R_{i-1})}{a_i \cdot (1 - r_{i-1} \cdot R_{i-1}) - c_i \cdot p_{i-1}} \qquad (4.109)$$

$$q_i = \frac{c_i \cdot (q_{i-1} + r_{i-1} \cdot Q_{i-1}) + d_i \cdot (1 - r_{i-1} \cdot R_{i-1})}{a_i \cdot (1 - r_{i-1} \cdot R_{i-1}) - c_i \cdot p_{i-1}} \tag{4.110}$$

$$r_i = \frac{e_i \cdot (1 - r_{i-1} \cdot R_{i-1}) + c_i \cdot r_{i-1} \cdot PP_{i-1}}{a_i \cdot (1 - r_{i-1} \cdot R_{i-1}) - c_i \cdot p_{i-1}} \tag{4.111}$$

Combining Equations 4.105 and 4.106 to eliminate $t_{a\ i-1}^{k}$ yields, after some rearranging,

$$t_{d\ i-1}^{k} = \frac{1}{1 - r_{i-1} \cdot R_{i-1}} \cdot (PP_{i-1} \cdot t_{d\ i}^{k} + R_{i-1} \cdot p_{i-1} \cdot t_{a\ i}^{k} + Q_{i-1} + R_{i-1} \cdot q_{i-1}) \tag{4.112}$$

Substituting Equation 4.112 into Equation 4.72 yields, after some rearranging,

$$t_{d\ i}^{k} = \frac{B_i \cdot (1 - r_{i-1} \cdot R_{i-1})}{A_i \cdot (1 - r_{i-1} \cdot R_{i-1}) - C_i \cdot PP_{i-1}} \cdot t_{d\ i+1}^{k}$$

$$+ \frac{C_i \cdot (Q_{i-1} + R_{i-1} \cdot q_{i-1}) + D_i \cdot (1 - r_{i-1} \cdot R_{i-1})}{A_i \cdot (1 - r_{i-1} \cdot R_{i-1}) - C_i \cdot PP_{i-1}}$$

$$+ \frac{E_i \cdot (1 - r_{i-1} \cdot R_{i-1}) + C_i \cdot R_{i-1} \cdot p_{i-1}}{A_i \cdot (1 - r_{i-1} \cdot R_{i-1}) - C_i \cdot PP_{i-1}} \cdot t_{a\ i}^{k} \tag{4.113}$$

Note that Equation 4.113 is identical to Equation 4.104 with

$$PP_i = \frac{B_i \cdot (1 - r_{i-1} \cdot R_{i-1})}{A_i \cdot (1 - r_{i-1} \cdot R_{i-1}) - C_i \cdot PP_{i-1}} \tag{4.114}$$

$$Q_i = \frac{C_i \cdot (Q_{i-1} + R_{i-1} \cdot q_{i-1}) + D_i \cdot (1 - r_{i-1} \cdot R_{i-1})}{A_i \cdot (1 - r_{i-1} \cdot R_{i-1}) - C_i \cdot PP_{i-1}} \tag{4.115}$$

$$R_i = \frac{E_i \cdot (1 - r_{i-1} \cdot R_{i-1}) + C_i \cdot R_{i-1} \cdot p_{i-1}}{A_i \cdot (1 - r_{i-1} \cdot R_{i-1}) - C_i \cdot PP_{i-1}} \tag{4.116}$$

To start the calculation process, applying Equations 4.109, 4.110, 4.111, 4.114, 4.115, and 4.116 for $i=1$ yields

$$p_1 = -\frac{b_1}{a_1} \tag{4.117}$$

$$q_1 = \frac{d_1}{a_1} \tag{4.118}$$

$$r_1 = \frac{e_1}{a_1} \tag{4.119}$$

$$PP_1 = -\frac{B_1}{A_1} \tag{4.120}$$

$$Q_1 = \frac{D_1}{A_1} \tag{4.121}$$

and $$R_1 = \frac{E_1}{A_1} \tag{4.122}$$

Next, Equations 4.109, 4.110, 4.111, 4.114, 4.115, and 4.116 should be used to obtain p_i, q_i, r_i, PP_i, Q_i, and R_i *for* $i=2, 3, \cdots, n$. Since $b_n = 0$ and $B_n = 0$, applying Equations 4.109 and 4.114 yields $p_n = 0$ and $PP_n = 0$, and then applying Equations 4.103 and 4.104 yields

$$t_{a\ n}^{k} = q_n + r_n \cdot t_{d\ n}^{k} \tag{4.123}$$

and $$t_{d\ n}^{k} = Q_n + R_n \cdot t_{a\ n}^{k} \tag{4.124}$$

Combining Equations 4.123 and 4.124 yields

$$t_{a\ n}^{k} = \frac{q_n + r_n \cdot Q_n}{1 - r_n \cdot R_n} \tag{4.125}$$

and $$t_{d\ n}^{k} = \frac{Q_n + R_n \cdot q_n}{1 - r_n \cdot R_n} \tag{4.126}$$

Finally, Equations 4.103 and 4.104 need to be employed for $i = n-1, n-2, \cdots, 3, 2, 1$ to yield the temperature of air stream in process channel t_a and the matrix temperature or the temperature of the moisture air in equilibrium with the solid phase t_d at all interior points.

4.6 Steps Used to Solve the Numerical Problem

The steps used to solve the numerical problem are as follows:

a. Estimate the t_a, t_d, w_d, and w_{da}.

b. Calculate the properties ρ_a, ρ_{da}, c_{pa}, c_{pda}, λ_a, μ_f, μ_w, ν_a, Pr, c_{pva}, c_{pvda}, and q_{st}, the heat and mass transfer coefficient α_h and α_m, the thermal conductivity of desiccant λ_d, and diffusion coefficient $D_{o,K,c}$ and $D_{s,e}$ needed in the discretized equations, which depend on t_a, t_d, w_d respectively.

c. Solve the w_a, w_d, t_a, t_d, and w_{da} fields with the moisture and energy conservation equations on both air stream and matrix and equilibrium isotherm equation.

d. Return to step 2 and iterate until a converged solution is reached.

e. Increment time, return to step 2 and iterate until a quasi-steady solution is obtained.

Trial and error established that the order of solution in step 3 seemed to give the most rapid convergence of the equations. There are two variables w_a and w_{da} in the moisture conservation equation on air stream, three variables w_a, w_d and w_{da} in the moisture conservation equation on desiccant, four variables w_a, t_a, t_d, and w_{da} in the energy conservation equation on air stream, and five variables w_a, w_d, t_a, t_d, and w_{da} in the energy conservation equation on matrix. w_{da} depends on w_d and t_d according equilibrium isotherm equation. To start the calculation process, w_{da} is estimated, and w_a is solved with the moisture conservation equation on air stream. Next, w_d is solved with the moisture conservation equation on desiccant, and then two energy conservation equations need to be employed to solve t_a and t_d. Finally, w_{da} is solved, utilizing equilibrium isotherm equation.

The transient solution is solved until quasi - steady state is reached. Even though the most important result is the quasi – steady solution, the model must be time accurate because the quasi – steady solution is a transient solution that varies periodically. The numerical solution is time accurate because time is only incremented when a converged solution is reached. The residuals of the governing equations are low because the central – difference formula and the Tridiagonal Matrix Algorithm are used. As a result, the convergence criteria are based on the dependent variables change from iteration to iteration. The following is satisfied for each dependent variable:

$$\left|w_{d\ i}^{k} - w_{d\ i}^{k\ *}\right| \le 10^{-3} \tag{4.127}$$

$$\left|t_{a\ i}^{k} - t_{a\ i}^{k\ *}\right| \le 0.1 \tag{4.128}$$

$$\left|t_{d\ i}^{k} - t_{d\ i}^{k\ *}\right| \le 0.1 \tag{4.129}$$

$$\left|w_{da\ i}^{k} - w_{da\ i}^{k\ *}\right| \le 10^{-5} \tag{4.130}$$

where $w_{d\ i}^{k\ *}$, $t_{a\ i}^{k\ *}$, $t_{d\ i}^{k\ *}$ and $w_{da\ i}^{k\ *}$ are estimated values.

Quasi-steady state can be determined using the periodicity of the desiccant wheel. This means that the dependent variable changes from revolution to revolution of the desiccant wheel are all zero (or, negligible). The quasi-steady conditions are defined when:

$$\left|w_{a\ i}^{k} - w_{a\ i}^{k\ *}\right| \le 10^{-5} \tag{4.131}$$

$$\left|w_{d\ i}^{k} - w_{d\ i}^{k\ *}\right| \le 10^{-3} \tag{4.132}$$

$$\left|t_{a\ i}^{k} - t_{a\ i}^{k\ *}\right| \le 0.1 \tag{4.133}$$

$$\left|t_{d\ i}^{k} - t_{d\ i}^{k\ *}\right| \le 0.1 \tag{4.134}$$

$$\left|w_{da\ i}^{k} - w_{da\ i}^{k\ *}\right| \le 10^{-5} \tag{4.135}$$

where $w_{a\ i}^{k\ *}$, $w_{d\ i}^{k\ *}$, $t_{a\ i}^{k\ *}$, $t_{d\ i}^{k\ *}$ and $w_{da\ i}^{k\ *}$ are values of last revolution of the wheel. Therefore, if Equations 4.131 to 4.135 are satisfied, the solution is deemed to be the quasi-steady solution.

The numbers of nodes have no effect on the simulation results in case of convergence, but when the numbers of nodes are little, the equations can not converge under some design and operation conditions. In the model developed in the thesis, n=100, so that the equations can converge under any design and operating conditions.

The time step for the model is

$$\Delta\tau = \frac{\Delta x}{v_c} \tag{4.136}$$

Chapter 5 Validation of the Numerical Model

Some numerical models and theoretical studies of desiccant wheels were reported, but few models and studies were validated by experiments. The purpose of this chapter is to validate the numerical model by comparisons with experimental data.

5.1 Test Rig and Test Method

The test rig was built in accordance with ASHRAE Standard 139 - 1998, Standard Method of Testing for Rating Desiccant Dehumidifiers Utilizing Heat for the Regeneration Process.

5.1.1 Test Loop

A test loop is illustrated in Figure 5.1. It employs a Pitot tube traverse arrangement (Figures 5.2 and 5.3) on the inlet and outlet of the dehumidifier test unit, plus necessary temperature and humidity – measuring stations, and pressure-measuring stations using static - pressure taps (Figure 5.4).

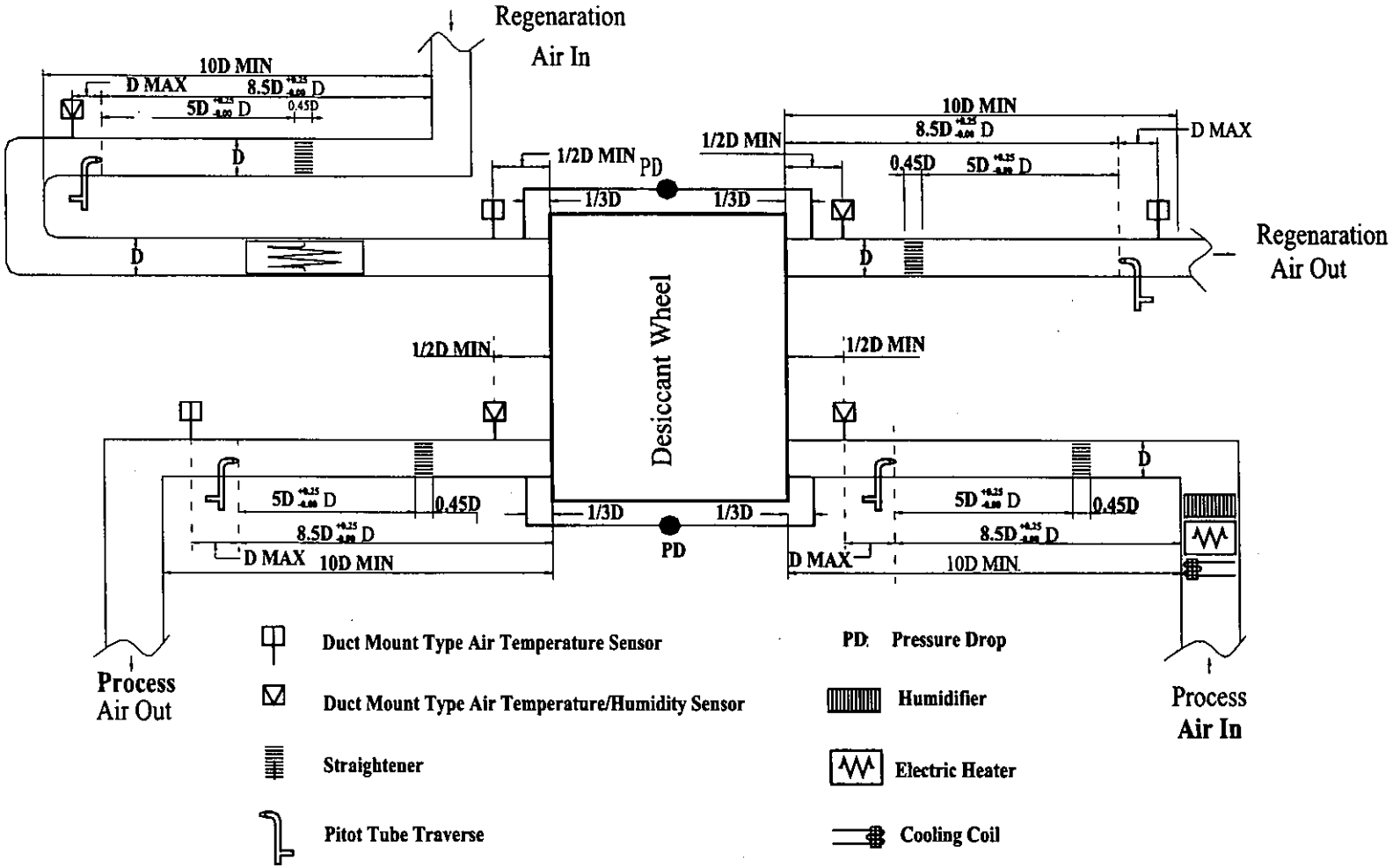

Note: 1.D=150mm

2.Dotted lines on the regeneration air outlet indicate a difuser cone which may be used to approach more nearly free delivery.

Figure 5.1 Test loop for desiccant wheel

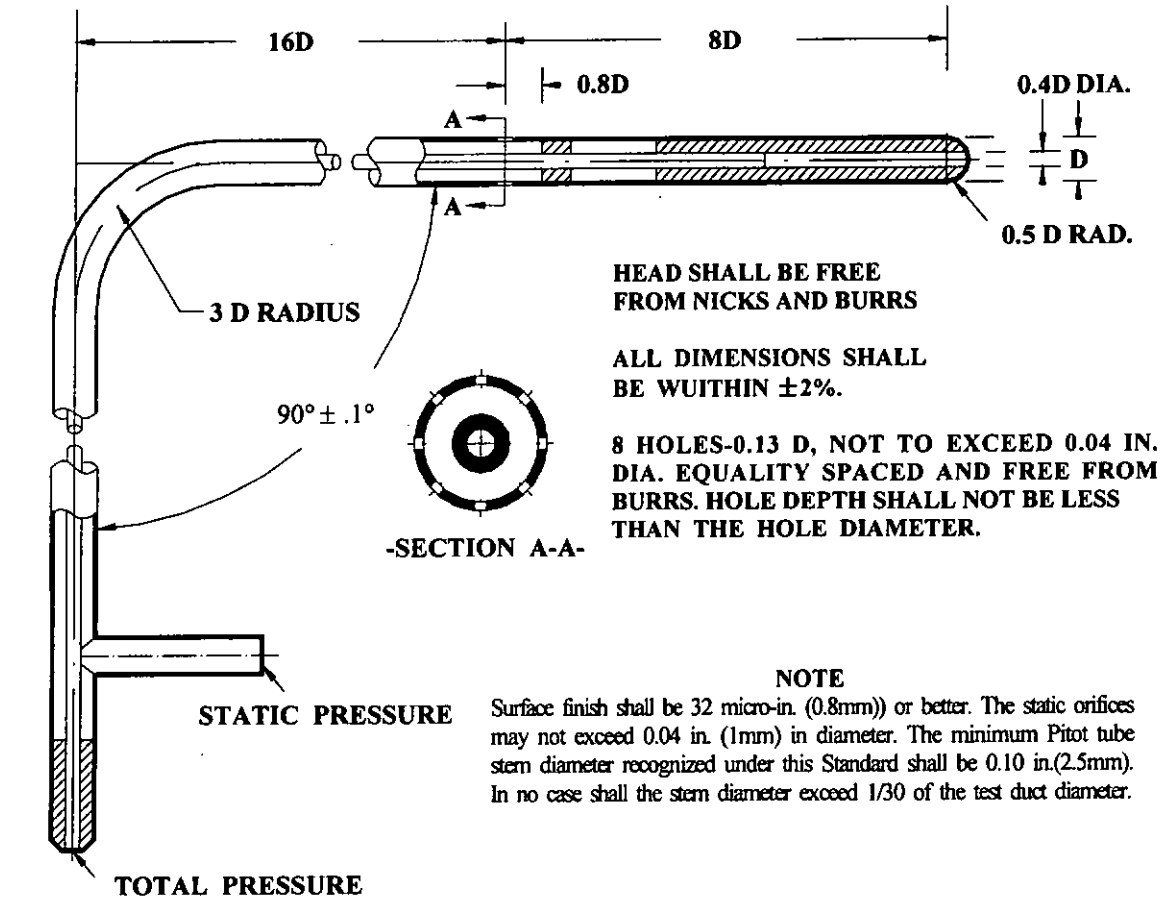

A. Pitot-static tube with spherical head

ALL OTHER DIMENSIONS ARE THE SAME AS FOR SPHERE HEAD PITOT-STATIC TUBES

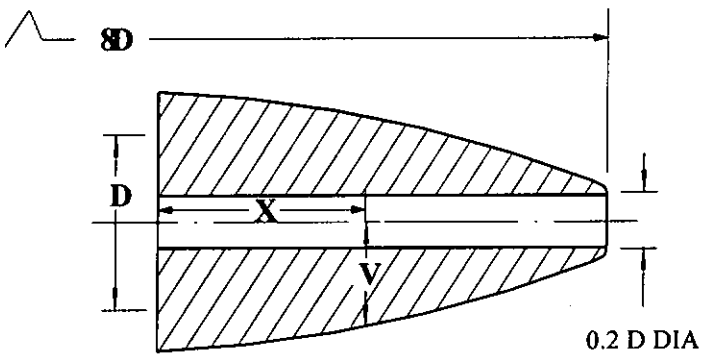

$\frac{X}{D}$	$\frac{V}{D}$	$\frac{X}{D}$	$\frac{V}{D}$
0.000	0.500	1.602	0.314
0.237	0.496	1.657	0.295
0.336	0.494	1.698	0.279
0.474	0.487	1.730	0.266
0.622	0.477	1.762	0.250
0.741	0.468	1.796	0.231
0.936	0.449	1.830	0.211
1.025	0.436	1.858	0.192
1.134	0.420	1.875	0.176
1.228	0.404	1.888	0.163
1.313	0.388	1.900	0.147
1.390	0.371	1.910	0.131
1.442	0.357	1.918	0.118
1.538	0.333	1.921	0.100
1.570	0.323		

B. Alternate Pitot-Static Tube with Ellipsoidal Head

Figure 5.2 Pitot-static tube

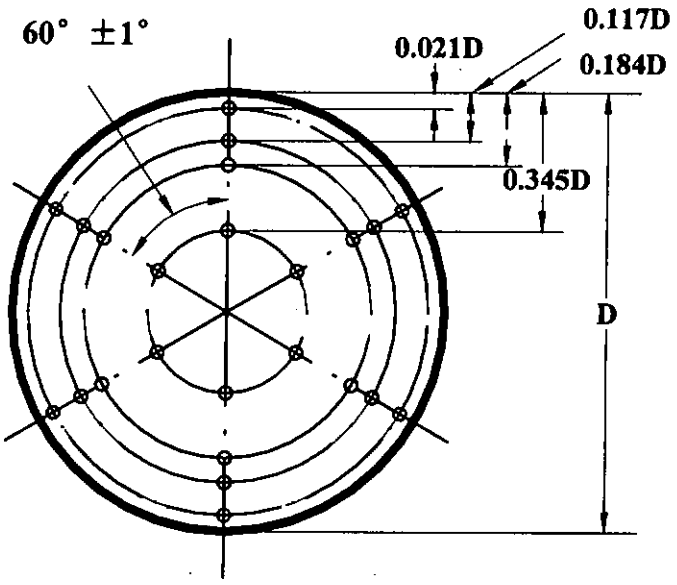

ALL PITOT POSITIONS ±0.0025 D RELATIVE TO INSIDE DUCT WALLS.

D IS THE AVERGE OF FOUR MEASUREMENTS AT TAAVERSE PLANE AT 45° ANGLES MEASURED TO ACCURACY OF 0.2% D.TRAVERSE.DUCT SHALL BE ROUND WITHIN 0.5% D AT TRAVERSE PLANE AND FOR A DISTANCE OF 0.5 D ON EITHER OF SIDE TRAVERSE PLANE.

Figure 5.3 Traverse points in a round duct

SURFACE SHALL BE SMOOTH AND FREE FROM IRREGULARITIES WITHIN 20 D OF HOLE. EDGE OF HOLE SHALL BE SQUARE AND FREE FROM BURRS.

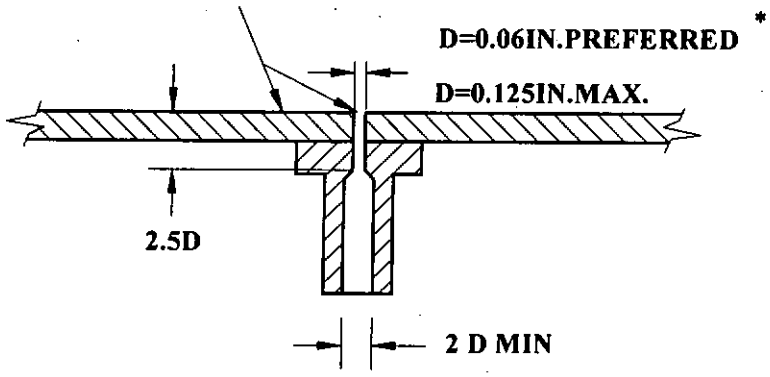

TO MANOMETER

*A 0.06 IN. HOLE IS THE MAXIMUM SIZE WHICH WILL ALLOW SPACE FOR SMOOTH SURFACE 20 D FROM THE HOLE WHEN INSTALLED 1.5 IN. FROM A PARTITION,SUCH AS IN FIGURES 13,14

Figure 5.4 Static pressure tap

The process air is passed by a fan through a conditioner including a cooling coil, a duct heater having a power of 0 - 2kW, and a humidifier having steam production of 1.5–5.0kg/h that adjust the temperature and moisture content of the inlet air conditions. Process air then passes through a flow straightener and airflow measuring station.

Regeneration air is passed through a flow straightener and airflow measuring station. And then regeneration air passes through a duct heater having a power of 0 - 9kW where it is heated to the test temperature.

5.1.2 Temperature and Relative Humidity Measuring

For the purpose of measuring the temperature and the humidity on the inlet and outlet of the dehumidifier test unit, duct detectors having an accuracy of $\pm 0.3°C$ for air dry – bulb temperature and $\pm 1\%$ RH for relative humidity are used. The smallest scale division is $0.1°C$ and $\pm 0.1\%$ RH. The measuring ranges are -20°C to +180°C for temperature and 0 to 100%RH for relative humidity.

The detector acquires the temperature with the aid of a thin – film measuring element whose electrical resistance changes in function of the temperature of the ambient air. The change in resistance is converted to 4 to 20 mA signals in correspondence with the temperature range –20 to +180°C.

The detector senses the relative humidity with the help of a capacitive humidity measuring element whose electrical capacity changes in function of the relative humidity of the ambient air. An electronic measuring circuit converts the detector's signal to a continuous 4 to 20 mA output signals, corresponding to 0 to 100% relative humidity.

For the purpose of measuring airflow rates, temperature readings are required in order to calculate air density and dependent properties such as specific heat. For these purposes, dry-bulb thermometers and transducers are used. Accuracy is $\pm 0.23^{\circ}C$ from $0^{\circ}C$ to $80^{\circ}C$ and $\pm 0.45^{\circ}C$ from $-43^{\circ}C$ to $97^{\circ}C$. The smallest scale division is $\pm 0.1^{\circ}C$. These temperature-measuring stations are uniformly located downstream of the Pitot traverse at each flow-measuring station.

5.1.3 Differential Pressure Measurements

The differential pressures between entering and leaving locations of equal airstream velocity, on each circuit of the dehumidifier test unit are determined. All pressure-measuring instruments are in accordance with ASHRAE Standard 41.3 – 1989, Standard Method for Pressure Measurement.

Pressure measurements were made with electronic micromanometer having an accuracy of $\pm 1\%$ of the reading ($\pm$ one digit). The smallest scale division of the

electronic pressure transducer is 0.01Pa. Differential pressure measurements can be obtained from 0.025Pa to 14946Pa.

The static pressure taps are illustrated in Figure 5.4. They consist of 6.0 mm (0.25 in.) diameter nipples soldered to the outer plenum walls and centered over 1.0 mm (0.04 in.) holes through the plenum walls. The edges of these holes are free of burrs and other surface irregularities.

The static pressure taps, four taps with manifold, are equally spaced around the perimeter of the ducts (Figure 5.5). The electronic micromanometer has one side connected to four externally manifolded pressure taps in the inlet plenum. The other side of the manometer is connected to four externally manifolded pressure taps in the discharge plenum. The inlet and outlet duct connections have cross-sectional dimentions equal to the duct flanges of the test unit enclosure. The diameters of the inlet and outlet plenums are 150mm.

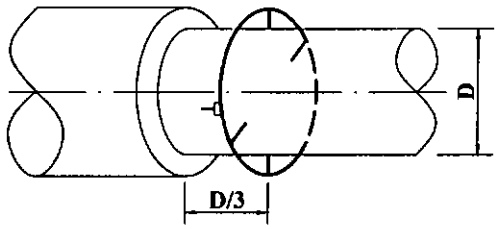

Figure 5.5 Typical plenum static pressure measurement

Pressure tap plenums of the inlet and outlet are used to determine the air friction loss of the desiccant dehumidifier test unit.

5.1.4 Airflow Rate Measurements

All airflow measurements were made in accordance with ASHRAE Standard 41.2 – 1987 RA 92, Standard Methods for Laboratory Airflow Measurement.

Flow rate shall be calculated from measurements of velocity obtained by a Pitot traverse in conjunction with an electronic micromanometer. A pattern of measuring points accurately located on each of several diameters of equal angular spacing constitutes a measuring station (Figure 5.3). The electronic micromanometer automatically corrects for density variations due to local temperature and barometric pressure. Velocity ranges are 0.127 – 152.4m/s using a pitot tube in conjunction with the electronic micromanometer. Accuracy is ± 3% of reading ± 0.0254m/s. The following are also noted:

a. The proper weighting of the readings taken across any given diameter, properly established, permits taking the arithmetic average of the readings of a traverse to determine the average velocity of the airstream (i.e. the average velocity is the arithmetic mean of the individual velocities). Best results occur when between 80% and 90% of the velocity measurements are

within 10% of the maximum velocity. The least acceptable result occurs if more than 75% of the velocity measurements exceed 10% of the maximum.

b. The flow streams should be perpendicular to the traverse plane. The angle between the flow stream and the traverse plane can be measured at a specific test point by tilting the nose of the Pitot tube so as to obtain a maximum pressure reading at that point. Variations from this flow condition resulting from swirl or other mass flow turbulence shall be acceptable when the angle between the flow stream and the traverse plane is greater than 80° at any point of measurement.

c. In making the traverse for that diameter, the nose of the Pitot tube must be maintained parallel to the duct wall and pointed against the flow of the airstream.

d. The length of the test duct, within one-half a duct diameter on each side of the traverse plane, is round within 0.5% of duct diameter as found by the average of four diameter measurements at 45° increments and the area of the duct then calculated by this result. The measurements shall be accurate within 0.2%.

e. Use the log – linear pattern, employing 4 diameters 60° apart and 6 points per diameter, for a total of 24 points per test (see Figure 5.3).

f. Note the required accuracy of Pitot positions from inside the duct walls and the maximum diameter of the Pitot head to avoid the necessity for correction of readings next to the duct wall.

5.1.5 Straighteners

Function of Straighteners

Straighteners are effective in producing a virtually uniform velocity of flow across the airstream. They eliminate eddies and the rotation of the airstream produced by the change in direction due to the test-unit configuration and/or the fan.

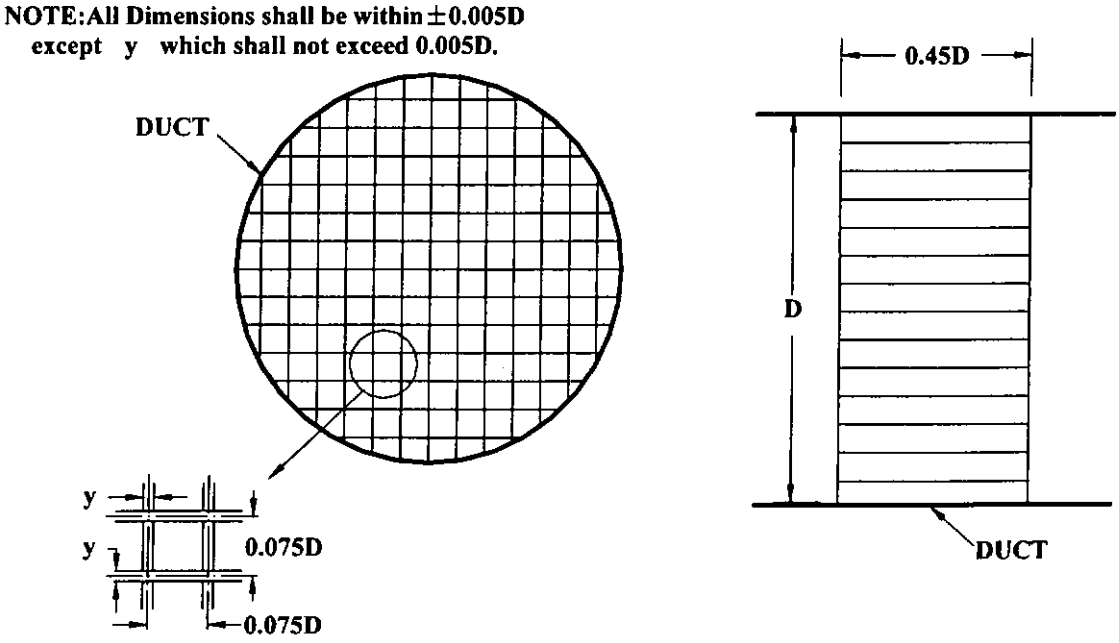

Figure 5.6 Flow straightener

Application of Straighteners

Straighteners are illustrated in Figure 5.6. The thickness of the straightener elements does not exceed 0.005D. The downstream plane of the straighteners is located between 5 and 5.25 duct diameters (D) upstream of the plane of the airflow measuring station. D is the inside diameter of the circular cross-sectional duct.

5.1.6 Plenum and Duct Sections

Plenum and duct sections are sealed to prevent air leakage, particularly at the connections to the dehumidifier test unit, and are insulated to prevent heat leakage between the dehumidifier test unit and the temperature-measuring instruments.

5.1.7 Method of Test

The test duct, measuring equipment, and desiccant dehumidifier test unit are operated until steady – state conditions have been maintained for at least 15 minutes. During any test, inlet temperature, humidity, and flow rate variations were less than ± 0.5°C, ± 1%rh, and ± 0.5%, respectively.

Airflow rates are determined at each of the four measurement stations as shown in Figure 5.1. The process and regeneration airflow rates are varied as required by means of two dampers.

5.2 Test Data and Calculations

5.2.1 Desiccant Wheel Test Unit

Desiccant wheel test unit is shown in Figure 5.7. Plane strips and corrugated strips of ceramic fiber paper were first stacked alternately with heat – resistant adhesive and rolled up into a honeycomb wheel with high voidage, thus forming a vast number of axial air channels running parallel through the structure, as show in Figure 5.8. A typical channel pitch is P(3.2)×H(1.8)mm, and a wall thickness is 0.2mm.

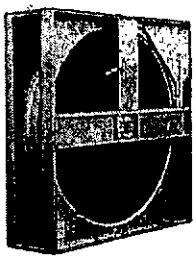

Figure 5.7 Desiccant wheel test unit

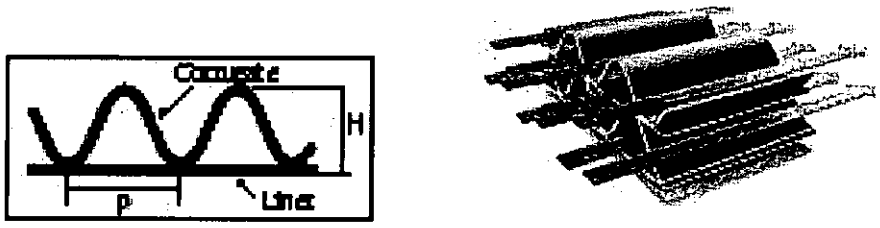

Figure5.8 The honeycomb of the desiccant

The ceramic wheel was then impregnated with aqueous sodium silicate solution. Silica gel was synthesized in the voids of the ceramic fiber sheet of the wheel matrix by treating with acidic solutions. The desiccant wheel was completed by rinsing, drying, heating and finishing.

The desiccant wheel test unit is divided into quadrants (three quadrants for supply flow and one quadrant for the exhaust) and the air flowed through opposite quadrants. The crossover leakage between the two air streams was measured by tracer gas (SF_6) tests. The test results show that the leakage driven by the differential pressure between the two air streams is usually less than 2% and always less than 4% of the flow rate. Table 5.1 shows the information on desiccant wheel test unit.

Table 5.1 Information on Desiccant Wheel Test Unit

Description	Value
Wheel parameters:	
1. wheel diameter	0.305 m
2. wheel deep l_c	0.203 m
3. rotation speed n_{rs}	32 rph
4. channel pitch	$3.2mm \times 1.8mm$
5. wall thickness	$0.2mm$
6. ratio of the desiccant surface area to the wheel volume r_{sv}	$4800\, m^2_{desiccant} / m^3_{wheel}$
7. ratio of the free flow area to the face area of a desiccant wheel r_a	0.9
8. ratio of the cross-sectional area of support material to the face area of a desiccant wheel r_m	0.03
9. volume fraction of the desiccant in the wheel f_v	$0.07\, m^3_{desiccant} / m^3_{wheel}$

Desiccant properties (metal silicate)

10. maximum water content of the desiccant

solid phase $w_{d\,max}$ $0.35\,kg_{H_2O}/kg_{dry\ \ desiccant}$

11. adsorption isotherm $w_d = w_{d\,\max} \cdot RH_{da}^{\,0.00912 \cdot T_d - 2.2}$ $kg_{H_2O}/kg_{dry\ \ desiccant}$

12. heat of sorption $q_{st} = -300 \cdot w_d + 2095$ kJ/kg_{H_2O}

$w_d \le 0.15$ $kg_{H_2O}/kg_{dry\ \ desiccant}$

$q_{st} = 2050$ kJ/kg_{H_2O}

$w_d > 0.15$ $kg_{H_2O}/kg_{dry\ \ desiccant}$

13. pore radius of desiccant a $68\times10^{-10}\,m$

14. tortuosity factor for intraparticle gas diffusion τ_g 2

15. specific surface area of pore of desiccant S_g $3.4\times10^5\,m^2_{surface\ \ area}/kg_{dry\ \ desiccant}$

16. tortuosity factor for intraparticle surface diffusion τ_s 2

17. specific heat of desiccant c_d $2.8\,kJ/kg_{dry\ \ desiccant}\cdot K$

Support material properties (ceramic fiber paper)

18. density of ceramic fiber paper ρ_m $190kg/m^3$

19. specific heat of ceramic fiber paper c_m $0.8\,kJ/kg\cdot K$

5.2.2 Data Record

Experiments were carried out using the honeycomb rotor dehumidifier mentioned above. Operating parameters studied were 1) flow rate of process air, 2) flow rate of regeneration air, 3) humidity of process feed air, 4) temperature of process feed air, 5) temperature of regeneration air and 6) humidity of regeneration air. Their influences on the humidity and the air temperature were measured at the outlet of the process zone ($0° < \theta < 270°$). The angle θ is taken from the starting point of the process zone. The test data were recorded for airflow measurement as shown in Table 5.2. The single point of performance data described in Table 5.3 were replicated over a number of regeneration air inlet conditions at which the test unit was tested. Appendix indicates the data recorded for each regeneration air inlet temperature.

5.2.3 Test Data Calculations

The following calculations were performed and included with Appendix.

Moisture Removal Capacity (MRC)

The moisture removal capacity of the test unit is calculated in kilograms per second as follows:

$$MRC = \dot{M}_{a,p,in} \cdot (\bar{w}_{a,p,in} - \bar{w}_{a,p,out}) \quad (kg_{H_2O}/s) \tag{5.1}$$

where MRC - moisture removal capacity (kg_{H_2O}/s);

$\dot{M}_{a,p,in}$ - total mass flow rate of process air inlet ($kg_{dry\ air}/s$);

$\bar{w}_{a,p,in}$ - average humidity ratio over cross-section at the process air inlet of desiccant wheel ($kg_{H_2O}/kg_{dry\ air}$);

$\bar{w}_{a,p,out}$ - average humidity ratio over cross-section at the process air outlet of desiccant wheel ($kg_{H_2O}/kg_{dry\ air}$)

Total Energy Transfer (TET)

The total energy transfer is:

$$TET = \dot{M}_{a,p,in} \cdot (\bar{h}_{a,p,out} - \bar{h}_{a,p,in}) \quad (kW) \tag{5.2}$$

where TET - total energy transfer (kW);

$\bar{h}_{a,p,in}$ - average enthalpy over cross-section at the process air inlet of desiccant wheel ($kJ/kg_{dry\ air}$);

$\bar{h}_{a,p,out}$ - average enthalpy over cross-section at the process air outlet of desiccant wheel ($kJ/kg_{dry\ air}$)

Regeneration Energy (RE)

The regeneration energy is defined as follows:

$$RE = \dot{M}_{a,r,in} \cdot (c_{pa,heater,out} \cdot t_{a,heater,out} - c_{pa,heater,in} \cdot t_{a,heater,in}) \quad (kW) \qquad (5.3)$$

where RE - regeneration energy (kW);

$\dot{M}_{a,r,in}$ - total mass flow rate of regeneration air inlet($kg_{dry\ air}/s$);

$t_{a,heater,in}$ - temperature of the regeneration air stream at the inlet of the heater (°C);

$t_{a,heater,out}$ - temperature of the regeneration air stream at the outlet of the heater (°C);

$c_{pa,heater,in}$ - specific heat of regeneration air stream at the inlet of the heater ($kJ/kg_{dry\ air} \cdot K$);

$c_{pa,heater,out}$ - specific heat of regeneration air stream at the outlet of the heater ($kJ/kg_{dry\ air} \cdot K$)

Regeneration Specific Heat Input (RSHI)

The specific heat input is defined as the ratio of the regeneration energy to the moisture removal capacity. The specific heat input is stated in terms of thermal

energy input per kilogram of moisture removal and expressed as kJ/kg_{H_2O}, and is calculated as follows:

$$RSHI = \frac{RE}{MRC} \quad (kJ/kg_{H_2O}) \tag{5.4}$$

Mass Balance

A calculation was performed to determine the ratio of the mass of moisture removed from the process air with respect to the mass of moisture rejected to the regeneration air at the test conditions. The mass ratio calculated for a specific test condition must be >0.95 and <1.05 in order to consider the data valid.

$$Mass \quad ratio = \frac{\dot{M}_{a,p,out} \cdot (\bar{w}_{a,p,in} - \bar{w}_{a,p,out})}{\dot{M}_{a,r,out} \cdot (\bar{w}_{a,r,out} - \bar{w}_{a,r,in})} \tag{5.5}$$

where $\dot{M}_{a,p,out}$ - total mass flow rate of process air outlet ($kg_{dry\ air}/s$);

$\dot{M}_{a,r,out}$ - total mass flow rate of regeneration air outlet($kg_{dry\ air}/s$);

$\bar{w}_{a,r,in}$ - average humidity ratio over cross-section at the regeneration air inlet of desiccant wheel ($kg_{H_2O}/kg_{dry\ air}$);

$\bar{w}_{a,r,out}$ - average humidity ratio over cross-section at the regeneration air outlet of desiccant wheel ($kg_{H_2O}/kg_{dry\ air}$)

Total Energy Balance

For a desiccant rotary dehumidifier, the total energy transfer is not an important performance parameter that is not involved in ASHRAE Standard 139 – 1998. The total energy transfer is for reference only.

A calculation was performed to determine the ratio of the rise in total energy of the process air with respect to the drop in total energy of the regeneration air at the test conditions. The total energy ratio calculated for a specific test condition must be >0.95 and <1.05 in order to consider the data valid.

$$Total \quad energy \quad ratio = \frac{\dot{M}_{a,p,out} \cdot (\bar{h}_{a,p,out} - \bar{h}_{a,p,in})}{\dot{M}_{a,r,out} \cdot (\bar{h}_{a,r,in} - \bar{h}_{a,r,out})} \tag{5.6}$$

where $\bar{h}_{a,r,in}$ - average enthalpy over cross-section at the regeneration air inlet of desiccant wheel ($kJ/kg_{dry\ air}$);

$\bar{h}_{a,r,out}$ - average enthalpy over cross-section at the regeneration air outlet of desiccant wheel ($kJ/kg_{dry\ air}$)

Table 5.2 Test Data Recorded for Airflow Measurement

Description	Units	Value
1. Process Airflow Inlet	m^3/s	0.04168
Temperature at Airflow Measuring Station	°C	28.6
Density of Air at Airflow Measuring Station	kg/m^3	1.1706
Mass Flow Rate	kg/s	0.04879
1a. Process Airflow Outlet	m^3/s	0.04610
Temperature at Airflow Measuring Station	°C	55.6
Density of Air at Airflow Measuring Station	kg/m^3	1.0745
Mass Flow Rate	kg/s	0.04953
2. Regeneration Airflow Inlet	m^3/s	0.02278
Temperature at Airflow Measuring Station	°C	29.8
Density of Air at Airflow Measuring Station	kg/m^3	1.1658
Mass Flow Rate	kg/s	0.02656
2a. Regeneration Airflow Outlet	m^3/s	0.02314
Temperature at Airflow Measuring Station	°C	42.2
Density of Air at Airflow Measuring Station	kg/m^3	1.1203
Mass Flow Rate	kg/s	0.02592

Table 5.3 Test Data Recorded for Each Regeneration Air Inlet Condition

Description	Units	Value
1. Process Air Inlet Temperature	°C	
2. Process Air Inlet Relative Humidity	%	
3. Process Air Inlet Humidity Ratio	$kg_{H_2O}/kg_{dry\ air}$	
4. Process Air Inlet Enthalpy	$kJ/kg_{dry\ air}$	
5. Process Air Outlet Temperature	°C	
6. Process Air Outlet Relative Humidity	%	
7. Process Air Outlet Humidity Ratio	$kg_{H_2O}/kg_{dry\ air}$	
8. Process Air Outlet Enthalpy	$kJ/kg_{dry\ air}$	
9.Experimental Moisture Removal Capacity	kg_{H_2O}/s	
10.Simulated Moisture Removal Capacity	kg_{H_2O}/s	
11.Deviation of Simulated Moisture Removal Capacity from Test Result	%	
12. Experimental Total Energy Transfer	kW	
13. Simulated Total Energy Transfer	kW	
14.Deviation of Simulated Total Energy Transfer from Test Result	%	
15.Process Air Pressure Drop	Pa	
16. Regeneration Air Inlet Temperature	°C	
17. Regeneration Air Inlet Relative Humidity	%	

18. Regeneration Air Inlet Humidity Ratio	$kg_{H_2O}/kg_{dry\ air}$	
19. Regeneration Air Inlet Enthalpy	$kJ/kg_{dry\ air}$	
20. Regeneration Air Outlet Temperature	°C	
21. Regeneration Air Outlet Relative Humidity	%	
22. Regeneration Air Outlet Humidity Ratio	$kg_{H_2O}/kg_{dry\ air}$	
23. Regeneration Air Outlet Enthalpy	$kJ/kg_{dry\ air}$	
24. Regeneration Air Pressure Drop	Pa	
25. Temperature of the Air at Inlet of Heater	°C	
26. Specific Heat of the Air at Inlet of Heater	$kJ/kg \cdot K$	
27. Temperature of the Air at Outlet of Heater	°C	
28. Specific Heat of the Air at Outlet of Heater	$kJ/kg \cdot K$	
29. Regeneration Energy	kW	
30. Regeneration Specific Heat Input	kJ/kg_{H_2O}	
31. Mass Ratio		
32. Total Energy Ratio		

5.3 Validation Results

In this section, the parameters predicted by the numerical model presented are compared with that measured experimentally on a commercially available desiccant wheel. Comparison with a few experimental tests will show that the numerical model does indeed accurately model the performance of desiccant wheel.

Figures 5.9 and 5.10 show the comparisons between the measured and simulated moisture removal capacity and total energy transfer, respectively. The process air inlet conditions are 29.1°C and 57.4%rh, and the process air and regeneration air mass flow rates are 0.04879 kg/s and 0.02656 kg/s respectively.

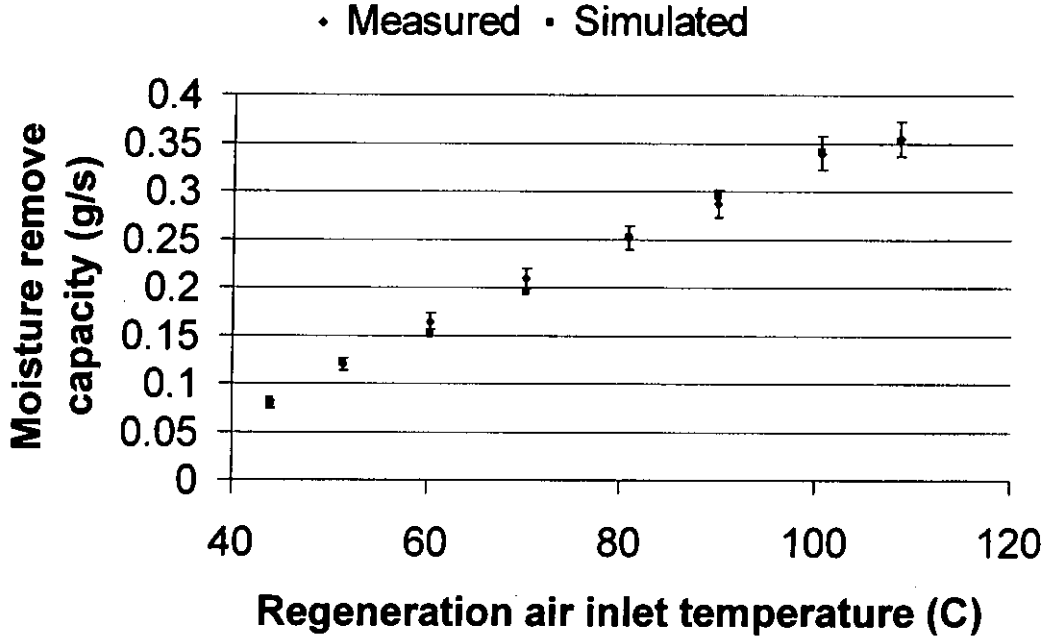

Figure 5.9 Comparison between the measured and simulated moisture removal capacity as a function of regeneration air inlet temperature for test conditions of process air inlet temperature 29.1°C and relative humidity 57.4%, and of process air and regeneration air mass flow rates 0.04879 kg/s and 0.02656 kg/s respectively

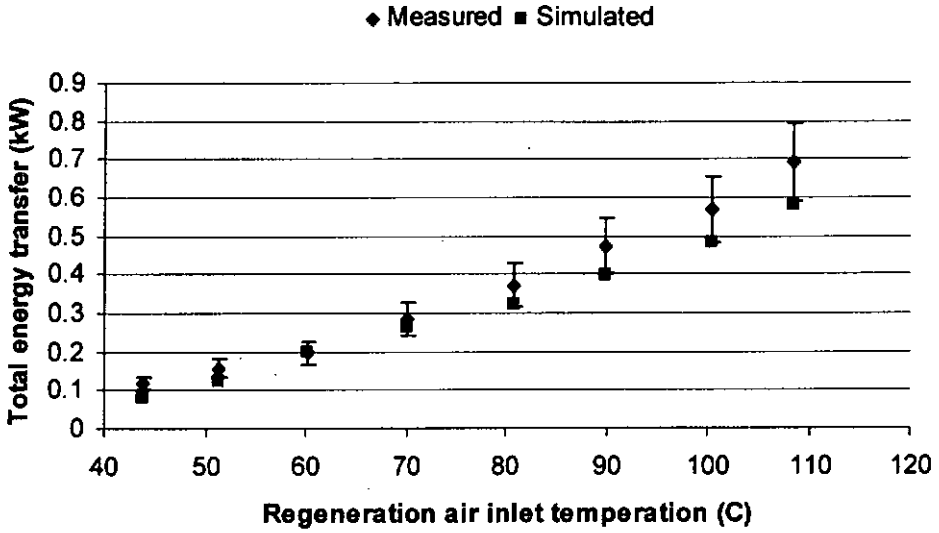

Figure 5.10 Comparison between the measured and simulated total energy transfer as a function of regeneration air inlet temperature for test conditions of process air inlet temperature 29.1°C and relative humidity 57.4%, and of process air and regeneration air mass flow rates 0.04879 kg/s and 0.02656 kg/s respectively

According to ASHRAE Standard 139 - 1998, Standard Method of Testing for Rating Desiccant Dehumidifiers Utilizing Heat for the Regeneration Process, if test rig, method and apparatus all accord with above standard, the uncertainties in measured data of moisture removal capacity is ± 5%.

In Figure 5.9, the error bars indicate ± 5% uncertainties in measured data, and it is showed that the simulated moisture removal capacity agrees with the test data within experimental uncertainty except two operating conditions in which the deviations of the simulated results from the test results are 8.2% and 7.0% respectively. Considering that the uncertainty in the predicted moisture removal

capacity for an existing desiccant wheel is, due to the uncertainty of the property data used in the model, likely ± 3 to ± 5%, the agreement between the measured and simulated results is acceptable in all cases. It is noted that a manufacturer may be able to reduce these uncertainty limits by using more accurate instrumentation and data to establish the wheel characteristics used in the model.

In Figures 5.10, the error bars indicate ± 15% difference from test data (not ± 15% uncertainties in measured data), and it is showed that the deviation of simulated total energy transfer from experimental results is within 16.8% except two rather extreme operating conditions in which the enthalpy of process air is approximately constant so that the uncertainties in measured data exceed the rise in the enthalpy of process air. The values of simulated total energy transfer are smaller than the test values of total energy transfer, because in the model developed in this thesis the sensible heat transfer from regeneration air to process air through the desiccant wheel case is not taken into account. For a desiccant rotary dehumidifier, the total energy transfer is not an important performance parameter that is not involved in ASHRAE Standard 139 – 1998. The total energy transfer is for reference only.

The experimental and simulated results show the same trends and display close agreement for each moisture removal capacity and each total energy transfer.

Chapter 6 Sensitivity Studies

The purpose of the simulations in this chapter is to confirm the relevancy of the numerical model by sensitivity studies. The effects of the design and the operation parameters of desiccant wheel (wheel parameters, mass flow rate, temperature, and humidity) on the dehumidifying performance will be studied. Investigating the effect of certain assumptions on the predicted performance is left to future studies. The variations in parameters of process and regeneration air with angular position and with depth into the tubes are simulated. The desiccant wheel simulated for the sensitivity studies in this chapter is the same as the test unit.

Optimal rotation speed of desiccant wheel is one of the most important factors in the design and the operation parameters of desiccant wheel. View the optimal rotation speed at the angle of adsorption. During adsorption, the higher the desiccant temperature, the higher is the relative humidity of the moisture air in equilibrium with the desiccant solid phase RH_{da} from the isotherms, and the smaller is the dehumidification potential between the desiccant and the process air. Therefore, at the beginning of the process zone section it takes some time before the adsorbent rotor is cooled down to the temperature at which the rotor has sufficient adsorbability. When the rotation speed is very high, cooling of the rotor occurs very late and the sector of the favorable adsorption zone becomes narrower.

As a consequence, the overall dehumidifying performance averaged over the whole process zone decreases. On the other hand, when the rotation speed is very slow, the rotor is subjected to a quick cooling at the beginning of the process zone section and recovered sufficient adsorbability. However, it is followed by a remarkable decrease in dehumidifying performance in the subsequent region of the process zone with increase in the amount adsorbed. Thus, the overall dehumidifying performance decreases again.

View the optimal rotation speed at the angle of desorption. When the rotation speed is very high, there is no enough time to desorb the desiccant. As a consequence, the overall dehumidifying performance decreases. On the other hand, when the rotation speed is very slow, the desiccant is subjected to a quick desorption at the beginning of the regeneration zone section and in the subsequent region of the regeneration zone desorption dose not take place again. It is followed by a decrease in dehumidifying performance in the region of the process zone with increase in the amount adsorbed. Thus, the overall dehumidifying performance decreases again. The rotation speed should be low enough for rapid cooling of the rotor in the process zoon and thorough desorption of desiccant in the regeneration zoon, but high enough to keep the adsorbent far from equilibrium in the process zoon.

The results of these conflicting effects yielded the optimal rotation speed. Many experiments were carried out by Kodama et al (1994) to investigate the effects of the rotation speed on dehumidifying performance under various operating conditions. They found the existence of an optimal rotation speed of the rotor for a given set of operation and design parameters. An empirical formula, Equation 6.1, was proposed to predict the optimal rotation speed in the practical operating range. The optimal rotation speed increases with increasing mass flow rate of regeneration air, decreasing total mass of desiccant wheel, decreasing bulk specific heat of desiccant wheel.

$$n_{rs,op} = \frac{1224 \cdot c_{pa} \cdot \dot{M}_{a,r}}{c_{pb} \cdot M_w} \tag{6.1}$$

where $\dot{M}_{a,r}$ - total mass flow rate of regeneration air (kg/s);

M_w - total mass of desiccant wheel (kg);

$$M_w = \frac{\pi}{4} \cdot D_w^2 \cdot l_c \cdot \rho_b \tag{6.2}$$

D_w - desiccant wheel diameter (m);

ρ_b - bulk density of desiccant wheel (kg/m^3_{wheel});

$$\rho_b = \rho_d \cdot f_v + \rho_m \cdot r_m \tag{6.3}$$

for the desiccant wheel simulated for the sensitivity studies in this chapter

$$\rho_b = 700 \times 0.07 + 190 \times 0.03 = 54.7 \ (kg/m^3_{wheel})$$

c_{pb} - bulk specific heat of desiccant wheel ($kJ/kg \cdot K$);

$$c_{pb} = \frac{c_d \cdot \rho_d \cdot f_v + c_m \cdot \rho_m \cdot r_m}{\rho_b} \tag{6.4}$$

for the desiccant wheel simulated for the sensitivity studies in this chapter

$$c_{pb} = \frac{2.8 \times 700 \times 0.07 + 0.8 \times 190 \times 0.03}{54.7} = 2.59(kJ/kg \cdot °C)$$

Substituting Equation 6.2 into 6.1 the optimal rotation speed can be expressed as

$$n_{rs,op} = \frac{1558 \cdot c_{pa} \cdot \dot{M}_{a,r}}{c_{pb} \cdot \rho_b \cdot D_w^2 \cdot l_c} \tag{6.5}$$

When the total mass flow rate of regeneration air $\dot{M}_{a,r}$ is $0.02656\ kg/s$, the optimal rotation speed for the desiccant wheel simulated for the sensitivity studies in this chapter is

$$n_{rs,op} = \frac{1558 \times 1.01 \times 0.02656}{54.7 \times 2.59 \times 0.305^2 \times 0.203} = 15.6 \approx 16 \quad (1/h)$$

Equation 6.5 correlates the optimal rotation speed with various operating and design parameters, but the effects of the process and regeneration air inlet conditions and process air flow rate on the optimal rotation speed were not taken into account. In what follows, discussion will be focused on the effects of the process and regeneration air inlet conditions and process air flow rate on the optimal rotation speed and dehumidifying performance.

The design and the operation parameters varied are the rotation speed of the rotor n_{rs}, the process air flow rate $\dot{M}_{a,p}$, the regeneration air inlet condition (i.e. humidity ratio $w_{a,r,in}$ temperature $t_{a,r,in}$), and the process air inlet conditions (i.e. humidity ratio $w_{a,p,in}$ and temperature $t_{a,p,in}$).

6.1 Effect of Regeneration Air Inlet Temperature on the Dehumidifying Performance and the Optimal Rotation Speed

The effect of regeneration air inlet temperature on the dehumidifying performance and the optimal rotation speed is simulated in this section. The process air inlet condition used in the simulations is the summer condition of the outdoor air in Hong Kong. The dry bulb is 33.2°C, and wet bulb temperature is 26.1°C (humidity ratio is 0.0186 $kg_{H_2O}/kg_{dry\ air}$), corresponding to 0.4% annual cumulative frequency of occurrence (ASHRAE Handbook, Fundamentals 26.31). The indoor thermal comfort design criteria is air temperature of 24°C and 60% relative humidity (humidity ratio 0.0112 $kg_{H_2O}/kg_{dry\ air}$). The indoor humidity ratio 0.0112 $kg_{H_2O}/kg_{dry\ air}$ is used as the regeneration air inlet humidity ratio in the simulations. The mass flow rate of process and regeneration airstreams is 0.04879 and 0.02656 kg/s respectively.

The relation between moisture removal capacity and regeneration air inlet temperature is shown in Figure 6.1, for rotation speed of desiccant wheel 16rph.

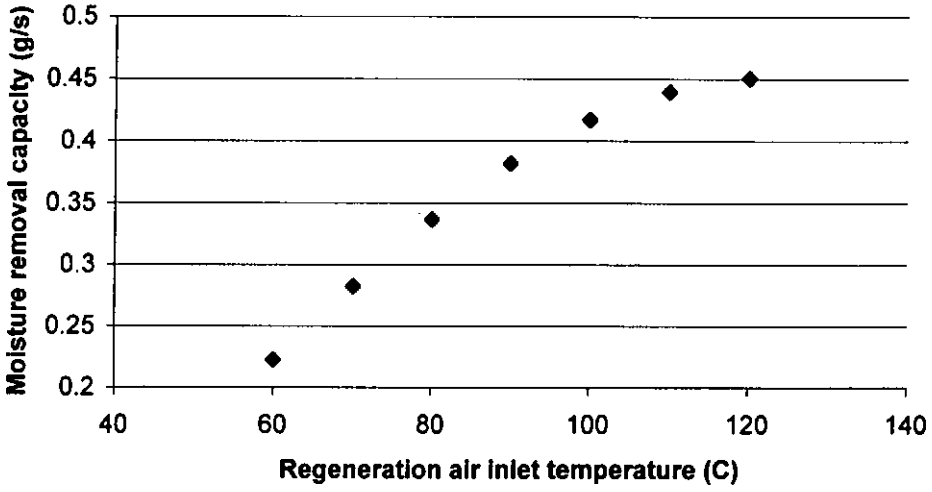

Figure 6.1 Effect of regeneration air inlet temperature on moisture removal capacity for the rotation speed of desiccant wheel 16 rph

Figure 6.1 shows that the moisture removal capacity becomes larger as the regeneration air inlet temperature increases. Since the amount adsorbed in the desiccant at equilibrium decreases at high regeneration temperature, the effective adsorption capacity of the rotor is increased as the adsorbent rotor is regenerated to a higher degree. However, the moisture removal capacity does not increase linearly with the regeneration air inlet temperature. The variation of the moisture removal capacity with the regeneration air inlet temperature is more pronounced for regeneration air inlet temperatures less than 100°C. The improvement on the moisture removal capacity by increasing the regeneration air inlet temperature at

the higher temperature levels is not as significant as at the lower temperatures. Since the water molecules adsorbed in desiccant get out almost thoroughly at high regeneration air inlet temperature, the increase in the regeneration potential of regeneration air by increasing the regeneration air inlet temperature at the higher temperature levels is not as significant as at the lower temperatures.

Figure 6.2 and Table 6.1 show the effect of the regeneration air inlet temperature $t_{a,r,in}$ and the rotation speed n_{rs} on the moisture removal capacity.

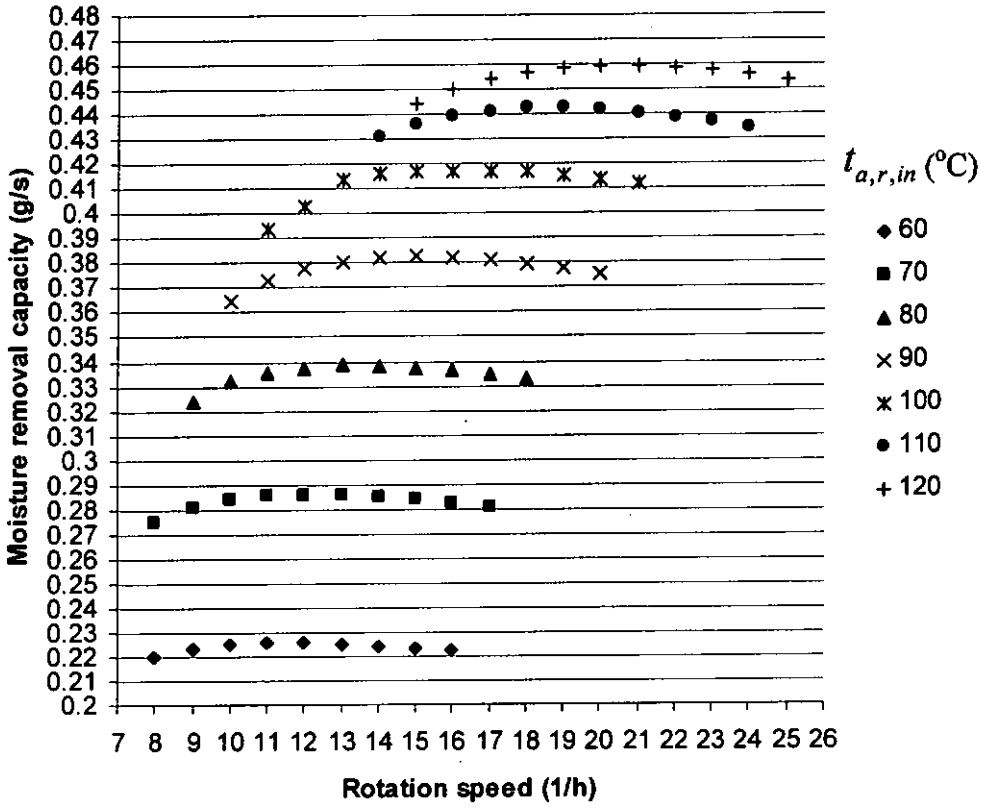

Figure 6.2 Effect of the regeneration air inlet temperature and the rotation speed on the moisture removal capacity

Table 6.1 Effect of the regeneration air inlet temperature and the rotation speed on the moisture removal capacity (g_{H_2O}/s)

Rotation Speed (1/h)	Moisture Removal Capacity (g_{H_2O}/s)						
	$t_{a,r,in}$ 60°C	$t_{a,r,in}$ 70°C	$t_{a,r,in}$ 80°C	$t_{a,r,in}$ 90°C	$t_{a,r,in}$ 100°C	$t_{a,r,in}$ 110°C	$t_{a,r,in}$ 120°C
8	0.2198	0.2745					
9	0.2230	0.2804	0.3242				
10	0.2247	0.2839	0.3317	0.3641			
11	0.2254	0.2855	0.3355	0.3728			
12	0.2255*	0.28591*	0.3373	0.3777	0.4030		
13	0.2251	0.28586	0.3386*	0.3804	0.4132		
14	0.2244	0.2850	0.3383	0.3823	0.4158	0.4309	
15	0.2235	0.2838	0.3373	0.3825*	0.4168	0.4360	0.4442
16	0.2224	0.2823	0.3365	0.3819	0.4169*	0.4394	0.4502
17		0.2805	0.3347	0.3812	0.4168	0.4413	0.4545
18			0.3326	0.3796	0.4165	0.4422	0.4571
19				0.3775	0.4153	0.4423*	0.4587
20				0.3756	0.4136	0.4416	0.4593*
21					0.4118	0.4404	0.4592
22						0.4388	0.4585
23						0.4369	0.4573
24						0.4346	0.4557
25							0.4538

* optimal rotation speed

As shown in Table 6.1 and Figure 6.2, the optimal rotation speed for the desiccant wheel simulated in this section is 16rph only for the regeneration air inlet temperature 100°C, which validates the numerical model at a different angle. The optimal rotation speed increases with increasing regeneration air inlet temperature, because the higher the regeneration air inlet temperature, the faster is the desorption. Figure 6.3 shows the relation between the optimal rotation speed and the regeneration air inlet temperature.

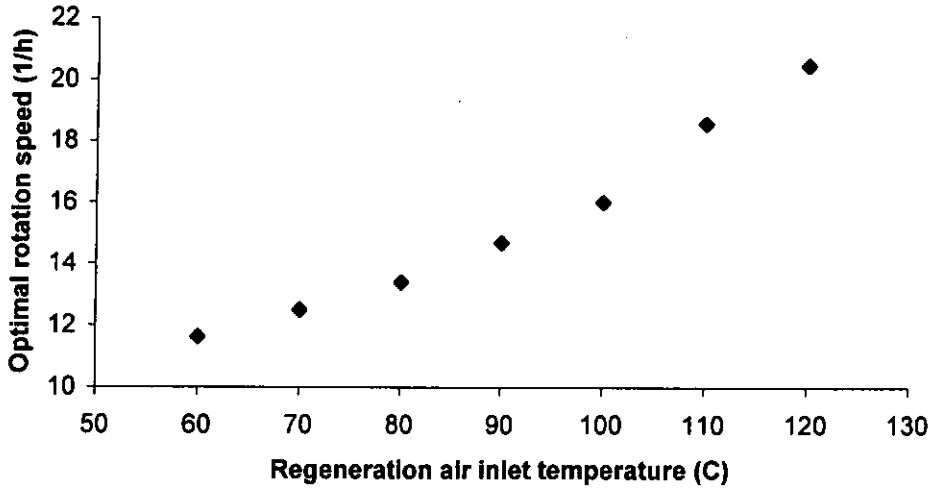

Figure 6.3 Relation between the optimal rotation speed and the regeneration air inlet temperature

Based on Equation 6.5, a recommendation for the optimal rotation speed is given by the following relationship to take the effect of the regeneration air inlet temperature on the optimal rotation speed into account.

$$n_{rs,op} = \frac{14.8 \cdot c_{pa} \cdot \dot{M}_{a,r} \cdot (T_{a,r,in} - 260)}{c_{pb} \cdot \rho_b \cdot D_w^2 \cdot l_c} \qquad (6.6)$$

where $T_{a,r,in}$ - absolute temperature of regeneration air stream inlet condition (K)

6.2 Effect of Process Air Inlet Temperature on the Dehumidifying Performance and the Optimal Rotation Speed

In this section, the effect of process air inlet temperature on the dehumidifying performance and the optimal rotation speed is simulated. The process and regeneration air inlet humidity ratio, and the process and regeneration air mass flow rate used in the simulations are the same as used in Section 6.1. The regeneration air inlet temperature is 100°C.

Figure 6.4 shows the variation of the dehumidification performance with the inlet temperature of the process air when all other operation parameters are held constant. During adsorption, the higher inlet temperature of the process air causes the higher temperature of desiccant, which results in higher relative humidity of the moisture air in equilibrium with the desiccant solid phase RH_{da} from the isotherms, and smaller dehumidification potential between the desiccant and the process air reducing the dehumidification capacity. As shown in Figure 6.4, the moisture removal capacity linearly decreases as the inlet temperature of the process air increases. Changing the inlet temperature of the process air from 22°C to 40°C, the moisture removal capacity decreases from 0.5025g/s to 0.3594g/s.

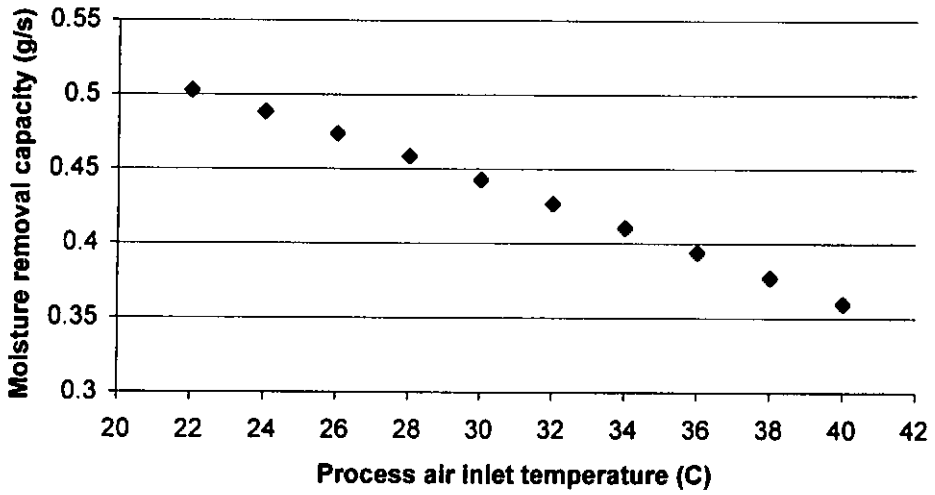

Figure 6.4 Effect of process air inlet temperature on moisture removal capacity for the rotation speed of desiccant wheel 16 rph

Figure 6.5 and Table 6.2 show the effect of the process air inlet temperature $t_{a,p,in}$ and the rotation speed n_{rs} on the moisture removal capacity.

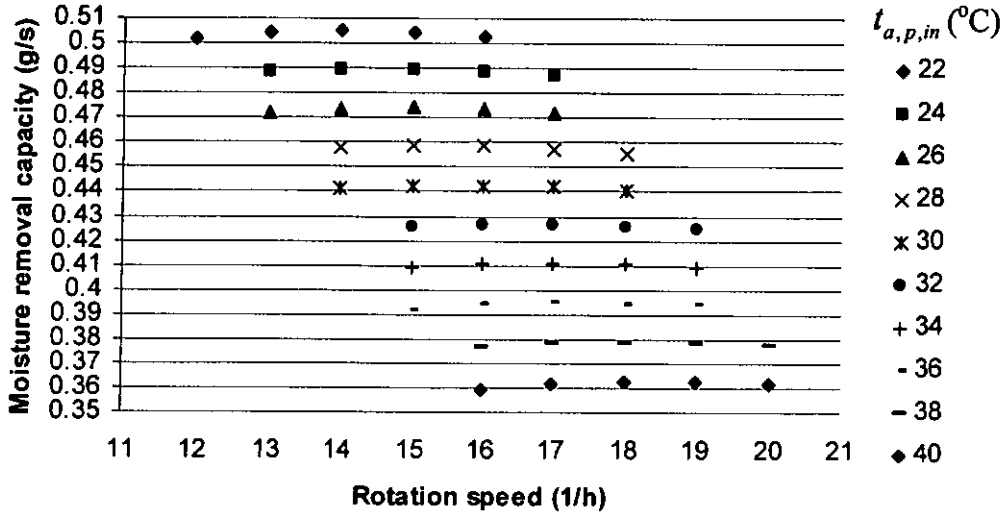

Figure 6.5 Effect of the process air inlet temperature and the rotation speed on the moisture removal capacity

Table 6.2 Effect of the process air inlet temperature and the rotation speed on the moisture removal capacity (g_{H_2O}/s)

Rotation Speed (1/h)	Moisture Removal Capacity (g_{H_2O}/s)									
	$t_{a,p,in}$ 22°C	$t_{a,p,in}$ 24°C	$t_{a,p,in}$ 26°C	$t_{a,p,in}$ 28°C	$t_{a,p,in}$ 30°C	$t_{a,p,in}$ 32°C	$t_{a,p,in}$ 34°C	$t_{a,p,in}$ 36°C	$t_{a,p,in}$ 38°C	$t_{a,p,in}$ 40°C
12	0.5014									
13	0.5039	0.4881	0.4718							
14	0.5048	0.4893	0.4736	0.4574	0.4408					
15	0.5042	0.4894*	0.4741*	0.4582	0.4422	0.4258	0.4090	0.3916		
16	0.5025	0.4882	0.4734	0.4583*	0.4424*	0.4265	0.4103	0.3937	0.3768	0.3594
17		0.4865	0.4719	0.4572	0.4421	0.4266*	0.4105*	0.3944*	0.3780	0.3614
18				0.4554	0.4407	0.4257	0.4103	0.3943	0.3783*	0.3622
19						0.4242	0.4092	0.3939	0.3780	0.3623*
20									0.3775	0.3618

*optimal rotation speed

As shown in Table 6.2 and Figure 6.5, the optimal rotation speed for the desiccant wheel simulated in this section is 16rph only for the process air inlet temperature 28°C and 30°C. The optimal rotation speed increases with increasing process air inlet temperature, because the higher the process air inlet temperature, the smaller is the dehumidification potential between the desiccant and the process air, and the faster the equilibrium arrives. Figure 6.6 shows the relation between the optimal

rotation speed and the process air inlet temperature. The optimal rotation speed linearly increases as the inlet temperature of the process air increases.

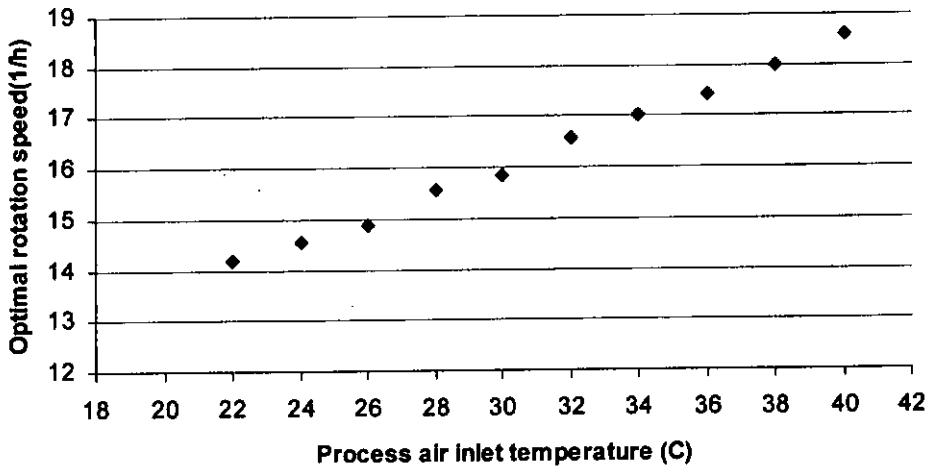

Figure 6.6 Relation between the optimal rotation speed and the process air inlet temperature

Based on Equation 6.6, a recommendation for the optimal rotation speed is given by the following relationship to take the effect of the process air inlet temperature on the optimal rotation speed into account.

$$n_{rs,op} = -\frac{1028 \cdot c_{pa} \cdot \dot{M}_{a,r} \cdot (T_{a,r,in} - 260)}{c_{pb} \cdot \rho_b \cdot D_w^2 \cdot l_c \cdot (T_{a,p,in} - 371)} \tag{6.7}$$

where $T_{a,p,in}$ - absolute temperature of process air stream inlet condition (K)

6.3 Effect of Regeneration Air Inlet Humidity Ratio on the Dehumidifying Performance and the Optimal Rotation Speed

The effect of regeneration air inlet humidity on the dehumidifying performance and the optimal rotation speed is simulated in this section. The process air inlet condition, and the mass flow rate of process and regeneration airstreams used in the simulation are the same as used in Section 6.1. The regeneration air inlet temperature is 100°C.

The effect of the inlet regeneration flow humidity ratio on the dehumidification performance of a rotary dehumidifier is presented in Figure 6.7, for rotation speed of desiccant wheel 16rph. At a constant regeneration air inlet temperature, increasing the moisture in the regeneration flow reduces the moisture uptake swing in the desiccant wheel, which deteriorates the dehumidification performance in the desiccant wheel. Figure 6.7 shows that the moisture removal capacity linearly decreases as the inlet regeneration flow humidity ratio increases.

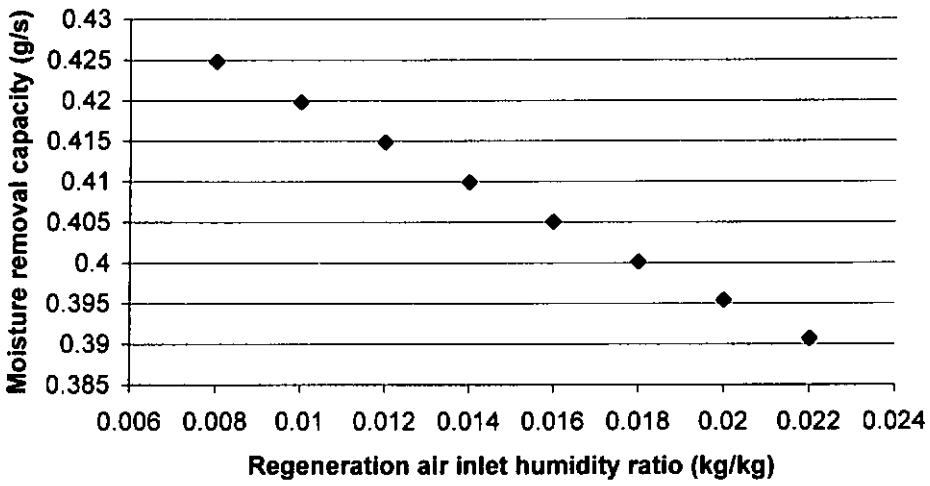

Figure 6.7 Effect of regeneration air inlet humidity ratio on moisture removal capacity for the rotation speed of desiccant wheel 16 rph

Table 6.3 and Figure 6.8 show the effect of the regeneration air inlet humidity ratio $w_{a,r,in}$ and the rotation speed n_{rs} on the moisture removal capacity.

Table 6.3 Effect of the regeneration air inlet humidity ratio and the rotation speed on the moisture removal capacity (g_{H_2O}/s)

Rotation Speed (1/h)	Moisture Removal Capacity (g_{H_2O}/s)							
	$w_{a,r,in}$ 0.008 kg/kg	$w_{a,r,in}$ 0.010 kg/kg	$w_{a,r,in}$ 0.012 kg/kg	$w_{a,r,in}$ 0.014 kg/kg	$w_{a,r,in}$ 0.016 kg/kg	$w_{a,r,in}$ 0.018 kg/kg	$w_{a,r,in}$ 0.020 kg/kg	$w_{a,r,in}$ 0.022 kg/kg
13					0.4007	0.3971	0.3935	0.3900
14			0.4115	0.4074	0.4033	0.3997	0.3958	0.39185*
15		0.4185	0.4140	0.4095	0.40497*	0.4005*	0.3962*	0.39185*
16	0.4248	0.4198	0.4148*	0.4099*	0.40496	0.4001	0.3954	0.3907
17	0.4256	0.4201*	0.4147	0.4093	0.4040	0.3991	0.3940	
18	0.42587	0.4200	0.4142	0.4084				
19	0.42592*	0.4190						
20	0.4242							

*optimal rotation speed

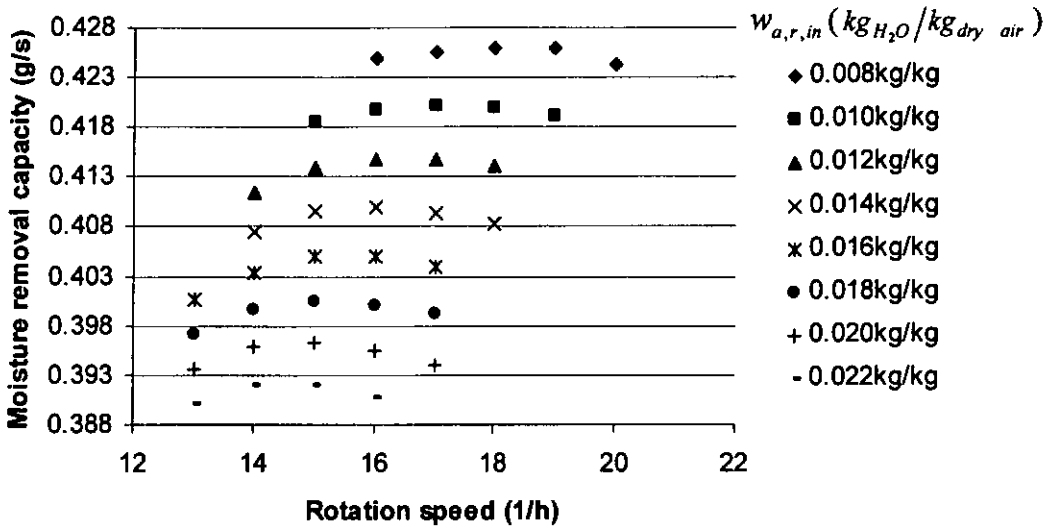

Figure 6.8 Effect of the regeneration air inlet humidity ratio and the rotation speed on the moisture removal capacity

As shown in Table 6.3 and Figure 6.8, the optimal rotation speed for the desiccant wheel simulated in this section is 16 rph only for the regeneration air inlet humidity ratio $0.012\,kg_{H_2O}/kg_{dry\ air}$ and $0.014\,kg_{H_2O}/kg_{dry\ air}$. The optimal rotation speed increases with decreasing regeneration air inlet humidity ratio, because the lower the regeneration air inlet humidity ratio, the larger is the desorption potential between the desiccant and the regeneration air, and the faster is the desorption. Figure 6.9 shows the relation between the optimal rotation speed and the regeneration air inlet humidity ratio.

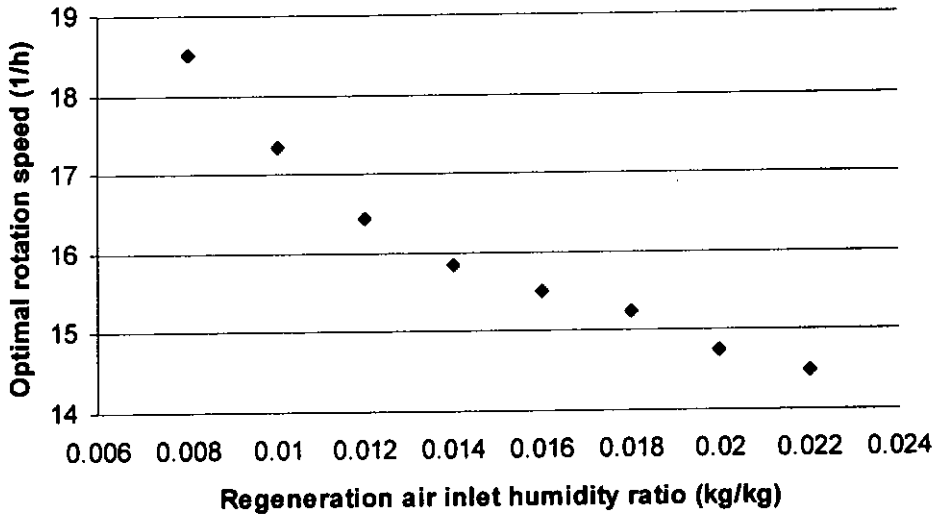

Figure 6.9 Relation between the optimal rotation speed and the regeneration air inlet humidity ratio

Based on Equation 6.7, a recommendation for the optimal rotation speed is given by the following relationship to take the effect of the regeneration air inlet humidity ratio on the optimal rotation speed into account.

$$n_{rs,op} = \frac{17618 \cdot c_{pa} \cdot \dot{M}_{a,r} \cdot (T_{a,r,in} - 260) \cdot (w_{a,r,in} - 0.0749)}{c_{pb} \cdot \rho_b \cdot D_w^2 \cdot l_c \cdot (T_{a,p,in} - 371)} \qquad (6.8)$$

Equation 6.8 is based on an empirical formula, Equation 6.1, proposed by Kodama et al (1994) and the simulation results of silica gel coated rotary dehumidifiers in this thesis. Many experiments on silica gel coated rotary dehumidifiers were carried out by Kodama et al (1994) to obtain the empirical formula, so Equation 6.8 can be applied to optimal rotation speed of silica gel coated rotary dehumidifiers.

6.4 Effect of Process Air Inlet Humidity Ratio on the Dehumidifying Performance and the Optimal Rotation Speed

The effect of process air inlet humidity ratio on the dehumidifier performance and the optimal rotation speed is simulated in this section. The regeneration air inlet condition and the mass flow rate of process and regeneration airstreams used in the simulations are the same as used in Section 6.2. The process air inlet temperature is 33.2°C.

Figure 6.10 shows that the moisture removal capacity increases as the process air inlet humidity ratio increases. For the same regeneration flow, the higher the moisture content in air, the larger is the dehumidification potential between the desiccant and the process air. Therefore more moisture will be removed from the process air. Figure 6.10 shows the dependence of the moisture removal capacity of a desiccant wheel with the inlet process air humidity ratio.

Table 6.4 and Figure 6.11 show the effect of the process air inlet humidity ratio $w_{a,p,in}$ and the rotation speed n_{rs} on the moisture removal capacity.

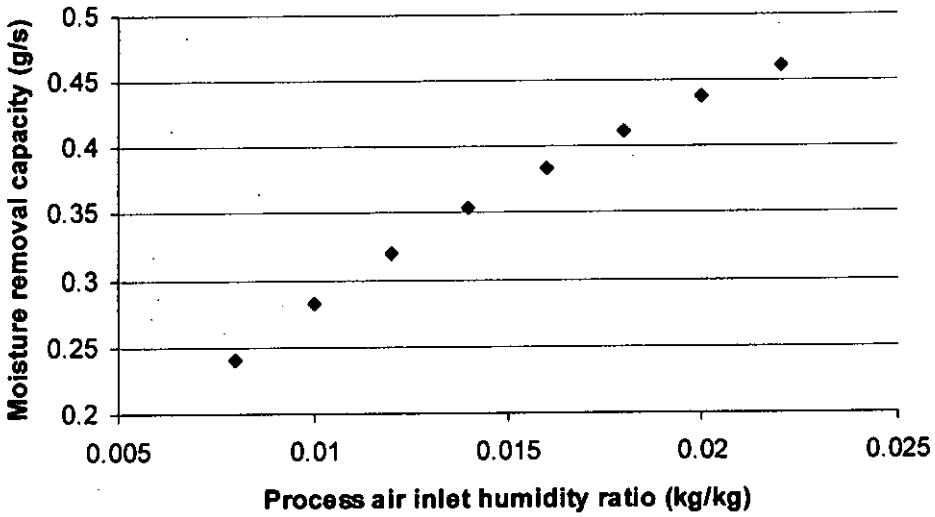

Figure 6.10 Effect of process air inlet humidity ratio on moisture removal capacity for the rotation speed of desiccant wheel 16 rph

Table 6.4 Effect of the process air inlet humidity ratio and the rotation speed on the moisture removal capacity (g_{H_2O}/s)

Rotation Speed (1/h)	Moisture Removal Capacity (g_{H_2O}/s)							
	$w_{a,p,in}$ 0.008 kg/kg	$w_{a,p,in}$ 0.010 kg/kg	$w_{a,p,in}$ 0.012 kg/kg	$w_{a,p,in}$ 0.014 kg/kg	$w_{a,p,in}$ 0.016 kg/kg	$w_{a,p,in}$ 0.018 kg/kg	$w_{a,p,in}$ 0.020 kg/kg	$w_{a,p,in}$ 0.022 kg/kg
13	0.2370							
14	0.2394	0.2811	0.3179	0.3508	0.3806	0.4080		
15	0.2403*	0.28238	0.3195	0.3526	0.3829	0.4105	0.4360	0.4598
16	0.2400	0.28243*	0.3199*	0.3534*	0.3837*	0.41152*	0.4372	0.4610
17	0.2389	0.2817	0.3193	0.3530	0.3835	0.41151	0.4377*	0.4618*
18		0.2800	0.3179	0.3518	0.3828	0.4111	0.4372	0.4615
19							0.4362	0.4607

*optimal rotation speed

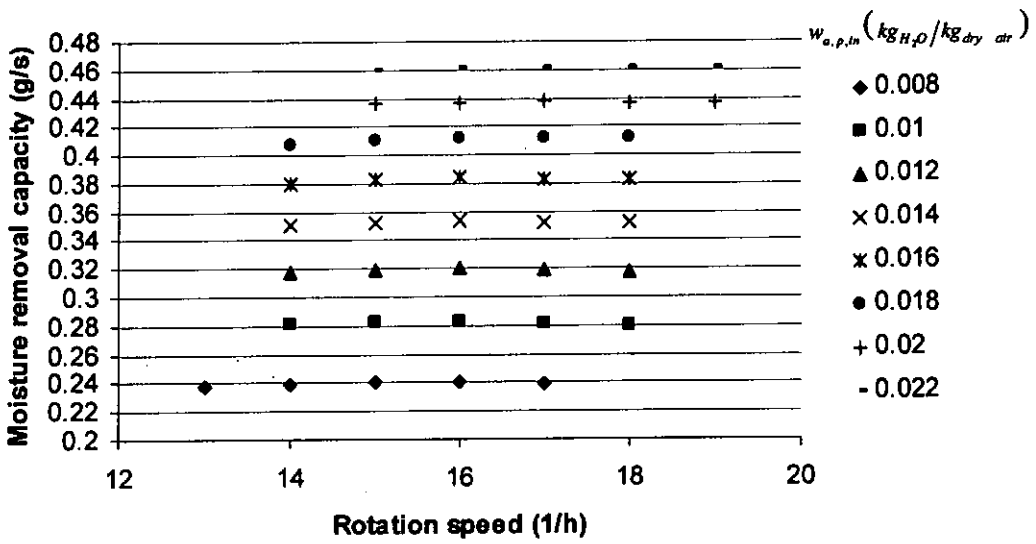

Figure 6.11 Effect of the process air inlet humidity ratio and the rotation speed on the moisture removal capacity

As shown in Table 6.4 and Figure 6.11, the optimal rotation speed for the desiccant wheel simulated in this section is 16 rph for almost all the process air inlet humidity ratio. The optimal rotation speed is independent of the process air inlet humidity ratio.

6.5 Effect of Mass Flow Rate of Process Airstream on the Dehumidifying Performance and the Optimal Rotation Speed

The discussion so far is based mainly on fixed value of the mass flow rate of process airstream. In this section, effect of the mass flow rate of process airstream on the dehumidifier performance and the optimal rotation speed is examined. For

this purpose, the moisture removal capacity is simulated at various mass flow rate of process airstream, with other parameters kept at constant values.

The process air inlet condition, regeneration air inlet humidity ratio, and the regeneration air mass flow rate used in the simulations are the same as used in Section 6.1. The regeneration air inlet temperature is 100°C.

The effect of the mass flow rate of process airstream on the dehumidification performance of a rotary dehumidifier is presented in Figure 6.12, for rotation speed of desiccant wheel 16rph. With other parameters kept at constant value, increasing the mass flow rate of process airstream enhances the moisture transfer between the process air stream and desiccant, which enhances the dehumidification performance in the desiccant wheel. Figure 6.12 shows that the moisture removal capacity increases as the mass flow rate of process airstream increases.

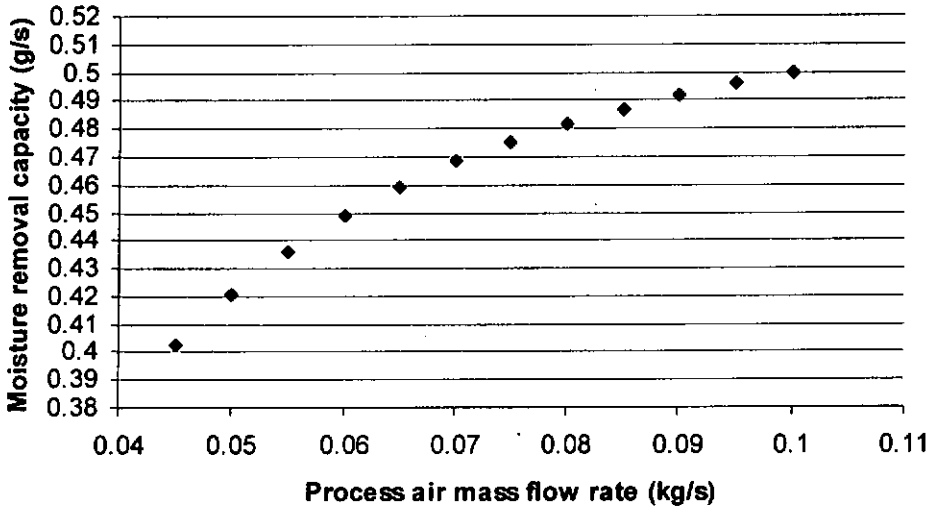

Figure 6.12 Effect of process air mass flow rate on moisture removal capacity for the rotation speed of desiccant wheel 16 rph

Table 6.5 and Figure 6.13 show the effect of the process air mass flow rate $\dot{M}_{a,p}$ and the rotation speed n_{rs} on the moisture removal capacity.

Table 6.5 Effect of the process air mass flow rate and the rotation speed on the moisture removal capacity (g_{H_2O}/s)

$\dot{M}_{a,p}(kg/s)$	Moisture Removal Capacity (g_{H_2O}/s)					
	14rph	15rph	16rph	17rph	18rph	19rph
0.045	0.3989	0.4015	0.4026	0.4027*	0.4024	0.4013
0.050	0.4173	0.4200	0.42095*	0.42094	0.4206	
0.055	0.4326	0.4353	0.4362*	0.4360	0.4356	
0.060	0.4453	0.4480	0.4488*	0.4485	0.4475	
0.065	0.4560	0.4578	0.4594*	0.4590	0.4579	
0.070	0.4650	0.4668	0.4682*	0.4678	0.4666	
0.075	0.4727	0.4744	0.4747	0.4753*	0.4741	0.4723
0.080	0.4792	0.4810	0.4813	0.4817*	0.4805	0.4786
0.085	0.4848	0.4866	0.4869*	0.4861	0.4860	
0.090	0.4896	0.4914	0.4917*	0.4910	0.4907	
0.095	0.4938	0.4956	0.4960*	0.4953	0.4937	
0.100	0.4974	0.4993	0.4997*	0.4990	0.4975	

*optimal rotation speed

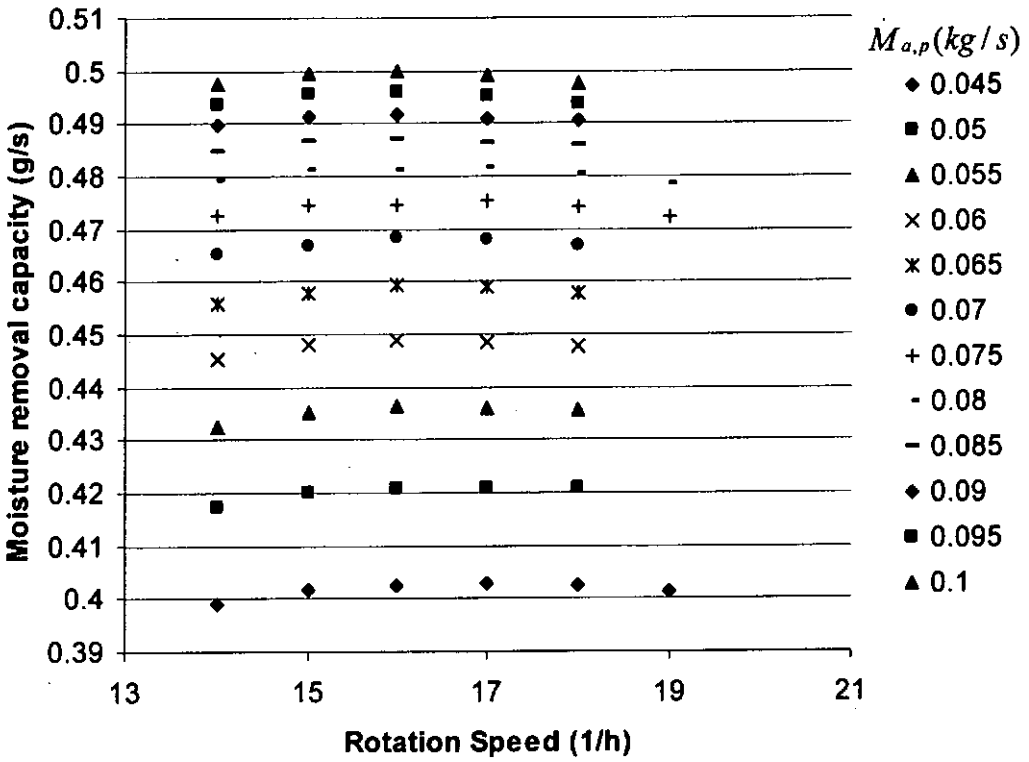

Figure 6.13 Effect of the process air mass flow rate and the rotation speed on the moisture removal capacity

As shown in Table 6.5 and Figure 6.13, the optimal rotation speed for the desiccant wheel simulated in this section is 16rph and 17rph for all process air mass flow rate. The optimal rotation speed is independent of the process air mass flow rate.

6.6 Variations in Outlet Parameters of Process and Regeneration Air with Angular Position

In this section, the variations in outlet parameters of process and regeneration air with angular position are simulated. The process and regeneration air inlet

humidity ratio, the process air inlet temperature, and the process and regeneration air mass flow rate used in the simulations are the same as used in Section 6.1. The regeneration air inlet temperature is 100°C. The rotation speed is 16rph which is optimal rotation speed in above operation conditions.

Figure 6.14 shows the variations in process air outlet humidity ratio and temperature with angular position.

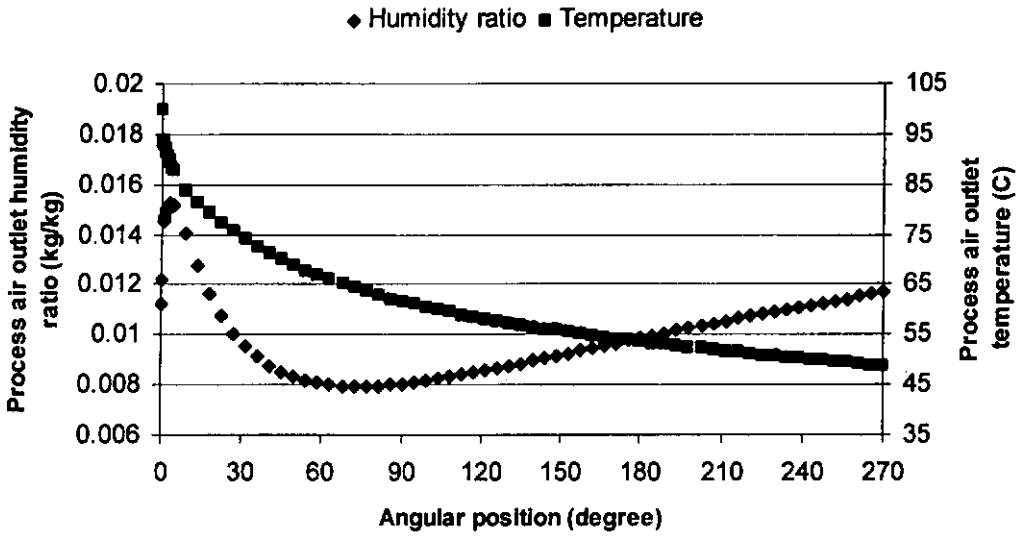

Figure 6.14 Variations in process air outlet humidity ratio and temperature with angular position

At the beginning of the process zone section, the desiccant temperature is higher, so the process air outlet temperature is higher. With increase of angular position, the process air outlet temperature decrease, as the desiccant wheel is cooled.

There is an equilibrium layer of moist air in contact with desiccant, shown in Figure 2.1. The temperature of the equilibrium layer is equal to the temperature of the desiccant surface. The isotherm determines the relations between the water content of desiccant and the relative humidity of moist air in the equilibrium layer at a given temperature. In other words, the air humidity ratio of the equilibrium layer depends on the temperature and the water content of desiccant. The mass transfer between the air flow and the desiccant depends on the difference of air humidity ratio between the air flow and the equilibrium layer in contact with desiccant. The higher the temperature and the moisture content of desiccant, the higher is the humidity ratio of moist air in the equilibrium layer.

At the beginning of the process zone section, the water content of desiccant is lowest, so the humidity ratio of moist air in the equilibrium layer is lower and the dehumidification potential between the desiccant and the process air is higher. As a result, the process air outlet humidity ratio is lower. With the increase of angular position, the process air outlet humidity ratio increases because of the increase of the water content of desiccant.

The desiccant wheel adsorbs water molecules as it is cooled. After the desiccant wheel is cooled down to certain temperature, the humidity ratio of moist air in the

equilibrium layer decreases with the decrease of desiccant temperature, so the process air outlet humidity ratio decreases with increase of angular position.

After the desiccant wheel is cooled down to the temperature at which the rotor has sufficient adsorbability, the process air outlet humidity ratio increases with increase of angular position, because of the increase in the amount adsorbed in the desiccant.

Figure 6.15 shows the variations in regeneration air outlet humidity ratio and temperature with angular position.

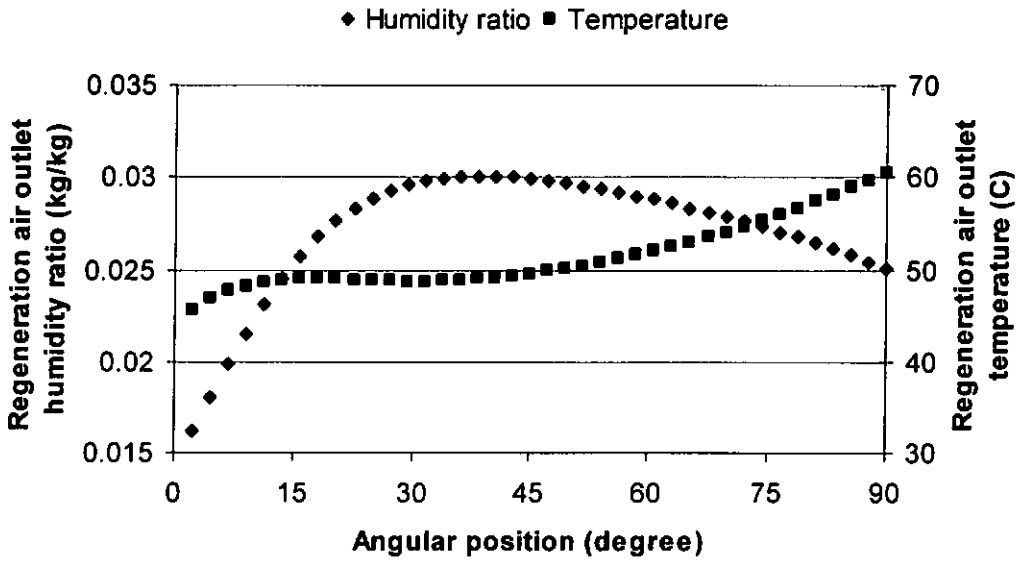

Figure 6.15 Variations in regeneration air outlet humidity ratio and temperature with angular position

At the beginning of the regeneration zone section, the desiccant temperature is lower, so the relative humidity of moist air in the equilibrium layer is lower and the

desorption potential between the desiccant and the regeneration air is smaller. As a result, the regeneration air outlet humidity ratio is lower.

At the beginning of the regeneration zone section, with increase of angular position, the desiccant temperature increases, so the regeneration air outlet humidity ratio increases.

After the desiccant wheel is heated up to certain temperature, the regeneration air outlet humidity ratio decreases with increase of angular position, because of the decrease in water content of the desiccant.

At the beginning of the regeneration zone section, the desiccant temperature is lower, so the regeneration air outlet temperature is lower. With increase of angular position, the regeneration air outlet temperature increase, as the desiccant wheel is heated. However, in the angular position in which the regeneration air outlet humidity ratio is at its maximum, the regeneration air outlet temperature decrease slightly with increase of angular position, because a large amount of heat is needed in the desorption process.

6.7 Variations in Parameters of Process and Regeneration Air with Depth into the Tubes

In this section, the variations in the parameters of process and regeneration air with depth into the tubes are simulated. Figures 6.16 and 6.17 show the variations in process air temperature and humidity ratio with depth into the tubes in different angular position, respectively. Figures 6.18 and 6.19 show the variations in regeneration air temperature and humidity ratio with depth into the tubes in different angular position, respectively. The operation conditions and the rotation speed of the desiccant wheel used in the simulations are the same as used in Section 6.6.

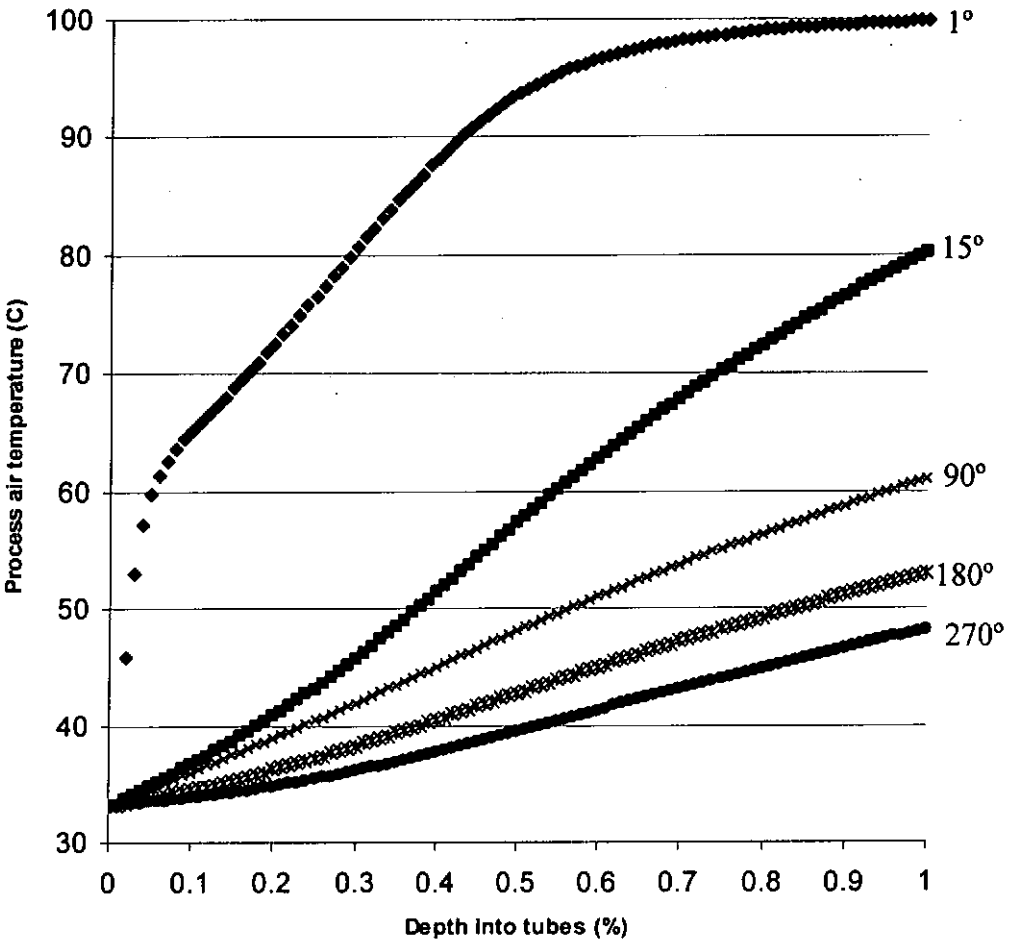

Figure 6.16 Variations in process air temperature with depth into tubes in different angular position

In Figure 6.16, the process air temperature increases with the increase of depth into the tubes, because the desiccant temperature is higher than the process air temperature.

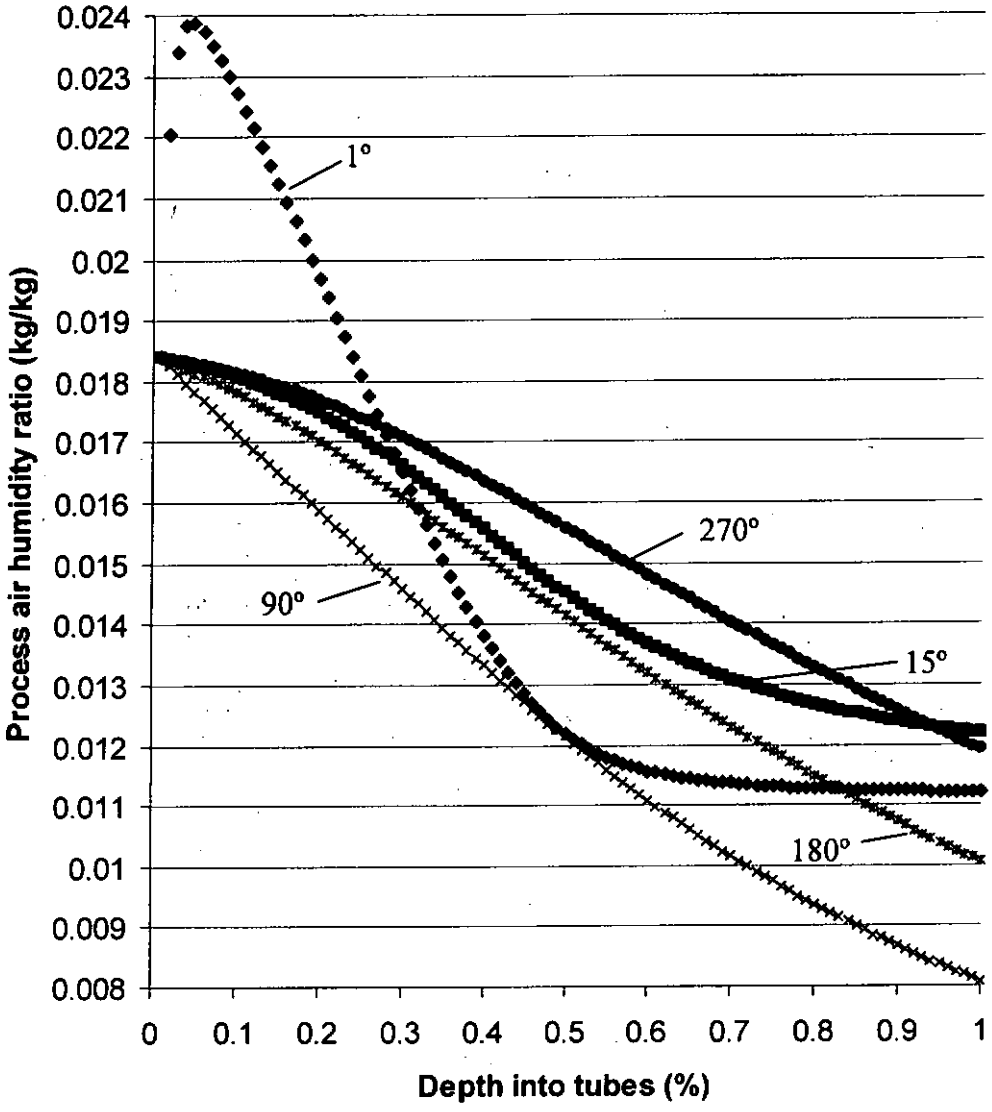

Figure 6.17 Variations in process air humidity ratio with depth into tubes in different angular position

In Figure 6.17, in the angular position 1° of the process zone section, the desiccant temperature is higher, so the relative humidity of moist air in the equilibrium layer in contact with the desiccant is higher. The water content of desiccant near the inlet of process air is larger than that of desiccant near the outlet of process air, because the regeneration and process air streams flow in opposite directions. The regeneration air outlet humidity ratio in the angular position 90° of the regeneration zone section is much higher than the process air inlet humidity ratio, by a comparison between Figure 6.17 and Figure 6.19. As a result, the air humidity ratio of the equilibrium layer in contact with the desiccant near the inlet of process air is larger than the process air inlet humidity ratio, and the process air humidity ratio increases with increase of depth into the tubes. After the process air is humidified up to certain humidity ratio, with increase of depth into the tubes, the process air humidity ratio decreases because of decrease of the water content of desiccant. The variations in process air humidity ratio with depth into the tubes for the depth more than 50% are not as pronounced as that for the depth less than 50%. Since in Figure 6.16 the process air temperature for the depth more than 50% approaches regeneration air inlet temperature 100°C and the desiccant temperature is higher than process air temperature, the desiccant temperature for the depth more than 50% approaches regeneration air inlet temperature 100°C too. As the process air humidity ratio for the depth more than 50% is lower, the dehumidification potential between the desiccant and the process air is very small at the desiccant temperature near 100°C.

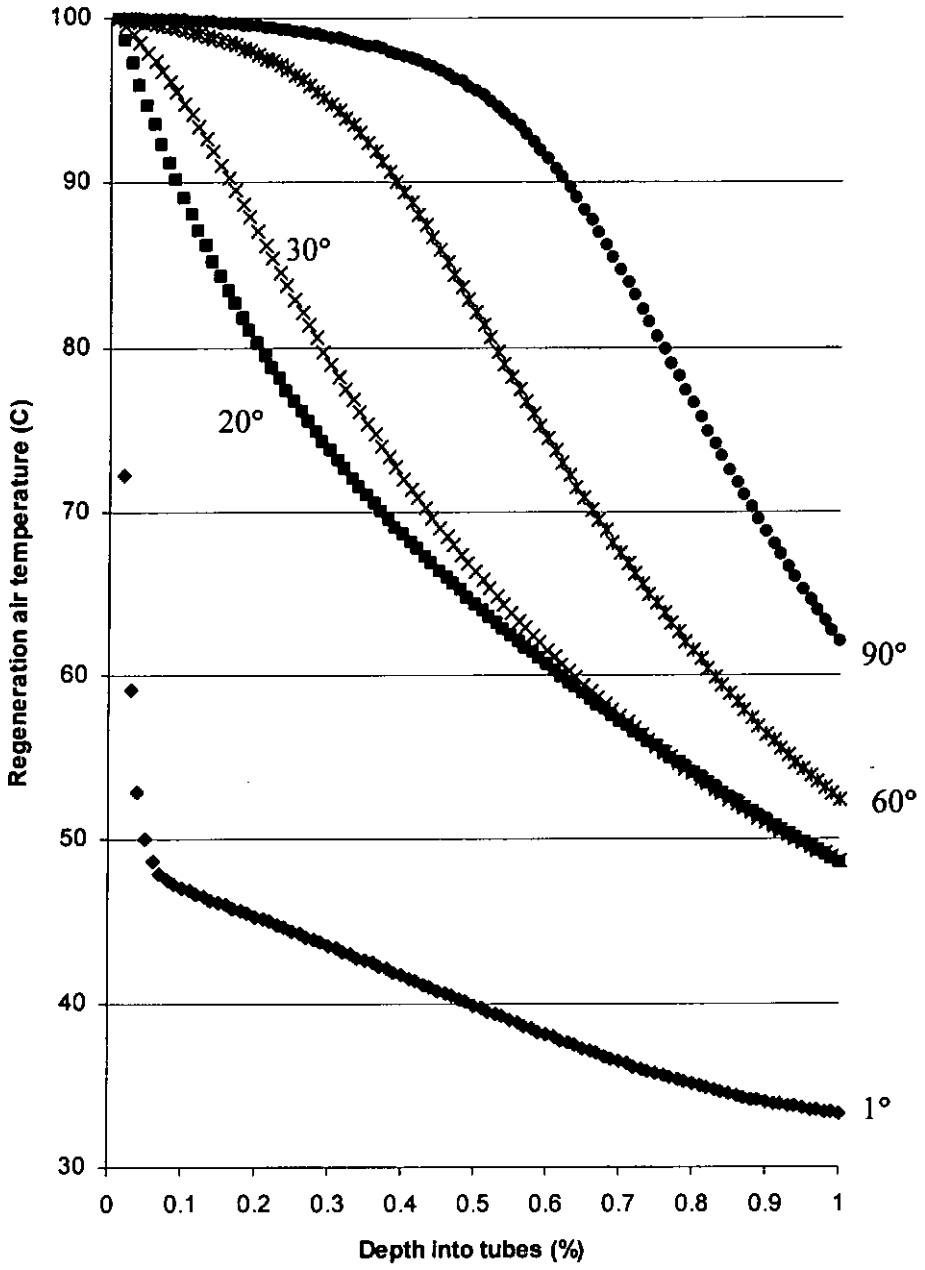

Figure 6.18 Variations in regeneration air temperature with depth into tubes in different angular position

In figure 6.17, with the increase of the angular position, the desiccant near the inlet of process air is cooled down to the temperature at which the desiccant has

adsorbability, so the process air is not humidified by desiccant near the inlet of process air and the process air humidity ratio decreases with increase of depth into the tubes.

In Figures 6.18, with increase of depth into the tubes, the regeneration air temperature decreases, because the desiccant adsorbs sensible heat from the regeneration air. In Figures 6.19, with increase of depth into the tubes, the regeneration air humidity ratio increases, because regeneration air adsorbs water molecules from the desiccant.

At the beginning of the regeneration zone section, the desiccant temperature is lower and the water content of desiccant is higher. The regeneration air temperature near the inlet is higher than that near the outlet, the regeneration air humidity ratio near the inlet is lower than that near the outlet, so temperature difference between the desiccant and the regeneration air near the inlet is higher than that near the outlet and the dehumidification potential between the desiccant and the regeneration air near the inlet is larger than that near the outlet. As a result, the variations of regeneration air temperature and humidity ratio with increase of depth near the inlet is more pronounced than that near the outlet.

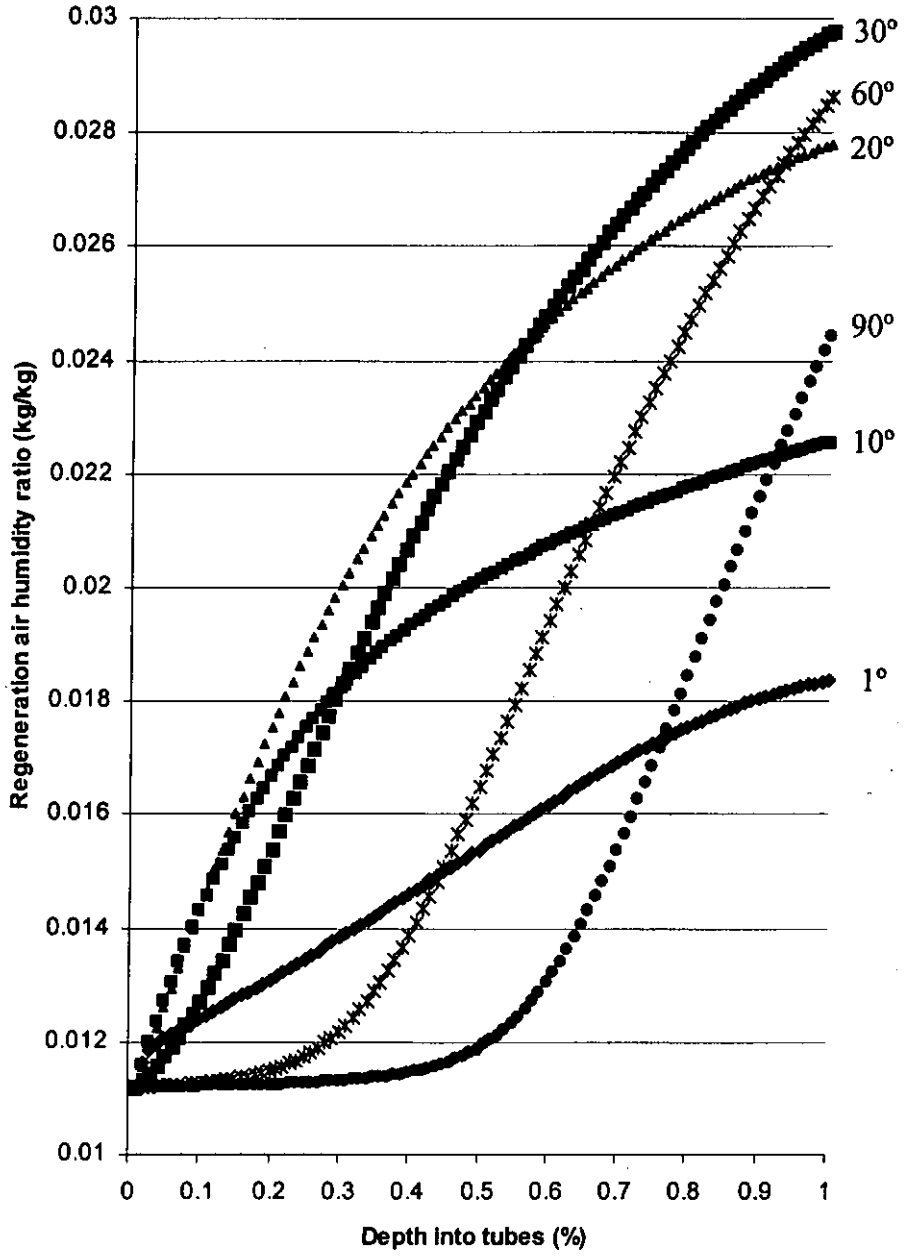

Figure 6.19 Variations in regeneration air humidity ratio with depth into tubes in different angular position

In the regeneration zone section, since the regeneration air temperature near the inlet is higher than that near the outlet and the regeneration air humidity ratio near the inlet is lower than that near the outlet, the desiccant near the inlet may reach

heat and mass equilibrium with regeneration air earlier than that near the outlet. As a result, the variations in regeneration air temperature and humidity ratio with increase of depth near the inlet is not as pronounced as near the outlet at the end of the regeneration zone section.

Chapter 7 Application of the Numerical Model to Prediction of the Performance of the Desiccant Dehumidification and Evaporative Cooling (DDEC) Systems

A desiccant dehumidification and evaporative cooling (DDEC) system relies on the processes of desiccant dehumidification, heat exchange, and evaporative cooling. This method of cooling and dehumidifying uses a variety of heat sources. The method is becoming more noticeable because of its electricity saving and CFC-free characteristics.

Figure 7.1 is a schematic representation of a single-stage DDEC system. Two air streams involved, and the supply air at point 3 is the stream that actually provides the cooling. The exhaust air at point 8 is always rejected to ambient, since it carries away all the heat and humidity entering the system either as air-conditioning load or as input energy. There are other configurations for creating a cooling system based upon the desiccation process as a starting point, but the system shown in Figure 7.1 is the topic of the discussion in this chapter.

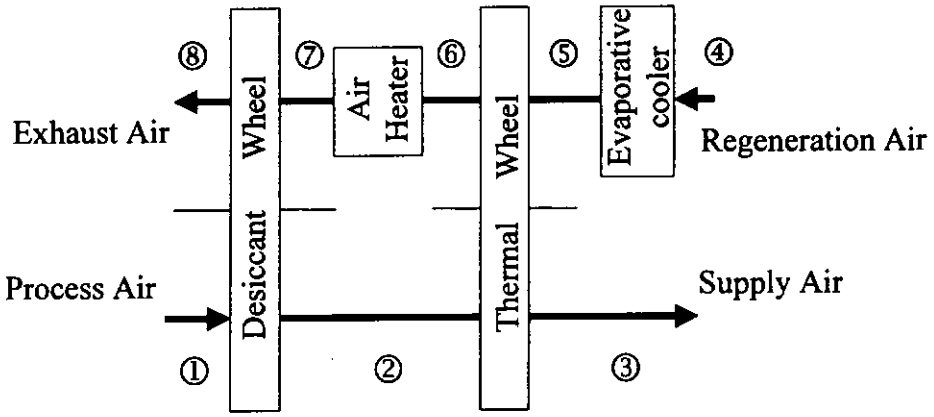

Figure 7.1 Schematic of a single - stage DDEC system

However, this system is deficient in that each desiccant is regenerated with high-temperature air. In temperate climate, the regeneration temperature is in the region of 60-80°C. In hot humid climate, the regeneration temperatures are more than 90°C. For the very low humidity ratio required of the supply air, such as in ice arenas, the regeneration temperature is even more than 100°C (Banks 1996). The high regeneration temperature limits utilization of waste heat. It is worth discussing how to reduce the regeneration temperature in order to make full use of low-temperature heat. If the process air flowed alternately over infinite desiccant wheels and intercoolers, the thermodynamics of the process air would be isothermal. Other conditions being equal, the regeneration temperature of an ideal, infinite multistage DDEC system is minimum. Figure 7.2 is a graphical representation of the thermodynamics properties of the cycle in a h-w chart.

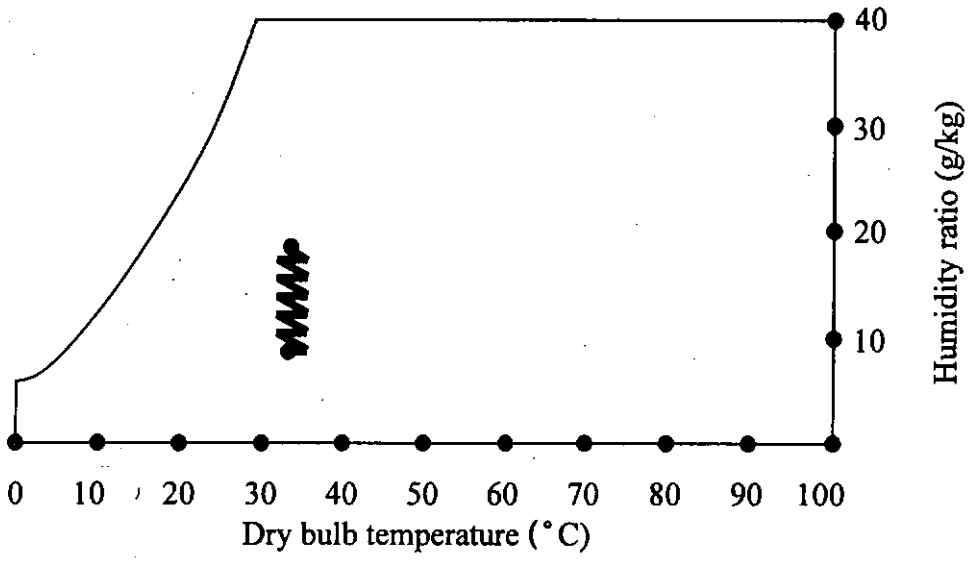

Figure 7.2 Cycle of an ideal infinite, multistage DDEC system

In this chapter, a two-stage DDEC system using low-temperature heat is proposed, and its performance is predicted. And then a comparison between a two-stage system and a single-stage system is made. The performance of desiccant wheel in the DDEC systems is simulated using the numerical model developed in the preceding chapters. Direct evaporative air coolers and thermal wheels are also the components of the DDEC systems. The experimental study of the direct evaporative air cooler is detailed in Section 7.2 and the mathematical model of the thermal wheel is described in Section 7.3.

7.1 Description of A Two-Stage DDEC System with Intercooling

Figure 7.3 shows a schematic diagram of a two-stage DDEC system with intercooling. The intercooler is first-stage thermal wheel. On condition that the regeneration temperature of each stage is equal, the required regeneration temperature is minimum.

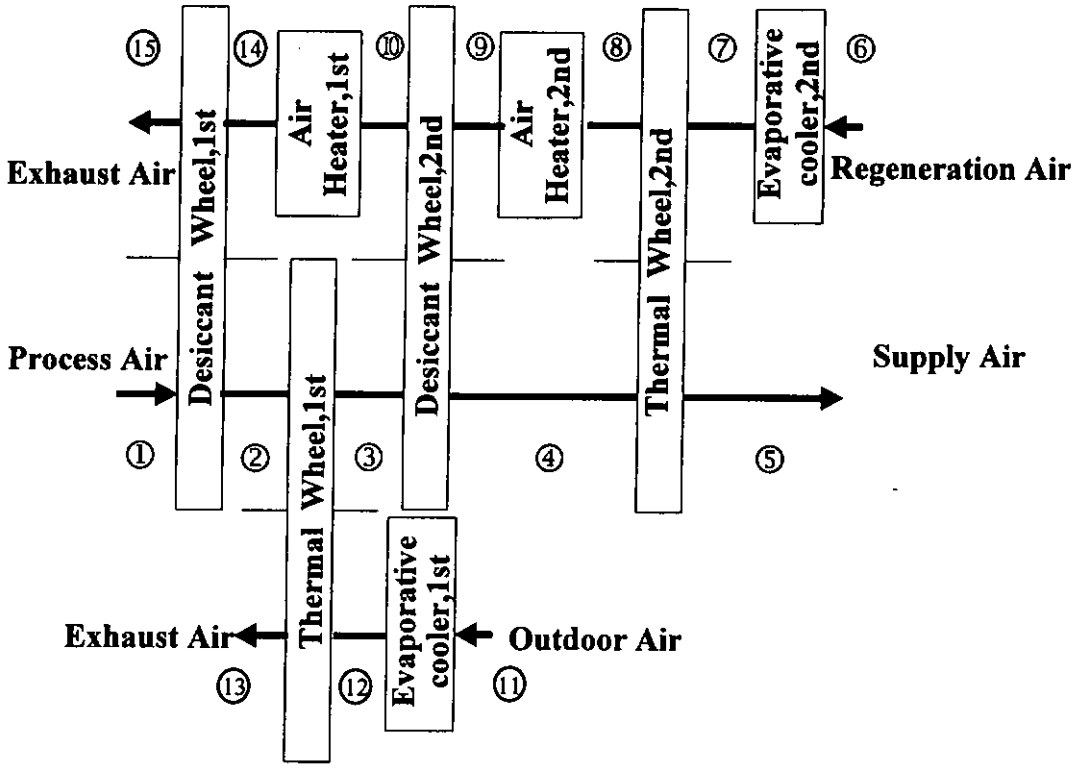

Figure 7.3 Schematic of a two-stage DDEC system

7.2 Experimental Study of Direct Evaporative Air Cooler (Zhang et al. 2000)

7.2.1 Introduction

Direct evaporative air coolers are also the components of the DDEC systems. Direct evaporative air coolers are regarded as energy-efficient, environmental friendly and cost-effective as air handling equipment (ASHRAE Handbook, HVAC Applications, 1999).

Applications of evaporative cooling range from comfort cooling in residential, agricultural, commercial and institutional buildings, to industrial applications for spot cooling in mills, foundries, power plants, and other hot environments (ASHRAE Handbook, HVAC Applications, 1999).

Media for direct evaporative air coolers can be classified as either random or rigid. Sheets of rigid, corrugated material make up the wetted surface of evaporative cooler and serve to bring the water and air into contact so that the air can absorb moisture and lower the dry-bulb temperature (cooling effect). The upper medium enclosure is fabricated of reinforced galvanized steel, stainless steel, other corrosion-resistant sheet metal, or plastic (ASHRAE Handbook, HVAC Equipment, 1996).

An ideal pad should have the following characteristics (Bom, 1999):

- minimum resistance to airflow
- maximum air-water contact for vaporization
- equal distribution of airflow resistance, air-water contact and water flow

- resistance to chemical or biological degradation
- ability to self-clean airborne matter
- durability and consistent performance over life cycle
- low cost.

In reality, all pads fall short of this ideal and thus require some trade-offs. Materials of rigid pads used at present include paper, cellulose and fiberglass that have been treated chemically with antirot and rigidifying resins, and typically use a honeycomb type structure. Saturation effectiveness of the evaporative coolers using this material varies from 70% to over 95%. The rigid medium is usually designed for a face velocity of 2-3*m/s* (Bom, 1999).

Some manufacturers supply pads made of woven plastic, but these have the disadvantage of poor cooling efficiency (low saturation effectiveness) because of the poor wetting characteristics of the plastic material. Other substances have been tried as pad materials such as woven expanded paper; fabrics; wood wool made of pine, fir, cottonwood, cedar, redwood or spruce; plain and etched glass fibres; copper, bronze and galvanized screening; but none of these is used extensively (Bom, 1999).

In each country where evaporative coolers are used or are intended to be used it may be advisable to look for an inexpensive and easily available indigenous pad

material. The objective, of course, is to avoid the need for continuous large – scale shipment of pad materials such as corrugated paper (Bom 1999).

So far, no reports have been found for the application of corrugated holed aluminum foil fillers (CHAF fillers), which have the following advantages:

- long and fairly constant service life
- self – cleaning (i.e., dust washes off)
- lack of biological deterioration
- ease of available to most of countries
- moderate cost.

If the saturation efficiency of 75-90% and low pressure drop are validated by the testing of an evaporative air cooler filled with CHAF, aluminum foil is a good pad material.

In this section, the theoretical and experimental analysis of evaporative coolers filled with CHAF is detailed.

7.2.2 Principles of Direct Evaporative Air Coolers

Direct evaporative cooling is an air-conditioning process that uses the evaporation of liquid water to cool an airstream directly so that the final dry bulb temperatures

of the airstream being cooled is lower than before undergoing the evaporative process. The direct evaporative air cooler consists of filler, a circulating pump, a distributor and a water tank, as shown in Figure 7.4. The filler is installed within a frame. Water is drawn by the circulating pump from the water tank, and distributed uniformly to the filler by the distributor. When an airstream contacts the water film directly, the processes of heat and mass transfer occur immediately. The remaining water drops down to the water tank and is recirculated. Because water is recirculated, the water temperature approaches the air wet-bulb temperature. Thus the process of direct evaporative cooling produces a constant wet-bulb temperature for an airstream, and can be regarded approximately as an isenthalpic process, as shown in Figure 7.5. Air enters the cooler at point 'e' and leaves the cooler at point 'l'. Evaporative cooling effectiveness, η_{ec}, is often used to assess the performance of a direct evaporative cooler, defined as

$$\eta_{ec} = \frac{t_e - t_l}{t_e - t_{ew}} \tag{7.1}$$

where t_e - temperature of air stream entering evaporative cooler (°C);

t_l - temperature of air stream leaving evaporative cooler (°C);

t_{ew} - wet-bulb temperature of air stream entering evaporative cooler (°C)

The effectiveness of evaporative cooling depends on the face velocity of the air flowing through the evaporative cooler, the water-air ratio for the mass flow rate of

the spraying water and the mass flow rate of the cooled air, and on the air inlet conditions and configurations of the wetted surface.

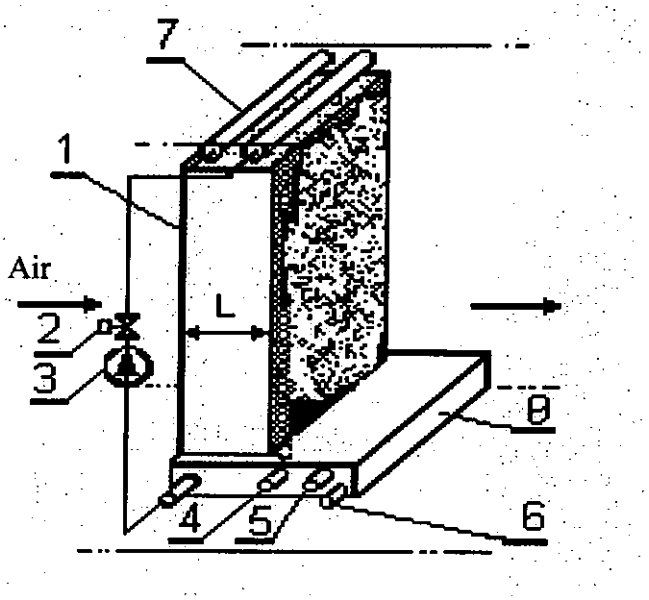

1. Filler
2. Valve
3. Circulating pump
4. Make-up water pipe
5. Overflow pipe
6. Discharging pipe
7. Distributor
8. Water tank

Figure 7.4 Schematic diagram of a direct evaporative air cooler

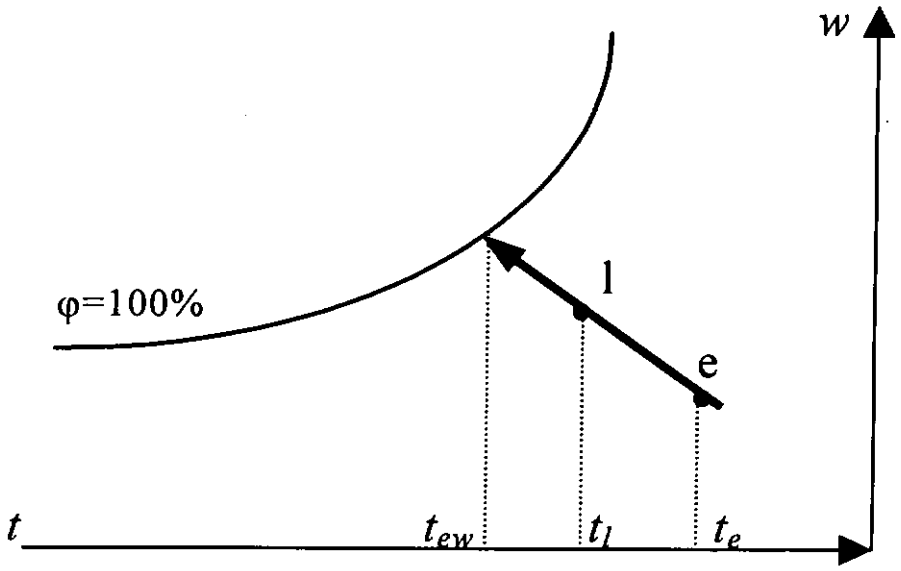

Figure7.5 Evaporative cooling process on psychometric diagram

In the evaporative cooling processes, the enthalpy is approximatively constant.

$$h_e = h_l \tag{7.2}$$

where h_e - enthalpy of air stream entering evaporative cooler ($kJ/kg_{dry\ air}$);

h_l - enthalpy of air stream leaving evaporative cooler ($kJ/kg_{dry\ air}$)

7.2.3 Experimental Study of the CHAF Cooler

The evaporative cooling effectiveness, η_{ec}, can be found from the energy and mass equations when the Lewis number is 1.0, i.e.

$$\eta_{ec} = 1 - \exp\left(-\frac{\alpha_v \cdot L}{\rho \cdot v_a \cdot c_{pa,ev}}\right) \tag{7.3}$$

where α_v - average volume heat transfer coefficient between air and water in evaporative air cooler ($kW/m^3 \cdot K$), defined as

$$\alpha_v = \alpha \cdot \frac{A_{ec}}{V} \quad (kW/m^3 \cdot K) \tag{7.4}$$

α - heat transfer coefficient between air and water in evaporative air cooler ($kW/m^2 \cdot K$);

A_{ec} - contact surface area between air and water in evaporative air cooler (m^2);

V - filler volume in evaporative air cooler (m^3);

L - filler thickness in evaporative air cooler (m);

ρ - air density in evaporative air cooler (kg/m^3);

v_a - face velocity of air in evaporative air cooler (m/s);

$c_{pa,ev}$ - specific heat capacity of air at constant pressure in evaporative air cooler ($kJ/kg \cdot K$)

The evaporative cooling effectiveness is a function of the filler thickness, air velocity and average volume heat transfer coefficient, among other factors. Apart from the structural parameters, the evaporative cooling effectiveness depends mainly on v_a and α_v, and the latter determined by the sprinkling density and air velocity.

A test rig was built to test the performance and find the relationships between the effectiveness and other parameters. The filler is made of JKB-700X aluminum foil, which was first holed then corrugated and then installed in series. The thickness of the CHAF filler is 200mm, the face area is 400mm (width)×800mm (height), the surface area ratio is 700 m^2/m^3 and the void ratio is 85%. The void ratio is defined as the ratio of the void volume of the filler to the product of face area and the thickness of the filler. Test results of the evaporative air cooler filled with CHAF are shown in Figure 7.6 to 7.10.

Effect of the Sprinkling Density on the Effectiveness

The sprinkling density q is defined as

$$q = \frac{m_w}{A_w} \quad (kg_{H_2O}/m^2 \cdot s) \tag{7.5}$$

where m_w - water flow rate in evaporative air cooler (kg_{H_2O}/s);

A_w - cross-sectional area of sprinkling water in evaporative air cooler (m^2)

The effect of the sprinkling density on the effectiveness is shown in Figure 7.6 when t_e = 28.3 °C, t_{ew} = 21.7 °C and v_a = 2.0 m/s. As sprinkling density increases, the falling water film on the filler surface forms water drops, and then changes into water streams in the filler. At the same time, as the contact area between air and water increases, the evaporative cooling effectiveness and average volume heat transfer coefficient increasing as shown in Figure 7.7 for the α_v-q relationship, but air flow resistant is also higher owing to narrow flow path as shown in Figure 7.8.

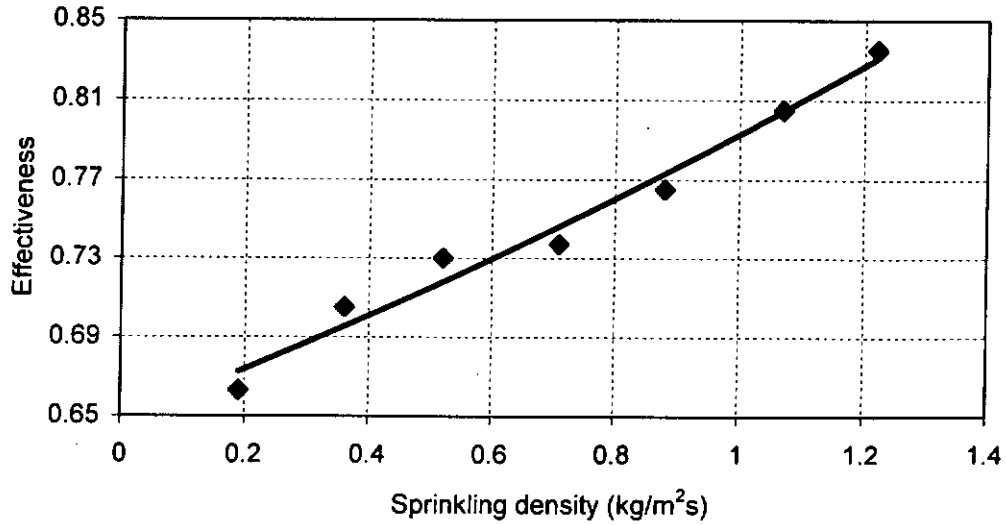

Figure 7.6 Effectiveness η_{ec} against sprinkling density q

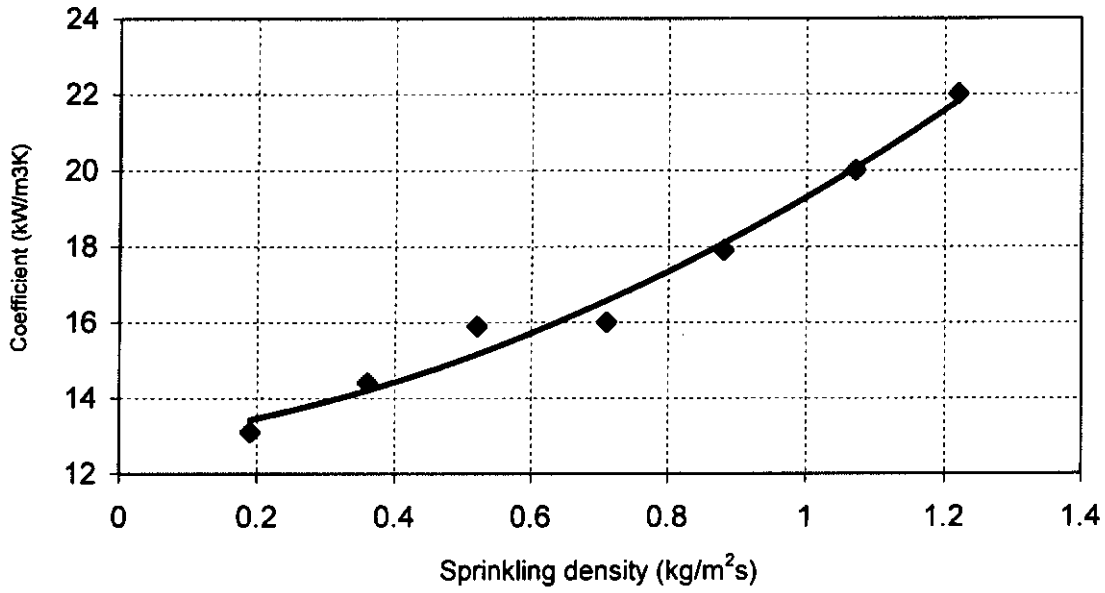

Figure7.7 Average volume heat transfer Coefficient α_v again sprinkling density q

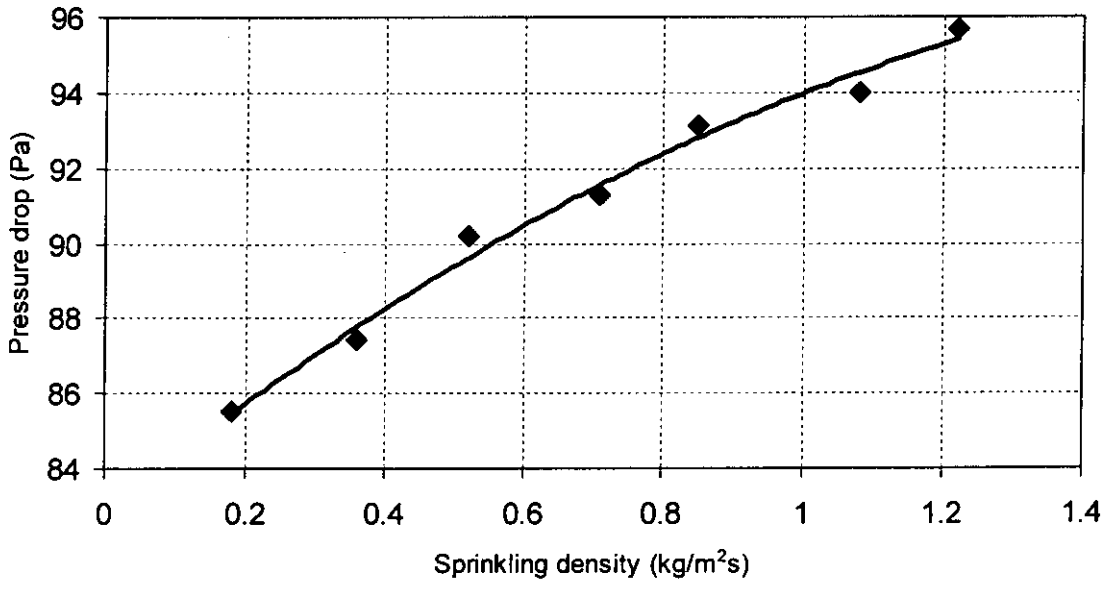

Figure7.8 Air pressure drop ΔP against sprinkling density q

Effect of the Air Velocity on the Effectiveness

Equation 7.3 shows that both the air velocity and the average volume heat transfer coefficient have an effect on the effectiveness of evaporative cooling. The effectiveness of evaporative cooling decreases with increase of the air velocity through the cooler when the average volume heat transfer coefficient is constant. This is because the contact time of air with water surfaces in the filler is shorter, so that the transfer of heat and moisture is not sufficient. The effectiveness of evaporative cooling is equal to unity when the air velocity is zero. However, the air velocity also has an effect on the average volume heat transfer coefficient. The following correlation of Nusselt number with Reynolds and Prandtl numbers was obtained experimentally by J.A.Dowdy and N.S. Karabash (1987) for the evaporative cooling process through various thickness of rigid impregnated cellulose evaporative media.

$$Nu = 0.10 \cdot (l_e / L)^{0.12} \cdot \mathrm{Re}^{0.8} \cdot \mathrm{Pr}^{1/3} \qquad (7.6)$$

where l_e - the characteristic length (m), defined as

$$l_e = V / A_{ec} \quad (m) \qquad (7.7)$$

Equation 7.6 shows that the higher the air velocity, the higher the heat transfer coefficient and thus the higher the effectiveness of evaporative cooling.

Combining the effect of the air velocity on Equation 7.3 and on Equation 7.6, the effectiveness of evaporative cooling does not necessarily increases with the increase or decrease of the air velocity through the cooler.

Figure 7.9 shows the effect of the enter air velocity on the effectiveness when t_e = 28.5 °C, t_{ew} = 22.5 °C and air velocity varies from 2.0 to 2.8m/s. When air velocity is low, the effectiveness decreases gradually with the increase of air velocity, because of shorter contact time period between the air stream and the filler surface. However, when the air velocity is above 2.4 m/s, the cooling effectiveness increases slightly with the increase of the air velocity because higher air velocity makes the heat and mass transfer coefficient greater.

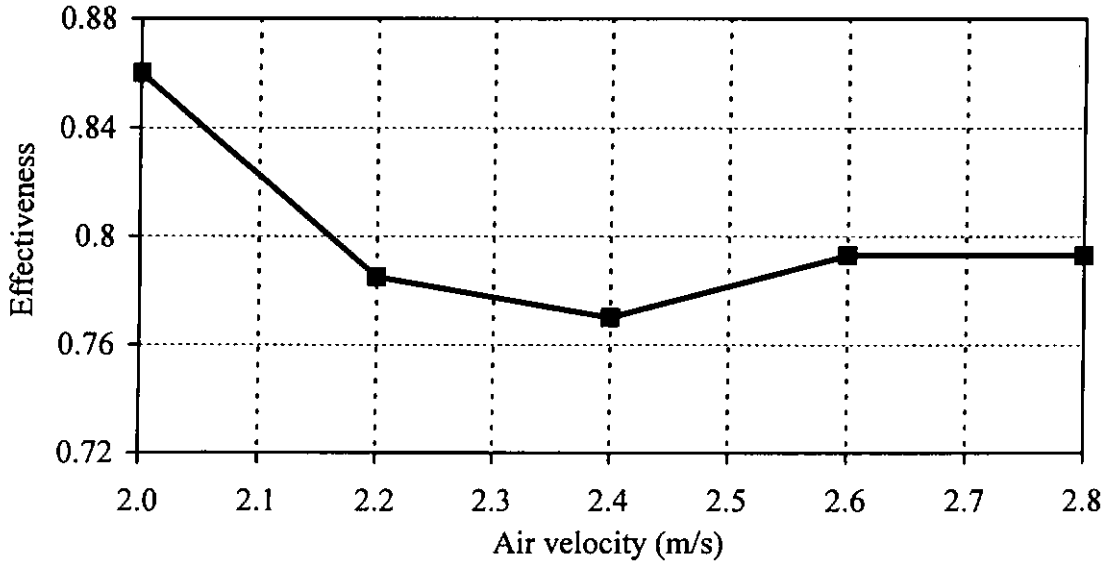

Figure 7.9 Effect of air velocity v_a on effectiveness η_{ec}

From Equations 7.3 and 7.4, the evaporative cooling effectiveness, η_{ec}, decreases with the increase of air velocity, but the average volume heat transfer coefficient increases with the increase of air velocity, and the effectiveness increases with the increase of heat transfer coefficient. The results of these conflicting effects yielded a turning point in effectiveness. Therefore, turning-point air velocity depends on filler thickness in evaporative air cooler, L, contact surface area between air and water in evaporative air cooler, A_{ec}, and filler volume in evaporative air cooler, V.

When the air velocity is no greater than 2.4 m/s, a lower air velocity can result in a higher cooling effectiveness, but will also produce a larger face area of the evaporative cooler for a given airflow rate. Therefore, the air velocity should usually not be lower than 2.0 m/s, and it should usually not be higher than 2.8 m/s in order to prevent the carryover of water droplets.

Figure 7.10 demonstrates that a linear relationship can be used for the air pressure loss Δp across the cooler and the air velocity when the sprinkling density is 1.04 $kg/m^2 \cdot s$. Optimum values of the sprinkling density and air velocity exist for different coolers. An air velocity of 2.0-2.8 *m/s* and a sprinkling density of 0.5-1.2 $kg/m^2 \cdot s$ lead to the maximum cooling effectiveness.

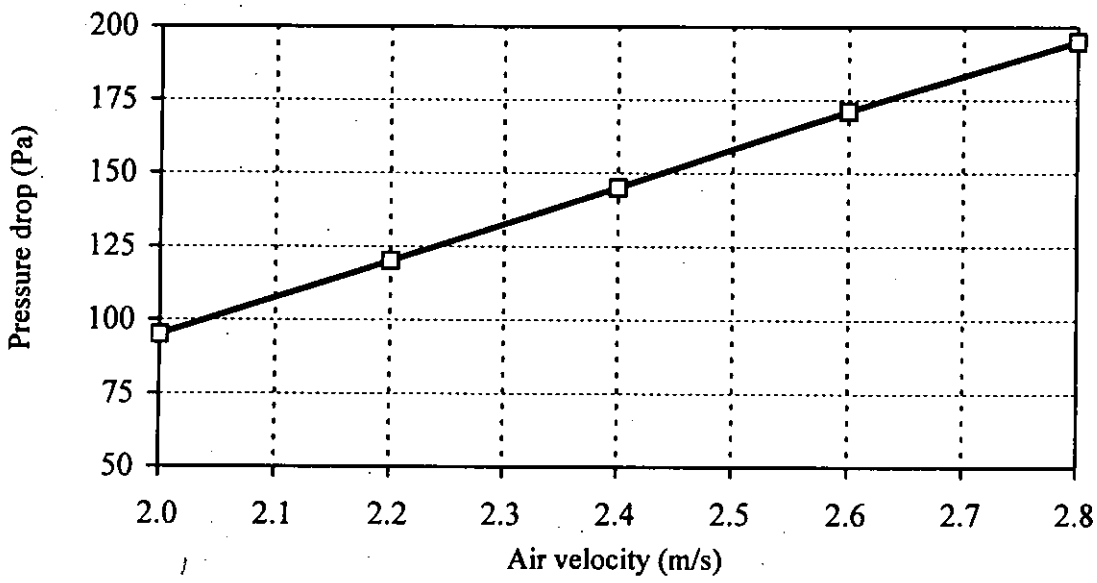

Figure 7.10 Pressure drop ΔP against air velocity v_a

7.2.4 Regression Analysis of Experimental Data

The air temperature at outlet and the energy loss through the filler have been obtained using linear multiple regression from the measured data. The experimental conditions are sprinkling density between 0.2 and $1.2\,kg/m^2 \cdot s$, the air velocity between 2.0 and $2.8m/s$ and $(T_e - T_{ew})/T_e$ between 0.015 and 0.045. T_e and T_{ew} are the absolute temperature and absolute wet-bulb temperature of air stream entering evaporative cooler respectively.

$$t_l = 1.015 \times t_e^{0.579} t_{ew}^{0.369} v_a^{0.082} q^{-0.03} \qquad (7.8)$$

$$\Delta P = 23.893 \times v_a^{2.032} q^{0.066} \qquad (7.9)$$

Thus, the cooling effectiveness can be found from equations 7.1 and 7.8:

$$\eta_{ec} = \frac{t_e - 1.015 \times t_e^{0.579} t_{ew}^{0.369} v_a^{0.082} q^{-0.03}}{t_e - t_{ew}} \tag{7.10}$$

7.3 Mathematical Model of Thermal Wheel

The static points of the cold fluid entering and leaving thermal wheel are 'ce' and 'cl'. The static points of the hot fluid entering and leaving thermal wheel are 'he' and 'hl'. The effectiveness of a thermal wheel η_{tw} is defined as the ratio of the actual rate of heat transfer between the hot and cold fluids to the maximum possible rate of heat transfer, that is

$$\eta_{tw} = \frac{C_h \cdot (t_{he} - t_{hl})}{C_{\min} \cdot (t_{he} - t_{ce})} \tag{7.11}$$

where C_h – heat capacity rate of the hot fluid flowing through the thermal wheel (kW/K);

$$C_h = \dot{m}_h \cdot c_{ph} \quad (kW/K) \tag{7.12}$$

$\dot{m}_h$ - mass flow rate of the hot fluid flowing through the thermal wheel (kg/s);

c_{ph} - specific heat of the hot fluid flowing through the thermal wheel $(kJ/kg \cdot K)$;

C_{min} – the smaller value between C_h and C_c (kW/K);

C_c – heat capacity rate of the cold fluid flowing through the thermal wheel (kW/K);

$$C_c = \dot{m}_c \cdot c_{pc} \quad (kW/K) \tag{7.13}$$

$\dot{m}_c$ - mass flow rate of the cold fluid flowing through the thermal wheel (kg/s);

c_{pc} - specific heat of the cold fluid flowing through the thermal wheel $(kJ/kg \cdot K)$;

t_{he} - air temperature of the hot fluid entering thermal wheel (°C);

t_{hl} - air temperature of the hot fluid leaving thermal wheel (°C);

t_{ce} - air temperature of the cold fluid entering thermal wheel (°C)

In the sensible cooling and heating processes, the humidity ratio is always constant.

$$w_{he} = w_{hl} \tag{7.14}$$

$$w_{ce} = w_{cl} \tag{7.15}$$

where w_{he} - air humidity ratio of the hot fluid entering thermal wheel $(kg_{H_2O}/kg_{dry\ air})$;

w_{hl} - air humidity ratio of the hot fluid leaving thermal wheel $(kg_{H_2O}/kg_{dry\ air})$;

w_{ce} - air humidity ratio of the cold fluid entering thermal wheel $(kg_{H_2O}/kg_{dry\ air})$;

w_{cl} - air humidity ratio of the cold fluid leaving thermal wheel $(kg_{H_2O}/kg_{dry\ air})$

The effectiveness of a thermal wheel, η_{tw}, varies from 0.80 to 0.95 (Jurinak and Beckman 1980).

7.4 Operating Parameters of the Two-Stage DDEC Cycle

Consider an office building air conditioning system in Hong Kong. Sensible cooling is performed by a mechanical refrigerating system and latent cooling by a DDEC system. The DDEC system as ventilation system should remove moisture from the supply air to maintain a specified indoor humidity ratio. The reactivation air is return air, and the process air is fresh air.

In Hong Kong, the summer condition of the outdoor air is dry bulb 33.2°C and wet-bulb temperature 26.1°C, corresponding to 0.4% annual cumulative frequency of occurrence (ASHRAE Handbook, Fundamentals 26.31). The indoor thermal comfort design criterion is air temperature of 24°C and 60% relative humidity. Fresh air supply is $0.008 m^3/s$ per person (ASHRAE Standard 55 – 1992). The latent heat and moisture from each occupant are $55W$ and $2.2\times10^{-5}\ kg/s$ (ASHRAE Handbook, Fundamentals 26.31). Occupants are the only source of moisture

generation. The static points of the outdoor air and the indoor air are 'o' and 'i'. The static point of the supply air is 's'.

From the psychrometric chart, the humidity ratios of outdoor and indoor air are

$$w_o = 0.01860 kg_{H_2O}/kg_{dry\ air}$$

and $$w_i = 0.01120 kg_{H_2O}/kg_{dry\ air}$$

To maintain a required indoor humidity ratio the humidity ratio of supply air is

$$w_s = w_i - \frac{0.000022}{0.008 \times \rho_{a,o}} \quad (kg_{H_2O}/kg_{dry\ air}) \tag{7.16}$$

where $\rho_{a,o}$ - dry air density of outdoor air, its value can be taken as

$$1.1532 kg_{dry\ air}/m^3$$

thus, the humidity ratio of supply air is

$$w_s = 0.0112 - \frac{0.000022}{0.008 \times 1.1532} = 0.00882 \quad (kg_{H_2O}/kg_{dry\ air})$$

The desiccant wheel used in the simulation of the two-stage DDEC system in this chapter is the same as the test unit, and the rotation speed is 20rph. Assume that the effectiveness of a thermal wheel η_{tw} is 0.80, and the saturation effectiveness of an evaporative cooler η_{ec} is 0.80. Each mass flow rate is equal, and is $0.045 kg/s$ (In case of the larger mass flow rate, the larger desiccant wheel diameter can be chosen). The calculations of the operating parameters of the two-stage DDEC cycle are shown in Table 7.1. Figure 7.11 shows the DDEC cycle of this system.

Table 7.1 Operation parameter calculations for the two-stage DDEC system

Point	Temperature (°C)	Humidity ratio ($kg_{H_2O}/kg_{dry\ air}$)	Enthalpy ($kJ/kg_{dry\ air}$)
Process air			
1 Outdoor air	33.2	0.01860	81.06
2 After the first desiccant wheel	47.8	0.01341	82.79
3 After the first thermal wheel	31.6	0.01341	66.08
4 After the second desiccant wheel	45.7	0.00882	68.71
5 Supply air	24.9	0.00882	47.47
Regeneration air			
6 Space air	24.0	0.01120	52.64
7 After the second evaporative cooler	19.7	0.01295	52.64
8 After the second thermal wheel	40.5	0.01295	74.03
9 After the second air heater	60.2	0.01295	94.38
10 After the second desiccant wheel	46.1	0.01756	91.76
11 Outdoor air	33.2	0.01860	81.06
12 After the first evaporative cooler	27.5	0.02092	81.06
13 After the first thermal wheel	43.7	0.02092	97.99
14 After the first air heater	60.2	0.01756	106.46
15 After the first desiccant wheel	45.6	0.02277	104.74

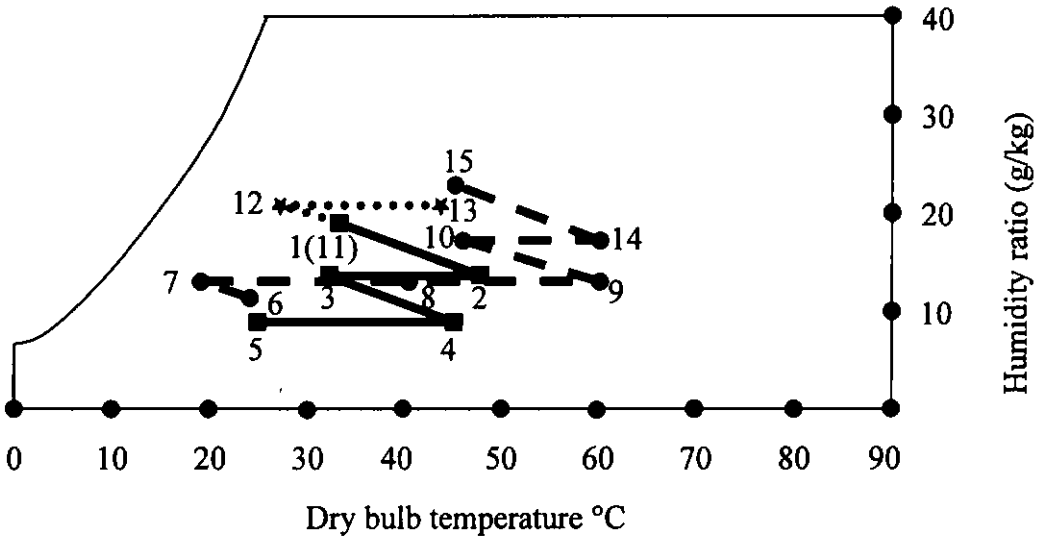

Figure 7.11 Cycle of a two-stage DDEC system

The humidity ratio and the enthalpy of air at point 'j' are expressed as w_j and h_j respectively. The dehumidifying capacity per $kg_{dry\ air}/s$, Δw_f of the first desiccant wheel is:

$$\Delta w_f = w_1 - w_2 = w_o - w_2 = 0.01860 - 0.01341 = 0.00519 \quad (kg_{H_2O}/kg_{dry\ air})$$

The dehumidifying capacity per $kg_{dry\ air}/s$, Δw_s of the second desiccant wheel is:

$$\Delta w_s = w_3 - w_4 = w_3 - w_s = 0.01341 - 0.00882$$

$$= 0.00459 \quad (kg_{H_2O}/kg_{dry\ air})$$

The regeneration air inlet temperatures of each stage desiccant wheel are equal. The humidity ratio of the regeneration air entering the first-stage desiccant wheel is 0.01756 $kg_{H_2O}/kg_{dry\ air}$ and 0.00461 $kg_{H_2O}/kg_{dry\ air}$ higher that than of the regeneration air entering the second-stage desiccant wheel, which will decrease the

dehumidification capacity of the first desiccant wheel. The temperature of the process air entering the first-stage desiccant wheel is 33.2°C and approximates the temperature 31.6°C of the process air entering the second-stage desiccant wheel. The humidity ratio of the process air entering the first-stage desiccant wheel is $0.01860\,kg_{H_2O}/kg_{dry\ air}$ and $0.00519\,kg_{H_2O}/kg_{dry\ air}$ higher than that of the process air entering the second-stage desiccant wheel, which will increase the dehumidification capacity of the first desiccant wheel. With these conditions, the dehumidifying capacity per $kg_{dry\ air}/s$ of the first desiccant wheel is $0.0006\,kg_{H_2O}/kg_{dry\ air}$ higher than that of the second desiccant wheel.

The total dehumidifying capacity per $kg_{dry\ air}/s$, Δw_t is:

$$\Delta w_t = w_1 - w_4 = w_o - w_s = 0.01860 - 0.00882$$

$$= 0.00978 \quad (kg_{H_2O}/kg_{dry\ air})$$

The cooling capacity per $kg_{dry\ air}/s$, $q_{cool,tf}$, of the first thermal wheel is:

$$q_{cool,tf} = h_2 - h_3 = 82.79 - 66.08 = 16.71 \quad (kJ/kg_{dry\ air})$$

The cooling capacity per $kg_{dry\ air}/s$, $q_{cool,ts}$, of the second thermal wheel is:

$$q_{cool,ts} = h_4 - h_5 = 68.71 - 47.47 = 21.24 \quad (kJ/kg_{dry\ air})$$

The cooling capacity per $kg_{dry\ air}/s$ of the first thermal wheel is $4.53\,kJ/kg_{dry\ air}$ lower than that of the second thermal wheel, because the temperature difference

between the two air streams entering the first thermal wheel is smaller than for the second thermal wheel.

The total cooling capacity per $kg_{dry\ air}/s$, $q_{cool,t}$, of the two-stage DDEC system is:

$$q_{cool,t} = h_1 - h_5 = 81.06 - 47.47 = 33.59 \quad (kJ/kg_{dry\ air})$$

The total cooling capacity per $kg_{dry\ air}/s$, $q_{cool,t}$, of the two-stage DDEC system is not equal to the sum of $q_{cool,tf}$ and $q_{cool,ts}$, because of the rise in enthalpy during the dehumidification of process air.

The regeneration heat input per $kg_{dry\ air}/s$, $q_{in,t}$, of the two-stage DDEC system is:

$$q_{in,t} = h_{14} - h_{10} + h_9 - h_8 = 106.46 - 91.76 + 94.38 - 74.03 = 35.05(kJ/kg_{dry\ air})$$

The coefficient of performance, COP, is:

$$COP = \frac{q_{cool,t}}{q_{in,t}} = \frac{33.59}{35.05} = 0.958$$

The regeneration specific heat input, *RSHI*, is:

$$RSHI = \frac{q_{in,t}}{\Delta w_t} = \frac{35.05}{0.00978} = 3584 \quad (kJ/kg_{H_2O})$$

7.5 A Comparison between the Two-Stage and A Single-Stage DDEC Systems

7.5.1 Operating Parameters of the Single-Stage DDEC Cycle

Similar calculations are done for a single-stage DDEC system. The components and the airstream inlet conditions in the single-stage DDEC system are the same as that in the two-stage DDEC system. The only difference is the desiccant wheel rotation speed 30rph for the single-stage DDEC system. The operating parameters of the process air and regeneration air at the exits of various components of the single-stage DDEC system are shown in Table 7.2. Figure 7.12 is a graphical representation of the thermodynamic properties of the cycle in a psychrometric chart.

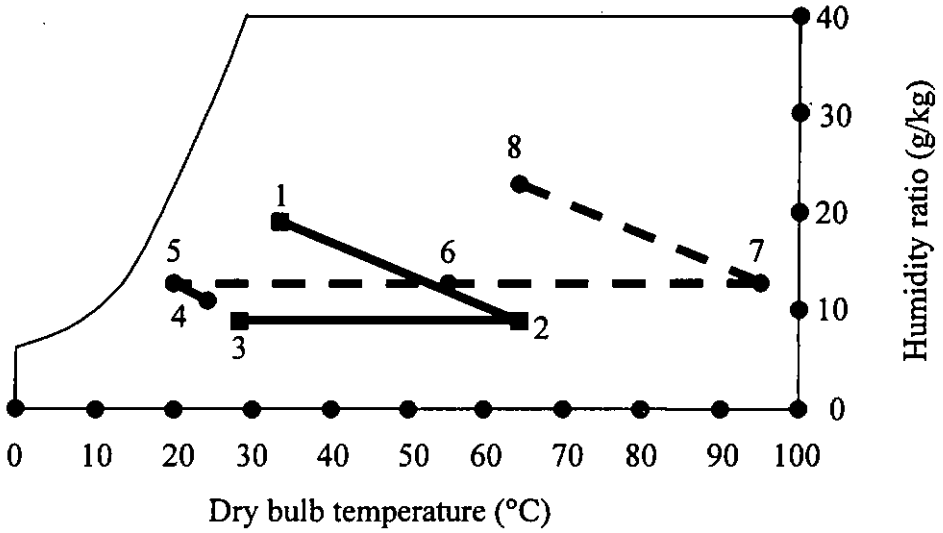

Figure 7.12 Cycle of a single-stage DDEC system

Table 7.2 Operation parameter calculations for the single-stage DDEC system

Point	Temperature (°C)	Humidity ratio ($kg_{H_2O}/kg_{dry\ air}$)	Enthalpy ($kJ/kg_{dry\ air}$)
Process air			
1 Outdoor air	33.2	0.01860	81.06
2 After desiccant wheel	64.3	0.00882	87.93
3 Supply air	28.6	0.00882	51.29
Regeneration air			
4 Space air	24.0	0.01120	52.64
5 After evaporative cooler	19.7	0.01295	52.64
6 After thermal wheel	55.4	0.01295	89.43
7 After air heater	95.2	0.01295	130.92
8 After desiccant wheel	63.8	0.02278	124.02

The total dehumidifying capacity per $kg_{dry\ air}/s$, Δw_t of each DDEC system is equal.

The cooling capacity per $kg_{dry\ air}/s$, $q_{cool,s}$, of the single-stage DDEC system is:

$$q_{cool,s} = h_1 - h_3 = 81.06 - 51.29 = 29.77 \quad (kJ/kg_{dry\ air})$$

The regeneration heat input per $kg_{dry\ air}/s$, $q_{in,s}$, is:

$$q_{in,s} = h_7 - h_6 = 130.92 - 89.43 = 41.49 \quad (kJ/kg_{dry\ air})$$

The coefficient of performance, COP, is:

$$COP = \frac{q_{cool,s}}{q_{in,s}} = \frac{29.77}{41.49} = 0.718$$

The regeneration specific heat input, *RSHI*, is:

$$RSHI = \frac{q_{in,s}}{\Delta w_t} = \frac{41.49}{0.00978} = 4242 \quad (kJ/kg_{H_2O})$$

7.5.2 A Comparison between the Two Systems

Comparison of Regeneration Air Inlet Temperature

The required regeneration air inlet temperature of the two-stage DDEC system is 60.2°C and 35.0°C lower than that of the single-stage system. The lowered regeneration air inlet temperature makes possible utilization of low-quality thermal energy such as solar energy and waste heat.

Comparison of Supply Air Parameters

The supply air temperature of the two-stage DDEC system is 24.9°C, approximates to the indoor air temperature 24.0°C, and is 3.7°C lower than that of the single-

stage system. At the conditioned space, the supply air of the two-stage DDEC system absorbs the latent heat from the occupants and rarely supplies sensible heat.

The supply air temperature of the single-stage DDEC system is 28.6°C and 4.6°C higher than the indoor air temperature. Besides absorbing the latent heat, the supply air of the single-stage system supplies sensible heat to the conditioned space.

The supply air enthalpy of the two-stage DDEC system is 47.47 $kJ/kg_{dry\ air}$ and 3.82 $kJ/kg_{dry\ air}$ lower than that of the single-stage system and 5.17 $kJ/kg_{dry\ air}$ lower than of the indoor air.

Comparison of Exhaust Air Temperature

There are two exhaust air streams in the two-stage DDEC system. The temperature of one exhaust air stream is 45.6°C and that of the other is 43.7°C. The two temperatures are both lower than the exhaust air temperature 63.8°C of single-stage DDEC system. That is, the two-stage DDEC system can decrease the heat pollution to the environment relatively to the single-stage system.

Comparison of Cooling Capacity

The cooling capacity per $kg_{dry\ air}/s$ of the two-stage DDEC system increases by 12.8% relatively to the single-stage system.

Comparison of COP and *RSHI*

The coefficient of performance, COP, of the two-stage DDEC system is 0.958 and 0.24 higher than that of the single-stage system, and regeneration specific heat input, *RSHI*, of the former is 3584 kJ/kg_{H_2O} and 658 kJ/kg_{H_2O} lower than that of the latter. The two-stage system not only has higher COP and lower *RSHI* but also requires the lower temperature heat used as regeneration heat. The required regeneration air inlet temperature of the two-stage DDEC system is 35.0°C lower than that of the single-stage system, so COP and *RSHI* are not reasonable index of performance for comparison between the two systems. The exergy method of energy system analysis should be used to evaluate rationally the heat energy consumption of the two systems.

Comparison of Exergy of Heat

For the two-stage system, the regeneration heat input per $kg_{dry\ air}/s$ of the first air heater, $q_{10,14}$, is:

$$q_{10,14} = h_{14} - h_{10} = 106.46 - 91.76 = 14.70 \quad (kJ/kg_{dry\ air})$$

For the process from state 10 to state 14, the exergy of heat is determined by the well-known expression

$$Ex_{q10,14} = \int_{10}^{14} dq - T_0 \cdot \int_{10}^{14} \frac{dq}{T} = q_{10,14} - T_0 \cdot \int_{10}^{14} \frac{c_p \cdot dT}{T} = q_{10,14} - T_0 \cdot c_p \cdot \ln \frac{T_{14}}{T_{10}} \tag{7.17}$$

where T_o - absolute temperature of ambient air, $300K$;

c_{pa} - specific heat of air at constant pressure, its value can be taken as $1.01 kJ/kg \cdot K$;

T_j - absolute temperature of air at point 'j' (K)

hence

$$Ex_{q10,14} = 14.70 - 300 \times 1.01 \times \ln \frac{60.2 + 273.16}{46.1 + 273.16} = 1.605 \quad (kJ/kg_{dry\ air})$$

Similarly, the regeneration heat input per $kg_{dry\ air}/s$ of the second air heater, $q_{8,9}$, is:

$$q_{8,9} = h_9 - h_8 = 94.38 - 74.03 = 20.35 \quad (kJ/kg_{dry\ air})$$

For the process from state 8 to state 9, Equation 7.17 gives

$$Ex_{q8,9} = \int_{8}^{9} dq - T_o \cdot \int_{8}^{9} \frac{dq}{T} = q_{8,9} - T_o \cdot \int_{8}^{9} \frac{c_p \cdot dT}{T} = q_{8,9} - T_o \cdot c_p \cdot \ln \frac{T_9}{T_8}$$

$$= 20.35 - 300 \times 1.01 \times \ln \frac{60.2 + 273.16}{40.5 + 273.16} = 1.893 \quad (kJ/kg_{dry\ air})$$

The total exergy of heat of a two-stage DDEC system is

$$Ex_{q,t} = Ex_{q10,14} + Ex_{q8,9} = 1.605 + 1.893 = 3.498 \quad (kJ/kg_{dry\ air})$$

For the single-stage system, the regeneration heat input per $kg_{dry\ air}/s$, $q_{6,7}$, is:

$$q_{6,7} = h_7 - h_6 = 130.92 - 89.43 = 41.49 \quad (kJ/kg_{dry\ air})$$

From Equation 7.17, the exergy of heat of the process from state 6 to state 7 is

$$Ex_{q,s} = Ex_{q6,7} = \int_6^7 dq - T_0 \cdot \int_6^7 \frac{dq}{T} = q_{6,7} - T_o \cdot \int_6^7 \frac{c_p \cdot dT}{T} = q_{6,7} - T_o \cdot c_p \cdot \ln\frac{T_7}{T_6}$$

$$= 41.49 - 300 \times 1.01 \times \ln\frac{95.2 + 273.16}{55.4 + 273.16} = 6.845 \quad (kJ/kg_{dry\ air})$$

It is thus evident that the exergy of heat per $kg_{dry\ air}/s$ of a single-stage DDEC system is higher than a two-stage system. The increment of the exergy of heat is

$$\Delta Ex_{q,st} = Ex_{q,s} - Ex_{q,t} = 6.845 - 3.498 = 3.347 \quad (kJ/kg_{dry\ air})$$

The exergy of heat per $kg_{dry\ air}/s$ of the two-stage DDEC system is only 51% of that of the single-stage system.

7.6 Conclusions

The required regeneration air inlet temperature of the two-stage DDEC system with intercooling is 35.0°C lower than of the single-stage system. The lowered regeneration temperature makes possible utilization of low-quality thermal energy such as solar energy and waste heat.

The cooling capacity per $kg_{dry\ air}/s$ of the two-stage DDEC system increases by 12.8 percent relatively to the single-stage system. The coefficient of performance, COP, of the two-stage DDEC system is 0.24 higher than that of the single-stage system, and regeneration specific heat input, *RSHI*, of the former is $658\,kJ/kg_{H_2O}$ lower than of the latter. The two-stage system not only has higher COP and lower *RSHI* but also requires the lower temperature heat used as regeneration heat. The required regeneration air inlet temperature of the two-stage DDEC system is much lower than of the single-stage system, so COP and *RSHI* are not reasonable index of performance for comparison between the two systems. The heat energy system analysis using exergy method shows that the exergy of heat per $kg_{dry\ air}/s$ of the two-stage desiccant cooling system is only 51% of that of the single-stage system.

The supply air enthalpy in both the two-stage system and the single-stage system is lower than the indoor air enthalpy. The supply air temperature of the two-stage DDEC system approximates to the indoor air temperature, so the supply air does not need further sensible cooling.

The exhaust air temperatures of the two-stage desiccant cooling system are lower than of the single-stage DDEC system. That is, the two-stage DDEC system can decrease the heat pollution to the environment relatively to the single-stage system.

The supply air of both the single-stage system and the two-stage system has sufficient low humidity to control indoor humidity, assuming that occupants are the major source of moisture generation. Mechanical cooling is required only for sensible heat removal purposes, so a higher evaporating temperature is required and consequently the coefficient of performance, COP, of a mechanical refrigerating system will be higher.

The direct evaporative cooling effectiveness η_{ec} of the evaporative air cooler using CHAF is about 0.8. The air flow resistance is not more than 200Pa for air velocity less than 3m/s. Therefore, the CHAF is a good pad material according to the characteristics which an ideal pad should have (Bom 1999) and the advantages which CHAF has.

Chapter 8 Summary and Recommendations

Rotary desiccant dehumidifiers are regarded as energy-efficient as air handling equipment, because of its low-cost requirements of thermal energy. The energy source in desorption can be provided from low-level energy such as waste heat from industries, hot air exhausted from refrigerators , solar collectors and so on.

The desiccant wheel has long been used in dehumidification and cooling systems, and is the primary component of a solid-desiccant cooling system. The desiccant wheel is the most difficult component to simulate, and the simulation of the desiccant wheel is the most time-consuming portion of all simulation programs of solid-desiccant cooling systems. The subject of heat and mass transfer in rotary desiccant dehumidifiers has been studied extensively over a period of many years.

In this thesis, a numerical model that predicts the heat and moisture transfer during adsorption and desorption processes in a desiccant-coated, rotary dehumidifier has been developed from physical principles. All the assumptions are explained. The model is one-dimensional and transient, and includes all important parameters that affect the performance of desiccant wheels, such as energy and mass storage in both air and matrix, convection, the axial thermal conduction through both desiccant and the support material, the axial water molecular diffusion within the

desiccant coating and the energy transfer between the air stream and the matrix. So far, no reports have been found on the model of desiccant coated rotary dehumidifier including all important parameters mentioned above, but literature review indicates a need for an accurate model of heat and mass transfer in a desiccant-coated, rotary dehumidifier. This model can be used in designing or optimizing the desiccant wheels and in predicting the performance of desiccant enhanced air-conditioning system.

The mathematical model of desiccant wheel is developed subject to the equilibrium relation of the desiccant material, the heat of adsorption, thermal conduction and moisture diffusion through desiccant material, the heat and mass transfer coefficient, the specific heat capacity, and the other desiccant properties which are detailed in Chapter 2.

Chapter 3 presented the four governing equations for coupled heat and mass transfer in desiccant wheel. The conservation equation of moisture on air stream includes moisture storage in air, moisture inflow by convection, and moisture transfer between the air stream and the desiccant. The conservation equation of moisture on desiccant includes moisture storage on the surface and in the pores of the desiccant felt material, moisture inflow by combined ordinary diffusion and Knudsen diffusion and surface diffusion through pores of the desiccant felt material, and moisture transfer between the air stream and the desiccant. The conservation

equation of energy on air stream includes energy storage in air, energy inflow by convection, and energy transfer between the air stream and the matrix. The conservation equation of energy on matrix includes energy storage in both the desiccant and the support material, energy inflow by heat conduction through matrix and moisture diffusion through pores of the desiccant felt material, and energy transfer between the air stream and the desiccant.

The discretization of the governing equations is performed and all the dependent variables and properties are solved at the nodes. The transient terms are solved using the implicit formulation. The numerical solution scheme is fully implicit for all of the dependent variables in that the most updated value is used in each algebraic equation. The discretized equations of moisture conservation are solved using the Thomas algorithm, also called the Tridiagonal Matrix Algorithm (TDMA), and the discretized equations of energy conservation are solved using the Tridiagonal Matrix Algorithm for double variables.

To validate the numerical model by comparisons with experimental data, a test rig has been built in accordance with ASHRAE Standard 139 - 1998, Standard Method of Testing for Rating Desiccant Dehumidifiers Utilizing Heat for the Regeneration Process.

The accuracy of the simultaneous heat and moisture transfer numerical model of desiccant coated rotary dehumidifier developed in this study has been confirmed by the good agreement with experimental data. The simulated moisture removal capacity agrees with the test data within experimental uncertainty. The model of the desiccant wheel has been used to predict the moisture removal capacity for various design and operation parameters. The wide range of change in each moisture removal capacity with design and operation parameters implies that an accurate model will be very important for the design of HVAC systems using desiccant coated rotary dehumidifier.

The simulation sensitivity results show that the moisture removal capacity becomes larger as the process air inlet humidity ratio and the regeneration air inlet temperature increase, and as the process air inlet temperature and the regeneration air inlet humidity ratio decrease. The moisture removal capacity also increases as the mass flow rate of process airstream increases.

Optimal rotation speed of desiccant wheel is one of the most important factors in the design and the operation parameters of a desiccant wheel. The effects of the rotation speed on dehumidifying performance under various operating conditions have been also investigated. An empirical formula proposed by Kodama et al. (1994) is used to predict the optimal rotation speed in a given set of operation and design parameters. The optimal rotation speed predicted by the empirical formula

is identical with the optimal rotation speed simulated by the numerical model developed in this thesis, which validates the numerical model at a different angle. The empirical formula correlates the optimal rotation speed with mass flow rate of regeneration air, bulk specific heat and total mass of desiccant wheel, but the effects of the process and regeneration air inlet conditions and process air flow rate on the optimal rotation speed were not taken into account. Based on empirical formula proposed by Kodama et al. (1994), a recommendation for the optimal rotation speed has been given to take the effect of the process and regeneration air inlet temperature and regeneration air inlet humidity ratio on the optimal rotation speed into account. The optimal rotation speed increases as the regeneration and process air inlet temperature increase, and as the regeneration air inlet humidity ratio decrease. The optimal rotation speed is independent of the process air inlet humidity ratio and mass flow rate.

The variations in outlet parameters of process and regeneration air with angular position and in the parameters of process and regeneration air with depth into the tubes are simulated.

The numerical model of desiccant-coated, rotary dehumidifier developed in this thesis has been also applied to the prediction of the performance of the desiccant dehumidification and evaporative cooling (DDEC) systems. The DDEC systems rely on the processes of desiccant dehumidification, heat exchange, and evaporative

cooling. This method of cooling and dehumidifying uses a variety of heat sources. The method is becoming more noticeable because of its electricity saving and CFC-free characteristics.

However, the single-stage DDEC system is deficient in that each desiccant is regenerated with high-temperature air. In temperate climate, the regeneration temperature is in the region of 60-80°C. In hot humid climate, the regeneration temperatures are more than 90°C. For the very low humidity ratio required of the supply air, such as in ice arenas, the regeneration temperature is even more than 100°C (Banks 1996). The high regeneration temperature limits utilization of waste heat. It is worth discussing how to reduce the regeneration temperature in order to make full use of low-temperature heat. If the process air flowed alternately over infinite desiccant wheels and intercoolers, the thermodynamics of the process air would be isothermal. Other conditions being equal, the regeneration temperature of an ideal, infinite multistage DDEC system is minimum.

A two-stage DDEC system using low-temperature heat has been proposed, and its performance is predicted. Then a comparison between a two-stage system and a single-stage system is made. The required regeneration air inlet temperature of the two-stage DDEC system with intercooling is 35.0°C lower than of the single-stage system. The lowered regeneration temperature makes possible utilization of low-quality thermal energy such as solar energy and waste heat.

The cooling capacity per $kg_{dry\ air}/s$ of the two-stage DDEC system increases by 12.8 percent relatively to the single-stage system. The coefficient of performance, COP, of the two-stage DDEC system is 0.24 higher than that of the single-stage system, and regeneration specific heat input, *RSHI*, of the former is $658\,kJ/kg_{H_2O}$ lower than of the latter. The two-stage system not only has higher COP and lower *RSHI* but also requires the lower temperature heat used as regeneration heat. The required regeneration air inlet temperature of the two-stage DDEC system is much lower than of the single-stage system, so COP and *RSHI* are not reasonable index of performance for comparison between the two systems. The heat energy system analysis using exergy method shows that the exergy of heat per $kg_{dry\ air}/s$ of the two-stage desiccant cooling system is only 51% of that of the single-stage system.

The supply air enthalpy in both the two-stage system and the single-stage system is lower than the indoor air enthalpy. The supply air temperature of the two-stage DDEC system approximates to the indoor air temperature, so the supply air does not need further sensible cooling.

The exhaust air temperatures of the two-stage desiccant cooling system are lower than of the single-stage DDEC system. That is, the two-stage DDEC system can decrease the heat pollution to the environment relatively to the single-stage system.

The supply air of both the single-stage system and the two-stage system has sufficient low humidity to control indoor humidity, assuming that occupants are the major source of moisture generation. Mechanical cooling is required only for sensible heat removal purposes, so a higher evaporating temperature is required and consequently the coefficient of performance, COP, of a mechanical refrigerating system will be higher.

Direct evaporative air coolers are also the components of the DDEC systems. Direct evaporative air coolers are regarded as energy-efficient, environmental friendly and cost-effective as air handling equipment (ASHRAE Handbook, HVAC Applications, 1999).

All media for direct evaporative air coolers fall short of the ideal pad and thus require some trade-offs. In each country where evaporative coolers are used or are intended to be used it may be advisable to look for an inexpensive and easily available indigenous pad material. The objective, of course, is to avoid the need for continuous large – scale shipment of pad materials such as corrugated paper (Bom, 1999).

So far, no reports have been found for the application of corrugated holed aluminum foil fillers (CHAF fillers), which have the following advantages:

- long and fairly constant service life
- self – cleaning (i.e., dust washes off)
- lack of biological deterioration
- ease of available to most of countries
- moderate cost.

The theoretical and experimental analysis of evaporative coolers filled with CHAF is detailed in Chapter 7. The experimental results show that the direct evaporative cooling effectiveness η_{ec} of the evaporative air cooler using CHAF is about 0.8, and the air flow resistance is not more than 200Pa for air velocity less than 3m/s. Therefore, the CHAF is a good pad material.

Further efforts are worth to be made on a few topics related to the research presented in this thesis. The numerical model of desiccant-coated, rotary dehumidifier developed in this thesis can be applied to the investigation of the effect of certain assumptions on the predicted performance, the optimization of the design and the operation parameters of desiccant wheel (wheel parameters, mass flow rate, temperature, and humidity), and the prediction of the performance of the desiccant enhanced air-conditioning system which has good performance in energy use, comfort and capital cost.

References

ASHRAE Handbook, Fundamentals 26.31

ASHRAE Handbook, HVAC Applications, 1999

ASHRAE Handbook, HVAC Equipment, 1996

ASHRAE Standard 41.1 – 1986 (RA 91), Standard Method for Temperature Measurement

ASHRAE Standard 41.2 – 1987 (RA 92), Standard Methods for Laboratory Airflow Measurement

ASHRAE Standard 41.3 – 1989, Standard Method for Pressure Measurement

ASHRAE Standard 55 – 1992

ASHRAE Standard 139 - 1998, Standard Method of Testing for Rating Desiccant Dehumidifiers Utilizing Heat for the Regeneration Process

ASHRAE, 1992, *Desiccant Cooling and Dehumidification*, Edited by L. Harriman, Atlanta: ASHRAE.

Banks, N. J., 1996, Desiccant dehumidifiers in ice arenas, *ASHRAE Transactions*, vol. 102, part 1

Banks, P. J., D. J. Close, and I. L. Maclaine-cross, 1970, Coupled heat and mass transfer in fluid flow through porous media-analogy with heat transfer, *Proceeding 4th Int. Heat Transfer Conference*, VII, CT3.1, Elsevier, Amsterdam.

Banks, P. J., 1972, Coupled equilibrium heat and single adsorbate transfer in fluid flow through a porous medium: I, Characteristic potentials and specific capacity ratios, *Chemical Engineering Science*, vol. 27, pp. 1143-1155.

Banks, P. J., 1985a, Prediction of heat and mass regenerator performance using nonlinear analogy method: Part 1, Basis, *ASME J. Heat Transfer*, vol. 107, pp. 222-229.

Banks, P. J., 1985b, Prediction of heat and mass regenerator performance using nonlinear analogy method: Part 2, Comparison of methods, *ASME J. Heat Transfer*, vol. 107, pp. 230-238.

Barlow, R. S., 1982, An analysis of the adsorption process and of desiccant cooling systems: A pseudo-steady-state model for coupled heat and mass transfer, Solar Energy Research Institute Rept. SERI/TR-1330, Golden, Colo..

Bom, Gert Jan., 1999, *Evaporative Air-conditioning Applications for Environmentally Friendly Cooling.*

Bullock, C. E., and J. L. Threlkeld, 1966, *ASHRAE Transactions*, vol. 72, 301.

Cejudo, J. M., R. Moreno and A. Carrillo, 2002, Physical and neural network models of a silica-gel desiccant wheel, *Energy and Buildings*, vol. 34, issue 8, pp. 837-844.

Charoensupaya, D., and W. M. Worek, 1988, Parametric study of an open-cycle adiabatic, solid, desiccant cooling system, *Energy*, vol. 13 (9), pp. 739-747.

Chau, C. K., and W. M. Worek, 1995, Interactive simulation tools for open – cycle desiccant cooling systems, *ASHRAE Transactions*, vol. 101, part 1, pp. 725-734.

Collier, R. K., T. S. Cal, and Z. Lavan, 1986, Advanced desiccant material assessment: Phase 1, Gas Research Institute Report GRI-86/0181, Chicago, Ill..

Collier, R. K., 1988, Advanced desiccant material assessment: Phase 2, Gas Research Institute Report GRI-88-0125, Chicago, Ill..

Close, D. J. and P. J. Banks, 1972, Coupled equilibrium heat and single adsorbate transfer in fluid flow through a porous medium: II, Predictions for a silica-gel air drier using characteristic charts, *Chemical Engineering Science*, vol. 27, pp. 1157-1169.

Dean, J. A., ed., 1973, Lange's Handbook of Chemistry, pp. 10, 11th ed., McGraw-Hill, New York.

Dowdy, J. A. and N. S. Karabash, 1987, Experimental Determination of Heat and Mass Transfer Coefficients in Rigid Impregnated Cellulose Evaporative Media, *ASHRAE Transactions*, vol.93, Part 2, P382-395

Dubinin, M. M., 1975, Physical adsorption of gases and vapors in micropores, Prog. Surf. Membrane Sci., vol. 9, pp. 1-70.

Dunkle, R. V., 1965, A method of solar air conditioning, in *Mechanical and Chemical Transactions, MCI*, vol. 1, pp. 73-78, Institute of Engineers, Australia.

(should delete)Eckert, E. R. G. and R. M. Drake, 1972, Analysis of heat and mass transfer, New York, McGraw-Hill, pp. 351.

Farooq, S., and D. M. Ruthven, 1991, Numerical Simulation of a desiccant bed for solar air conditioning applications, *ASME J. Solar Energy Engineering*, vol. 113, pp. 80-88.

Gilliland, E. R., R. F. Baddour, G. P. Perkinson, and K. J. Sladek, 1974, Diffusion on surfaces. I . Effect of concentration on the diffusivity of physically adsorbed gases, *Industrial Chemical Fundamental*, vol.13, No.2, pp. 95-99.

Gregg, S. J. and K. S. W. Sing, 1967, Adsorption, surface area and porosity, pp. 121, pp187.

Gunderson, M. E., K. C. Hwang, and S. M. Railing, 1978, Development of a solar desiccant dehumidifier, SAN-1591-1, AiResearch Manufacturing Co., CA.

Gurgel, J. M., and R. P. Klüppel, 1996, Thermal conductivity of hydrated silica-gel, *The Chemical Engineering Journal*, vol.61, pp. 133-138.

Husky, B., J. Sharp, A. Venero, and H. Yen, 1982, Advance solar/gas desiccant cooling system, GRI-81/0064, Gas Research Institute, Chicago, IL.

Incropera, F. P. and Dewitt, D. P., 1996, *Fundamentals of Heat and Mass Transfer*. John Wiley & Sons, New York, 886pp

Jekel, T. B., J. W. Mitchell, and Sanford A. Klein, 1993, Equilibrium performance evaluation of desiccant dehumidifiers, Joint Solar Engineering Conference, ASME.

Jurinak, J. J., 1982, Open cycle solid desiccant cooling : Component models and system simulation, Ph.D. thesis, University of Wisconsin-Madison.

Jurinak, J. J., and W. A. Beckman, 1980, A comparison of the performance of open cycle air conditioners utilizing rotary desiccant dehumidifier, ISES – As 1980 Annual Conference Phoenix 80, v3.1

Kays, W. M., and M. E. Crawford, 1980, *Convective heat and mass transfer*, New York: McGraw – Hill.

Kreith, F. and Black, W. Z., 1980, *Basic heat transfer*. Harper and Row, New York, 556pp, pp. 243.

Kodama, A., M. Goto, T. Hirose, and T.Kuma, 1994, Temperature profile and optimal rotation speed of a honeycomb rotor adsorber operated with thermal swing, *Journal of Chemical Engineering of Japan*, vol.27, no.5, pp. 644-649.

Kruckles, W. W., 1976, On gradient dependent diffusivity, *Chemical Engineering Science*, vol.28, pp. 1565-1576.

Löf, G. O. G., 1955, House heating and cooling with solar energy, in *Solar Energy Research*, University of Wisconsin Press, Madison, Wisc..

Lu, L. T., D. Charoensupaya, and Z. Lavan, 1991, Determination of sorption rate and apparent solid-state diffusivity of pure H_2O in silica gel using constant volume/variable pressure apparatus, *Journal of solar Energy*, vol. 113, pp. 257-263.

Lu, Y. Q., 1996, *A guide to HAVC Design*. Architectural Industry Press of China, Beijing, 418pp

Lunde, P., 1975, Solar powered desiccant air-conditioning system, Center for the Environment and Man Rept. CEM 4171-526, Hartford, Conn..

Maclaine-cross, I. L., and P. J. Banks, 1972, Coupled heat and mass transfer in regenerators: Predictions using an analogy with heat transfer, *Int. J. Heat Mass Transfer*, vol. 15, pp. 1225-1242.

Maclaine-cross, I. L., 1974, A theory of combined heat and mass transfer in regenerators, Ph.D. thesis, Monash University, Australia.

Majumdar, P., 1998, Heat and mass transfer in composite desiccant pore structures for dehumidification, *Solar Energy*, vol.62, no.1, pp. 1-10.

Mathiprakasam, B., 1979, Performance predictions of silica gel desiccant cooling systems, PhD. thesis, Illinois Institute Technology, Chicago, Ill..

Mathiprakasam, B., and Z. Lavan, 1980, Performance predictors for adiabatic desiccant dehumidifiers using linear solutions, *ASME J. of Solar Energy Engineering*, vol. 102, pp. 73-79.

Meckler, M, 1995, Desiccant outdoor air preconditioners maximize heat recovery ventilation potentials, *ASHRAE Transactions*, vol. 101, part 2, pp. 992-1000.

Mei, V. C., 1979, Heat and mass transfer in air cooled desiccant dehumidifiers, Ph.D. thesis, Illinois Institute of Technology, Chicago, Ill..

Mei, V. C., F.C. Chen, Z. Lavan, R. K. Collier, and G. Meckler, 1992, An assessment of desiccant cooling and dehumidification technology, pp87.

Nimmo, B. G., R. K. Collier Jr., and K. Rengarajan, 1993, DEAC: Desiccant enhancement of cooling-based dehumidification, *ASHRAE Transactions*, vol. 99, part 1, pp. 842-848.

Niu, J. L. and L. Z. Zhang, 2002, Effects of wall thickness on the heat and moisture transfers in desiccant wheels for air dehumidification and enthalpy recovery, *International Communications in Heat and Mass Transfer*, vol. 29, issue 2, pp. 255-268.

Pennington, N. A., 1995, Humidity changer for air-conditioning, U.S. Patent 2,700,537, Jan..

Pesaran, A. A., and A., F., Mills, 1987 a, Moisture transport in silica gel packed beds – I. Theoretical study, *International Journal of Heat and Mass Transfer*, vol.30, pp. 1037-1049.

Pesaran, A. A., and A., F., Mills, 1987 b, Moisture transport in silica gel packed beds – I.I Experimental study, *International Journal of Heat and Mass Transfer*, vol.30, pp. 1051-1060.

Polanyi, M., 1932, Section III-theories of the adsorption of gases. A general survey and some additional remarks, Trans. Far. Soc., vol. 28, pp. 316-333.

Raghavan, V., and D. Gidaspow, 1985, Diffusion and adsorption of moisture in desiccant sheets, AIChE Journal vol. 31, no. 11, pp. 1791-1800.

Rengarajan, K., and B. G. Nimmo, 1993, Desiccant enhanced air conditioning (DEAC): An approach to improved comfort, in: Heat Pump and Refrigeration systems Design, Analysis and Applications, ASME AES-vol. 29, pp. 129-138.

Roy, D. and D. Gidaspow, 1972, A cross flow regenerator: A Green's Matrix Representation, *Chem. Eng. Sci.*, vol. 27, pp. 779-793.

San, J. Y., and S. C. Hsiau, 1993, Effect of axial solid heat conduction and mass diffusion in a rotary heat and mass regenerator, *International Journal of Heat and Mass Transfer*, vol.36, no.8, pp. 2051-2059.

Shah, R. K. and A. L. London, 1978, *Advances in heat transfer: Laminar flow forced convection in ducts: A source book for compact heat exchanger analytical data*, edited by T. F. Irvine, Jr. and J. P. Hartnett, New York: Academic Press.

Simonson, C. J. and R. W. Besant, 1997, Heat and moisture transfer in desiccant coated rotary energy exchangers, *HVAC&R Research*, vol.3, No.4, October, pp. 325-368.

Sladek, K. J., E. R. Gilliand, and R. F. Baddour, 1974, Diffusion on surfaces. II. Correlation of diffusivities of physically and chemically adsorbed species, *Industrial Chemical Fundamental*, vol.13, No.2, pp. 101-105.

Staats, W. R., J. Wurm, L. R. Wright, V. Kunc, and H. A. Banasiuk, 1977, Field testing of solar-MEC systems, Final Report, Institute of Gas Technology, Chicago, IL.

Štěpánek, F., M. Kubíček and M. Marek, 1998, Modeling and optimization of continuous adsorption in a desiccant rotor, *Industrial and Engineering Chemistry Research*, vol.37, No.4, pp.1435-1443.

Van den Bulck, E., J. W. Mitchell, and S. A. Klein, 1985, Design theory for rotary heat and mass exchange, *International Journal of Heat and Mass Transfer*, vol.28, pp. 1575-1595.

Van den Bulck, J. W. Mitchell, 1986, The use of dehumidifiers in desiccant cooling and dehumidification, *ASME J. Heat Transfer*, vol. 108, pp. 684-692.

Van den Bulck, E., 1987, Convective heat and mass transfer in compact regenerative dehumidifiers, Ph.D. thesis, University of Wisconsin-Madison

Van den Bulck, E., S. A. Klein, and J. W. Mitchell, 1988, Second law analysis of solid desiccant rotary dehumidifiers, *ASME J. Solar Energy Engineering*, vol. 110, pp. 2-9.

Venhuizen, D., 1984, Solar King's cooling gambit, *Solar Age*, pp. 9-25 (1984 (10)).

Walas, S. M., 1985, Phase equilibria in chemical engineering, 1th ed., Butterworth.

Worek, W. M., 1980, Experimental performance of a cross-cooled desiccant dehumidifier prototype, Ph.D. thesis, Illinois Institute of Technology, Chicago, Ill..

Zhang, Huan and Jianlei Niu, 1998, Two-stage desiccant cooling system and its energy consumption analysis, *journal of Heating Ventilating and Air Conditioning* (in Chinese), Vol. 28, No 6, pp. 2-5.

Zhang, Huan and Jianlei Niu, 1999, A two-stage desiccant cooling System using low temperature heat, *Building Services Engineering Research and Technology*, Vol. 20, No 2, pp. 51-55.

Zhang, Huan, S. J. You, H. X. Yang and Jianlei Niu, 2000, Enhanced performance of air-cooled chillers using evaporative cooling, *Building Services Engineering Research and Technology*, Vol. 21, No 4, pp. 213-217.

Zhang, X. J., Y. J. Dai and R. Z. Wang, 2003, A simulation study of heat and mass transfer in a honeycombed rotary desiccant dehumidifier, *Applied Thermal Engineering*, vol. 23, issue 8, pp. 989-1003.

Zhang, X. M., Z. P. Ren and F. M. Mei, 1993, Heat transfer (in Chinese), edited by Architectural publishing House of China, Beijing.

Zheng, W., and W. M. Worek, 1993, Numerical simulation of combined heat and mass transfer processes in a rotary dehumidifier, *Numerical Heat Transfer*, Part A, vol. 23, pp. 211-232.

Zheng, W., W. M. Worek, and D. Novosel, 1993, Control and optimization of rotational speeds for rotary dehumidifiers, *ASHRAE Transactions*, vol. 99, part 1, pp. 825-833.

Zheng, W., W. M. Worek, and D. Novosel, 1995, Performance optimization of rotary dehumidifiers, *Transactions of the ASME*, February, vol. 117, pp.40-44.

Appendix Test Data Recorded and Simulated Results

Table A1 shows the test data recorded for airflow measurement.

Table A1 Test Data Recorded for Airflow Measurement

Description	Units	Value
1. Process Airflow Inlet	m^3/s	0.04168
Temperature at Airflow Measuring Station	°C	28.6
Density of Air at Airflow Measuring Station	kg/m^3	1.1706
Mass Flow Rate	kg/s	0.04879
1a. Process Airflow Outlet	m^3/s	0.04610
Temperature at Airflow Measuring Station	°C	55.6
Density of Air at Airflow Measuring Station	kg/m^3	1.0745
Mass Flow Rate	kg/s	0.04953
2. Regeneration Airflow Inlet	m^3/s	0.02278
Temperature at Airflow Measuring Station	°C	29.8
Density of Air at Airflow Measuring Station	kg/m^3	1.1658
Mass Flow Rate	kg/s	0.02656
2a. Regeneration Airflow Outlet	m^3/s	0.02314
Temperature at Airflow Measuring Station	°C	42.2
Density of Air at Airflow Measuring Station	kg/m^3	1.1203
Mass Flow Rate	kg/s	0.02592

The single point of performance data described in Table A2 was replicated over a number of regeneration air inlet conditions at which the desiccant wheel was tested.

Table A2 Test Data Recorded and Simulated Results for Each Regeneration Air Inlet Temperature

Description	Units	Value
1. Process Air Inlet Temperature	°C	
2. Process Air Inlet Relative Humidity	%	
3. Process Air Inlet Humidity Ratio	$kg_{H_2O}/kg_{dry\ air}$	
4. Process Air Inlet Enthalpy	$kJ/kg_{dry\ air}$	
5. Process Air Outlet Temperature	°C	
6. Process Air Outlet Relative Humidity	%	
7. Process Air Outlet Humidity Ratio	$kg_{H_2O}/kg_{dry\ air}$	
8. Process Air Outlet Enthalpy	$kJ/kg_{dry\ air}$	
9.Experimental Moisture Removal Capacity	kg_{H_2O}/s	
10.Simulated Moisture Removal Capacity	kg_{H_2O}/s	
11. Uncertainty in Simulated Moisture Removal Capacity	%	
12. Experimental Total Energy Transfer	kW	
13. Simulated Total Energy Transfer	kW	
14. Uncertainty in Simulated Total Energy Transfer	%	

15.Process Air Pressure Drop	Pa	
16. Regeneration Air Inlet Temperature	°C	
17. Regeneration Air Inlet Relative Humidity	%	
18. Regeneration Air Inlet Humidity Ratio	$kg_{H_2O}/kg_{dry\ air}$	
19. Regeneration Air Inlet Enthalpy	$kJ/kg_{dry\ air}$	
20. Regeneration Air Outlet Temperature	°C	
21. Regeneration Air Outlet Relative Humidity	%	
22. Regeneration Air Outlet Humidity Ratio	$kg_{H_2O}/kg_{dry\ air}$	
23. Regeneration Air Outlet Enthalpy	$kJ/kg_{dry\ air}$	
24. Regeneration Air Pressure Drop	Pa	
25. Temperature of the Air at Inlet of Heater	°C	
26. Specific Heat of the Air at Inlet of Heater	$kJ/kg \cdot K$	
27. Temperature of the Air at Outlet of Heater	°C	
28. Specific Heat of the Air at Outlet of Heater	$kJ/kg \cdot K$	
29. Regeneration Energy	kW	
30. Regeneration Specific Heat Input	kJ/kg_{H_2O}	
31. Mass Ratio		
32. Total Energy Ratio		

Table A3 to Table A10 indicate the data recorded for each regeneration air inlet temperature.

Table A3 Test Data Recorded and Simulated Results for Regeneration Air Inlet Temperature 43.8°C

Description	Units	Value
1. Process Air Inlet Temperature	°C	28.9
2. Process Air Inlet Relative Humidity	%	59.2
3. Process Air Inlet Humidity Ratio	$kg_{H_2O}/kg_{dry\ air}$	0.01484
4. Process Air Inlet Enthalpy	$kJ/kg_{dry\ air}$	66.961
5. Process Air Outlet Temperature	°C	35.2
6. Process Air Outlet Relative Humidity	%	37.1
7. Process Air Outlet Humidity Ratio	$kg_{H_2O}/kg_{dry\ air}$	0.01324
8. Process Air Outlet Enthalpy	$kJ/kg_{dry\ air}$	69.379
9.Experimental Moisture Removal Capacity	kg_{H_2O}/s	0.0781×10^{-3}
10.Simulated Moisture Removal Capacity	kg_{H_2O}/s	0.0812×10^{-3}
11.Uncertainty in Simulated Moisture Removal Capacity	%	4.0
12. Experimental Total Energy Transfer	kW	0.1180
13. Simulated Total Energy Transfer	kW	0.0819
14. Uncertainty in Simulated Total Energy Transfer	%	30.6
15.Process Air Pressure Drop	Pa	434.9
16. Regeneration Air Inlet Temperature	°C	43.8
17. Regeneration Air Inlet Relative Humidity	%	22.9

18. Regeneration Air Inlet Humidity Ratio	$kg_{H_2O}/kg_{dry\ air}$	0.01282
19. Regeneration Air Inlet Enthalpy	$kJ/kg_{dry\ air}$	77.579
20. Regeneration Air Outlet Temperature	°C	31.7
21. Regeneration Air Outlet Relative Humidity	%	54.4
22. Regeneration Air Outlet Humidity Ratio	$kg_{H_2O}/kg_{dry\ air}$	0.01603
23. Regeneration Air Outlet Enthalpy	$kJ/kg_{dry\ air}$	72.924
24. Regeneration Air Pressure Drop	Pa	465.9
25. Temperature of the Air at Inlet of Heater	°C	29.8
26. Specific Heat of the Air at Inlet of Heater	$kJ/kg \cdot K$	1.005
27. Temperature of the Air at Outlet of Heater	°C	43.8
28. Specific Heat of the Air at Outlet of Heater	$kJ/kg \cdot K$	1.005
29. Regeneration Energy	kW	0.3737
30. Regeneration Specific Heat Input	kJ/kg_{H_2O}	4784.89
31. Mass Ratio		0.952
32. Total Energy Ratio		0.993

Table A4 Test Data Recorded and Simulated Results for Regeneration Air Inlet Temperature 51.3°C

Description	Units	Value
1. Process Air Inlet Temperature	°C	28.9
2. Process Air Inlet Relative Humidity	%	58.6
3. Process Air Inlet Humidity Ratio	$kg_{H_2O}/kg_{dry\ air}$	0.01468
4. Process Air Inlet Enthalpy	$kJ/kg_{dry\ air}$	66.568
5. Process Air Outlet Temperature	°C	38.1
6. Process Air Outlet Relative Humidity	%	29.3
7. Process Air Outlet Humidity Ratio	$kg_{H_2O}/kg_{dry\ air}$	0.01223
8. Process Air Outlet Enthalpy	$kJ/kg_{dry\ air}$	69.774
9.Experimental Moisture Removal Capacity	kg_{H_2O}/s	0.1195×10^{-3}
10.Simulated Moisture Removal Capacity	kg_{H_2O}/s	0.1205×10^{-3}
11.Deviation of Simulated Moisture Removal Capacity from Test Result	%	1.0
12. Experimental Total Energy Transfer	kW	0.1564
13. Simulated Total Energy Transfer	kW	0.1245
14.Deviation of Simulated Total Energy Transfer from Test Result	%	20.4
15.Process Air Pressure Drop	Pa	434.5
16. Regeneration Air Inlet Temperature	°C	51.3

17. Regeneration Air Inlet Relative Humidity	%	14.9
18. Regeneration Air Inlet Humidity Ratio	$kg_{H_2O}/kg_{dry\ air}$	0.01234
19. Regeneration Air Inlet Enthalpy	$kJ/kg_{dry\ air}$	83.671
20. Regeneration Air Outlet Temperature	°C	33.6
21. Regeneration Air Outlet Relative Humidity	%	51.9
22. Regeneration Air Outlet Humidity Ratio	$kg_{H_2O}/kg_{dry\ air}$	0.01705
23. Regeneration Air Outlet Enthalpy	$kJ/kg_{dry\ air}$	77.499
24. Regeneration Air Pressure Drop	Pa	467.7
25. Temperature of the Air at Inlet of Heater	°C	29.8
26. Specific Heat of the Air at Inlet of Heater	$kJ/kg \cdot K$	1.005
27. Temperature of the Air at Outlet of Heater	°C	51.3
28. Specific Heat of the Air at Outlet of Heater	$kJ/kg \cdot K$	1.005
29. Regeneration Energy	kW	0.5710
30. Regeneration Specific Heat Input	kJ/kg_{H_2O}	4778.24
31. Mass Ratio		0.994
32.Total Energy Ratio		0.993

Table A5 Test Data Recorded and Simulated Results for Regeneration Air Inlet Temperature 60.3°C

Description	Units	Value
1. Process Air Inlet Temperature	°C	29.0
2. Process Air Inlet Relative Humidity	%	57.7
3. Process Air Inlet Humidity Ratio	$kg_{H_2O}/kg_{dry\ air}$	0.01454
4. Process Air Inlet Enthalpy	$kJ/kg_{dry\ air}$	66.301
5. Process Air Outlet Temperature	°C	41.3
6. Process Air Outlet Relative Humidity	%	22.6
7. Process Air Outlet Humidity Ratio	$kg_{H_2O}/kg_{dry\ air}$	0.01118
8. Process Air Outlet Enthalpy	$kJ/kg_{dry\ air}$	70.340
9.Experiment Moisture Removal Capacity	kg_{H_2O}/s	0.1639×10^{-3}
10.Simulated Moisture Removal Capacity	kg_{H_2O}/s	0.1505×10^{-3}
11.Deviation of Simulated Moisture Removal Capacity from Test Result	%	8.2
12. Experiment Total Energy Transfer	kW	0.1971
13. Simulated Total Energy Transfer	kW	0.1958
14. Deviation of Simulated Total Energy Transfer from Test Result	%	0.7
15.Process Air Pressure Drop	Pa	434.4
16. Regeneration Air Inlet Temperature	°C	60.3

17. Regeneration Air Inlet Relative Humidity	%	10.2
18. Regeneration Air Inlet Humidity Ratio	$kg_{H_2O}/kg_{dry\ air}$	0.01291
19. Regeneration Air Inlet Enthalpy	$kJ/kg_{dry\ air}$	94.379
20. Regeneration Air Outlet Temperature	°C	36.6
21. Regeneration Air Outlet Relative Humidity	%	49.8
22. Regeneration Air Outlet Humidity Ratio	$kg_{H_2O}/kg_{dry\ air}$	0.01938
23. Regeneration Air Outlet Enthalpy	$kJ/kg_{dry\ air}$	86.604
24. Regeneration Air Pressure Drop	Pa	463.8
25. Temperature of the Air at Inlet of Heater	°C	29.8
26. Specific Heat of the Air at Inlet of Heater	$kJ/kg \cdot K$	1.005
27. Temperature of the Air at Outlet of Heater	°C	60.3
28. Specific Heat of the Air at Outlet of Heater	$kJ/kg \cdot K$	1.00512
29. Regeneration Energy	kW	0.8143
30. Regeneration Specific Heat Input	kJ/kg_{H_2O}	4968.27
31. Mass Ratio		0.992
32.Total Energy Ratio		0.993

Table A6 Test Data Recorded and Simulated Results for Regeneration Air Inlet Temperature 70.2°C

Description	Units	Value
1. Process Air Inlet Temperature	°C	29.2
2. Process Air Inlet Relative Humidity	%	56.1
3. Process Air Inlet Humidity Ratio	$kg_{H_2O}/kg_{dry\ air}$	0.01429
4. Process Air Inlet Enthalpy	$kJ/kg_{dry\ air}$	65.883
5. Process Air Outlet Temperature	°C	45.6
6. Process Air Outlet Relative Humidity	%	16.2
7. Process Air Outlet Humidity Ratio	$kg_{H_2O}/kg_{dry\ air}$	0.01000
8. Process Air Outlet Enthalpy	$kJ/kg_{dry\ air}$	71.711
9.Experimental Moisture Removal Capacity	kg_{H_2O}/s	0.2093×10^{-3}
10.Simulated Moisture Removal Capacity	kg_{H_2O}/s	0.1946×10^{-3}
11.Deviation of Simulated Moisture Removal Capacity from Test Result	%	7.0
12. Experimental Total Energy Transfer	kW	0.2843
13. Simulated Total Energy Transfer	kW	0.2629
14.Deviation of Simulated Total Energy Transfer from Test Result	%	7.5
15.Process Air Pressure Drop	Pa	433.5
16. Regeneration Air Inlet Temperature	°C	70.2

17. Regeneration Air Inlet Relative Humidity	%	6.4
18. Regeneration Air Inlet Humidity Ratio	$kg_{H_2O}/kg_{dry\ air}$	0.01269
19. Regeneration Air Inlet Enthalpy	$kJ/kg_{dry\ air}$	104.253
20. Regeneration Air Outlet Temperature	°C	38.9
21. Regeneration Air Outlet Relative Humidity	%	47.4
22. Regeneration Air Outlet Humidity Ratio	$kg_{H_2O}/kg_{dry\ air}$	0.02095
23. Regeneration Air Outlet Enthalpy	$kJ/kg_{dry\ air}$	93.034
24. Regeneration Air Pressure Drop	Pa	465.3
25. Temperature of the Air at Inlet of Heater	°C	29.8
26. Specific Heat of the Air at Inlet of Heater	$kJ/kg \cdot K$	1.005
27. Temperature of the Air at Outlet of Heater	°C	70.2
28. Specific Heat of the Air at Outlet of Heater	$kJ/kg \cdot K$	1.009
29. Regeneration Energy	kW	1.086
30. Regeneration Specific Heat Input	kJ/kg_{H_2O}	5188.72
31. Mass Ratio		0.992
32.Total Energy Ratio		0.993

Table A7 Test Data Recorded and Simulated Results for Regeneration Air Inlet Temperature 80.8°C

Description	Units	Value
1. Process Air Inlet Temperature	°C	29.3
2. Process Air Inlet Relative Humidity	%	56.9
3. Process Air Inlet Humidity Ratio	$kg_{H_2O}/kg_{dry\ air}$	0.01459
4. Process Air Inlet Enthalpy	$kJ/kg_{dry\ air}$	66.739
5. Process Air Outlet Temperature	°C	49.6
6. Process Air Outlet Relative Humidity	%	12.5
7. Process Air Outlet Humidity Ratio	$kg_{H_2O}/kg_{dry\ air}$	0.00944
8. Process Air Outlet Enthalpy	$kJ/kg_{dry\ air}$	74.340
9.Experimental Moisture Removal Capacity	kg_{H_2O}/s	0.2513×10^{-3}
10.Simulated Moisture Removal Capacity	kg_{H_2O}/s	0.2519×10^{-3}
11.Deviation of Simulated Moisture Removal Capacity from Test Result	%	0.2
12. Experimental Total Energy Transfer	kW	0.3709
13. Simulated Total Energy Transfer	kW	0.3241
14.Deviation of Simulated Total Energy Transfer from Test Result	%	12.6
15.Process Air Pressure Drop	Pa	432.1
16. Regeneration Air Inlet Temperature	°C	80.8

17. Regeneration Air Inlet Relative Humidity	%	4.0
18. Regeneration Air Inlet Humidity Ratio	$kg_{H_2O}/kg_{dry\ air}$	0.01211
19. Regeneration Air Inlet Enthalpy	$kJ/kg_{dry\ air}$	113.691
20. Regeneration Air Outlet Temperature	°C	42.0
21. Regeneration Air Outlet Relative Humidity	%	42.2
22. Regeneration Air Outlet Humidity Ratio	$kg_{H_2O}/kg_{dry\ air}$	0.02203
23. Regeneration Air Outlet Enthalpy	$kJ/kg_{dry\ air}$	99.059
24. Regeneration Air Pressure Drop	Pa	466.2
25. Temperature of the Air at Inlet of Heater	°C	29.8
26. Specific Heat of the Air at Inlet of Heater	$kJ/kg \cdot K$	1.005
27. Temperature of the Air at Outlet of Heater	°C	80.8
28. Specific Heat of the Air at Outlet of Heater	$kJ/kg \cdot K$	1.009
29. Regeneration Energy	kW	1.370
30. Regeneration Specific Heat Input	kJ/kg_{H_2O}	5451.65
31. Mass Ratio		0.992
32.Total Energy Ratio		0.993

Table A8 Test Data Recorded and Simulated Results for Regeneration Air Inlet Temperature 89.9°C

Description	Units	Value
1. Process Air Inlet Temperature	°C	29.0
2. Process Air Inlet Relative Humidity	%	57.6
3. Process Air Inlet Humidity Ratio	$kg_{H_2O}/kg_{dry\ air}$	0.01451
4. Process Air Inlet Enthalpy	$kJ/kg_{dry\ air}$	66.235
5. Process Air Outlet Temperature	°C	53.2
6. Process Air Outlet Relative Humidity	%	9.6
7. Process Air Outlet Humidity Ratio	$kg_{H_2O}/kg_{dry\ air}$	0.00864
8. Process Air Outlet Enthalpy	$kJ/kg_{dry\ air}$	75.949
9.Experiment Moisture Removal Capacity	kg_{H_2O}/s	0.2864×10^{-3}
10.Simulated Moisture Removal Capacity	kg_{H_2O}/s	0.2944×10^{-3}
11.Deviation of Simulated Moisture Removal Capacity from Test Result	%	2.8
12. Experiment Total Energy Transfer	kW	0.4739
13. Simulated Total Energy Transfer	kW	0.3942
14.Deviation of Simulated Total Energy Transfer from Test Result	%	16.8
15.Process Air Pressure Drop	Pa	436.7
16. Regeneration Air Inlet Temperature	°C	89.9

17. Regeneration Air Inlet Relative Humidity	%	2.6
18. Regeneration Air Inlet Humidity Ratio	$kg_{H_2O}/kg_{dry\ air}$	0.01154
19. Regeneration Air Inlet Enthalpy	$kJ/kg_{dry\ air}$	121.657
20. Regeneration Air Outlet Temperature	°C	43.7
21. Regeneration Air Outlet Relative Humidity	%	40.0
22. Regeneration Air Outlet Humidity Ratio	$kg_{H_2O}/kg_{dry\ air}$	0.02285
23. Regeneration Air Outlet Enthalpy	$kJ/kg_{dry\ air}$	102.957
24. Regeneration Air Pressure Drop	Pa	464.4
25. Temperature of the Air at Inlet of Heater	°C	29.8
26. Specific Heat of the Air at Inlet of Heater	$kJ/kg \cdot K$	1.005
27. Temperature of the Air at Outlet of Heater	°C	89.9
28. Specific Heat of the Air at Outlet of Heater	$kJ/kg \cdot K$	1.009
29. Regeneration Energy	kW	1.614
30. Regeneration Specific Heat Input	kJ/kg_{H_2O}	5635.47
31. Mass Ratio		0.992
32.Total Energy Ratio		0.993

Table A9 Test Data Recorded and Simulated Results for Regeneration Air Inlet Temperature 100.5°C

Description	Units	Value
1. Process Air Inlet Temperature	°C	29.1
2. Process Air Inlet Relative Humidity	%	57.6
3. Process Air Inlet Humidity Ratio	$kg_{H_2O}/kg_{dry\ air}$	0.01460
4. Process Air Inlet Enthalpy	$kJ/kg_{dry\ air}$	66.558
5. Process Air Outlet Temperature	°C	57.9
6. Process Air Outlet Relative Humidity	%	6.8
7. Process Air Outlet Humidity Ratio	$kg_{H_2O}/kg_{dry\ air}$	0.00764
8. Process Air Outlet Enthalpy	$kJ/kg_{dry\ air}$	78.160
9.Experimental Moisture Removal Capacity	kg_{H_2O}/s	0.3396×10^{-3}
10.Simulated Moisture Removal Capacity	kg_{H_2O}/s	0.3401×10^{-3}
11.Deviation of Simulated Moisture Removal Capacity from Test Result	%	0.1
12. Experimental Total Energy Transfer	kW	0.5661
13. Simulated Total Energy Transfer	kW	0.4815
14.Deviation of Simulated Total Energy Transfer from Test Result	%	14.9
15.Process Air Pressure Drop	Pa	436.7
16. Regeneration Air Inlet Temperature	°C	100.5

17. Regeneration Air Inlet Relative Humidity	%	1.6
18. Regeneration Air Inlet Humidity Ratio	$kg_{H_2O}/kg_{dry\ air}$	0.01047
19. Regeneration Air Inlet Enthalpy	$kJ/kg_{dry\ air}$	129.687
20. Regeneration Air Outlet Temperature	°C	45.4
21. Regeneration Air Outlet Relative Humidity	%	38.2
22. Regeneration Air Outlet Humidity Ratio	$kg_{H_2O}/kg_{dry\ air}$	0.02385
23. Regeneration Air Outlet Enthalpy	$kJ/kg_{dry\ air}$	107.352
24. Regeneration Air Pressure Drop	Pa	464.4
25. Temperature of the Air at Inlet of Heater	°C	29.8
26. Specific Heat of the Air at Inlet of Heater	$kJ/kg \cdot K$	1.005
27. Temperature of the Air at Outlet of Heater	°C	100.5
28. Specific Heat of the Air at Outlet of Heater	$kJ/kg \cdot K$	1.009
29. Regeneration Energy	kW	1.898
30. Regeneration Specific Heat Input	kJ/kg_{H_2O}	5588.93
31. Mass Ratio		0.994
32.Total Energy Ratio		0.993

Table A10 Test Data Recorded and Simulated Results for Regeneration Air Inlet Temperature 108.5°C

Description	Units	Value
1. Process Air Inlet Temperature	°C	29.3
2. Process Air Inlet Relative Humidity	%	55.7
3. Process Air Inlet Humidity Ratio	$kg_{H_2O}/kg_{dry\ air}$	0.01427
4. Process Air Inlet Enthalpy	$kJ/kg_{dry\ air}$	65.935
5. Process Air Outlet Temperature	°C	61.4
6. Process Air Outlet Relative Humidity	%	5.3
7. Process Air Outlet Humidity Ratio	$kg_{H_2O}/kg_{dry\ air}$	0.00700
8. Process Air Outlet Enthalpy	$kJ/kg_{dry\ air}$	80.082
9.Experimental Moisture Removal Capacity	kg_{H_2O}/s	0.3547×10^{-3}
10.Simulated Moisture Removal Capacity	kg_{H_2O}/s	0.3522×10^{-3}
11.Deviation of Simulated Moisture Removal Capacity from Test Result	%	0.7
12. Experimental Total Energy Transfer	kW	0.6902
13. Simulated Total Energy Transfer	kW	0.5783
14.Deviation of Simulated Total Energy Transfer from Test Result	%	16.2
15.Process Air Pressure Drop	Pa	426.7
16. Regeneration Air Inlet Temperature	°C	108.5

17. Regeneration Air Inlet Relative Humidity	%	1.3
18. Regeneration Air Inlet Humidity Ratio	$kg_{H_2O}/kg_{dry\ air}$	0.01145
19. Regeneration Air Inlet Enthalpy	$kJ/kg_{dry\ air}$	140.711
20. Regeneration Air Outlet Temperature	°C	47.3
21. Regeneration Air Outlet Relative Humidity	%	36.9
22. Regeneration Air Outlet Humidity Ratio	$kg_{H_2O}/kg_{dry\ air}$	0.02545
23. Regeneration Air Outlet Enthalpy	$kJ/kg_{dry\ air}$	113.475
24. Regeneration Air Pressure Drop	Pa	461.3
25. Temperature of the Air at Inlet of Heater	°C	29.8
26. Specific Heat of the Air at Inlet of Heater	$kJ/kg \cdot K$	1.005
27. Temperature of the Air at Outlet of Heater	°C	108.5
28. Specific Heat of the Air at Outlet of Heater	$kJ/kg \cdot K$	1.009
29. Regeneration Energy	kW	2.112
30. Regeneration Specific Heat Input	kJ/kg_{H_2O}	5954.33
31. Mass Ratio		0.992
32.Total Energy Ratio		0.993